UNIVERSITAT POLITÈCNICA DE VALÈNCIA

INSTITUTO INTERUNIVERSITARIO DE INVESTIGACIÓN DE
RECONOCIMIENTO MOLECULAR Y DESARROLLO TECNOLÓGICO

Impact of brain endothelial senescence on neurogenesis: application of novel strategies for age-related senescence detection

PhD. THESIS

Submitted by:

Sara Rojas Vázquez

PhD. Supervisors:

Prof. Isabel Fariñas Gómez

Prof. Ramón Martínez-Máñez

Valencia, May 2023

Mr. Ramón Martínez-Máñez, Full professor in the Department of Chemistry at the Universitat Politècnica de València, and Ms. Isabel Fariñas Gómez, Full Professor in the Department of Cellular Biology, Functional Biology and Physical Anthropology and the Research Institute in Biotechnology and Biomedicine (BIOTECMED) at the Universitat de València,

Certify:

That the work "Impact of brain endothelial senescence on neurogenesis: application of novel strategies for age-related senescence detection" has been developed by Sara Rojas Vázquez under their supervision, at the Instituto Interuniversitario de Investigación de Reconocimiento Molecular y Desarrollo Tecnológico (IDM) of the Universitat Politècnica de València, as a Thesis Project in order to obtain the degree of PhD in Chemistry at the Universitat Politècnica de València.

Valencia, April 28th 2023

Prof. Ramón Martínez-Máñez

Prof. Isabel Fariñas Gómez

Index

Figure index

Introduction

Results

Material and methods

List of acronyms and abbreviations

AAV	adeno-associated vector
aNSC	activated neural stem cell
ATP	adenosine triphosphate
B1	neural stem cell
B2M	β2-microglobulin
BBB	blood-brain-barrier
BCL-2	B-cell lymphoma 2
BEC	brain endothelial cell
BEnd.3	brain endothelial cell line
bFGF	basic fibroblast growth factor
BLBP	brain lipid-binding protein
BrdU	5-Bromo-2'-deoxyuridine
BSA	bovine serum albumin
CAG	hybrid synthetic promoter
CCL	chemokine ligand
C-CM	control EC-conditioned medium
CDK	cyclin-dependent kinase
CKI	cyclin-dependent kinase inhibitor
CNS	central nervous system
CP	choroid plexus
CSF	cerebrospinal fluid
DAS	days after senolytics/senolysis
D+Q	dasatinib and quercetin
DDR	DNA damage response
DFFDA	CellTraceTM Oregon GreenTM 488 Carboxy-DFFDA-SE
DG	dental gyrus
DIV	days in vitro
DMEM	Dulbecco's modified eagle medium
DNA	deoxyribonucleic acid
DSBs	DNA double-strand breaks
e.g.	*exempli gratia* (for example)
EBSS	Earle's Balanced Salt Solution
ECM	extracellular matrix
EC	endothelial cell
EDTA	ethylenediaminetetraacetic acid
EGF	epidermal growth factor
EGFR	EGFR receptor
ENB	early neuroblast
eNOs	endothelial nitric oxide synthase
EPM	Elevated Plus Maze
FACS	fluorescence-activated cell sorting
FBS	foetal bovine serum
FC	flow cytometry
FDR	false discovery rate
FSC	forward scatter detector
GC	granule cell
gc	genomic copies
GCL	granule cell layer
GDF11	growth differentiation factor 11
GFAP	glial fibrillary acidic protein
GL	glomerular layer
GLAST	glutamate aspartate transporter
GLUT1	glucose transporter 1
GO	gene ontology
HBSS	Hanks balanced salt solution
HIF-1α	hypoxia-inducible factor alpha
HPLC	high performance liquid chromatography
hUVECs	human umbilical vein endothelial cells
i.c./IC	intracardiac
ICC	immunocytochemistry
i.e.	id est (that is)
IGC	intermediate granule cell
IHC	immunohistochemistry
IL	interleukin
i.p./IP	intraperitoneal
IPC	intermediate progenitor cell
IRS	insulin receptor substrate
i.v./IV	intravenous
Lin$^-$	lineage-negative (negative for TER119, O4, CD45 and CD31)
LNB	late neuroblast
LV	lateral ventricle

-m	month-old
M.A.S	Motor Ability Scale
MFI	median fluorescence intensity
MI	mean fluorescence intensity
min/h	minutes/hours
MOI	multiplicity of infection
NB	neuroblast
Non-CM	non-conditioned medium
NOR	Novel Object Recognition
NSC	neural stem cell
NT-3	neurotrophic factor 3
OB	olfactory bulb
p38MAPK	p38-mitogen activated protein kinase
PB	phosphate buffer
PBS	phosphate-buffered saline
PCR	polimerase chain reaction
PD	Parkinson disease
PEDF	epithelial-derived factor
PEI	polyethylenimine
PFA	paraformaldehyde
pNSCs	primed neural stem cell
qNSCs	quiescent neural stem cell
Rb	retinoblastoma protein
RGL	radial quiescent glia-like cells
rhEGF	recombinant human epidermal growth factor
RMS	rostral migratory stream
RNA	ribonucleic acid
ROS	reactive oxygen species
RSV	Rous sarcoma virus
SA-β-Gal	senescence-associated beta-Galactosidase
SAMP	senescence-accelerated mouse prone
SAMR	senescence-accelerated mouse resistant
SASP	senescence-associated secretory phenotype
SC	stem cell
SCAP	senescent cells anti-apoptotic pathway
S-CM	senescent EC-conditioned medium
SDF1	stromal-derived chemokine factor
SEM	standard error of mean
sEVs	small extracellular vesicles
SEZ	subependymal zone
SGZ	subgranular zone
SSC	side scatter detector
SOD	superoxide dismutase
TGFβ1	transforming growth factor beta 1
TH	tyrosine hydroxylase
TNF-α	tumour necrosis factor alpha
V-SVZ	ventricular-subventricular zone
w/o	without
WM	whole-mount
β-Gal	beta-Galactosidase

Introduction

Preview

Ageing is conceived as a progressive process of functional decline that occurs over the course of life. In general, advancing age is accompanied by the deterioration of multiple tissues, altered homeostasis and increased frailty. Age is considered to be the main risk factor for a large number of diseases with high mortality rates, such as cardiovascular pathologies, cancer, pulmonary fibrosis, hepatic steatosis, and neurodegenerative disorders, among others. As the elderly population grows, these pathologies are becoming increasingly prevalent in our society and are now the leading health concerns in primary care. Consequently, comprehending the mechanisms that cause ageing and resulting health decline is a major challenge for the scientific community, backed by significant socio-economic interest. Achieving this goal would allow for targeted interventions against age-related diseases, promote healthy ageing, and extend human lifespan. In this context, cellular senescence has emerged as an important focus of research, as this cellular fate is considered a contributing factor to the functional and structural deterioration of tissues with increasing age, leading to chronic health conditions.

Neurodegenerative disorders are mostly of unknown etiology, and only palliative treatments are currently available. Neurodegeneration may be prompted by the decline in neurogenesis that occurs with ageing. In this regard, the brain vasculature represents an essential component of the neurogenic niches, where cells with the capacity to generate new neurons reside. Brain microvessels contribute substantially to preserving the homeostasis and neurogenic potential of these regions, but they also undergo structural and functional changes with age. However, whether these alterations are linked to cellular senescence it is not yet clear. Hence, the purpose of this thesis is to delve deeper into the intricacies of age-related senescence and its impact on the process of brain ageing.

1. How do we age?: unlocking the connection between ageing and cell senescence

Ageing is characterised by a progressive functional decline which is accompanied by the development of age-related diseases (López-Otín et al., 2013; 2023). One of the hallmarks of ageing is a rise in the number of senescent cells in most organs (Childs et al., 2017). Senescence is a biological process that cells can undergo in response to different intra and extracellular stressors, including oncogene activation, epigenetic remodelling, hypoxia, oxidative stress, telomere attrition and other forms of DNA damage (**Figure 1**) (Hernández-Segura et al., 2018). Interestingly, these stress factors have been classically recognised as primary hallmarks of ageing (López-Otín et al., 2013). One of the most prominent traits of senescent cells is their irreversible replicative arrest. Senescence inducers trigger a cell DNA damage response (DDR) that promotes up-regulation of cyclin-dependent kinase inhibitor (CKI) proteins. Senescent cells activate the tumour suppressor protein p53 leading to increased levels of the CKI protein $p21^{CIP1}$ (p21) and to cell cycle blockade. Additionally, in response to persistent DNA damage, CKI $p16^{INK4a}$ (p16) can be activated through various pathways, including those mediated by p38-MAPK-induced mitochondrial dysfunction and ROS production (**Figure 1**). This consolidates permanent cell cycle arrest and leads to altered expression of many genes and epigenetic DNA changes in senescent cells (Rayess et al., 2012; Herranz and Gil, 2018; Kumari and Jat, 2021). Cell cycle withdrawal is frequently accompanied by substantial deterioration of the nuclear lamina, as a result of reduced levels of the nuclear envelope protein Lamin B1, as well as an increase in heterochromatin foci of DNA damage responsive proteins, particularly γH2AX (histone H2AX phosphorylated at serine 139) (Herranz and Gil, 2018). Although senescent cells do not proliferate, they are metabolically active and display augmented lysosomal mass with elevated activity of the lysosomal β-Galactosidase enzyme (β-Gal). Furthermore, they exhibit a potent secretory function known as senescence-associated secretory phenotype (SASP) (**Figure 1**) (Kurz et al., 2000; Coppé et al., 2010; Muñoz-Spín and Serrano, 2014).

The SASP comprises a complex mixture of molecules, including cytokines, chemokines, proteases,

growth factors and exosomes, which are released into the extracellular space. Broadly, the secretome of senescent cells has a potent proinflammatory effect, exerts immunomodulatory actions and influences the growth of neighbouring cells (Tchkonia et al., 2013; van Deursen, 2014, Childs et al., 2017; Borghesan et al., 2019). In healthy adult tissues, the SASP is transient and may even contribute to the restoration of tissue homeostasis (Tchkonia et al., 2013). However, chronic SASP is a key driver of the major deleterious effects of senescence, as it is responsible for many pathological features of ageing, such as chronic inflammation, tumorigenesis and impaired adult stem cell (SC) renewal (Coppé et al., 2010; van Deursen, 2014; Muñoz-Spín and Serrano, 2014; Schafer et al., 2020). Although cellular senescence prevents damage progression by permanently halting cell proliferation and acting as a defence mechanism against cancer, the accumulation of senescent cells can accelerate tumour progression due to growth factors and proteases released in the SASP (Campisi, 2013; Childs et al., 2017; Yang et al., 2021). Importantly, senescent cell-secreted factors also have the potential to induce senescence in surrounding cells in a paracrine manner (Tchkonia et al., 2013; Acosta et al., 2013; Gonzalez-Meljem et al., 2018). Indeed, while some of these SASP factors may be restricted to a specific tissue affecting adjacent cells, others circulate in the systemic milieu and reach distant cells even in other tissues (e.g. via exosomes), and both play an active role in the spread of senescence (Takasugi, 2018; Borghesan et al., 2019; Mao and Xu., 2020). Intriguingly, the content of the secretome varies according to cellular origin, tissue location or senescence inducer and is susceptible to modulation by hormones, drugs or pathogens (Coppé et al., 2008; Malaquin et al., 2018). Moreover, regarding other aspects of cell metabolism, senescent cells often show altered mitochondrial function that favours a shift from fatty acid use for energy production towards glucose utilisation (Sabbatinelli et al., 2019). This reliance on glycolysis can lead to lipid droplet accumulation and lipotoxicity, which is reported to promote neuroinflammation as well as impaired microcirculation in the brain (Flor et al., 2017; Ogrodnik et al., 2019; Hidalgo-Lanussa et al., 2020).

Senescent cells develop pro-survival mechanisms to avoid immune clearance and apoptosis (Yosef et al., 2016; Hu et al., 2022), which, together with their ability to induce paracrine senescence, contributes to their accumulation in tissues (**Figure 1**) (Nelson et al., 2012; Ovadya et al., 2018). The progressively elevated incidence of these cells also reflects the loss of cell repair mechanisms and the reduced capacity of the immune system to clear both damaged and senescent cells with advancing age (Montecino-Rodriguez et al., 2013; Childs et al., 2017; Ovadya et al., 2018). Increased senescence burden results in the loss of functional cells in tissues and a wide range of non-autonomous alterations, such as impaired extracellular matrix remodelling, decreased cell proliferation, and SC exhaustion in their attempt to regenerate tissue. These changes correlate with impaired tissue renewal and performance, leading to organ dysfunction and promoting the development of age-related diseases (Childs et al., 2015; 2017; Herranz and Gil, 2018). Therefore, persistent senescence has been described as a driver of several chronic diseases, including neurodegenerative disorders that constitute a major challenge to medicine and public health in developed and developing countries (Childs et al., 2017; Martínez-Cué and Rueda, 2020). In this context, the senescent cell burden has emerged as one of the main hallmarks of ageing and its proper detection has become a priority for developing therapeutic strategies.

Unfortunately, there is no single specific marker to identify senescent cells, hence a combination of different ones is required for accurate detection (Hernández-Segura et al., 2018). As the characteristics of senescent cells can be influenced by their origin, placement and senescence induction, the recognition of senescent cell markers can be a complex task (González-Gualda et al., 2021). Nonetheless, senescence-associated β-Gal (SA-β-Gal) is one of the most common features shared among senescent cells and represents one of the most widely used biomarkers in the field (Dimri et al., 1995; Kurz et al., 2000). The increased activity of lysosomal β-Gal in senescent cells has traditionally been examined by a histochemical reaction involving the use of the specific substrate X-gal. Once hydrolyzed in lysosomes, the chromogen X-gal labels senescent cells blue. Because β-Gal is an enzyme present in all cell lysosomes, the technique is carried out under suboptimal pH conditions for the enzyme to ensure that only cells with very high β-Gal activity will turn blue (Debacq-Chainiaux et al., 2009). Although frequently used, this staining method has

strong limitations, such as: it cannot be performed on living cells, its results vary depending on the fixation conditions, and it is difficult to combine with other senescence-associated markers. In this regard, there is a growing interest in the search for other methods that may facilitate the reliable detection of SA-β-gal, overcoming the barriers of traditional X-gal staining. For instance, new fluorogenic probes are emerging that can fluorescently identify β-Gal activity in live cells (Ogawa et al., 2021). Building on this, our group has synthesised probes that consist of a fluorophore bound to a galactose derivative. This bond is susceptible to hydrolysis by the β-Gal enzyme, releasing the fluorophore, which then becomes intensely fluorescent. We have designed several fluorogenic probes for senescent cell recognition, containing fluorophores with different emission ranges to facilitate the development of flow cytometry strategies for *ex vivo* detection of senescent cells (Lozano-Torres et al., 2017; 2023; Rojas-Vázquez et al., submitted).

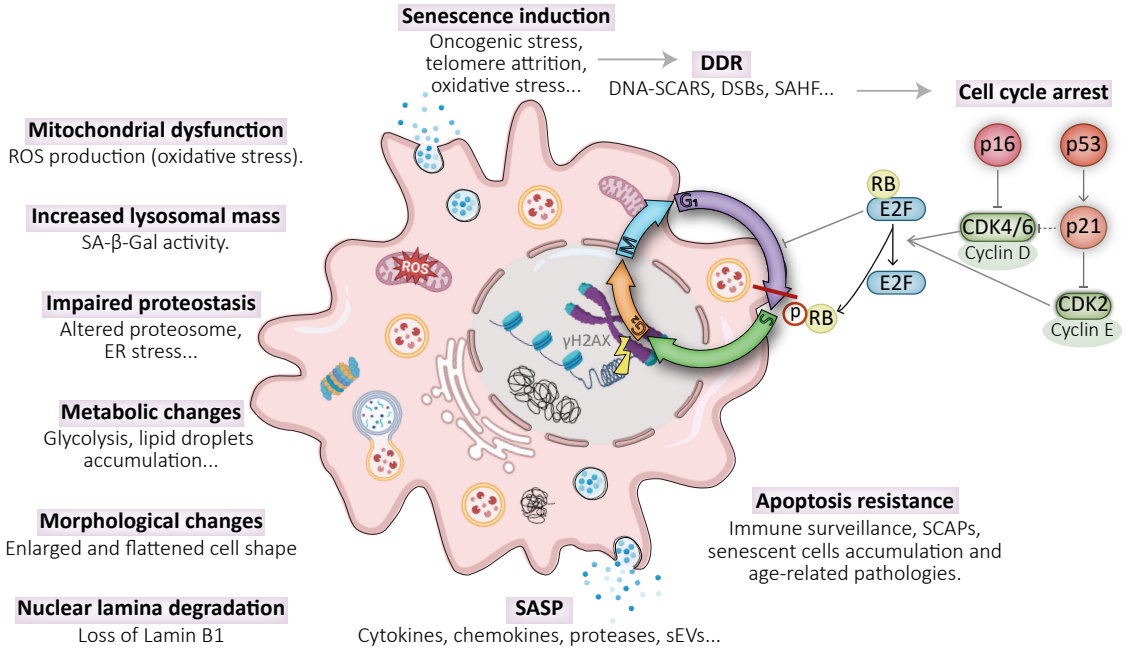

Figure 1. Main features of age-related cell senescence. Senescence is a cellular response to different types of stressors, such as oncogenic stress, telomeric attrition, or oxidative stress, among others. These stressors lead to DNA double-strand breaks (DSBs), scars, or chromatin reorganisation (senescence-associated heterochromatin foci or SAHFs), triggering a cascade reaction for cell cycle arrest. This is achieved by activating one or more senescence-promoting transcription factor cascades through the upregulation of p16 or/and p53-p21 cell cycle inhibitors, leading to irreversible proliferation arrest and inducing a series of changes that compromise the functionality of the cell. For example, senescent cells can exhibit high β-gal activity, increased mitochondrial ROS production, endoplasmic reticulum (ER) stress, as well as a potent SASP in which they release mainly pro-inflammatory factors. All these features create an environment conditioned by stressful signals that affect senescent cells itself, in an autocrine manner, and neighbouring tissue cells, in a paracrine manner, contributing to the spread of cellular senescence. In addition, these cells develop anti-apoptotic mechanisms (SCAPs) that favour their accumulation in tissues with ageing.

Nevertheless, longitudinally associating the phenotypic changes of ageing with the senescent cell burden of the organism remains a rather difficult task today. This is mainly due to the absence of reliable and non-invasive tools to detect senescent cells in live animals (González-Gualda et al., 2021). Longitudinal characterisation of ageing enables tracking the age-related progressive deterioration of the organism. Such studies are based on different specific tests performed at multiple age points, which reveal the general health status of the individual simply by external assessment (Yanai and Endo, 2021). Their combination with the measurement of senescence burden can provide valuable information, for example, for determining the biological age of an individual, for identifying key ages for diagnosing senescence-associated diseases, or for developing targeted therapies to rejuvenate tissues.

2. Ageing in murine models: the consequences of senescence

Similar to humans, mouse models of natural ageing experience progressive overall physiological deterioration that affects different organs as they age. At the neurological level, the performance of basic functions in the mouse is altered at advanced ages, as even olfaction, one of the main drivers for tasks requiring exploration and socialisation, is impaired with ageing (Patel and Larson, 2009; Yanai and Endo, 2021; Radulescu et al., 2021). Therefore, increasing age is accompanied by substantial changes in animal welfare that can be observed through the longitudinal evaluation of different parameters related to ageing. In this sense, strength, motor skills, memory, cognition and emotion, among other aspects, begin to deteriorate, creating an imbalance in health status between young and old mice that can be externally evaluated by specific tests. For instance, the wild-type C57BL/6 mouse strain undergoes a gradual functional decline with ageing (Yanai and Endo, 2021). The middle-aged C57BL/6 mice show decreased locomotor activity, as revealed by Rotarod and Open Field tests, while at older ages they display increased anxious behaviour, decreased social skills and reduced spatial memory, as evidenced by Open Field, Elevated Plus Maze (EPM) and social interaction tests, among others (Shoji et al., 2016; Yanai and Endo, 2021; Radulescu et al., 2021). Interestingly, senolytic strategies to selectively eliminate senescent cells have shown promising outcomes, contributing to improved physical function, reduced anxiety and prolonged lifespan in aged C57BL/6 animals (Xu et al., 2018; Ogrodnik et al., 2019; Fielder et al., 2022). These results imply that many of the changes exhibited with ageing are directly proportional to the prevalence of senescent cells in tissues.

The increasing incidence of neurological disturbances and neurodegenerative diseases represents one of the major concerns in medicine today (Gorelick et al., 2017; Zheng and Chen, 2022). However, research progress in these pathologies lags behind that of other peripheral issues due to the numerous unanswered questions surrounding brain ageing and the complexity of its study. Animal behavioural assessment is a valuable tool for studying neurological disorders that affect emotion, memory, and/or cognition, as it provides insight into the ageing process within the brain (Revest et al., 2009; Costa et al., 2015; Anacker and Hen, 2017). In naturally ageing C57BL/6 mice, age-dependent alterations are not noticeable until around 10 months of age, but brain dysfunction-associated behavioural changes are not typically observed until the mice reach more than 12 months old (Yanai and Endo, 2021). Consequently, identifying brain-related deficits in naturally ageing mouse models requires not only a large cohort of animals to overcome inter-individual variability, but also a long period of time for the mice to age. In this context, mouse strains that experience accelerated ageing may facilitate longitudinal studies and represent the best alternative, in terms of time and cost, in gerontological research.

The senescence-accelerated mouse (SAM) strains are considered one of the most interesting pro-ageing animal models. They were developed from the AKR/J strain through inbreeding and selection for manifestation of different signs of early ageing, leading to the separate breeding of mice that were genetically prone to accelerated senescence (SAMP) and those that were, comparatively, resistant (SAMR). SAMP mice exhibited a general decrease in activity, hair loss, periophthalmic lesions, weight loss and reduced lifespan, among others, which were also inherited by subsequent generations (Takeda et al., 1981; Hosokawa et al., 1984). From these progenitors, and with more than 20 generations of inbreeding, several series of SAMP and SAMR animals were obtained and have been established as pure strains with a consistent expression of phenotypes that vary among the different series (Takeda et al., 1981; Takeda, 1999; Takeda, 2009). Thus, while other SAMP strains develop severe early osteoporosis (as SAMP6), SAMP8 has become one of the most recognized mouse strains in gerontology for its characteristic learning and memory deficits from an early age (Ito, 2013; Chen et al., 2009; Takeda, 2009; Akiguchi et al., 2017; Fernández et al., 2021).

SAMP8 mice show age-related symptoms and loss of function several months earlier than normal ageing or SAMR1 mice (commonly used in comparative studies with the SAMP8 strain) (**Figure 2**)

(Yanai and Endo, 2016). SAMP8 animals have attracted special attention in neurodegenerative disease research because they closely mimic age-associated pathologies of the human brain, such as Alzheimer's disease (AD) (Butterfield and Poon, 2005; Morley et al., 2012; Fernández et al., 2021). Indeed, several pathomorphological alterations and blood-brain barrier (BBB) dysfunctions, affecting glia, neurons, and vessels, have been identified in the SAMP8 mouse brain. Specifically, neuropathological changes shared with the human brain include morphological alteration in thalamic and hippocampal neurons, astrogliosis in neurogenic areas and formation of amyloid plaques that form aggregates in various brain regions such as the hippocampus, cerebellum or cortex, among other anomalies (Pelegrí et al., 2007; Banks et al., 2007; Del Valle et al., 2009; Takeda, 2009).

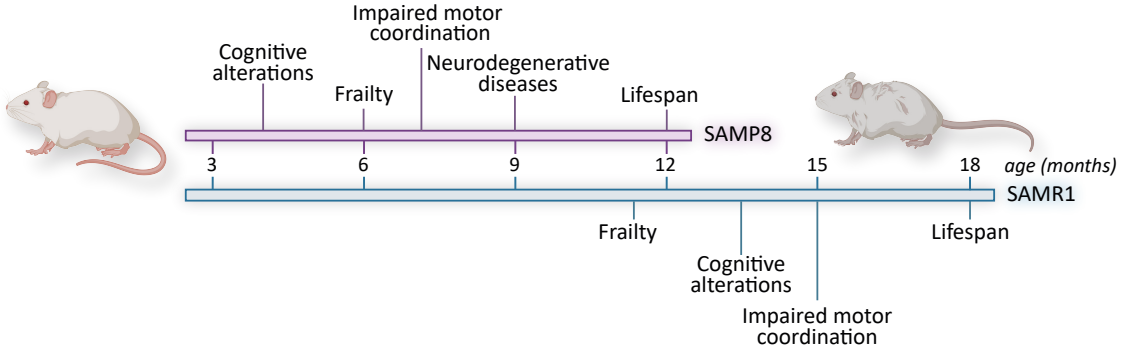

Figure 2. Timeline of the onset of age-related deficits in SAMP8 and SAMR1 mouse strains. SAMP8 mice, prone to accelerated ageing, experience early functional decline and have a shorter mean life expectancy than SAMR1 mice. The SAMP8 strain shows early signs of physical frailty, suffer from metabolic alterations and, relevantly, develop cognitive and memory deficits at early ages, making them a reference model for the study of neurodegenerative diseases. The age-related conditions shown in this figure include information from the literature and from our own study.

Notably, the SAMP8 brain is exposed to high levels of oxidative stress from an early age compared to the SAMR1 strain. Antioxidant enzyme activities decrease with age in SAMP8 animals compared to SAMR1 (Sureda et al., 2006; Bayram et al., 2013). In addition, impaired mitochondrial respiratory control has been described in SAMP8 mice with the consequent rise in ROS (Nishikawa et al., 1998). The reduction of the antioxidant system and the elevated ROS generate a pro-oxidant environment, which alters proper cellular function and contributes to ageing (Chandrasekaran et al., 2017). In fact, the use of antioxidants in SAMP8 has led to reduced levels of lipid peroxidation and protein carbonylation, and improved memory in SAMP8 mice (Butterfield et al., 1997; Okatani et al., 2002; Morley et al., 2012). This points to elevated oxidative status as a possible underlying cause of the learning and memory impairment of this strain (Kim and Choi, 2000; Morley et al., 2012). Moreover, increased oxidative stress could also contribute to astrogliosis and microgliosis in the brain of SAMP8 mice (Takeda, 2009), affecting BBB permeability with pathological consequences.

Some of these disorders are demonstrated in SAMP8 mice behaviour as early as 4 months old, with worse memory in the Novel Object Recognition (NOR) test, reduced freezing in the Cued Conditioning test and impaired spatial memory in the Morris Water Maze test (Yanai and Endo, 2016; Wang et al., 2014). However, first reports did not find remarkable differences at this level between SAMP8 and SAMR1 mice until 8-12 months of age (Miyamoto et al, 1986). Accordingly, the current literature is divided on the onset of age-related alterations in the SAMP8 strain (Butterfield and Poon, 2005; Yanai and Endo, 2016; Fernández et al., 2021). The early deterioration of these mice is a consequence of physiological senescence, whose incidence and severity increase with age. Therefore, using the SAM model to elucidate the mechanisms behind accelerated ageing can provide insights into the fundamental mechanisms of natural ageing. Despite the significant interest that the SAMP8 mice have generated in the gerontological field, most of the published research focuses on its cognitive disturbances and markers related to AD.

There are currently no comprehensive longitudinal studies linking the onset of health deficits to rising levels of cellular senescence during ageing, neither in animal models of accelerated ageing nor in natural ageing. This constraint is largely due to the limited non-invasive methods for measuring senescent cell levels *in vivo*. Importantly, this procedure would enable to identify target ages at which there is still room for improvement in health, which could be useful in devising therapeutic interventions to prevent or relieve age-related diseases.

3. Adult SCs and ageing: a brain case report

In recent years, it has been widely recognized that dysfunction of tissue-specific SCs may underlie the gradual age-related decline in tissue and organ performance. Self-renewing SCs reside in adult tissues and support the continuous production of specialised cell progeny, enabling physiological cell turnover and recovery after injury (Simons and Clevers, 2011). However, ageing negatively impacts SCs, compromising their maintenance and activity (Schultz and Sinclair, 2016; López-Otín et al., 2023). Unlike in other somatic cells, telomerase expression is sustained in tissue-specific SCs after birth. Nonetheless, these cells experience telomere shortening at advanced ages (Martinez and Blasco, 2017) and elevated levels of the cell cycle inhibitors p16 or p21 are also found in some SCs with ageing (Schultz and Sinclair, 2016; Herranz and Gil, 2018). Regardless of whether or not SCs undergo senescence with ageing, they can certainly sense the consequences of senescent cell accumulation (Childs et al., 2017). Given that SCs are at the top of the cell lineage hierarchy of mature cell production in many tissues, it is not surprising that they have become a major focus of current research aimed at improving their regenerative capacity in adult tissues.

The adult mammalian brain contains two distinct germinal regions harbouring neural SCs (NSCs) that sustain a steady production of new neurons destined for specific circuits: the subependymal zone (SEZ; also called the ventricular-subventricular zone, or V-SVZ) in the walls of the lateral ventricles (LVs) and the subgranular zone (SGZ) in the dentate gyrus (DG) of the hippocampal formation. In these microenvironments, or niches, NSCs find a unique set of signals and interactions conducive to their maintenance, self-renewal, and differentiation. The SEZ is by far the largest and most prolific neurogenic niche in mice, producing millions of neurons over the mouse lifespan as shown by cell lineage tracing experiments (Silva-Vargas et al., 2013; Obernier and Alvarez-Buylla, 2019). Subependymal NSCs give rise to new neurons intended to integrate into the olfactory bulb (OB) circuits, while those residing in the SGZ generate granule cells (GCs) for the DG itself (**Figure 3a**) (Ruddy and Morshead, 2018; Obernier and Alvarez-Buylla, 2019). Nevertheless, despite the persistence of NSCs, adult neurogenesis declines over time for reasons that are poorly understood (Ben-Abdallah et al., 2010; Lugert et al., 2010; Encinas et al., 2011; Conover and Shook, 2011; Shook et al., 2012; Kalamakis et al., 2019).

Much of our knowledge on adult NSCs comes from early definitions of their astrocytic nature and from the establishment of conditions to allow their growth in culture (Reynolds and Weiss, 1992; Ferrón et al., 2007). SEZ single-cell homogenates plated under non-adhesive conditions in a defined medium containing mitogens, epidermal growth factor (EGF) with or without basic fibroblast growth factor (bFGF), generate floating clonal aggregates known as neurospheres (Belenguer et al., 2016). Neurosphere-initiating cells are self-renewing, as evidenced by the generation of additional neurospheres after dissociation and reseeding, and multi-potent, as they can differentiate into neurons, astrocytes, and oligodendrocytes when exposed to appropriate stimuli (Ferrón et al., 2007; Belenguer et al., 2016). Although neurosphere assays have contributed considerably to our understanding of adult neurogenesis, the relationship between neurosphere-initiating cells and *in vivo* NSCs remained uncertain for many years (Reynolds and Rietze, 2005; Pastrana et al., 2011). A better definition of *in vivo* cell heterogeneity and potential was later achieved through the integration of structural studies with cell lineage tracing analyses and the prospective isolation of SEZ cells via fluorescence-activated cell sorting (FACS) (Beckervordersandforth et al., 2010; Mich et al., 2014; Codega et al., 2014; Belenguer et al., 2021).

In the SEZ, NSCs (also known as B1 cells) lie immediately underneath the ependymal cell monolayer that lines the LVs. Subependymal NSCs present a thin apical cytoplasmic process that intercalates between multi-ciliated ependymal cells ending in a primary cilium immersed in the cerebrospinal fluid (CSF) of the LVs. NSCs also exhibit a long basal cell process that extends into the tissue to contact the blood vessels that supply the SEZ (Tavazoie et al., 2008; Silva-Vargas et al., 2013; Obernier and Alvarez-Buylla, 2019). Therefore, B1 cells adopt a radial morphology that allows them to access factors secreted by the choroid plexus (CP) into the CSF and by the blood vessels, such as angiocrine factors produced by endothelial cells (ECs), which are known to influence NSC maintenance and neurogenic potential (Silva-Vargas et al., 2016; Rojas-Vázquez et al., 2021). In addition, these SCs interact through adhesive contacts and are responsive to other niche cells, including parenchymal astrocytes, ependymal cells, microglia and neurons, from which they also receive specific signals and factors (Morante-Redolat and Porlan, 2019; Obernier and Alvarez-Buylla, 2019; Porlan et al., 2013; Sirerol-Piquer et al., 2019). Comprehending the complex interplay between NSCs and their microenvironment is crucial for developing strategies to promote brain repair, as both extrinsic and intrinsic factors modulate NSC behavior and likely underlie the age-related decline in adult neurogenesis.

B1 NSCs descend from embryonic radial glial cells from which they inherit their elongated form and biochemical features typical of the astrocytic lineage, such as the expression of the glial fibrillary acidic protein (GFAP), glutamate-aspartate transporter (GLAST, also known as SLC1A3), or brain lipid binding protein (BLBP). Adult NSCs are specified during mid-embryonic development and most remain quiescent until adulthood (Fuentealba et al., 2015; Furutachi et al., 2015). When activated, 20% of NSC divisions are self-renewing, whereas 80% produce neural progenitor cells (NPCs, also known as C cells) that divide symmetrically 3-4 times before converting into neuroblasts (NBs) (Ponti et al., 2013; Obernier et al., 2018). Newly spawned NBs can cycle once or twice while migrating forward in groups to collectively form the rostral migratory stream (RMS) towards the OB. NBs can be categorised into two subpopulations, one proliferating and one post-mitotic, known as early NBs (ENBs) and late NBs (LNBs), respectively. Within the OB, LNBs migrate radially to localise in specific layers and differentiate into interneurons that integrate into existing circuits involved in odour discrimination (**Figure 3b**) (Katsimpardi and Lledo, 2018). Although neurons represent the predominant progeny, NSCs can also produce, albeit to a lesser extent, oligodendrocytes destined for the corpus callosum and striatal astrocytes (Menn et al., 2006; Silva-Vargas et al., 2013; Sohn et al., 2015).

Unravelling the complexities of NSC *in vivo* heterogeneity has been one of the major challenges in the neurogenic field. Indeed, for many years, it was not possible to specifically discriminate NSCs from niche astrocytes, let alone NSC populations with different activation dynamics. Subependymal NSCs have been classically regarded as primarily quiescent, as they could retain traceable nucleosides and survive antimitotic treatments (Doetsch et al., 1999; Maslov et al., 2004; Mich et al., 2014). Interestingly, cumulative nucleoside-based labelling indicated that a portion of these cells undergo rapid division, suggesting cyclic heterogeneity among NSCs (Ponti et al., 2013). This led to the design of strategies based on the use of fluorescent EGF for the live cell detection of the activation-related EGF receptor (EGFR) in order to distinguish quiescent and activated NSCs, and proliferative and non-proliferative progeny.

Labelling with antibodies against different surface antigens (GLAST, Prominin 1/CD133, Plexin B2, LeX) and/or expression of a GFAP reporter, together with fluorescent binding of EGF, has been used to separate by FACS $EGFR^{low/-}$ quiescent (qNSCs) and $EGFR^{+}$ activated (aNSCs) from the SEZ (Codega et al., 2014). These NSC subpopulations differ phenotypically and transcriptionally from each other (Codega et al., 2014; Dulken et al., 2017; Belenguer et al., 2021). For instance, aNSCs are characterised by the expression of genes involved in cell cycle and DNA repair, are metabolically dependent on oxidative phosphorylation and show increased proteasome activity and protein synthesis. On the other hand, the transcriptome of qNSCs is enriched in genes related to cell adhesion and communication, inflammatory response and extracellular matrix (ECM). Moreover, qNSCs metabolically rely on glycolysis, lipid metabolism and lysosomal function.

Regarding this information, it is evident that the behaviour of aNSCs and qNSCs, as well as the balance between quiescence and activation, must be tightly regulated (Llorens-Bobadilla et al., 2015; Chaker et al., 2016; Urbán et al., 2019; Belenguer et al., 2021).

New deep RNA sequencing techniques at the single-cell level of GLAST$^+$ cells revealed that there are NSCs whose molecular signature differs from quiescent and activated B1 cells, showing a shallow quiescent profile, meaning they are quiescent but prone to activation. Therefore, this work supported the existence of an ordered transition from a deeply quiescent "dormant" (qNSCs) state, through a "primed" for activation 'shallow' quiescent (pNSCs) state, to an active (aNSCs) state (Llorens-Bobadilla et al., 2015; Urbán et al., 2019). Importantly, this finding has led to the optimization of the isolation procedure in our laboratory, allowing to set up a novel method to selectively separate aNSCs, pNSCs and qNSCs using FACS. The prospective isolation of these three populations of NSCs has enabled us to verify that only aNSCs (with high levels of EGFR) and pNSCs (with very low levels of EGFR) are able to grow and generate neurospheres *in vitro*, whereas qNSCs cannot be cultured in commonly used neurosphere growth medium (Belenguer et al., 2021).

Despite the heterogeneous cellular composition of the SEZ, our group has pioneered the development of a FACS protocol that permits the identification and cell sorting of NSC populations and their progeny in a reproducible and standardised manner for functional studies. This procedure consists of two steps. In the first one, dead cells and non-neurogenic cells (e.g. TER-199$^+$ erythrocytes, CD45$^+$ microglia, O4$^+$ oligodendrocytes, neurons and ependymal cells) are excluded, while the second strategically differentiates each of the populations that constitute the neurogenic lineage. Regarding this second step, cells are classified into NSCs, astrocytes, NPCs or NBs, according to the expression of the glial marker GLAST, the activation-associated receptor EGFR and the neuroblast adhesion molecule CD24. Additionally, the CD9 tetraspanin is used to discriminate NSCs from niche astrocytes (Belenguer et al., 2021). This strategy represents a valuable breakthrough in the field of neurogenesis, providing insight into NSC biology and a better understanding of the underlying processes that regulate neurogenesis. Furthermore, it allows for the analysis of neurogenic function in different scenarios, such as specific diseases or during ageing.

Within the SGZ, radial quiescent glia-like cells (RGL or type 1 cells) are found in contact with blood vessels and represent the pinnacle of the neurogenic lineage in this region. Neurogenesis takes place when RGL cells give rise to intermediate proliferative progenitors (IPCs, also known as type 2 cells or D cells). These cells are more differentiated and divide to a lesser extent than NPCs in the SEZ, but can ultimately differentiate into neuroblasts (or intermediate GCs: IGCs). IGCs migrate very short distances to the overlying granule cell layer (GCL) of the DG, where they mature into GCs (**Figure 3c**) (Ruddy and Morshead, 2018). Mature GCs constitute the neuronal circuitry of the DG. Hippocampal NSCs also display molecular heterogeneity with dynamic expression profiles that delineate a progression from quiescence to neuronal maturation (Shin et al., 2015; Artegiani et al., 2017).

It is widely accepted that increasing age correlates with progressive depletion of neurogenic output of both the SGZ and SEZ niches (Luo et al., 2006; Ahlenius et al., 2009; Ben-Abdallah et al., 2010; Lugert et al., 2010; Encinas et al., 2011; Conover and Shook 2011; Shook et al., 2012). Conventional analyses had shown a decrease in the number of proliferative cells with ageing, suggesting that the low level of neurogenesis in the elderly was mainly due to a reduction in the overall number of NSCs (Maslov et al., 2004; Molofsky et al., 2006; Luo et al., 2006; Ahlenius et al., 2009). B1 cells remaining in the aged SEZ were considered primarily quiescent, as they appeared less prone to divide than NSCs in the young adult brain. However, cycling NSCs exhibited higher rates of cell cycle re-entry and transient expansion prior to lineage progression than their young counterparts (Stoll et al., 2011), suggesting potentially complex changes at the level of cycle dynamics and gene expression (Daynac et al., 2016; Ziebell et al., 2018; Shi et al., 2018). Recently, deep sequencing analyses of cardinal SC features over time have revealed an increased fraction of NSCs with a quiescence-related molecular profile in the elderly (Apostolopoulou et al., 2017; Ziebell et

al., 2018; Kalamakis et al., 2019). Kalamakis and colleagues have reported that old qNSCs become more resistant to activation at advanced ages. Remarkably, under certain external stimuli, such as exercise, NSCs have been shown to regain some of their neurogenic potential and can be reactivated showing similar levels of proliferation and differentiation as young NSCs (Lugert et al., 2010; Katsimpardi et al., 2014; Kalamakis et al., 2019). Together, the data suggest that NSCs are less likely to become activated in an aged environment and that cell-extrinsic factors may play a crucial role in the decline of neurogenesis with ageing. Therefore, exploring the extrinsic signalling involved in this phenomenon represents a valuable strategy for understanding age-related neurogenic impairment.

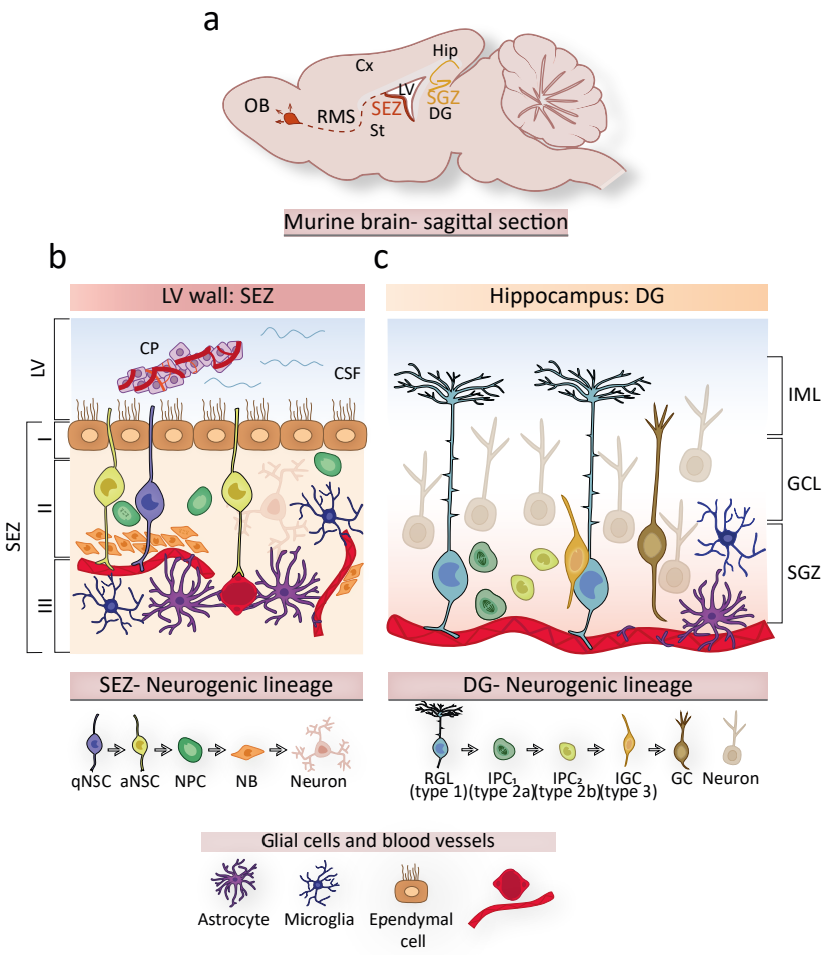

Figure 3. Depiction of adult brain neurogenic niches. a) Representation of murine brain-sagittal section and location of the main neurogenic niches, the SEZ and the SGZ. **b**) Illustration of the organisation of the adult SEZ neurogenic niche. NSCs contact the ependymal cell layer apically and blood vessels through a basal process. Due to their specific position, NSCs receive signals from the vascularised CP through their access to the CSF (domain I), from other cell components of the niche (domain II), and from the vascular plexus (domain III). The components of the SEZ niche are outlined below, providing an overview of the neurogenic lineage progression from qNSCs to aNSCs, NPCs, and NBs that migrate and generate new neurons in the OB. **c**) Illustration of the organisation of the hippocampal neurogenic niche. In the SGZ, NSCs or RGLs contact blood vessels and give rise to IPCs that progress into type 3 NBs or IGCs, to finally differentiate into GCs that are mainly located in the GCL and the inner molecular layer (IML). Mature GCs constitute the neuronal circuitry of the DG. Find below an overview of the RGL lineage (adapted from Rojas-Vázquez et al., 2021).

The intrinsic molecular mechanisms that regulate NSC activity and their role in the age-related loss of neurogenesis remain a major challenge to be uncovered. Decreased levels of specific growth factors and their signalling receptors have been observed in the SEZ with advancing age, while the expression of the cell cycle inhibitors p16 and $p19^{ARF}$ rises in proliferating cells, reducing cell growth with ageing. SC telomerase activity has been described to decrease with age, as well as its expression, which also contributes to the reduction of NSC proliferation and p53 activation (Ferrón et al., 2004; 2009). Although in the process of senescence p53 activation triggers an increase of p21 in many senescent cells (Herranz and Gil, 2018), NSCs already exhibit p53-independent high levels of p21 that are crucial for the preservation of their stem properties (Marqués-Torrejón et al., 2013; Porlan et al., 2013). Despite the progress in unveiling some aspects of NSC ageing, the mechanisms behind are still largely unknown.

With regards to accelerated senescence, most reports agree on a non-productive hyperproliferation of NSCs in both the SEZ and the SGZ of SAMP8 mice. Concerning the SEZ, NSCs are abnormally positioned

in SAMP8 mice resulting in an altered niche cytoarchitecture from early ages. These anomalies are accompanied by hyperproliferation of NSCs leading to premature depletion of the NSC pool at advanced ages. Primary cultures of NSCs from the SEZ of SAMP8 mice experience a rapid decrease in proliferation and heightened levels in senescence-related markers, including γH2AX heterochromatin foci denoting DNA damage, p53 and p19ARF cell cycle inhibitors, lysosomal β-Gal activity, and ROS production, in contrast to those obtained from SAMR1 mice (Soriano-Cantón et al., 2015). Importantly, oxidative stress is closely related to cellular senescence (Pole et al., 2016) and SAMP8 NSCs *in vitro* appear to be susceptible of a senescent fate. Considering the high level of oxidative stress described in aged and SAMP8 animals, they are likely to be sensitive to cell senescence consequences *in vivo* as well (Bayram et al., 2013; Soriano-Cantón et al., 2015).

4. The vascular niches and their transformation over time

NSCs occupy a strategic position within the SEZ that allows them to receive signals from CSF through receptors at the membrane of their primary cilium, and from ependymal cells through adhesive interactions (Lehtinen et al., 2013; Silva-Vargas et al., 2016; Morante-Redolat and Porlan, 2019). In the basal domain, away from the LV, NSCs are in close contact with blood vessels, accessing both local (vascular cell-derived) factors and distant (blood-borne) molecules that permeate the SEZ parenchyma (Tavazoie et al., 2008; Shen et al., 2008; Mirzadeh et al., 2008; Rafii et al., 2016; Smith et al., 2018). Although NSCs in the SGZ are located deeper in the brain parenchyma and do not have direct access to the CSF, they possess a single radial process that extends through the GCL and interacts tightly with the blood vessels located underneath the DG (Palmer et al., 2000; Vicidomini et al., 2020).

The vascular network that supplies the entire central nervous system (CNS) constitutes the BBB, a highly specialised structure that plays an essential role in maintaining brain homeostasis. Unlike other organs, brain ECs (BECs) are strongly sealed by tight junctions on the luminal face of brain vessels, devoid of fenestrations, and display restricted transcellular transport. Moreover, BECs are surrounded by mural cells with contractile properties, such as pericytes in capillaries, vascular smooth muscle cells in large vessels, as well as by astrocytic end-feet that are involved in vascular-to-neuronal communication (Obermeier et al., 2013). A basement membrane rich in different ECM components envelopes the cellular variety that builds the BBB (**Figure 4a**) (Morante-Redolat and Porlan, 2019). This particular multicellular assembly provides an interface between the blood (peripheral compartment) and the neural parenchyma, strictly regulating the transfer of blood-borne molecules and immune cells to the brain (Obermeier et al., 2013).

In contrast to the tortuous morphology of blood vessels in non-neurogenic regions, the vasculature of neurogenic niches exhibits singular features and architecture. An extensive planar vascular plexus flows parallel to the SEZ, and stem and progenitor cells lie adjacent. Subependymal NSCs and NPCs directly contact blood vessels at specific sites that lack astrocytic end-feet and pericyte coverage (Shen et al., 2008; Tavazoie et al., 2008). Notably, the specialised BBB makes the SEZ a more permeable region to systemic signals from the blood, which will be accessible to NSCs (Tavazoie et al., 2008). On the other hand, the DG vascular plexus also differs structurally and functionally from the rest of the hippocampus and its singular pattern appears to be influenced by proliferative progenitor cells. IPCs are located close to microvessels, and have been described as a potential regulator of neurogenesis-angiogenesis cross-talk (Kempermann et al., 2015; Pombero et al., 2018). Furthermore, the activity of pre-existing DG neurons increases blood flow and permeability to growth factors, enhancing the survival of newly born neurons (Shen et al., 2019).

In this context, neurogenic niches are considered functional units between neural precursor cells and their environment, in which blood vessels play an active role (Ehret et al., 2015; Apple and Kokovay, 2017). The vascular niche provides a rich source of regulatory signals to the neurogenic regions, including locally secreted and systemically released factors, as well as cell-cell and cell-ECM interactions (**Figure 4b**) (Ottone

et al., 2014; Morante-Redolat and Porlan, 2019; Rojas-Vázquez et al., 2021). BECs secrete angiocrine factors that have been shown to play a substantial role in the homing, self-renewal and differentiation of NSCs and their neurogenic lineage (Rafii et al., 2016; Karakatsani et al., 2019). These diffusible signals have attracted research attention for years, as they constitute one of the main pathways for intercellular communication at this level. Among them, pigmented epithelial-derived factor (PEDF) was the first endothelial-derived soluble factor described to be involved in the regulation of NSCs within the SEZ, leading to increased self-renewal by facilitating Notch signalling (Ramírez-Castillejo et al., 2006; Andreu-Agulló et al., 2009). Thereafter, placental growth factor 2 (PIGF-2), β-cellulin, VEGF (vascular endothelial growth factor) or the stromal-derived chemokine factor (SDF1) (Kokovay et al., 2010; Sun et al., 2010; Gomez-Gaviro et al., 2012; Crouch et al., 2015; Zhu et al., 2019) secreted by ECs have been reported to enhance NSC proliferation. In contrast, other soluble factors, such as neurotrophin-3 (NT-3), are reportedly involved in maintaining quiescence (Delgado et al., 2014). In this regard, angiocrine-mediated BEC-NSC communication signalling appears to play a very active role in regulating NSC behaviour and thus in the maintenance of adult neurogenesis. Cell adhesion-mediated signalling between NSCs and vessels has been less explored. Nevertheless, some studies have revealed that binding of NSCs to ECM components of blood vessels, or physical contact with vascular cells, promotes quiescence (Ottone and Parrinello, 2015).

With increasing age, neurogenic niches undergo structural and functional remodelling. Ageing drives LV stenosis and results in a marked increase in the number of astrocytes interposed in the ependymal layer, while the quantity of ependymal cells progressively decreases (Luo et al., 2008; Capilla-Gonzalez et al., 2014). In addition, the remaining ependymal cells show altered morphology and protein expression, and exhibit numerous lipid droplets, which reflect metabolic changes that have been associated with an elevated secretion of pro-inflammatory cytokines (Capilla-Gonzalez et al., 2014; Ogrodnik et al., 2019). Different niche elements change with physiological ageing; for instance, astrocytes and microglia show functional decline with age and even manifest a senescent profile in response to different stressors both *in vitro* and *in vivo* (Conover and Shook, 2011; Capilla-Gonzalez et al., 2014; Cohen and Torres, 2019; Ogrodnik et al., 2021). However, one of the components most significantly affected by ageing is the vasculature. Blood vessel disorders include endothelial and pericyte degeneration, increased BBB permeability and impaired transport, as well as ECM remodelling. Consequently, barrier integrity appears to be compromised in the elderly, leading to abnormal transfer of blood-borne proteins and impaired blood flow regulation (**Figure 4c**) (Obermeier et al., 2013; Segarra et al., 2021). Importantly, the described changes not only alter signalling interactions between vascular elements and NSCs, but also the supply of nutrients and oxygen to the brain parenchyma, and expose neurogenic niches to circulating pro-ageing factors. All of this contributes to a relentless cycle of deterioration resulting in chronic diseases at the brain level (Apple and Kokovay, 2017; Silva-Vargas et al., 2013; Smith et al., 2018), but further research will be needed to understand the origin and development of this series of detrimental events in the vascular niches.

Remarkably, studies using heterochronic parabiosis or transient blood exchange have identified systemic circulating factors in the blood that may influence adult neurogenesis. Several pro-ageing molecules have been noticed to rise in the bloodstream with age and negatively impact adult neurogenesis, such as β2-microglobulin (B2M), transforming growth factor beta 1 (TGFβ1), chemokine (C-C motif) ligand 11 and 2 (CCL11 and CCL2), interleukin 6 (IL-6) and tumour necrosis factor α (TNF-α) (Villeda et al. 2011; Smith et al. 2015; Rebo et al. 2016; Smith et al, 2018; Tominaga and Suzuki, 2019). These blood-borne factors are all linked to cellular senescence. While B2M can be found on the membrane surface of senescent cells in response to p53, the others have been described as components of the SASP. Although reported as anti-neurogenic factors, increased levels of these circulating molecules have been related to disruption of endothelial tight junctions, vascular hypertrophy and dysfunction, and impaired BBB integrity, which in turn affects adult neurogenesis (Rebo et al., 2016; Rea et al., 2018). The age-related rise in the senescent cell burden, in combination with these pro-ageing blood-borne factors, can ultimately promote inflammation and oxidative stress in the brain leading to serious pathologies (Tominaga and Suzuki, 2019).

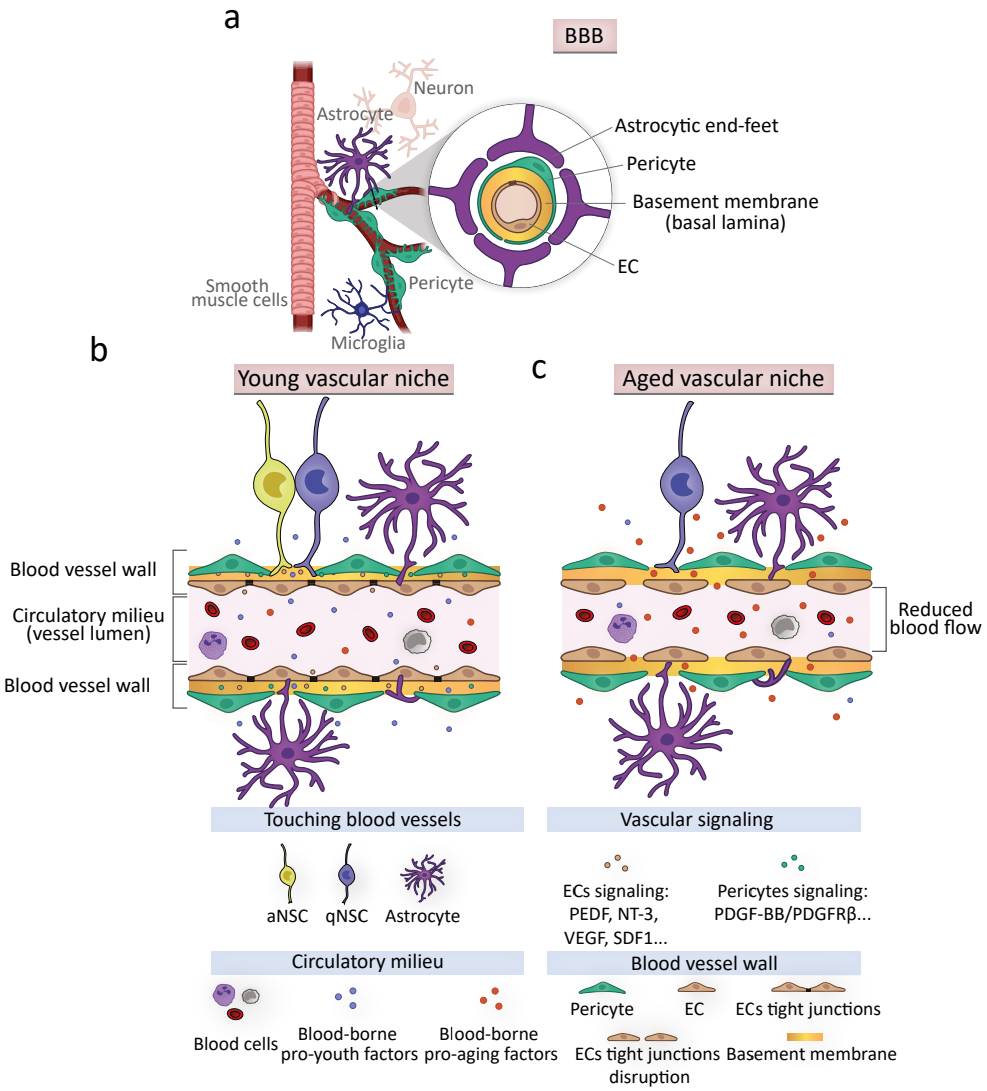

Figure 4. Overview of age-related alterations in the SEZ vascular niche. a) Depiction of the BBB main components. **b**) Representation of the SEZ vascular niche at the cellular level in a young mouse. NSCs contact blood vessels at specific sites where astrocytic endfeet and pericytes are absent, and receive signals from ECs and other vascular components, as well as blood-borne factors. Notably, ECs exert an important control on signals and molecules that reach the parenchyma through their tight junctions, and also play an active role in regulating NSC behaviour. **c**) Depiction of age-related alterations in the SEZ vascular niche. Note that as the tight junctions of ECs are lost, circulating pro-ageing and anti-neurogenic factors reach the brain parenchyma. In addition, vascular cells begin to secrete pro-inflammatory and pro-oxidant factors, which negatively impact the neurogenic potential of NSCs. Blood flow is reduced and blood pressure increased, thus limiting the nutrient supply (adapted from Rojas-Vázquez et al., 2021).

On the other hand, certain factors detected in young blood are reportedly reduced in blood at older ages, such as growth differentiation factor 11 (GDF11). GDF11 has been shown to exert pro-youth effects on neurogenesis within the SEZ, accompanied by vessel remodelling, improved blood flow and enhanced angiogenesis (Katsimpardi et al., 2014). These results suggest that young blood may have indirect beneficial effects on aged neurogenesis through the restoration of vascular architecture. Similarly, pro-ageing circulating factors could exert their anti-neurogenic effect through disruption of the BBB and alteration of local communication pathways between neurogenic and vascular cells. However, the potential mechanisms responsible for these effects remain largely unexplored.

5. Brain endothelial senescence: a potential bridge between ageing and neurogenesis decline

Senescent cells accumulate in tissues with age and, through their SASP, contribute to chronic inflammation and lead to profound tissue damage (Hernández-Segura et al., 2017; Herranz and Gil, 2018). This cell fate could be involved in age-related brain deterioration that occurs when SCs fail to fulfil their neurogenic function. However, the role of senescence at this level has not been studied in depth, not only because of the limited tools for reliable detection of these cells in the brain, but also because of the countless mechanisms by which senescent cells can potentially impair the activity of NSCs and their progeny at advanced ages. As previously discussed, the relationship of NSCs and NPCs with the vasculature constitutes a regulatory core with a rich source of reciprocal signalling between neurogenic and vascular cells, essential for sustaining adult neurogenesis (Crouch et al., 2015; Karakatsani et al., 2019). Central to this interaction are ECs that actively regulate NSC behaviour by maintaining a balance between quiescence and activation in neurogenic niches, which is largely mediated by EC-derived angiocrine factors (Rojas-Vázquez et al., 2021). Therefore, the accumulation of ECs with a senescent profile could account for the age-related loss of neurogenesis, as senescence may impair the regulatory function of ECs on NSCs. Senescent cell-secreted factors play an important role in intercellular communication leading to non-autonomous changes in the recipient cells. In this respect, BEC senescence could alter not only the signalling pathways involved in modulating NSC activity, but also their intrinsic regulation (Fabian-Labora and O'Loghlen, 2020; Rojas-Vázquez et al., 2021). Different types of glial cells and neurons have been shown to exhibit senescent traits in the aged rodent brain that contribute to neurodegeneration, but functional studies on age-related BEC senescence are yet to be conducted (Jurk et al., 2012; Bussian et al., 2018; Ogrodnik et al., 2019; Zhang et al., 2019).

Although the X-gal histochemical reaction has been commonly used to identify senescent cells (Debacq-Chainiaux et al., 2009), a systematic description of whether X-gal staining can be used to reliably monitor BEC senescence *in vivo* is still lacking, with few examples reported (Minamino et al., 2002). Nevertheless, ECs begin to exhibit a variety of phenotypic changes with increasing age, including greater morphological complexity, decreased proliferation, increased secretory activity, signs of DNA damage, as well as elevated levels of CKI proteins (p53-p21 and p16) (Zhan et al., 2010; Bhayadia et al., 2016; Jia et al., 2019; Grosse et al., 2020; Mühleder et al., 2021). The age-related increase in ECs with these attributes correlates with severe vascular dysfunction, also in humans (Katsuumi et al., 2018).

The transcriptomes of BECs from aged mice differ from those of young ones (Kalamakis et al., 2019; Kiss et al. 2020). Interestingly, many of the genes up-regulated in older BECs are strongly associated with a senescent molecular profile, including biological programs of response to cell damage, release of pro-inflammatory factors and generation of reactive oxygen species (ROS), among others (**Figure 5**) (Zhang et al., 2019; Kalamakis et al., 2019; Kiss et al., 2020). In particular, bulk RNA-sequencing analysis of NSCs, microglia and ECs obtained from the SEZ of 2- and 19-month-old mice revealed that ECs exhibit the most drastic changes in transcripts related to inflammatory cytokines that promote NSC quiescence in the elderly (Kalamakis et al., 2019). Moreover, senescence-induced ECs *in vitro* have been shown to secrete a greater number of extracellular vesicles that may collaborate with soluble factors to induce paracrine senescence in healthy cells (Riquelme et al., 2020). Importantly, an altered secretory phenotype in BECs involves impaired signalling in vascular niches (Apple and Kokovay, 2017).

From a metabolic point of view, p53 activation triggered by DNA damage in senescent ECs alters glucose homeostasis and reduces nitric oxide synthase (eNOS) activity, leading to decreased expression of proliferator-activated receptor-gamma coactivator-1a (PGC-1a), with subsequent impairment of mitochondrial biogenesis (Yokoyama et al., 2014). Senescence-associated mitochondrial degradation (Chapman et al., 2019) significantly affects ECs, as these cells rely heavily on mitochondria to support

normal function of ATP-dependent transporters for the regulation of vascular exchange. Their energy shifts towards a more glycolytic profile, presumably to sustain the high metabolic demands of the SASP (Sabbatinelli et al., 2019). In addition, decreased eNOS activity, and consequent reduced levels of the vasodilation regulator NO (Matsushita et al., 2001; Van Der Loo et al., 2000), could lead to hypoperfusion of brain cells, decreasing the bioavailability of nutrients and oxygen at this level (Graves and Baker, 2020). In this regard, ageing also entails a decrease in GLUT1 expression in BECs, resulting in a reduction in glucose transport across the BBB, thus interfering with the metabolism of surrounding cells (Lee et al., 2018).

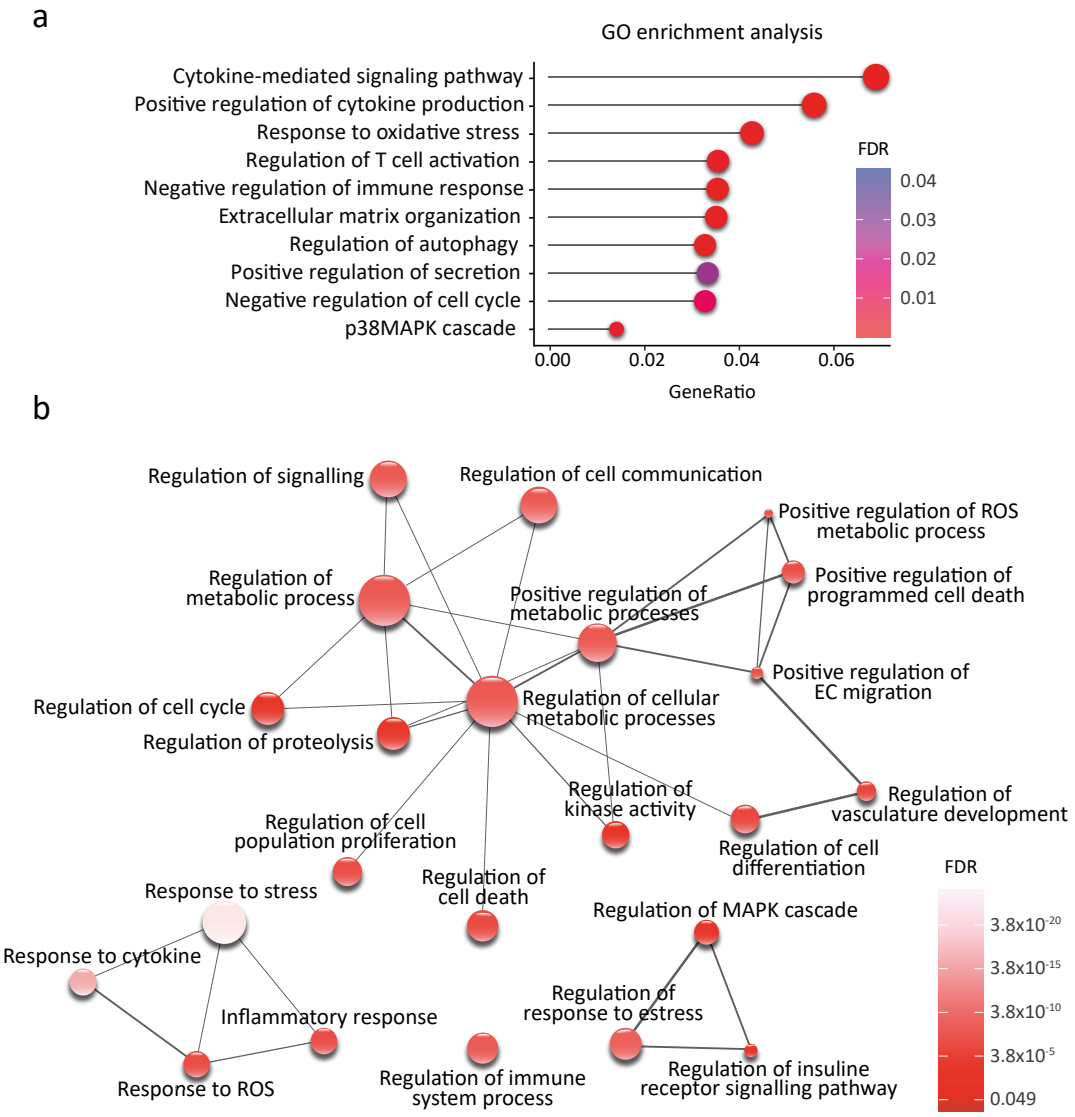

Figure 5. Functional analysis of comparative transcriptomic results of BECs from 2- versus 22-month old C57BL/6 mice. a) Representative Gene ontology (GO, Biological Process) terms enriched in upregulated BECs from 22 compared to 2-month-old mice. The length of the bars indicates the proportion of genes from the input list annotated to that GO term. The size of bubbles reflects the log2 number of genes annotated to the term, and the colour of the bubbles indicate the GO p-values adjusted by multiple testing by the False Discovery Rate (FDR) method. **b**) GO term similarity network of representative terms enriched in BECs from 22 compared to 2-month-old mice. Bubble colours indicate the FDR of the GO term, and their sizes indicate the log number of genes annotated to that GO term. Highly similar GOs are linked by edges in the graph, where the line width indicates the degree of similarity between them. All data represented was obtained from the bulk RNA-sequencing analysis published by Kalamakis and colleagues in 2019. Note that there are several GOs related to metabolic activities, regulation of cell proliferation, cell death and immune response that fit a senescent cell profile .

Considering the close proximity of BECs and NSCs, the metabolic rewiring associated with cell senescence could have a detrimental impact on tissue renewal. The biochemical changes prompted by EC senescence could affect the metabolic transition from glycolysis to oxidative phosphorylation that occurs when NSCs become activated (Llorens-Bobadilla et al., 2015), acting as a contributing factor to the increased propensity of NSCs to remain quiescent with age. Furthermore, EC senescence induces global metabolic disturbances through actions on white adipose tissue, leading to elevated insulin resistance in the organism as part of the metabolic syndrome (Barinda et al., 2020). The acquisition of a senescent phenotype is, therefore, accompanied by a reduction in insulin receptor substrate (IRS) expression and insulin resistance. This systemic effect could be detrimental to the maintenance of NSCs, as the insulin signalling pathway is critical for their proliferation (Chirivella et al., 2017). The resulting elevated glucose levels in the circulation also down-regulate eNOS and telomerase expression (Hayashi et al., 2006), promoting the spread of senescence.

Mitochondrial deficiency in ECs causes high levels of ROS, which act as a spreader of senescence in a paracrine manner. ROS cause DNA damage (Srinivas et al., 2019) and also act as NO scavengers, producing peroxynitrite, which inhibits mitochondrial superoxide dismutase (SOD2), thereby increasing $O_2^{\cdot-}$ (Van Der Loo et al., 2000). Excess $O_2^{\cdot-}$ can damage mitochondrial complexes generating a positive loop for enhanced mitochondrial ROS generation (Maranzana et al., 2013). Additionally, deficits in SOD1 (cytosolic) or SOD2 have been associated with a senescent phenotype (Treiber et al., 2012; Zhang et al., 2017), as well as the increased NADPH oxidase (NOX) activity (particularly NOX1), both contributing to elevate ROS levels (Salazar, 2018). The increased oxidative stress during ageing is also partly related to pericyte alterations. These cells upregulate the expression of inducible NOS (iNOS), producing a rise in NO that can result in higher levels of peroxynitrite when reacting with $O_2^{\cdot-}$ anions (Van Der Loo et al., 2000). Nonetheless, the role of ROS in senescence is not clear-cut, as it functions both as a consequence and as a causal factor.

Overall, EC senescence appears to be a relevant contributing factor to the impaired neurogenic activity in aged niches, as its altered metabolism can promote pro-oxidant and pro-inflammatory stimuli creating a dysfunctional vascular profile (Regina et al., 2016; Katsuumi et al., 2018). Assessing the role of senescent BECs in the age-related decline of neurogenesis is challenging because the burden of senescence increases in nearly all tissues. In this sense, there is a pressing need for strategies that can specifically discern the impact of brain endothelial senescence on neurogenic niches. The information presented herein renders BECs senescence a highly promising subject of investigation, not only for comprehending the intricacies of brain ageing, but also for revealing novel therapeutic avenues with the potential to augment the longevity of brain health.

6. Senolysis: a road to rejuvenation?

The impaired phagocytic immune response and the selective activation of anti-apoptotic pathways by senescent cells are likely to contribute significantly to the increased senescent cell burden observed with age (Nelson et al., 2012; Ovadya et al., 2018). Due to the undeniable role of cellular senescence in the spread of ageing and its pathological consequences, targeting senescent cells and the pathways involved in their maintenance has become a major focus of research (Zhang et al., 2022). Consequently, senolytic and senomorphic strategies have gained great scientific interest in recent years. The first approach consists of selectively eliminating senescent cells, while the second targets senescence-inducing pathways and factors involved in SASP to prevent paracrine senescence and reduce the deleterious effects of inflammation and oxidative stress on tissues (Zhu et al., 2015; Zhang et al., 2022; Zhu and Lerman, 2022).

Since the accumulation of senescent cells with ageing at the systemic level affects tissues through multiple mechanisms and leads to numerous diseases (Van Deursen, 2014), the clearance of these cells has become one of the most compelling therapeutic approaches against many age-related disorders, such

as cancer (Short et al., 2019). For example, targeting transcription factor cascades involved in inducing senescence, such as those driven by p16 or p21, can exacerbate tumour development, while eliminating senescent cells can prevent tumour growth and delay multiple forms of cancer in aged mice (Kirkland and Tchkonia, 2020; Schmitt et al., 2022). In this regard, pharmacological interventions with senolytic drugs are gaining ground over other strategies. The most promising senolytic drugs facilitate the selective elimination of these cells through inhibition of their pro-survival mechanisms known as senescent cell anti-apoptotic pathway (SCAP) networks (Robbins et al., 2021). These drugs were selected after a comprehensive screening of proteomic and transcriptomic databases in order to find the SCAPS most highly expressed by senescent cells. Through bioinformatics approaches, potential senolytic drugs were selected, with special interest in compounds already marketed and naturally occurring that target SCAP nodes, to facilitate translation to clinical application (Kirkland and Tchkonia, 2020; Chaib et al., 2022). Given that senescent cells share some features with cancer cells, such as resistance to apoptosis, many anticancer agents have been tested as senolytics.

The SCAP network may vary between senescent cells; thus, senolytic drugs that target a specific SCAP only remove a subset of these cells (Kirkland and Tchkonia, 2020). In fact, senolytic compounds that act on multiple SCAP networks show greater specificity for senescent cells and reduced off-target effects than those that act on a limited range of SCAP-related molecules. For instance, Navitoclax (ABT-263) inhibits the anti-apoptotic proteins BCL-2, BCL-W and BCL-XL, which are upregulated in some senescent cells (Zhu et al., 2016). Its oral administration in aged mice has been shown to promote clearance of senescent SCs in bone marrow and muscle, leading to rejuvenation of these tissues. However, the use of Navitoclax is limited due to its significant apoptotic effects on non-senescent cell types, such as platelets and immune cells, and its side effect of thrombocytopenia (Chang et al., 2016). Other senolytic compounds have been shown to reduce senescence burden *in vivo* with minimun effect on non-senescent cells. Among these, one of the most widely used strategies is the combination of the senolytic drugs dasatinib (D) and quercetin (Q). D inhibits tyrosine kinases related to anti-apoptotic pathways and has been approved for clinical use in the US (since 2006) in cancer treatments. Q is a natural flavonoid that targets members of the BCL-2 family, HIF-1α and specific PI3-kinase and p21 nodes involved in SCAP, resulting in the elimination of senescent cells, especially, senescent ECs (**Figure 6**) (Zhu et al., 2015; Hickson et al., 2019; Dagher et al., 2021).

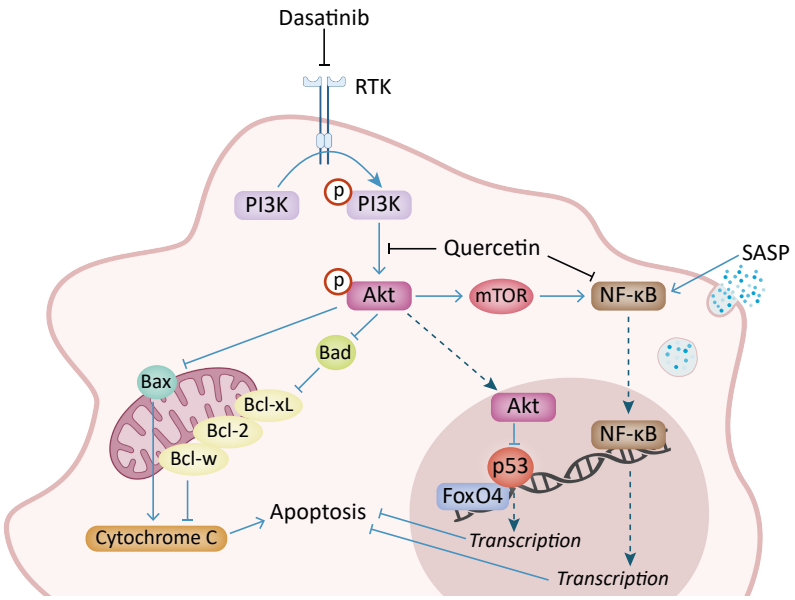

Figure 6. Potential intracellular targets of D and Q senolytic drugs. The drug D works by suppressing the PI3K/Akt (phosphatidylinositol 3-kinase/protein kinase B) pathway via receptor tyrosine kinase (RTK). On the other hand, Q inhibits Akt phosphorylation and then induces apoptosis of senescent cells and blocks the SASP secretome via FoxO4 and mTOR, respectively. Additionally, Q exerts senolytic effects through the inhibition of the NF-κB (nuclear factor-κB) pathway (adapted from Wu et al., 2022).

Mixed use of D+Q orally has been reported to decrease senescence load with beneficial effects on tissue renewal and health span in mice (Xu et al., 2018; Ogrodnik et al., 2019; Ogrodnik et al., 2021). For example, intermittent administration of these drugs has been demonstrated to increase insulin sensitivity in obese mice, alleviate renal fibrosis and idiopathic pulmonary fibrosis, improve bone strength, and enhance endurance and physical performance, among other beneficial outcomes. Furthermore, clinical trials with D+Q are currently being conducted to effectively eliminate senescent cells in humans with certain pathologies (Hickson et al., 2019). Interestingly, these drugs are able to cross the BBB and have been reported to reduce senescent oligodendrocyte progenitors by decreasing Aβ plaque inflammation and improving cognitive function in mouse models of AD (Zhang et al., 2019), as well as to eliminate senescent periventricular cells in the SEZ of obese mice, improving neurogenesis (Ogrodnik et al., 2019). Importantly, the D+Q strategy exerts beneficial effects also at the vascular level in aged mice, enhancing carotid artery relaxation, leading to improved vasomotor function (Roos et al., 2016). These results suggest that senolytic drugs may have the potential to reverse age-related changes in the brain, such as vascular remodelling and impaired adult neurogenesis.

Although the underlying mechanisms involved in the loss of NSC neurogenic activity with age have not yet been clarified, cell senescence has arisen as an important source of deleterious effects and chronic inflammation in the brain (Apple and Kokovay, 2017). The inhibition of pro-ageing or senescence-associated factors could be a therapeutic option but, given their multifaceted origin and effects, targeting senescent cells themselves may offer more efficient and lasting results. Selective removal of senescent cells appears as a promising novel approach that could enhance neurogenesis and extend brain health. The pursuit of rejuvenating brain tissue by depleting senescent cells and stimulating neuronal regeneration has exciting potential, but still faces substantial challenges. The mechanisms behind ageing at the brain level are not yet fully understood, and the specific effects of senolytic drugs on neurogenic function require further investigation.

Objectives

Ageing encompasses the development of several diseases that have been associated with an increased burden of senescence, such as neurodegenerative ones (Martínez-Cué and Rueda, 2020). Indeed, neurogenesis has been reported to decrease over time in the two main neurogenic niches of the mammalian brain, the SEZ and the SGZ (Encinas et al., 2011; Conover and Shook, 2011). However, it is unclear how senescence contributes to this end. Intriguingly, a definitive longitudinal correlation between ageing and senescence has yet to be established, due to the lack of tools for reliable detection of senescent cells *in vivo*. In this regard, our group is developing new strategies to identify senescent cells both *in vivo* and *ex vivo* with the aim of better understanding the impact of senescence on ageing in different organs, including the brain.

NSCs are exposed to multiple signals that extrinsically regulate their behaviour. The vasculature, especially BECs, exert a significant influence on NSC neurogenic function through diverse mechanisms (Rojas-Vázquez et al., 2021). The intimate relationship between BECs and NSCs makes the brain endothelium an attractive target of study. These vascular cells undergo functional alterations with ageing that may promote the loss of neurogenesis in the elderly. However, whether BECs can experience a senescent fate, let alone whether this affects the neurogenic function of NSCs, has hardly been studied. In this context, our work is based on the hypothesis that ageing-associated senescence of BECs has deleterious effects on neurogenesis. To investigate this hypothesis, we have addressed two different primary objectives:

1. Development of novel strategies for longitudinally monitoring ageing-associated senescence *in vivo*.

2. Characterisation of ageing-associated brain endothelial senescence and its impact on adult neurogenesis.

Material and methods

1. Experimental animals

1.1. *Mice handling*

Mice were bred and housed at the animal housing facility of the Universitat de València (Servei Central de Suport a la Investigació Experimental – SCSIE, Burjassot). Housing established 12 h periods of light/darkness, room temperature of 20-22 °C, and free accessible diet of pellets and water, following European Union 2010/63/UE and Spanish RD-53/2013 guidelines and under official veterinary supervision. All experimental procedures were approved by the Universitat de València Ethics Committee for Research and Animal Welfare (CEBA) and conducted in accordance with the recommendations of the Federation of European Laboratory Animal Science Associations (FELASA).

1.2. *Mouse strains*

Experiments were performed on mouse models of natural and accelerated ageing at different ages. The SAMP8 mouse strain, prone to accelerated senescence, and the SAMR1 mouse strain, resistant to accelerated senescence (Takeda, 2009), were obtained from the Universitat de Barcelona and bred and maintained in the animal housing facility of the Universitat de València. C57BL/6 were obtained from The Jackson Laboratory (stock no. 000664) and aged in the same facility.

2. *In vitro* methods

2.1. *Cellular models of endothelial senescence*

Primary venous ECs from the human umbilical cord (hUVECs) were obtained from EndoGRO™ (Sigma-Aldrich), cultured using EndoGRO-LS medium specific for these cells (SCME001, Sigma-Aldrich) (**see Annex II, table 4**), and maintained at 37 °C and 5% CO_2. For experimental setups, cells were seeded in 60 mm cell culture plates with 56 cm^2 growth area (p100) at a density of 500,000 cells *per* plate for pharmacological senescence induction and 2.5-fold less for control (untreated) cells. To trigger a senescent fate, cells were treated with 1 µM palbociclib (PD-0332991 HCl, Selleckchem) for 7 days *in vitro* (DIV) (Estepa-Fernández et al., 2021). Palbociclib stock was prepared at 10 mM by dissolving the drug in sodium lactate and HCl to obtain a working solution of pH 4.0. This stock was aliquoted and stored at -20 ^oC for later experimental use. After the 7-day treatment period, the cells were washed twice with phosphate-buffered saline (PBS; 0.9% NaCl in 0.1M phosphate buffer, PB, pH 7.0) to remove residual palbociclib from the medium.

For hUVECs to enter replicative senescence, the cells were passaged 29 times *in vitro* and their senescence phenotype was studied in comparison to hUVECs at shorter passages (less than 10) (Jong et al., 2013; Ohori et al., 2021; Chala et al., 2021).

The immortalised bEnd.3 cell line consists of ECs isolated from brain tissue derived from BALB/c mice with endothelioma. These cells were obtained from ATCC (CRL-2299™), cultured with DMEM F12, 10% fetal bovine serum (FBS) and 1% antibiotic-antimycotic (see **Annex II, table 5**), and maintained at 37 °C and 5% CO_2 in a humidified incubator. BEnd.3 cells were seeded in a p100 culture dish at a density of 10,000 cells/cm^2 and exposed to a subcytotoxic oxidative stress with 300 µM H_2O_2 (hydrogen peroxide, PanReac AppliChem) diluted in DMEM-F12. Cells were first incubated with this stressor for 3 h to induce premature senescence and then washed with PBS to remove residual H_2O_2 from the medium. Finally, fresh medium was added and 24 h later the cells were ready for experimental use. Bend.3 cells exposed

to H_2O_2 (senescent) were used in parallel with bEnd.3 cells not exposed to this oxidative stress (controls) in experimental issues (Han et al., 2021).

HUVECs and bEnd.3 cells grow adherent to the plate surface. These cells were passaged when the culture reached approximately 80% confluence. After washing with 0.1 M PBS, the cells plated on a p100 were detached with 1 ml of 0.05% trypsin/0.02% EDTA solution within 1-3 min. Then, 5 ml of medium supplemented with protein serum is added to neutralise the enzymatic digestion. Finally, the cells were passaged at a ratio of 1:3 to 1:4 for an interval of 3-4 days in culture until the next passage. Importantly, all cells were tested negative for mycoplasma contamination by PCR using specific primers.

2.2. *Primary culture of BECs from SAMP8 and SAMR1 mouse brains*

SAMP8 (n=3) and SAMR1 (n=3) mice aged 4-months were euthanized by cervical dislocation and their brains were collected. After discarding the bulbs and cerebellum, the brains were minced and pooled for each SAM strain. Tissue samples were then enzymatically digested using the Neural Tissue Dissociation Kit (P) (Miltenyi, cat. no. 130-092-628) and following the instructions of the manufacturer, with the exception that P (papain) was diluted at a ratio of 1:10 to preserve the CD31 epitope. Tissue dissociation was carried out in a gentleMACS™ Octo Dissociator with heaters (Miltenyi). Next, 3 ml of ECs blocking buffer (**Annex II, table 8**) was added to neutralise the enzymatic digestion and tissue pieces were mechanically dissociated by pipetting up and down 25-30 times using a plastic Pasteur pipette. The cell suspension was filtered through a 70 µm nylon filter (pre-wetted with 1 ml of EC blocking buffer). Subsequently, the sample and filter were washed with an additional 5 ml of EC blocking buffer. Filtered cells were pelleted (300 x*g*, 10 min) and resuspended in 190 µl of ECs blocking buffer with 10 µl of CD31 magnetic beads (Miltenyi, cat. no. 130-097-418) and maintained at 4 °C in the dark for 15 min. 1 ml of EC blocking buffer was added to centrifuge the magnetically labelled cells (300 x*g*, 10 min) which were resuspended in another 1 ml of EC blocking buffer and passed through a MS column (Miltenyi, cat. no. 130-042-201) on an OctoMACS® magnetic separator (Miltenyi, cat. no. 130-042-109). In this case, as our samples were very rich in myelin, we separated them on two MS columns to optimise the isolation of magnetically labelled $CD31^+$ cells, i.e. BECs. The columns were washed 3 times with EC blocking buffer and all eluted fractions were collected together for each mouse strain. Finally, the cells were pelleted (300 x*g*, 5 min), resuspended in Endothelial Cell Growth Medium MV2 (Promocell, cat. no. C-22022) and seeded in a 48-well culture plate at a density of 40,000 cells/cm^2 as well as in a specific chamber for optical imaging (8-well Ibidi® chamber) (**Graphical method 1**). Within 5 days of seeding, the cell medium was replaced with fresh medium and the cells were maintained in culture at 37 °C and 5% CO_2 for 7 DIV before initiating senescence analysis (see Ouellette and Lacoste, 2021 for a comparable protocol).

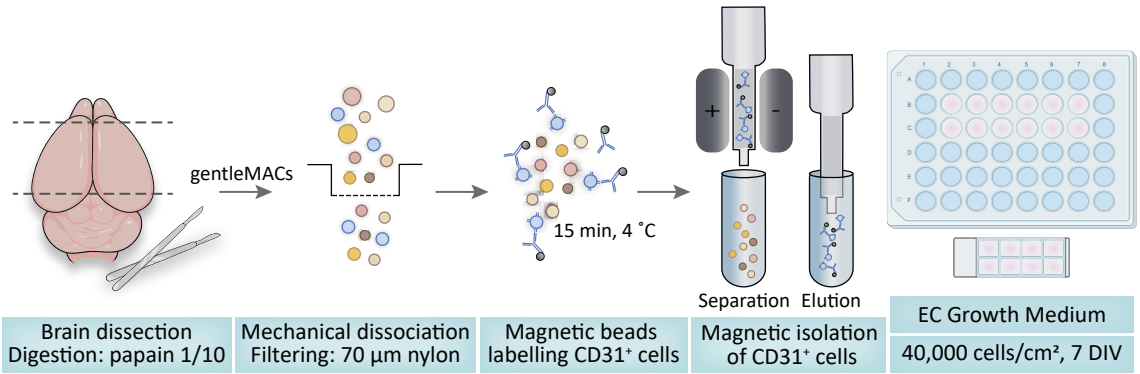

Graphical method 1. BECs primary culture procedure.

2.3. *EC senescence detection and characterization*

2.3.1. *Cytochemical detection of senescence-associated markers*

SA-β-Gal activity detection was performed using the Sigma-Aldrich kit for X-gal histochemical staining (cat. no. CS0030-1KT) and following the provided protocol for fixation and cytochemical reaction. Senescent and control hUVECs were seeded in a 48-well culture plate at a density of 25,000 cells/cm^2 and 12,500 cells/cm^2, respectively. After X-gal cytoenzymatic reaction, blue-labelled senescent cells were detected and photographed using a Nikon ECLIPSE TE2000-S inverted microscope coupled to a Nikon digital camera (DXM1200F).

We also analysed other senescence-associated markers by immunofluorescence. To do this, cells were seeded at the same density but on a round glass coverslip and fixed 24 h later with 2% paraformaldehyde (PFA) in PB for 15 min and then washed thoroughly with PB. Prior to antigen-specific detection with primary antibodies, potential non-specific sites were blocked by incubating the cells in blocking buffer (10% foetal bovine serum-FBS and 0.1% Triton™ X-100 in PBS) for 1 h at room temperature (RT). Cells were then incubated with primary antibodies to Ki67 (Abcam, cat. no. ab15580), p21 (Abcam, cat. no. Ab109520), Lamin B1 (Abcam, cat. no. Ab16048) and γH2AX (Millipore, cat. no. 05-636-I) (**Annex I, table 1**) overnight at 4 °C. After 3 washes in PBS at 5 min intervals, the cells were labelled with fluorescent secondary antibodies (Jackson ImmunoResearch/ Molecular probes) (**Annex I, table 2**) for 1 h at RT in the dark. Remnants of secondary antibodies not bound to primary antibodies were washed with PB and cell nuclei were stained with 4',6-diamidino-2-phenylindole (DAPI, 1 µg/ml in distilled water) for 4 min at RT in the dark. After thorough washing of the cells, the glass coverslips were mounted with FlourSave™ reagent (Calbiochem, cat. No. 345789) on a slide for image acquisition with an Olympus FV10i confocal laser microscope (60x objective). In the case of BECs isolated from SAMP8 and SAMR1 mice, the cells were photographed in the 48-well culture plate using an IN CELL analyser 2000 (40x objective).

2.3.2. *Quantification of immunofluorescence data and bioinformatics analysis*

As all mentioned antibodies recognise a nuclear epitope, quantitative analysis was performed by counting the number of nuclei positive for each senescence marker *per* DAPI labelled nucleus in all images obtained *per* sample. However, cells labelled with p21 and Lamin B1 are not as easy to identify as positive or negative, as the distinction lies mainly in the level of fluorescence intensity. For these two, we used Image J's Fiji software, where positive cells were identified using a bioimage analysis workflow. The quantification of these senescence markers was deployed as a Fiji macro (Schindelin et al., 2012) that was divided into three main steps: 1) segmentation of nuclei performed in the DAPI channel using the pre-trained StarDist Versatile (fluorescent nuclei) model (Schmidt et al., 2018) setting a score threshold of 0.5 and an overlap threshold of 0.4; 2) selection of segmented regions of interest (ROIs) per area to discard those with abnormal size, setting a selection range of 50-600 square microns; 3) single-cell quantification of the mean grey value (sum of the grey values of all pixels divided by the number of total pixels) by measuring the intensities of the selected ROIs in the channel(s) corresponding to the senescence marker.

2.3.3. *Flow cytometric evaluation of senescence-associated markers in the cell nucleus*

For *in vitro* endothelial senescence models of hUVECs under replicative senescence and bEnd.3 cells exposed to H_2O_2, senescence-associated markers were assessed by flow cytometry, including p16 or γH2AX. Prior to incubation with the primary antibodies, cells were fixed and permeabilized using the BD Pharmingen™ Transcription-Factor Buffer Set (cat. no. 562725) for 20 min at RT in order to detect (intra) nuclear senescent markers. Cells were then incubated with primary antibodies against p16 (Abcam, cat. no. ab211542) and γH2AX for 40 min at 4 °C, and subsequently with secondary antibodies labelled with Alexa

Fluor™ (Invitrogen-Molecular Probes) for 30 min at 4 °C. Finally, after pelleting the cells and resuspending them in 0.5 ml of FACS buffer (**Annex II, table 7**), senescent markers levels (median fluorescence intensity or MFI) were assessed on a LSR-Fortessa X-20 cytometer (Becton Dickinson) equipped with 355 nm, 405 nm, 488 nm, 561 nm and 640 nm lasers. Results were analysed with FlowJo_v10.8.1 software.

2.4. *New fluorogenic probes for SA-β-Gal detection*

2.4.1. *Generation of new molecular probes for senescent cell detection*

The chemistry laboratory of Prof. Ramón Martínez-Máñez is devoted to the generation of molecular probes for the detection of biologically relevant enzymatic activities, such as SA-β-Gal activity (**Graphical method 2**). The AHGa probe is based on a naphthalimide fluorophore containing an acetylated galactose attached to one of the aromatic nitrogen atoms of L-histidine via a hydrolysable N-glycosidic bond. AHGa has a molecular weight of 764 g/mol and is preferentially transformed into AH in senescent cells, resulting in an increased fluorescent emission (λ_{ex}=405 nm and λ_{em}=540 nm, in PBS- 0.01% DMSO). The NBGal probe has a molecular weight of 648.8 g/mol and consists of a Nile Blue (NB) fluorophore linked, via an N-glycosidic bond, to a galactosamine group but, in this case, the dye emits fluorescence in the far-red spectrum range (λ_{ex}=635 nm and λ_{em}=666 nm, in PBS- 0.01% DMSO). On the other hand, the WOS-Cy7Gal probe contains a cyanine-7 (Cy7) fluorophore as a signalling unit that binds to a galactose derivative via an O-glycosidic bond, hydrolysable by the β-Gal enzyme. The probe has a molar mass of 876 g/mol and the released Cy7 dye has maximum excitation and emission wavelengths in PBS of 580 nm and 660 nm, respectively.

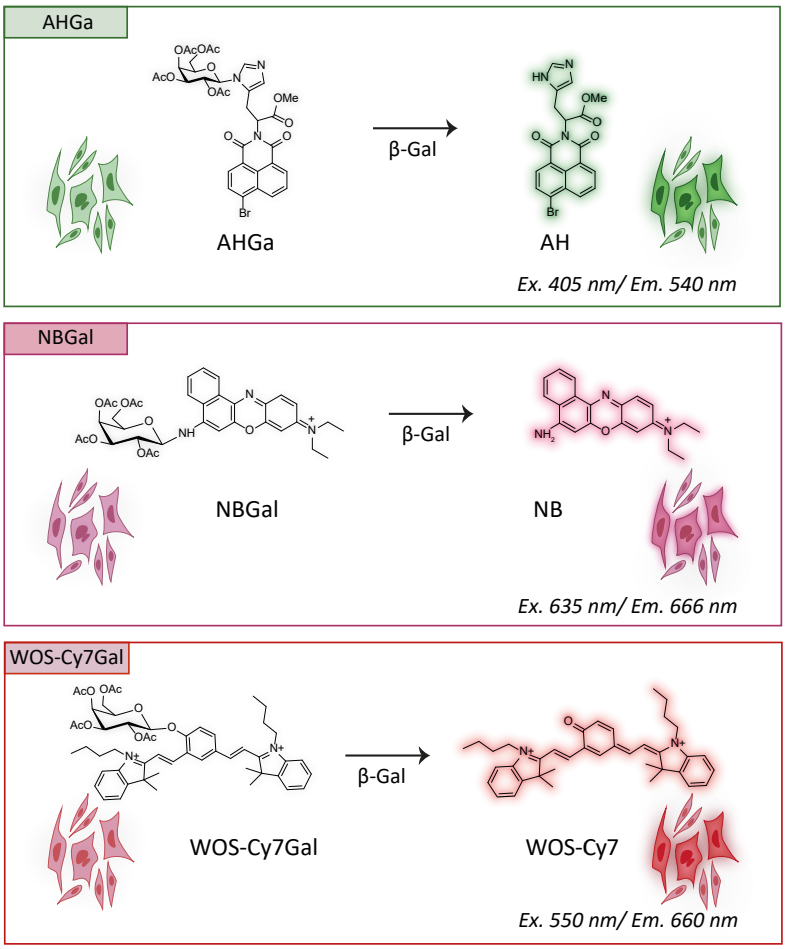

Graphical method 2. New fluorogenic probes for SA-β-Gal detection.

The probes were synthesised and chemically characterised by ^{1}H and ^{13}C-NMR spectra (Bruker FT-NMR Avance 400 spectrometer) at 300 K, using TMS as internal standard and by high resolution mass spectrometry (HRMS) (TRIPLETOF T5600 spectrometer). The specificity and selectivity of hydrolysis of the probes, at the chemistry level, was characterised as described in the published works by our group (Lozano-Torres et al., 2017; Lozano-Torres et al., 2023; Rojas-Vázquez et al., *submitted*). All probes were diluted in DMSO to a stock concentration of 20 mM, which can be stored in aliquots at -80°C maintaining its functional qualities for 3 months.

2.4.2. *Confocal microscopy imaging of β-Gal activity-based fluorogenic probes*

For all the molecular probes mentioned, the released fluorophore is retained in cell lysosomes emitting a fluorescence signal that can be measured by flow cytometry or confocal microscopy imaging. Accordingly, all of them were validated in our endothelial senescence model with hUVECs treated with the senescence-inducing drug palbociclib. For confocal images acquisition cells were seeded in an 8-well Ibidi® chamber at a density of 20,000 cell/cm^2 and 10,000 cell/cm^2 for senescent and control cells, respectively. Once adhered to the plate surface, cells were incubated with 10 µg/ml Hoechst 33342 (Invitrogen) in EndoGRO-hUVECs medium for 30 min for nuclear labelling, with the exception of the AHGa probe whose emission range coincides with that of Hoechst 33342. After careful washing of the cells, each molecular probe was added at a different concentration, for optimal fluorescence detection without toxicity, diluted in DMEM basal medium: 10 µM AHGa, 2 µM NBGal and 20 µM WOS-Cy7Gal (Lozano-Torres et al., 2017; 2023; Rojas-Vázquez et al., submitted). Images were obtained within the first hour of cells with the probe using a 60x objective of an Olympus FV10i confocal microscope fitted with 405 nm, 458 nm, 488 nm and 633 nm lasers.

To assess SA-β-Gal activity in primary cultures of SAMP8 and SAMR1 mouse BECs (seeded in 8-well Ibidi®), we used the AHGa probe. First, we incubated the cells for 20 min with 5 µM far-red fluorescent DNA dye Draq5™ (Abcam, cat. no. ab108410) to label cell nuclei. Subsequently, after washing the cells, AHGa was added under the same conditions described above. Images were obtained with an Olympus FV1000 microscope equipped with 405 nm, 488 nm, 515 nm, 559 nm, 595 nm y 635 nm lasers.

2.4.3. *Flow cytometry analysis of β-Gal activity-based fluorogenic probes*

All these molecular probes were also tested by flow cytometry using palbociclib-treated hUVECs. Senescent and control cells were detached from the culture plate (p100) using 1 ml of 0.05% trypsin/ 0.02% EDTA solution and, after a few minutes, collected with EndoGRO-medium and pelleted (300 x*g*, 5 min) in order to incubate cells with each probe at the appropriate concentration (WOS-Cy7Gal at 20 µM, AHGa at 10 µM, and NBGal at 2 µM) 15 min in FACS buffer (**Annex II, table 7**). Next, cells were centrifuged (300 x*g*, 5 min) and resuspended in 0.5 ml of FACS buffer ready for analysis. DAPI (0.1 µg/ml) was added prior to flow cytometry analysis to discard dead cells. For cells labelled with the AHGa probe, 1 µg/ml propidium iodide (Sigma, cat. no. P4864) replaced DAPI for dead cell exclusion. Cells were analysed in a BD-LSR-Fortessa and the probe-associated MFI was compared between control and senescent cells with FlowJo_v10.8.1 software.

2.5. ***Establishment, propagation, and proliferative analysis of neurosphere cultures***

Primary cultures of adult subependymal NSCs were obtained from 2- to 4-month-old C57BL/6 mice. Mice were euthanized by cervical dislocation and after peeling off the skull, the brain was extracted and placed on a silicone dissection pad with cold sterile Dulbecco's phosphate buffered saline (1X DPBS) (Biowest, cat. no. X0515). The rest of the samples remain with cold DPBS in independent wells of a culture plate placed on ice until dissection is complete. Briefly, the cerebellum and olfactory bulbs were discarded

to obtain a thick slice containing the lateral ventricles. Both hemispheres were then separated along the brain midline. The lateral ventricle of each hemisphere was exposed by separating the hippocampus, septum, and diencephalon from the cortex along the line of the corpus callosum. Next, each SEZ was trimmed by removing the surrounding tissue with the white matter tracts (corpus callosum and capsule/ terminal striatum) as reference lines. Finally, each SEZ block was cut to obtain a thin tissue slice of approximately 1 mm, separating the SEZ from the underlying striatal parenchyma (see Belenguer et al., 2016 for details).

Once the SEZ was isolated, it was minced and enzymatically digested with papain 12U (Worthington Biochemical Corporation, cat. no. LS003120) in an enzymatic solution for 30 min in a thermostatic bath at 37 °C. The solution included 0.2 mg/ml L-cysteine hydrochloride (Sigma, cat. no. C8277) and 0.2 mg/ml EDTA (Sigma, cat. no. E6511) in Earle's balanced salt solution (EBSS) (Gibco, cat. no. 24010-043). Tissue digestion was interrupted by adding 3 ml of washing medium (**Annex II, table 1**) and the SEZ pieces were centrifuged (100 x*g* for 3 min) and the supernatant removed. 1 ml of washing medium was added to mechanically dissociate the tissue by gently pipetting up and down several times until the cell suspension became homogeneous. Next, another 10 ml of washing medium was added to remove dead cells and debris (200 x*g*, 10 min). Finally, primary cells were resuspended in NSC complete medium (see **Annex II, table 3**) and 15,000 cells/cm^2 were plated in a 48-well culture plate at a final volume of 0.5 ml *per* well and incubated for 7-10 days at 37 °C and 5% CO_2 in a humidified incubator (**Graphical method 3**). During this period, differentiated cells die while NSCs and some progenitors begin to proliferate and form floating neurospheres (Belenguer et al., 2016).

Primary neurospheres from the SEZ can be expanded by seeding individual cells under the same conditions. All experiments were performed before passage 9 since, although NSCs retain their self-renewal capacity, we have previously observed signs of cellular stress and telomere shortening at later passages (Ferrón et al., 2004). Primary neurospheres, once grown and harvested *in vitro,* were collected and centrifuged at 130 x*g* for 7 min. The spheres were then enzymatically dissociated with 200 µl of Accutase® solution (Sigma, cat. no. A6964) for 10 min at RT. Subsequently, 1 ml of washing medium was added to cease digestion and the cells were mechanically dissociated by gently pipetting 10-14 times. Cell suspension was washed with 5 ml of wash medium (**Annex II, table 1**) (200 x*g*, 10 min) and individual cells were resuspended in complete medium to determine the concentration of viable cells using an ADAM automatic cell counter system. For culture passage and bulk expansion, 10,000 viable cells/cm^2 were seeded in fresh pre-warmed complete medium and incubated at 37 °C in 5% CO_2 (**Graphical method 3**). After 4-6 days, the new secondary neurospheres were ready for subculturing.

To track cell division and assess the proliferative capacity of NSCs with the membrane-permeable fluorescent tracer CellTrace™ Oregon Green™ 488 Carboxy-DFFDA-SE (hereafter DFFDA, Thermo Fisher, cat. no. C34555), 1 million of individual cells were washed with DPBS (200 x*g*, 10 min) to avoid sequestration of the tracer by BSA. Cells were then incubated with 2 µg/ml DFFDA in DPBS for 7 min at 37 °C in a thermostatic bath in the dark. Probe excess was removed with washing medium (200 x*g*, 10 min) and loaded NSCs were seeded in complete medium. For analysis after different treatments and times, neurospheres were collected in 15 ml falcons for digestion with Acutase® to obtain a single cell suspension, which was centrifuged and resuspended in FACS buffer (**Annex II, table 7**). Heterogeneous dilution of the tracer within the culture defined label-retaining cells (DFFDA^{high}: 10% brightest) and highly proliferative cells (DFFDA^{low}: 40% faintest or negative) that were determined on an LSR-Fortessa cytometer (BD) (**Graphical method 3**).

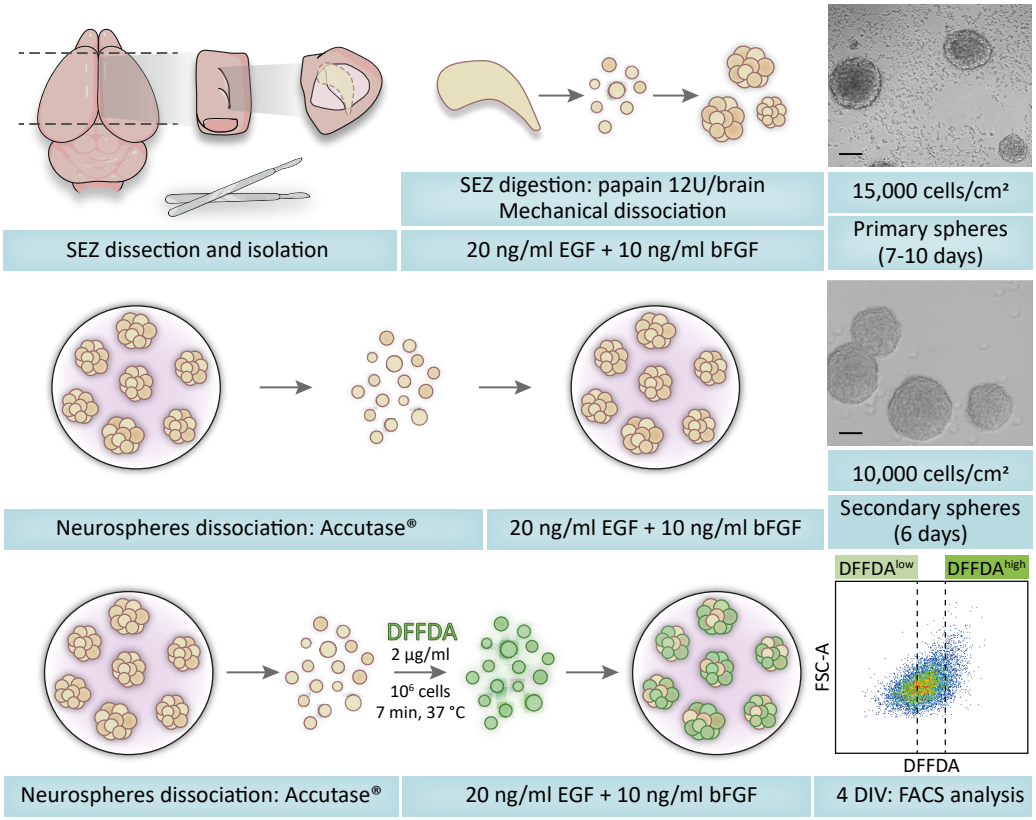

Graphical method 3. Primary culture, subculture and proliferative analysis of NSCs *in vitro.*

2.6. *Evaluation of the paracrine effects of EC senescence in NSC cultures*

In order to explore the effects that the secretome of senescent ECs may have on NSC activity, we first used the EC senescence model with palbociclib-treated hUVECs. After induction of senescence in p100-seeded cells, we thoroughly, but carefully, washed both senescent and control cells with 1X DPBS with Ca^{2+} and Mg^{2+} (Gibco, cat. no. 14080055) 3 times before adding complete NSC medium (**Annex II, table 3**) without BSA, and ECs were conditioned with this medium for 24 h. After this period, the cell medium was collected in 50 ml falcons and the debris was removed by two consecutive centrifugations. Following the first centrifugation (200 x*g*, 5 min), the supernatant was centrifuged again (1200 x*g*, 10 min) and recovered. During this protocol, we maintained the medium samples at 4 °C (on ice) to ensure a stable temperature and to avoid any possible heat shock that could favour protein denaturation. In addition, control and senescent cells were collected to quantify the number of cells per plate and its viability using a propidium iodide-based automatic ADAM cell counter system (Digital Bio). It should be noted that the number of viable senescent cells was always lower than the control cells, but the experiments were always performed with a cell viability of over 75%.

The supernatant obtained could be used to study the effect of the senescent endothelial secretome on NSCs but, in our study, we were interested in discerning the effects of soluble angiocrine factors from small extracellular vesicles (sEVs). Therefore, we ultracentrifuged (Hitachi-Himac Microultracentrifuge, C5150FNX, rotor: fixed angle S50A) the supernatant at 10,000 x*g* for 1 h at 4 °C and then carefully passed with a 20 ml syringe through a 0.22 µm nylon filter. The filtered medium was then ultracentrifuged (100,000 x*g*, 1h 20 min) to pellet the sEVs and recover the soluble fraction in the supernatant (**Graphical method 4**). This soluble fraction was kept at 4 °C until it was added to the NSC cultures within 24 h.

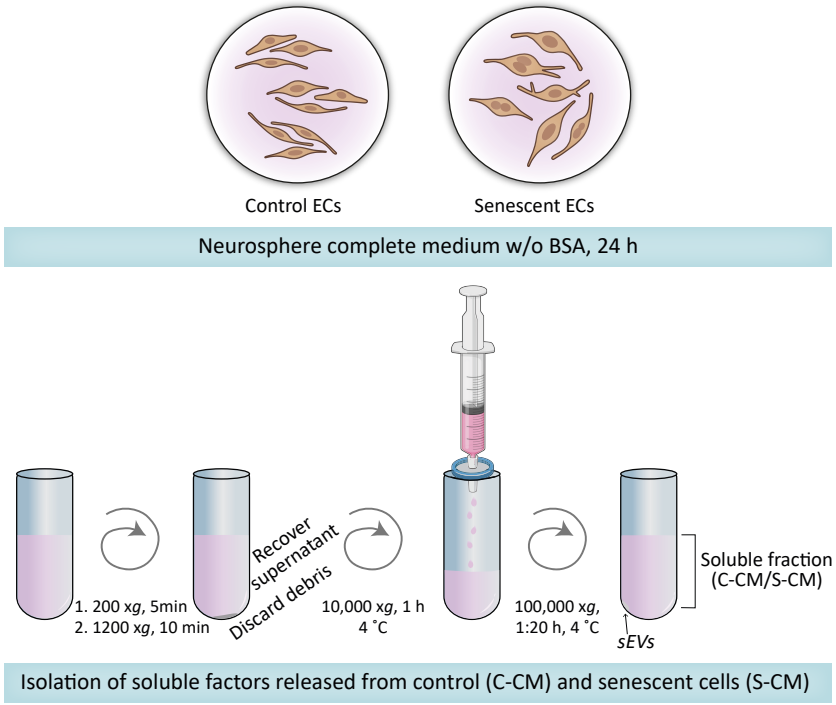

Graphical method 4. Isolation protocol of the soluble fraction secreted by ECs.

Moreover, to further investigate the paracrine impact of BEC-derived soluble factors on NSCs and whether these SCs are susceptible to a senescent fate, we used senescent and control bEnd.3 cells. Because during the development of these experiments we realised that bEnd.3 cells have an attenuated secretory profile, compared to hUVECs, and that they are also more resistant to serum-free medium, these cells were incubated for 48 h with the complete NSC medium without BSA. The same protocol as described above for hUVECS was followed to obtain the soluble fraction released by bEnd.3 cells.

Individual neurospheres were seeded in a 48-well plate at a density of 20,000 cells/cm^2 with complete NSC medium at a volume of 0.375 ml *per* well. Right away, a final volume of 0.5 ml was reached by adding 0.125 ml *per* well of the soluble fraction obtained from senescent or control ECs (1/4 dilution) or, in the case of unconditioned NSCs, fresh complete NSC medium.

In order to identify a potential increase in the lysosomal β-Gal activity of NSCs exposed to senescent EC-derived factors, cells were incubated with 20 µM WOS-Cy7Gal for 15 min (at RT and in the dark) prior to flow cytometry analysis. In addition, other senescence-associated markers, such as Lamin B1 and ROS generation, were also examined by FACS. For the evaluation of cellular ROS production, the fluorogenic probe mitoSOX™ red (Invitrogen, cat. no. M36008) was used in DFFDA labelled cells. MitoSOX™ is a commercially available fluorogenic probe that becomes oxidised by superoxide anions in the mitochondria of living cells and then emits fluorescence. This probe was prepared according to the manufacturer's instructions and cells were incubated with mitoSOX™ for 20-30 min at 37 °C in a thermostatic bath in the dark. Cells were then pelleted (300 x*g*, 8 min) and resuspended in 0.5 ml FACS buffer and ready for analysis. On the other hand, for the assessment of Lamin B1 we proceeded as for other nuclear markers, following the steps described in **Method 2.3.3.** We analysed the levels of Lamin B1 by comparing the percentage of Lamin B1$^-$ cells, in order to measure the senescence-associated decrease of this marker. Ultimately, unconditioned and conditioned NSCs by senescent or control ECs (hUVECs or bEnd.3 cells) were comparatively examined using the LSR-Fortessa cytometer (BD). FlowJo_v10.8.1 software was used to analyse the results.

2.7. *Adeno-associated vector (AAV2-BR1-p16-GFP) construction for BEC senescence induction*

2.7.1. *Viral vector production, isolation and quantification*

We obtained the plasmid encoding NRGTEWD (BR1) capsid vector protein and ampicillin resistance from Körbelin and his group (Körbelin et al., 2016) and transformed 100 µl of competent Escherichia coli bacteria DH5alpha (ThermoFisher, cat. no. 18265017). These cells were stored in an eppendorf® tube at -80 °C and thawed for 10 min on ice before plasmid was added at a concentration of 100 ng/µl. After plasmid addition, we maintained the bacteria on ice for 2 min and then heat-shocked them for 45 seconds at 42 °C in a thermoblock, transferring them back to ice for another 2 min. Next, we seeded the cells on a p100 dish with LB agar and ampicillin and left it upside down for 18 h at 37 °C. After this period, we took a single colony of bacteria using a 10 µl pipette tip which we dipped into a liquid culture containing 200 ml of LB + ampicillin (diluted 1:1000) to amplify the plasmid, and kept it on shaking at 37 °C overnight. Finally, we purified and isolated the plasmid DNA following the instructions specified in the Genopure Plasmid Maxi Kit (Roche, cat. no. 03143422001). In addition, we sequenced some DNA fragments to ensure that we had increased the number of plasmid copies properly for our experiments. Indeed, we selected 3 primers defined in the genetic map of the plasmid (**Annex III**) and PCR results confirmed that the product is specific and of the expected size. The purified plasmid encoding the viral capsid (pREPCAP_BR1) was sent to a virus production centre (CEBATEG- UAB, Barcelona) that carried out the assembly of the modified AAV2-BR1, including the genetic material for the expression of p16 (provided by Prof. Pura Muñoz) and GFP.

The expression cassettes (CAG-p16 and RSV-GFP) were cloned into the pAAV plasmid which contained the ITRs of the AAV2 genome, a multicloning site to facilitate cloning of expression cassettes, and ampicillin resistance gene for selection. rAAV vector was produced by triple transfection of $4x10^8$ HEK293 cells with 500 µg of pAAV-CAG-p16-RSV-GFP, 500 µg of pRepCap_BR1, and 1000 µg of pXX6 plasmid (kindly provided by Dr. Jude Samulsky, University of North Carolina at Chapel Hill) mixed with polyethylenimine (PEI; branched, MW 25,000; Sigma). Briefly, 48 h after transfection, cells were harvested by centrifugation (200 x*g*, 10 min), resuspended in 60 ml of 20 mM NaCl, 2 mM $MgCl_2$, and 50 mM Tris-HCl (pH 8.5), and lysed by three freeze–thaw cycles. Cell lysate was clarified by centrifugation (2000 x*g*, 10min) and the rAAV particles were purified from the supernatant by iodixanol gradient. The clarified lysate was treated with 50 U/ml of Benzonase (Novagen) for 1 h, 37 °C and centrifuged (3000 x*g*, 20 min). The vector-containing supernatant was collected and adjusted to 200 mM NaCl using a 5 M stock solution. To precipitate the virus from the clarified cell lysate, polyethylene glycol (PEG 8000; Sigma) was added to a final concentration of 8% and the mixture was incubated (3 h, 4 °C) and centrifuged (8000 x*g*, 15 min). The rAAV-containing pellets were resuspended in 20 mM NaCl, 2 mM $MgCl_2$, and 50 mM Tris-HCl (pH 8.5) and incubated for 48 h at 4 °C. rAAV particles were purified using the iodixanol method as previously described (Zolotukhin et al., 1999). rAAV concentration was performed in PBS using Amicon Ultra-15 Centrifugal Filter Device (Millipore). rAAV particles were titrated following a method based on the quantitation of encapsidated DNA with the fluorescent dye PicoGreen® (Piedra et al., 2015).

2.7.2. *Evaluation of viral vector transduction in ECs in vitro*

The GFP gene expression of the generated AAV2-BR1-p16-GFP vector was tested in cell culture using bEnd.3 cells. To this end, cells were seeded in a 96-well plate (p96) at a density of 1,500 cells/well. When cells reached approximately 60% confluence, the vector was added. For cellular infection, the cell medium was removed and the adeno-associated vector was added in bEnd.3 cell medium with depleted protein serum (2% FBS) at a reduced volume *per* well (50 µl). A multiplicity of infection (MOI) of 100,000 genomic copies (gc) *per* cell was used and, after 24 h, the volume of the wells was restored to 100 µl with 10% FBS bEnd.3 cell medium. After 8 DIV, the cells were detached and pelleted (300 x*g*, 5 min). BEnd.3 cells were resuspended in 0.5 ml of FACS blocking buffer and run on a LSR-Fortessa cytometer (BD) to analyse

the potential increase in the percentage of GFP⁺ cells in those incubated with the viral vector (**Graphical method 5**).

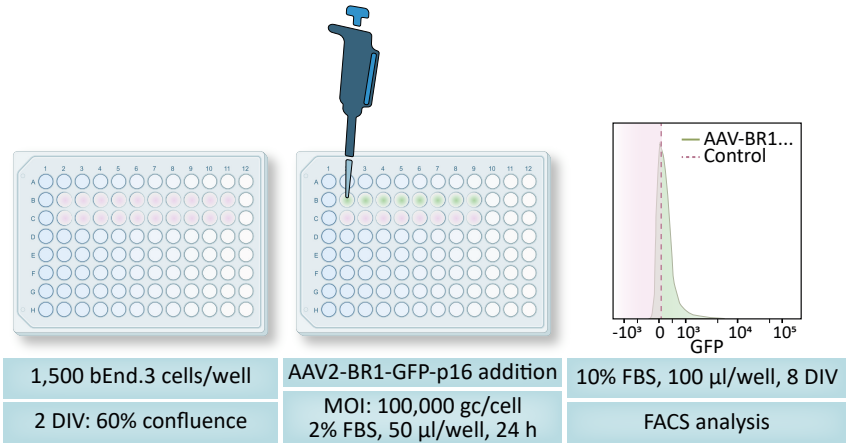

Graphical method 5. Evaluation of *in vitro* viral vector transduction in ECs.

3. *Ex vivo* methods

3.1. Histochemical X-gal staining of SEZ whole-mount preparations

The brains of 7-month-old SAMP8 and SAMR1 mice were extracted after they were euthanized by cervical dislocation. Under magnification (Leica MZ6 25x) and with the aid of scalpels, we dissected the SEZ as described above (see **Method 2.5.**). Freshly obtained SEZs were placed in a 48-well plate, washed with PBS and fixed in a solution of 1% PFA and 0.2% glutaraldehyde in PBS for 1 h at RT. Next, SEZ whole-mounts were incubated for 30 h at 37 °C in the staining solution described in the protocol reported by Debacq-Chainiaux and colleagues in 2009 for histochemical X-gal staining (Debacq-Chainiaux et al., 2009). Of note, sufficient volume of both fixative and staining solutions was used to completely cover the SEZ whole-mount preparation (0.5 ml). After this period, the staining solution was removed and the SEZ whole-mount preparations were washed with PBS. Subsequently, they were placed on a slide with a coverslip in a glycerol mount for analysis of the samples right afterward. Blue-stained cells were detected and photographed using a Nikon Eclipse-Ni microscope coupled to a Nikon Digital DS-Ri1 camera.

3.2. *Analysis of brain endothelial senescence by flow cytometry*

Mice under study were euthanized by cervical dislocation and, after peeling off the skull, their brains were extracted and placed in a 12-well dish with ice-cold PBS. Meninges were removed and bulbs and cerebellum were discarded. The remaining brain tissue, with the exception of the SEZs which were processed in parallel to phenotype the neurogenic lineage (see **Method 3.4.**), was minced and subjected to enzymatic digestion (Czupalla et al., 2018). Brain tissue was digested with a mixture of 1 mg/ml collagenase/dispase (Sigma, cat. no. 10269638001) and 0.2 mg/ml DNAse (Labclinics, cat. no. LS002007) diluted in 2 ml RPMI *per* sample using a gentleMACS™ Octo Dissociator with heaters (Miltenyi). The digested pieces were mechanically dissociated by pipetting up and down 30 times with a plastic Pasteur pipette and the cell suspension was filtered through a 70 µm nylon filter pre-wetted with 1 ml of FACS buffer. After washing the filter with 5 ml of FACS buffer, the cells were pelleted (300 x*g*, 10 min) and processed for myelin removal following the protocol specified by the Debris Removal Solution manufacturer (Miltenyi, cat. no. 130-109-398). Cells were then incubated in 100 µl of FACS blocking buffer with the primary antibodies

specific for labelling CD31⁺ ECs and CD45⁺ immune cells (BD Bioscience, see **Annex I, table 3**) at 4 °C (ice) for 30 min in the dark. Next, cells were washed with 2 ml of FACS buffer (300 x*g*, 10 min), and the labelled samples were divided into two fractions, one for cell fixation and one for live cells determination of SA-β-gal activity or ROS generation.

For the detection of intranuclear senescence markers, the labelled cells were fixed according to the instructions of the BD Pharmingen™ Transcription-Factor Buffer Set (cat. no. 562725). Briefly, cells were first incubated with primary antibodies to p16 and γH2AX for 40 min at 4 °C in the dark. After washing the primary antibodies (500 x*g*, 5 min), secondary antibodies labelled with Alexa Fluor™ (Invitrogen-Molecular Probes) were added for 30 min at 4 °C in the dark. On the other hand, unfixed cells were incubated for 15 min with WOS-Cy7Gal at RT or NBGal at 37 °C and 5% CO_2, for β-gal activity evaluation. For the assessment of mitochondrial ROS production, cells were incubated with mitoSOX™ (Invitrogen, cat. no. M36008) for 25 min at 37 °C in a thermostatic bath in the dark. Finally, after pelleting the cells (500 x*g*, 5 min) and resuspending them in 0.5 ml FACS blocking buffer, senescence marker levels were measured on a LSR-Fortessa cytometer (BD) (**Graphical method 6**). The samples remained on ice during the whole procedure, except for the incubation times with the probes or with the primary and secondary antibodies, where the samples were kept at 37 °C or at 4 °C in a refrigerator, respectively. FlowJo_v10.8.1 software was used to analyse the results by comparing the MFI of each senescence marker between the different experimental conditions.

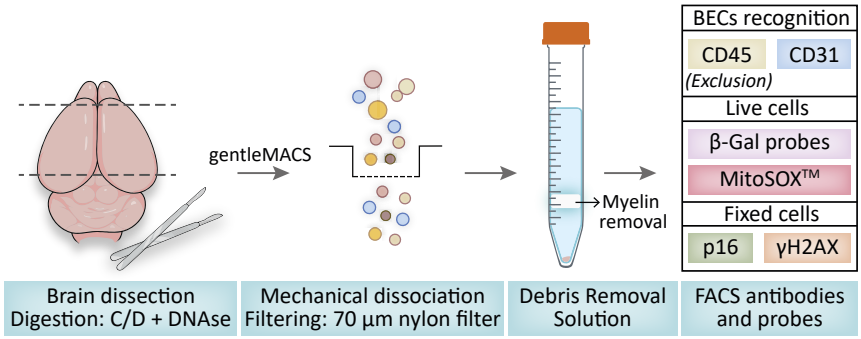

Graphical method 6. Procedure for phenotyping senescent BECs.

The FACS gating strategy to isolate individual BECs was performed following the analysis workflow described below. First, brain cells were gated by size (FSC) and cellular complexity (SSC), discarding cellular debris, dead cells and myelin remnants. Second, singlets were gated using SCC-H and SCC-A. Next, live or DAPI- cells were selected and CD45⁻ cells were gated to exclude microglia and other myeloid cells. Finally, CD31⁺ cells were isolated and all senescence markers were assessed within this cell population (**Graphical method 7**). Cells were first incubated with the primary rabbit antibodies to p16 or Lamin B1 and then with secondary anti-rabbit antibodies labelled with Alexa Fluor™ (Invitrogen-Molecular Probes) and analysed in LSR-Fortessa cytometer (BD). FlowJo_v10.8.1 software was used to interpret the results.

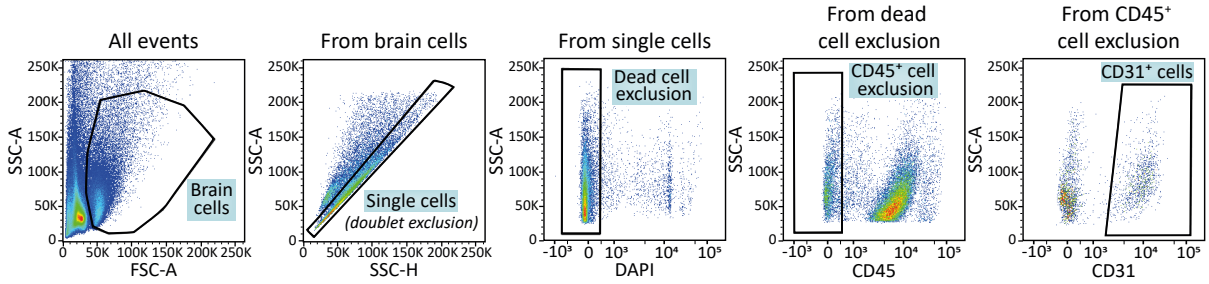

Graphical method 7. FACS gating strategy for BECs identification.

3.3. *Measurement of the senescent cell burden in different organs*

SAMP8 and SAMR1 mice of 7 months old were euthanized by cervical dislocation and the right kidney and a piece of the right lobe of the liver were extracted. These tissues were subjected to enzymatic digestion with a mixture of 1 mg/ml collagenase/dispase (Sigma, cat. no. 10269638001) and 0.2 mg/ml DNAse (Labclinics, cat. no. LS002007) diluted in 2 ml RPMI per sample. Tissue enzymatic dissociation was performed using a gentleMACS™ Octo Dissociator with heaters (Miltenyi) selecting "37 °C_Multi-tissue_C" program. Next, 5 ml of FACS buffer was added and the digested tissue pieces were mechanically dissociated with a plastic Pasteur pipette and filtered through a 40 µm nylon filter to obtain a single cell suspension. In order to reduce the background noise caused to auto-fluorescence in some cells and to target cell populations that are widely found in many organs, cells were incubated with a 100 µl mixture of CD31 and CD45 antibodies (BD Bioscience, see **Annex I, table 3**), for 30 min in the dark at 4 °C, to label endothelial and immune cells, respectively. Thus, the results obtained are the product of the analysis of senescence markers in both cell populations. After adding extra volume of FACS buffer and pelleted the cells, a portion of live cells was incubated with 20 µM of WOS-Cy7Gal for 15 min prior to the flow cytometry assay for SA-β-Gal detection, together with 0.1 µg/ml DAPI to exclude dead cells. The remaining cells were fixed and permeabilized using BD Pharmingen™ Transcription-Factor Buffer Set for detection of intranuclear senescent markers. Cells were first incubated with the primary rabbit antibodies to p16 or Lamin B1 and then with secondary anti-rabbit antibodies labelled with Alexa Fluor™ (Invitrogen) and analysed in LSR-Fortessa cytometer (BD). FlowJo_v10.8.1 software was used to interpret the results.

3.4. *FACS strategy for the analysis of the SEZ neurogenic lineage*

In Prof. Isabel Fariñas' group we have developed a flow cytometry-based protocol to phenotype the different SEZ populations of the neurogenic lineage: qNSCs, pNSCs, aNSCs, NPCs, ENBs and LNBs (Belenguer et al., 2021). After dissection, SEZs from each mouse were minced and enzymatically digested using the Neural Tissue Dissociation kit (T) (Miltenyi, cat. no. 130-093-231) following the instructions of the manufacturer in a gentleMACS™ Octo Dissociator with heaters (Miltenyi). Digestion was quenched with 3 ml of 100 µg/ml trypsin inhibitor (Sigma, cat. no. T6522) diluted in FACS buffer (**Annex II, table 7**) and the digested pieces were mechanically dissociated pipetting up and down 25 times through a plastic Pasteur pipette. The cell suspension was filtered through a 40 µm nylon filter to break up cell aggregates and an additional 5 ml of FACS buffer was used to wash the filter. Cells were then pelleted (300 x*g*, 10 min) and resuspended in 100 µl of FACS blocking buffer with the specific antibodies and reagents (see **Annex I, table 3**) and incubated for 30 min at 4 °C in the dark. Next, after washing with 1 ml of FACS buffer (300 x*g*, 10 min), the labelled samples were resuspended in 0.5 ml FACS blocking buffer for flow-cytometry analysis using a LSR-Fortessa cytometer (BD). DAPI (0.1 µg/ml) was added to exclude dead cells.

Graphical method 8 includes the detailed strategy for the identification of SEZ populations based on our protocol (Belenguer et al., 2021). Briefly, SEZ cells are gated by FSC and SSC to discard cell debris, dead cells, myelin, as well as ependymal cells and neurons (Murayama et al., 2002). Then, $CD45^+$ (microglia), $CD31^+$ (EC), $TER\text{-}119^+$ (erythrocyte) and $O4^+$ (oligodendrocyte) cells are negatively selected or excluded in order to analyse the remaining lineage-negative (Lin^-) cells. Lin^- cells are stratified using fluorescent labelled antibodies to GLAST and CD24 as well as anti-EGF to stain EGFR (Codega et al., 2014). The $GLAST^-/CD24^{high}$ fraction delimits NBs (Belenguer et al., 2021; Llorens-Bobadilla et al., 2015; Pastrana et al., 2009), that can be subdivided into $EGFR^+$ or $EGFR^{low/-}$ pools of proliferating (ENBs) and non-proliferating or migrating NBs (LNBs), respectively. $GLAST^-/CD24^{-/low}/EGFR^+$ and $GLAST^+/CD24^{high}/EGFR^+$ cells have been previously characterised as NPCs (NPC1 and NPC2), but were considered as a single NPC population throughout this thesis in order to facilitate interpretation of data. Within the $GLAST^+/CD24^{-/}$low fraction, cells with low levels of CD9 are considered mature non-neurogenic astrocytes whereas $CD9^{high}$ NSCs can be classified into different states by GLAST levels and EGF-binding (Belenguer et al., 2021; Llorens-Bobadilla et al., 2015):

GLAST^{high}/CD24$^{-/low}$/CD9^{high}/EGFR$^{-/low}$ qNSCs and GLAST^{low}/CD24$^{-/low}$/CD9^{high}/EGFR$^{-/low}$ pNSCs are quiescent, whereas GLAST^{low}/CD24$^{-/low}$/CD9^{high}/EGFR^{+} aNSCs are actively proliferative (Belenguer et al., 2021). The relative abundance of each population is calculated as the percentage of total live cells selected. We can also calculate the number of cells in each population from this percentage by quantifying the number of total viable cells in the SEZ with the ADAM automatic cell counter equip (Digital Bio), which is how we have represented our data.

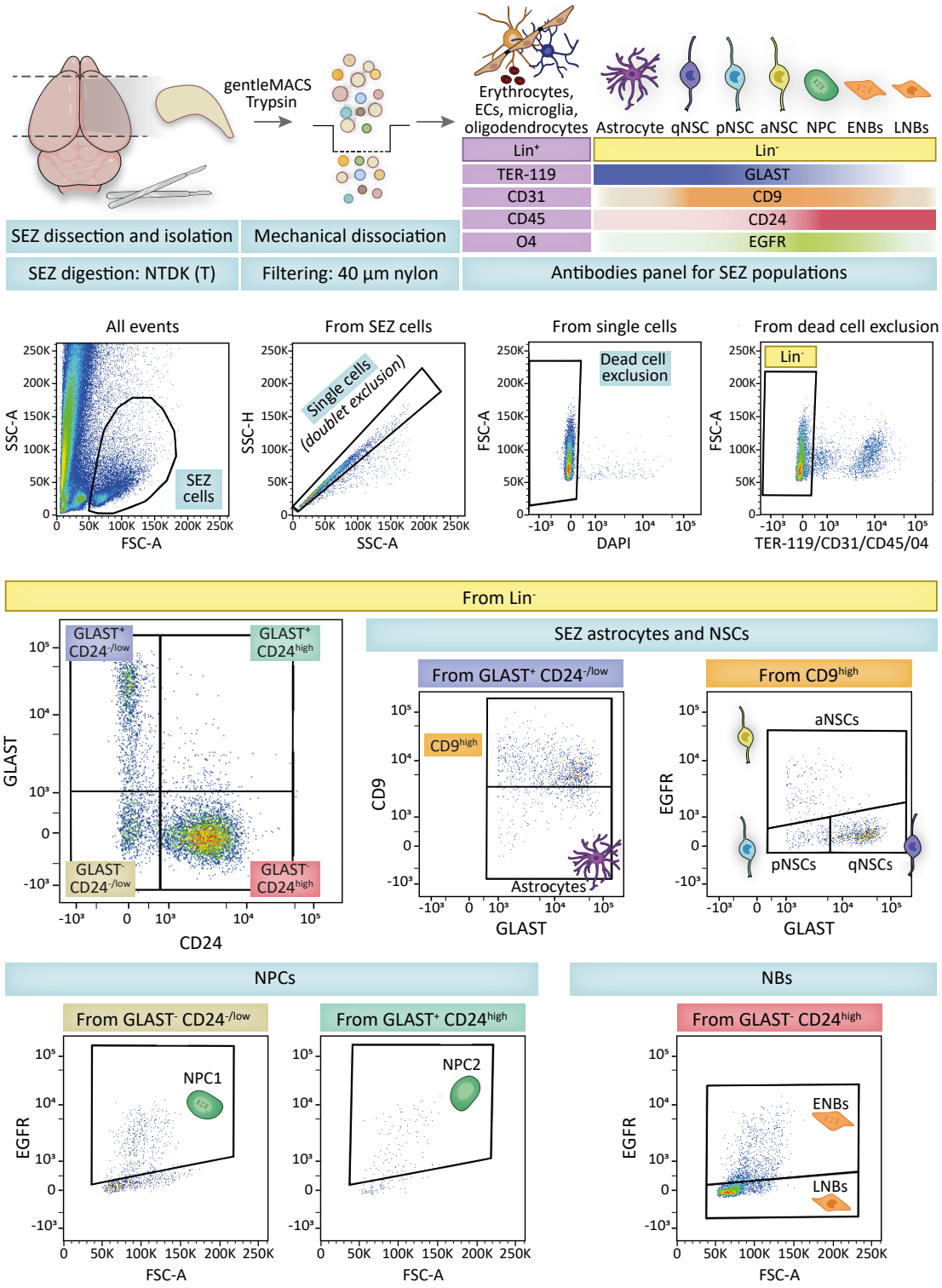

Graphical method 8. Analysis of the SEZ neurogenic lineage by flow cytometry (Belenguer et al., 2021).

4. *In vivo* methods

4.1. *Longitudinal characterisation of ageing through external assessment*

We tracked the progression of ageing from 2 to 12 months of age in SAMP8 and SAMR1 male mice by examining different phenotypic traits that are typically associated with increasing age, using specific tests conveniently distributed over time. The SAMP8 strain of mice is characterised by early ageing and short lifespan, while SAMR1 animals follow a relatively normal ageing pattern. In this regard, we were able to detect age-associated disorders in SAMP8 mice by comparatively studying both strains, and this allowed us to characterise the accelerated ageing process. In addition, behavioural tests were also used to monitor senolytic treatments in SAMP8 and C57BL/6 mice.

4.1.1. *Physical fitness*

To evaluate physical fitness each animal body weight was recorded monthly by using a Kern 440-45N balance and subjected to the following specific tests:

Grip strength: The Grip Strength test was used to assess the neuromuscular function of the mice by measuring the maximal strength of their front paws (Gomez-Cabrera et al., 2017). The readout was obtained by measuring the grip force applied by the mouse's forelegs on a bar sensor using a Bioseb metre (Panlab) that provided a strength value in units of grams. To proceed with the measurement of grip strength, the mouse was brought close to the grip bar, allowing only its forepaws to grasp the bar. The mouse was then pulled horizontally by its tail and the value of the grip strength was recorded. To obtain reliable data, five trials *per* mouse were performed with 1 min rest between each repetition. The mean of the values recorded for each mouse was normalised to its body weight to interpret the results.

Weight test: This test allowed further assessment of muscle strength in SAMP8 and SAMR1 mice, especially the force associated with forelimb and torso musculature (Deacon, 2013). To perform this test, a metal hook of known weight was placed on a grid that the mice could easily grasp. The mouse was placed on the grid in such a way that it could grasp the grid with its front paws. Next, the mouse was lifted from the base of its tail (closest to the body) for 5 seconds while holding a given weight. This process was repeated three times with a 2 min rest between each trial. If the animal was able to hold the weight during the 3 trials, the weight was increased by inserting an additional hook and the procedure was repeated. The weight limit for this test was 120% of the animal's body weight. However, if the mouse fails in one of the trials, it will not continue with the test. The maximum weight that the mice were able to lift was recorded for statistical analysis.

Grid test: The Grid test was used to assess the overall muscle strength and endurance of the mice (Graber el al., 2020). The dimensions of the grid were large enough for the mice to fully place its paw inside each square, and the material was strong enough to support the weight and movement of the animal. The grid used was circular in shape with a diameter of 80 cm. This grid was placed horizontally over a bucket (1 m high and 50 cm wide) high enough to prevent the mice from easily reaching the ground and, therefore, to encourage them to try to hold on for as long as possible. Accordingly, sufficient sawdust was placed at the base to cushion the mice's fall and prevent damage. Mice were lifted by their tail, carefully placed in the central area of the grid and held until they grasped the grid with their front and hind paws. The grid was then inverted, leaving the mouse clutching it upside down. With a maximum time of 96 seconds *per* animal to complete the test, the latency time until the mice left the grid and fell onto the sawdust was recorded. The results were normalised to the body weight of the animal for statistical analysis. This test was only performed once *per* animal at the selected ages to avoid the learning factor

which could lead to false results, since falling on the sawdust does not harm the mice and they may prefer to drop rather than hold on.

4.1.2. *Motor coordination and locomotion.*

These parameters were specifically evaluated in two different behavioural tests.

Pole test: The Pole test has previously been reported to assess mouse movement disorders due to striatal dopamine depletion or basal ganglia abnormality (Ogawa et al., 1985; Matsuura et al., 1997; Fernagut et al., 2003; Fleming et al., 2004; Recasens et al., 2014). Each mouse was placed head upwards on top of an inclined (10-15°) wooden pole (1 cm-diameter and 45 cm-long) with a thick layer of bedding on the basement to prevent damage in the falls. When placed on the pole, the mouse oriented himself downward and descended the length of the pole. The time between the placement on the pole and the moment when the four paws touched the floor was measured (T-down), with a time limit of 90 seconds. All experimental subjects were tested for 3 trials. Mice that descended the pole in a different way in more than one trial, like slipping away or jumping, were discarded from the experiment.

We considered the motor strategy used during the task performance for analysis. In this sense, a Motor Ability Scale (M.A.S.; see Recasens et al., 2014) was defined to score mice's behaviour in three degrees: 0 points for dragging or falling from the pole, 1 point for T-down between 7 and 49 seconds and 2 points for T-down < 7 seconds. Therefore, the higher the score in the M.A.S., the better motor performance in the Pole test. The average of those three trials was calculated and considered for statistical analyses including mathematical transformations for normality tests.

Open Field test: General motor activity was examined as previously reported (Perez-Villalba et al., 2018) in a squared open field (50 cm^2) (Panlab, S.L., Harvard Apparatus) homogenous and dimly illuminated. We used a tracking software (SMART, Panlab SL, Harvard Apparatus) to analyse the spatiotemporal distribution of mouse movement in addition to spontaneous locomotor activity. The movement trajectory beside total distance travelled and mean speed were analysed for statistical analysis.

4.1.3. *Hind limb clasping reflex*

Hind limb clasping is a marker of neurodegenerative disease progression in several mouse models (Chou et al., 2008), occurring, for example, in mice with cerebellar ataxia (see Guyenet et al., 2010 for protocol setup). Briefly, mice were lifted by the tail in 3 trials, 10 seconds each trial, and were continuously videotaped for further evaluation. Hind limb position was assessed on a 4-stage scale: 0 represented no alteration in hind limb position, 1 was assigned when one hind limb retracted close to the body, 2 when two hind limbs retracted close to the body and 3 when the hind limbs not only retracted, but folded and tightened completely along the belly, referred to as "hind limb clasping". This scale represents a gradual deterioration of the hind limb reflex response associated with neurodegeneration (Komatsu et al., 2006) of motor areas such as the striatum, cerebellum and spinal cord (Lalonde and Strazielle, 2011).

4.1.4. *Anxious behaviour*

Anxiety was evaluated in two different behavioural tests.

Open Field test: Anxious behaviour analysis was conducted with the Open Field test using a grey squared Plexiglas open box (50 cm^2) (Panlab, S.L.). Briefly, mice were gently introduced in the open field and videotaped for 10 min in a dim light room to which they have been previously habituated. Periphery/centre areas were automatically established by the Smart video tracking software (Smart Junior, Panlab S.L., Harvard Apparatus). Trajectory of movement and motor behaviour were analysed.

Elevated Plus Maze test: Anxiety was also evaluated with the EPM test as previously reported (Moya-Pérez et al, 2017). We used a grey-painted Plexiglas apparatus with four 30 cm-long and 5 cm-wide arms (two open and two enclosed by 15.25 cm-high walls). Each arm of the maze was attached to sturdy metal legs so that it was raised 40 cm off the ground. Each mouse under study was gently left in the middle of the EPM for a free-moving task during 5 min. The time spent in the open arms was measured by tracking software (Smart Junior, Panlab S.L., Harvard Apparatus, Spain). Time in the open arm was scored when all four paws were in the open arm of the maze.

4.1.5. *Olfactory Habituation-Dishabituation*

An Olfactory Habituation-Dishabituation test was performed to analyse mice odorant detection as described in the protocol published by Perez-Villalba and colleagues in 2015 (Perez-Villalba et al., 2015). Briefly, the experimental mouse was placed in a Pexiglas box (22.5 x 22.5 x 29.5 cm) with a hole (1 cm diameter) on one side of the box accessible to the mice. A transparent methyl methacrylate lid was used to prevent odour dissipation of the essences during the test. Ordinary cotton sticks impregnated with essences were inserted through this hole. First, a stick impregnated with mineral oil (Sigma-Aldrich, cat. no. M8410-100ML), which is practically odourless to the animal, was positioned through the hole, just to accustom the mouse to the presence of this item. For this purpose, a new stick with mineral oil was inserted every minute for a total of 5 times. Next, a new stick was impregnated with vanillin (Sigma-Aldrich, cat. no. W310700-sample-k) diluted 1/20 in mineral oil to introduce a vanilla aroma, which is an odorous stimulus that the mouse should recognise. We repeated the process of replacing the stick, renewing the vanillin essence every minute for 5 consecutive times, while the interest of the mouse in this odour decreased. Finally, we introduced a new odorous stimulus with (-)-carvone (Sigma-Aldrich, cat. no. 22060-5ML-F) diluted 1/20 in mineral oil, which provided a mint aroma that aroused again the attention of the mouse, and we proceeded in the same way as before. This whole process was recorded, and the time of exploration detecting new odours was evaluated. The critical points of analysis in this test are the exploration time of the vanilla aroma with the first sticks (V1 and V2) and, especially, the recognition of the second odour stimulus, the mint aroma (from V5 to M1), as it requires increased sensitivity for odour discrimination.

4.1.6. *Novel Object Recognition*

The NOR test assesses several cognitive tasks in mice, in particular recognition memory (Lueptow, 2017). This test relies on the spontaneous tendency of rodents to spend more time exploring a novel object than a familiar one. To do this, the experimental mouse was placed in an open field box containing two matching objects with which the animal became familiar for 5 min. After 1 h, one of these objects is changed by a new different one and mice are allowed to explore both objects for 5 minutes. The time spent exploring each object was carefully assessed from video recordings.

4.1.7. *Glucose Tolerance*

Impaired glucose metabolism is an age-associated event and its assessment provides a measurable biochemical parameter to characterise the health status of SAMP8 and SAMR1 mice (Fülöp et al., 1987; Chia et al., 2018). We evaluated glucose metabolism in these animals performing a Glucose Tolerance test (Stevic et al., 2007; Pedro et al., 2020). First, the baseline blood glucose level measurement was performed after 6 h of fasting. Subsequently, a dose of 2 g of glucose *per* kg of mouse weight was administered via oral gavage in these animals. The blood glucose level was measured at 15, 30, 45, 60, 120 and 180 min after administration. The glycaemia was analysed in a drop of blood obtained by slightly pricking mice in the saphenous vein. The readout was performed with test strips and a glucometer (My Counter Next®) that provided the values of glucose concentration in blood in mg/dl.

4.1.8. *Hair recovery (follicle regeneration assessment)*

In order to assess the time required for complete renewal of a hair patch, animals were shaved with an approximately 1 x 1 cm square on the lower back. Each animal's hair regrowth was monitored weekly, and pictures were taken to assess their hair growth progress. In our work, we compared SAMP8 with SAMR1 animals by quantifying the number of days elapsed from the shaving to the complete hair recovery in the shaved area. This test provides an idea of stem cell activity based on the renewal rate of the follicular population (Orasan et al., 2016).

4.2. ***Systemic β-Gal activity assessment with the renally clearable Cy7Gal probe***

We decided to chemically modify the WOS-Cy7Gal probe through the addition of sulfonic groups to the releasable Cy7 fluorophore in order to promote its diffusion out of the cells and its recovery in the urine when injected *in vivo*. This way, we obtained a probe with the ability to act as an *in vivo* readout of SA-β-Gal activity. Therefore, upon administration, the non-emissive Cy7Gal probe becomes hydrolyzed by the β-Gal enzyme in cells to release the highly fluorescent dye Cy7. Furthermore, Cy7 is rapidly cleared in the kidneys, due to appropriate modifications, which allows its detection in urine simply by using a fluorometer (**Graphical method 9**). This probe was chemically characterised in the same way as WOS-Cy7Gal (see **Method 2.4.1.**) (Rojas-Vázquez et al., submitted).

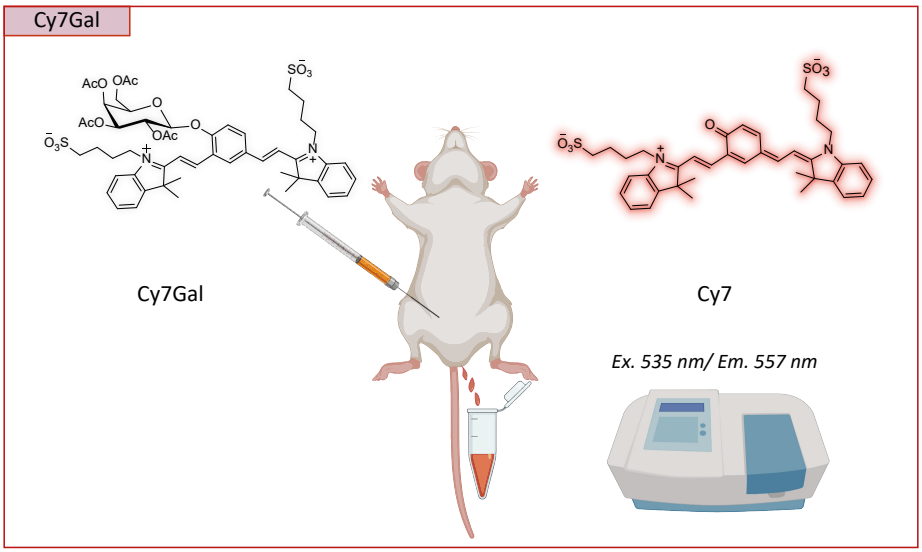

Graphical method 9. Cy7Gal, a renal clearable fluorogenic probe for β-Gal *in vivo* detection.

For biodistribution analysis of Cy7Gal compared to the probe without sulfonic groups WOS-Cy7Gal, 15-m SAMP8 mice were intraperitoneally (i.p.) injected with each of the probes (13 mg/ml, 200 µl) or the vehicle (DMEM) using Micro-Fine™ insulin syringes of 29G (BD, cat. no. 324827). Mice were anaesthetised with isoflurane (2%) for 10 min. After this time, blood samples were obtained by submandibular puncture of mice with a 25G needle (BD) and collected in heparinized tubes. Subsequently, these samples were centrifuged (350 x*g*, 4 min) and the supernatant (plasma) was rescued. For plasma fluorescence analysis, 10 µl of sample was diluted in 90 µl of distilled water and fluorescence readout (λ_{ex}= 535 nm; λ_{em}= 560 nm) was performed in a fluorometer (Horiba Scientific Fluoromax-4 spectrofluorometer). Urine samples were collected manually (using a 200 µl pipette and 1.5 ml eppendorf® tubes) 15 min post-injection and fluorescence measurement was performed diluting 5 µl of urine in 95 µl of distilled water (λ_{ex}= 535 nm; λ_{em}= 557 nm). Both plasma and urine samples were kept in the dark at 4 °C until fluorescence was

measured (on the same day of collection). Of note, urine samples can be stored for several months at -80 °C for further analysis.

To estimate the senescent cell burden related to ageing or monitoring of senolytic treatments, mice were i.p. injected with Cy7Gal. The dose administered was adjusted to the body weight of each animal (140 mg/kg). After Cy7Gal injection, mice were anaesthetised with isoflurane (2%) for 15 min to equalise probe distribution time and, upon awakening, urine samples were collected individually. Given that urine output can vary substantially between young and old animals (or between SAMP8 and SAMR1 mice), we measured in a fluorometer the counts *per* second (CPS) of 5 µl of urine sample diluted 1/20 in distilled water. Subsequently, the CPS, or arbitrary units (a.u.), obtained was multiplied by the volume of urine collected for that sample. In this way, we obtained a result that allowed us to evaluate the amount of fluorophore released, independently of the variability in micturition volume that conditions the concentration of the fluorophore in the bladder and, therefore, the fluorescence measurement.

Fluorometer measurements of urine from young versus old C57BL/6 mice were confirmed with an analogous method, HPLC-MS. The HPLC-MS measurements were obtained using an eluent gradient method from H_2O-methanol (100:0 v/v) to H_2O-methanol (0:100 v/v) at 10 min with a flow rate of 0.5 ml/min with a kromasil C18 column. Mass spectroscopy chromatograms were recorded with an Agilent Ultivo mass spectrometer equipped with a triple Q-TOF detector using a dual selected ion monitoring (SIM) function at 1034 m/z and 705 m/z simultaneously, corresponding to the Cy7Gal probe and Cy7 fluorophore, respectively. The calibration curve was obtained by measuring known concentrations of the Cy7Gal probe and Cy7 fluorophore in H_2O using the dual SIM method. The amount of Cy7Gal and Cy7 excreted was calculated by measuring 5 µl of urine sample diluted in 500 µl H_2O and multiplying the corresponding concentration (obtained with the calibration curve) by the volume of urine collected for each sample. The percentage of probe or dye excreted in the urine was obtained relative to the amount of Cy7Gal injected.

4.3. *Senolytic treatments*

Mice were treated via oral gavage with a combination of the senolytic drugs D+Q: D (5 mg/kg) and Q (50 mg/kg) dissolved in 20% PEG-n400 and 0.9% NaCl (vehicle) (Xu et al., 2018). SAMP8 mice received the drug mixture for 5 consecutive weeks at 7 months of age, alternating a regime of 5 or 1 administrations *per* week. Cy7Gal and behavioural monitoring was assessed either short term (within 21 days) or long term (within 58 days) after the end of the senolytic treatment. The same cohort of animals received another cycle of treatment at 10 months and senescence burden and behaviour were assessed only in the short term after the end of this second cycle. Furthermore, to evaluate the impact of the treatment on adult neurogenesis in the OB and the SGZ, another group of 8-month-old SAMP8 mice was treated with the combination of D+Q senolytic drugs for 5 weeks with the same regimen as previous. On the other hand, 15-month-old C57BL/6 mice received a 5-week treatment cycle with 2 doses *per* week and were tested for Cy7Gal and behavioural monitoring within 15 days after the senolytic intervention.

Of note, groups were assigned prior to the onset of any experimental procedure, and created by matching mice based on body weight, without using randomization. Moreover, during the analysis of behavioural tests and BrdU quantification, the experimenter was blind to the group assignment of each animal.

4.4. *Immunohistochemical analysis of adult neurogenesis in the SEZ and the SGZ*

SAMP8 mice were treated with a senolytic regimen of D+Q for 5 weeks and administered 5-Bromo-2'-deoxyuridine (BrdU) 5 days laters. BrdU is a synthetic thymidine analogue that incorporates newly

synthesised DNA during the S phase of the cell cycle. It can be used in combination with different chase time points to assess neurogenesis in specific regions of the brain (Wojtowicz and Kee, 2006). In this study, we used a long chase protocol to evaluate neurogenesis in the OB and the hippocampal DG. We prepared a 10 mg/ml solution of BrdU (Sigma, cat. no. B5002) in sterile 0.9% NaCl, using a bath sonicator and vortex. Mice were i.p. injected (using 30G needle) with a dosage of 50 mg/kg twice daily, with 6 h interval, for 3 consecutive days. The mice were euthanized 26 days after the first injection. Since cells dilute BrdU labelling after 3-4 cell divisions, this long chase protocol allowed us to identify slow-proliferating NSCs, immature neurons (LNBs or IGCs), as well as newly-generated neurons that exited the cell cycle shortly after BrdU incorporation. We quantified the number of $BrdU^+$ cells in the GL of the OB, and the SGZ and inner GCL of the DG, as a measure of neurogenesis.

For immunohistochemical detection of BrdU and neurogenic cell populations, animals were first deeply anaesthetized by i.p. injection of a mixture of medetomidine (0.5-1 mg/kg) and ketamine (50-75 mg/kg) diluted in saline (0.09% NaCl). Mice were then transcardially perfused with approximately 28 ml of 0.9% NaCl and 83 ml of 4% PFA in 0.1 M PB (pH 7.4) at a flow rate of 5.5 ml/min. The fixed brains were carefully removed preserving the OBs and then post-fixed for 2 h by immersion in 4% PFA. After thoroughly washing the fixative with 0.1 M PBS, brains and OBs were embedded separately in 4% agar and sectioned with vibratome at 40 µm (Leica VT1000). Serially collected coronal sections were stored at 4 °C in 0.05% sodium azide (in PBS) until use. For BrdU detection, sections were preincubated in 2 N HCl for 17 min at 37 °C to denature chromatin and neutralised in 0.1 M sodium borate (pH 8.5) before incubation with blocking solution for 1h. Next, OB sections were incubated for 48 h with specific primary antibodies to BrdU (Abcam, cat. no. ab6326) and tyrosine hydroxylase (TH, Novus Biologicals, cat. no. NB300-120) (**Annex I, table 1**) for labelling dopaminergic neurons, while hippocampal ones were incubated with BrdU. After thoroughly washing, tissue sections were incubated with fluorescently-labelled secondary antibodies (Jackson ImmunoResearch) (see **Annex I, table 2**) for 1 h at RT in the dark and under gentle movement. Next, the sections were washed again and nuclei were counterstained with DAPI (0.1 µg/ml) for 3 min in the dark. Finally, after removal of DAPI remnants with PBS, tissue sections were mounted using FluorSave™ reagent.

Immunostained brain sections were photographed on an Olympus FV10i confocal microscope using 60x objective. Panoramic images (2x objective) were captured using a Zyla sCMOS ANDOR camera attached to a Nikon ECLIPSE Ni-fluorescence microscope. The total number of $BrdU^+$ cells in the GL and the SGZ were manually counted in one every 3 sections under Nikon ECLIPSE Ni- fluorescence microscope. During the quantification of $BrdU^+$ cells, the investigator was blinded to the group assignment of each animal.

4.5. *Analysis of AAV2-BR1-p16-GFP transduction in BECs and its effects on neurogenesis*

C57BL/6 mice of 3-months-old received an intravenous (i.v.) injection of $1x10^{12}$ gc of the adeno-associated AAV2-BR1-p16-GFP virus vector into the tail vein (using BD Micro-Fine™ insulin syringes u-100, 29G). To serve as a control, another group of age-matched C57BL/6 mice received an injection of PBS instead. In addition, 14 days after vector/PBS administration, mice were i.p. injected with BrdU twice for 3 consecutive days (see **Method 4.4**). Mice were euthanized by cervical dislocation 31 days after virus injection, and the brain and a portion of the right lobe of the liver were extracted. The bulbs were isolated and the hippocampus was dissected and both were immersed in 4% PFA (diluted in PB) for 24 h for subsequent sectioning (vibratome, Leica VT1000). Immunohistochemical analysis of neurogenesis was performed by quantifying $BrdU^+$ cells in the OB and the SGZ (see **Method 4.4.**). The remaining brain tissue was processed for assessment of vector transduction and endothelial senescence by FACS (see **Method 3.2.**)**.** Liver tissue was minced and digested following the same procedure exposed in **Method 3.3**. After tissue digestion and cell suspension filtration, liver and brain samples were incubated with CD45 and CD31 antibodies to analyse the percentage of GFP^+ cells in the endothelium by flow cytometry.

For senescence assessment in BECS, live cells were incubated with 2 µM NBGal for 15 min for the detection of SA-β-Gal activity. DAPI (0.1 µg/ml) was used for the exclusion of dead cells. On the other hand, the remaining brain cells were fixed and permeabilized according to the protocol of the BD Pharmingen™ Transcription-Factor Buffer Set (cat. no. 562725). Fixed cells were first incubated with the primary antibodies p16, γH2AX and GFP (Aveslab, cat. no. GFP-1020), and then with the appropriate fluorescently-labelled secondary antibodies (Alexa Fluor™) (**Annex I, table 1 and 2**). Finally, cell pellets (500 x*g*, 5 min) were resuspended in 0.5 ml FACS buffer and samples were analysed on an LSR-Fortessa cytometer (BD). Results were obtained using FlowJo_v10.8.1 software.

The flow cytometry analysis strategy consisted of selecting $CD31^+$ cells following the gating protocol previously described (**Method 3.2**) and evaluating the percentage of GFP^+ BECs in adeno-associated vector-injected mice compared to PBS-injected controls. In parallel, BECs from virus-administered mice were compared to liver ECs and $CD31^-$ brain cells in order to assess the selectivity of the vector for targeting BECs. The overexpression of p16 in these same cell populations was also examined to ensure the specificity of the strategy. Furthermore, we evaluated the levels of p16 within the most positive (20% of most immunopositive, or GFP^{high}, cells) and most negative (20% of most immunonegative, or GFP^{low}, cells) subpopulations of BECs for GFP in the animals injected with the vector. Additionally, we also checked the levels of other markers associated with senescence in BECs, such as β-Gal activity and γH2AX, not only comparing virus-injected and control mice, but also within the $GFP^{high/low}$ subpopulations of BECs in vector recipient mice.

4.6. *Fluorescent tomato lectins for imaging of blood vessels in SEZ whole-mount preparations*

C57BL/6 mice were deeply anaesthetised by i.p. injection of a mixture of medetomidine (0.5-1 mg/kg) and ketamine (50-75 mg/kg) diluted in saline (0.09% NaCl). Subsequently, mice were intracardiac (i.c.) injected (using BD Micro-Fine™ insulin syringes, 29G) with 488 fluorescently-labelled tomato lectins from *Lycopersicon esculentum* (Sigma-Aldrich, cat. no. L0401) at a concentration of 0.8 mg/ml (100 µl/animal). After 1 min, mice were transcardiac perfused with 0.09% NaCl for 5 min. The brains were then extracted and the SEZ isolated as a whole-mount. Moreover, the SEZ tissue was incubated with 2 µM NBGal in EndoGRO-LS (Sigma-Aldrich, SCME001) basal medium in a 48-well plate for 15 min at 37 °C and 5% CO_2. After washing the SEZ whole-mount 3 times with PBS, it was carefully placed on an Ibidi® 35 mm dish (Ibidi®, cat. no. 81158). The remnants of liquid were removed to favour the adhesion of the fresh tissue to the dish surface. We avoided using fixatives in order to ensure the efficiency of the β-Gal activity-based probe. The animals were processed in a staggered manner and images were captured for 40 min *per* sample using an Olympus FV10i confocal laser microscopy and 60x objective (**Graphical method 10**).

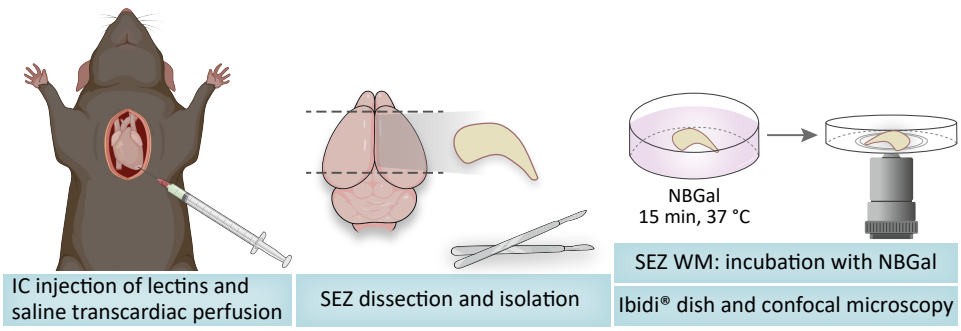

Graphical method 10. Lectin-labelling of brain blood vessels and imaging of SEZ whole-mount preparations.

5. Statistical analysis and data representation

All statistical tests were performed using the GraphPad Prism 8.0.2 software for Windows. Analyses of significant differences between means were assessed by unpaired or paired two-tailed Student's t-test when appropriate. In addition, two-way ANOVA and Tukey's multiple comparisons post-hoc test were used when applicable. P-values lower than 0.05 were considered as statistically significant and referred as *p<0.05, **p<0.01, ***p<0.001 and ****p<0.0001. Graphs always present data as the mean ± standard error of the mean (SEM). Statistical analysis details and the number of experiments performed with independent cultures/animals (n) are indicated in the figure legends or shown in the graphs.

The figures of this thesis, and the graphical representation of the results, were designed and created using GraphPad Prism 8.0.2 and Adobe Illustrator 2020 software. Furthermore, some of the images included were obtained from BioRender.

Results

1. Development of novel strategies for longitudinally monitoring ageing-associated senescence *in vivo*

Chronic accumulation of senescent cells in tissues has been identified as a major driver of ageing and a cause of many age-related pathologies (Herranz and Gil, 2018; López-Otín et al., 2023). Nevertheless, the impact of increased senescence burden on ageing-associated disorders has been scarcely investigated, mainly due to the lack of reliable reagents for non-invasive *in vivo* detection of senescent cells. We set out to delve deeper into the relationship between the burden of senescent cells and ageing. To this end, we closely monitored the progression of ageing in mouse models of accelerated (SAMP8) and natural (C57BL/6) ageing, and analysed its correlation with systemic β-Gal activity using non-invasive fluorescence methods.

1.1. *Longitudinal characterisation of ageing progression*

SAMP8 mice are a well-established model of accelerated ageing, characterised for exhibiting an earlier functional decline compared to naturally ageing mice (Takeda et al., 1981; Hosokawa et al., 1984). For the gerontological field, this strain has the advantage of allowing longitudinal assessment of age-related alterations over a relatively short period of time. However, except for their impaired memory and learning skills that have been extensively evaluated, studies on the course of ageing and its associated phenotypic changes from an early age are still lacking in this model (Akiguchi et al., 2017; Fernández et al., 2021). Analyses of this magnitude can be useful in understanding the physiological deterioration of SAMP8 mice, enabling the identification of turning points at which severe deficits appear compared to naturally ageing mice. Following this idea, we decided to perform a comprehensive characterisation of the progression of ageing in SAMP8 animals compared with their control strain resistant to accelerated senescence, SAMR1. On this basis, we have conducted several meticulously selected tests covering an age range of 2 to 12 months, which have allowed us to detect the onset of deficits at physical, neurological, tissue renewal and metabolic levels.

As weight can vary with increasing age, we tracked the mean body weight of the SAM mice through different ages and found clear disparities between both strains almost from the beginning. SAMP8 mice are heavier from very early adulthood compared to age-matched SAMR1 mice. They experience a significant increase in body weight from 2 to 6 months of age (when peak weight was recorded) (**Figure 7a**). The elevated body weight of SAMP8 mice may be associated with their low physical activity, which contributes to exacerbated functional impairment and disability. Nonetheless, from 9-months onwards, the weight of the mice equalises between the two strains, which is the period when a rapid decrease in muscle mass has been reported in SAMP8 animals (Guo et al., 2015).

Ageing entails a progressive decrease in tissue capacity for repair and regeneration. We have previously described how the dynamics of SAMP8 NSCs include hyperproliferation followed by NSC depletion (Soriano-Cantón et al., 2015). Along the same lines, changes in the SC compartments of the interfollicular epidermis of 12-month-old SAMP8 mice have been reported (Changarathil et al., 2019). Ageing drives cell-cycling defects that can ultimately result in impaired SC follicle regeneration. Here, we report dramatic differences in hair recovery after shaving between SAMP8 and SAMR1 mice as early as 5 months of age. Of note, there is a substantial slowdown in hair growth from 3 to 5 months of age in SAMP8 animals (**Figure 7b**). These results suggest that SC depletion in the epidermis may be occurring earlier than expected and remains until advanced ages, leading to the characteristic alopecia that elderly SAMP8 mice exhibit.

Metabolic disorders, such as metabolic syndrome, are also commonly associated with advancing age (Goldsworthy and Potter, 2014). SAMP8 mice have been reported to develop metabolic disturbances, including insulin resistance and visceral fat expansion, which are responsible for impaired glucose tolerance in the elderly (Liu et al., 2017). In order to assess potential age-related impairment of glucose processing,

we performed a Glucose Tolerance test in SAMP8 and SAMR1 mice by administering a certain dose of glucose and monitoring its levels in the blood. Although there were no significant differences at 4 months, 6-month-old SAMP8 mice took longer to control the rise in blood glucose, showing significantly higher glycaemic peaks than their SAMR1 counterparts (**Figure 7c**). Hence, from middle age onwards, metabolic processing of glucose differs between SAMP8 and SAMR1 mice, with the SAMP8 mice regulating blood glucose levels less efficiently. This is likely due to the age-related increase in insulin resistance, which can have serious systemic effects, particularly in the brain, as the primary consumer of glucose-derived energy. Elevated insulin resistance in the brain can impair cognitive function and contribute to the distinctive cognitive deficits observed in SAMP8 animals (Rhea and Banks, 2017).

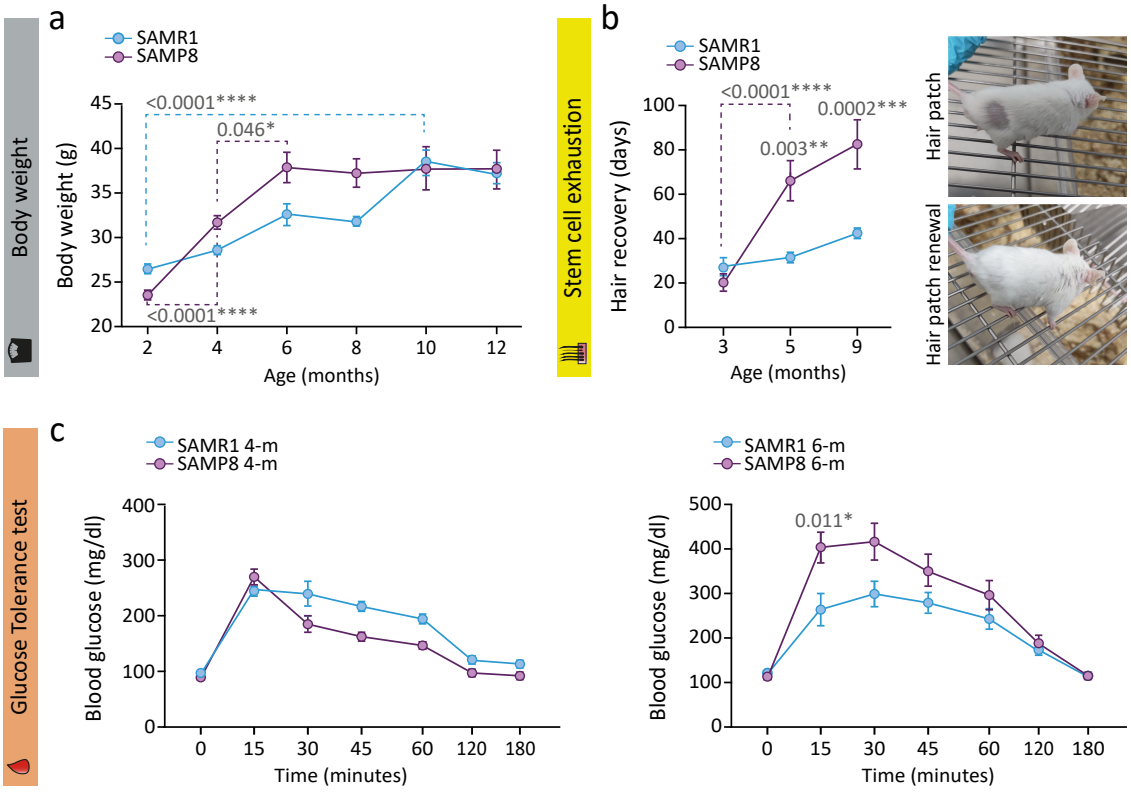

Figure 7. Assessment of premature ageing-related parameters in SAMP8 and SAMR1 strains. a) Body weight recording of SAMP8 and SAMR1 mice from 2 to 12 months of age (minimum of n= 8 animals *per* strain and age). **b**) Measurement of the time required for mouse hair to recover after shaving a small area. Note that SAMP8 mice take longer to renew the hair patch. The number of SAMR1 animals used for this test was as follows: 3-month-old (-m) n=9, 6-m n=6, 9-m n=7; whereas of SAMP8 mice: 3-m n=10, 6-m n=5, 9-m n=5. **c**) Glucose tolerance evaluation in SAMP8 and SAMR1 mice. For this test, 4-m SAMR1 (n=6) and SAMP8 (n=6) and 6-m SAMR1 (n=7) and SAMP8 (n=7) mice were used. Observe that while glucose metabolism is not affected at 4-m of age, regulation of blood glucose levels is impaired at 6-m in sAMP8 mice. The graphs show the mean ± SEM. Two-way ANOVA, simultaneously comparing SAM "strain" and "age", and Tukey's multiple comparisons post hoc test were used for statistical analysis of the data represented in graphs *a* and *b*. Of note, unpaired Student's t-test analysis of body weight comparing only "mouse strain" (at the same ages) shows significant differences at 4 (p-value=0.0019) and 6 months of age (p-value=0.044) between SAMP8 and SAMR1 mice. Two-way repeated-measures ANOVA was used for the analysis of glucose tolerance, i.e. data shown in graphs *c*. The exact p-values are indicated in the graphs.

Focusing on the physical fitness of SAMP8 mice, we performed various tests specifically designed to assess the age-associated decline in skeletal muscle strength and muscular endurance. For instance, the Grip Strength and Weight tests provide insight into the neuromuscular function of the mice by measuring the maximum strength of their front paws and the maximum weight they are able to lift, respectively. SAMP8 mice showed no signs of muscle deterioration in these tests at 3 months, but a clear drop in

strength was observed from 5 months onwards. As expected, both tests showed an earlier decline in muscle function in SAMP8 compared to SAMR1 mice (**Figure 8a,b**). Interestingly, this weakness in the SAMP8 strain is almost maintained from onset throughout adulthood, suggesting that these animals suffer severe deficits in skeletal muscle that plateau from an early age. On the other hand, SAMR1 mice experience a progressive decline in muscle strength with age, and thus the differences between one strain and another diminish at older ages.

Furthermore, we conducted a Grid test to evaluate the muscle endurance of mice limbs, albeit it also involves certain motor coordination skills. Mice exert greater grip strength and direct their movements with their front paws, using their hind paws for support and the tail as a guide for positioning. Therefore, the Grid test involves strength to grip the grid and endurance to hold on for a period of time, but also requires coordination of movements. In concordance with the other fitness tests, the results indicated that SAMP8 animals experience an abrupt decline in limb grip resistance between 3 and 5 months of age (P= <0.0001, as in the Grip Strength and Weight tests). On the contrary, SAMR1 animals show a gradual decrease in physical endurance, but still perform better in this test at older ages than SAMP8 mice (**Figure 8c**). The data revealed a marked early decline in muscle strength and endurance in SAMP8 mice, which likely precedes the loss of skeletal muscle mass and function (sarcopenia) described in these animals at older ages (Sousa-Victor et al., 2014; Huang et al., 2021).

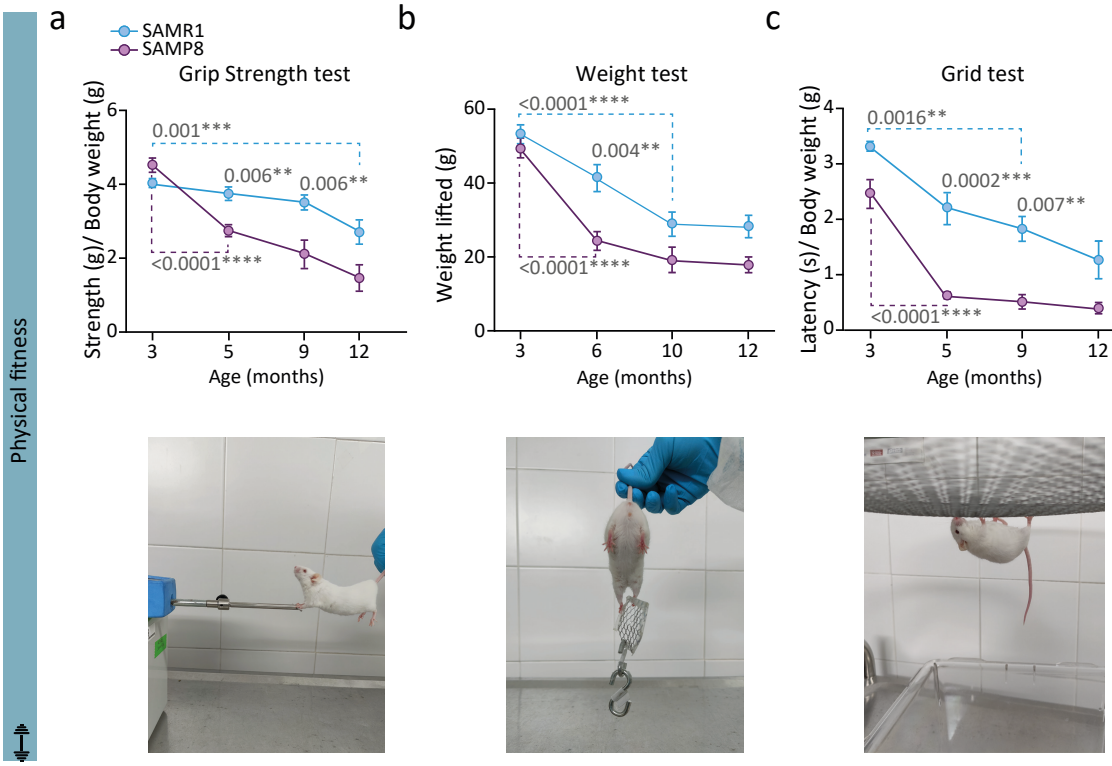

Figure 8. Physical fitness evaluation of SAMP8 and SAMR1 mice over time. a) Measurement of forelimb grip strength normalised by animal body weight, comparing SAMP8 and SAMR1 mice at different ages (SAMR1 mice: 3-m n=8, 5-m n=8, 9-m n=5, 12-m n=5; SAMP8 mice: 3-m n=11, 5-m n=12, 9-m n=5, 12-m n=5). Illustrative photograph of a mouse performing the Grip Strength test. **b**) Measurement of the maximum weight lifted by mice in the Weight test, comparing SAMP8 and SAMR1 mice at different ages (SAMR1 mice: 3-m n=8, 6-m n=12, 10-m n=8, 12-m n=10; SAMP8 mice: 3-m n=5, 6-m n=10, 10-m n=9, 12-m n=7). Illustrative photograph of a mouse performing the Weight test. **c**) Comparison of the latency times, normalised by the body weight, of SAMR1 and SAMP8 mice at different ages during the Grid test (SAMR1 mice: 3-m n=6, 5-m n=7, 9-m n=9, 12-m n=6; SAMP8 mice: 3-m n=15, 5-m n=11, 9m n=7, 12-m n=6). Illustrative photograph of a mouse performing the Grid Test. The graphs show the mean ± SEM. Two-way ANOVA, simultaneously comparing SAM "strain" and "age", and Tukey's multiple comparisons post hoc test were used for statistical analysis. The exact p-values are indicated in the graphs.

The motor system represents the main component of interaction with the environment for a mouse. Accordingly, when impaired, it can lead to disruptions in a variety of functions, including exploration, feeding, social interaction and learning. Although the Grid test has a motor coordination component, we decided to specifically examine whether a failure at this level might be contributing to the poor physical performance of SAMP8 animals. Motor coordination was examined with the Pole test, in which mice learn to walk down a stick by coordinating the movement of their front and hind limbs. Despite its experimental simplicity, many types of neuronal dysfunction and basal ganglia disorders can alter mouse performance in this test (Fernagut et al., 2003; Fleming et al., 2004; Recasens et al., 2014). Indeed, from 7 months onwards, SAMP8 mice were notably less adept at synchronising their front and rear limbs to accomplish the task than SAMR1 mice (**Figure 9a**). Additionally, we used the "hind limb clasping" severity score to further assess motor behaviour. The hind limbs of a healthy mouse generally open and stretch when held by the tail for a few seconds. This positioning reflex depends on the spinal motor pathways responsible for fore and hind limbs movement (Lalonde and Strazielle, 2011). However, in the context of neurodegeneration, this reflex begins to deteriorate and the hind limbs start to retract rather than stretch (Chou et al, 2008; Guyenet et al, 2010). Remarkably, we found a mild hind limb clasping in SAMP8 mice from 4 months of age that became more evident with increasing age, while it was absent in SAMR1 mice at all ages evaluated (**Figure 9b**). This progressively deteriorating motor coordination reflex suggests neurodegenerative processes that evolve with age in SAMP8 animals and can be easily monitored. Unlike motor coordination, locomotion analysis from the Open Field test show no differences between SAMR1 and SAMP8 mice. Nonetheless, both strains displayed a greater speed and distance travelled as they aged, which is consistent with the hyperactivity disorders reported in these mice (Yagi et al., 1988) (**Figure 9c**).

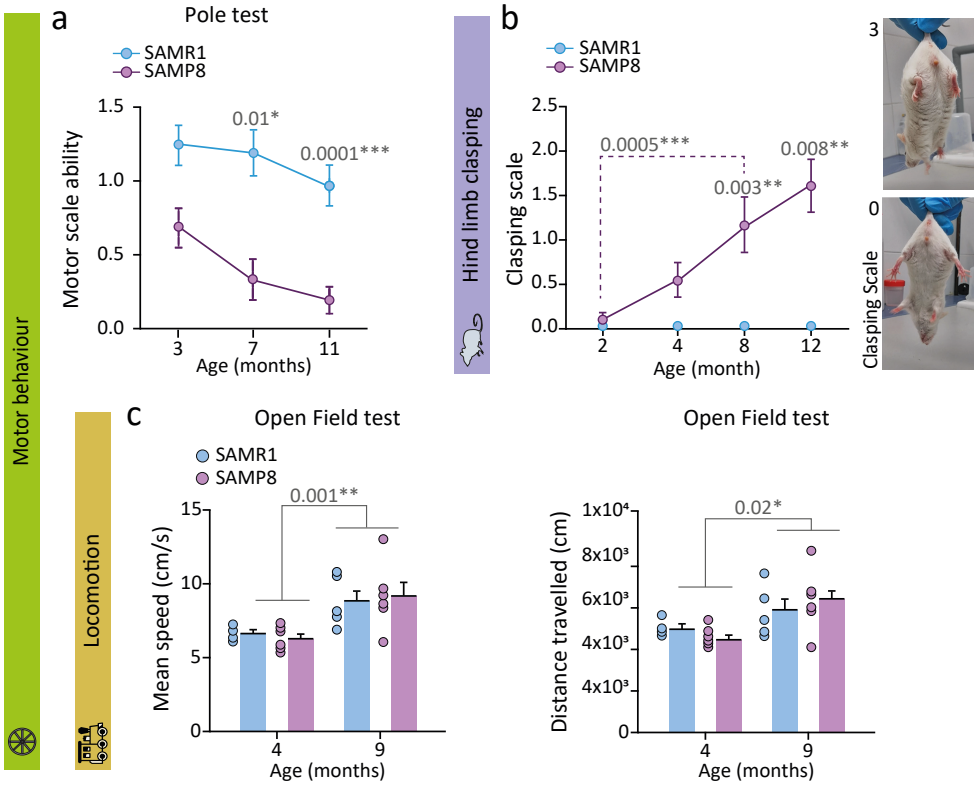

Figure 9. Assessment of general motor behaviour during accelerated ageing. a) Evaluation of motor coordination of SAMP8 and SAMR1 mice using the Pole test at 3, 7 and 11 months of age (SAMR1 mice: 3-m n=11, 7-m n=7, 11-m n=19: SAMP8 mice: 3-m n=11, 7-m n=9, 11-m n=16). **b**) Assessment of hind paw motor reflex through the Hind limb Clasping test in SAMP8 and SAMR1 mice at different ages (SAMR1 mice: 2-m n=14, 4-m n=10 , 8-m n=10, 12-m n=7; SAMP8 mice: 2-m n=10, 4-m n=6, 8-m n=8 , 12-m n=5). On the right, representative illustration of the clasping scale score when the hind limb clasping reflex is not affected (0) and when it is severely affected (3).

(Figure 9. Continued) **c)** Assessment of locomotion parameters, such as mean speed and total distance travelled, in 4- and 9-m SAMR1 and SAMP8 mice, using the Open Field test. Note that there are no significant differences in locomotion between both strains. The graphs show the mean ± SEM. Two-way ANOVA, simultaneously comparing SAM "strain" and "age", and Tukey's multiple comparisons post hoc test were used for statistical analysis. The exact p-values are indicated in the graphs.

One of the most prominent signs of brain ageing, is the increase in anxious behaviour (Meeker et al., 2013; Yanai and Endo, 2021). Anxiety is also measured in the Open Field test. Anxious mice spend less time in the unprotected central area of the open field, displaying an anxiety-related phenomenon called thigmotaxis. This was evaluated by analysing the time mice spent in a delimited central area versus the time spent in the peripheral area closer to the walls of the box (Tucker and McCabe, 2021). We observed that thigmotaxis appears as early as 4 months of age in the SAMP8 strain and in the absence of deficits in locomotion, as shown before. SAMP8 mice spent significantly more time in the peripheral zone during the Open Field test, as they presumably perceive more safety and security in this area, and this fact persisted with age (**Figure 10a,b**). This means that there are anxiety-like signs that emerge in young SAMP8 animals and will remain a stable trait of altered behaviour. Therefore, anxiety appears as a feature of functional ageing in the SAMP8 strain in which emotional deficits are prevalent from an early age.

Given that anxiety has been shown to be a robust characteristic of ageing in SAMP8 mice, we decided to also evaluate this behavioural trait in naturally ageing C57BL/6 mice. In this regard, we analysed anxious behaviour by comparing 3- and 17-month-old C57BL/6 mice using the Open Field test (**Figure 10c,d**), as before, but also the EPM. In the latter, anxious mice tend to spend more time in the closed than in the open arm of the elevated maze, as they perceive this area as safer. Notably, both tests showed increased signs of thigmotaxis in the older mice (**Figure 10e,f**), overall, pointing to anxious behaviour as a useful parameter for monitoring ageing and/or anti-ageing therapies.

This work has allowed us to accurately characterise the ageing process in mice with the SAM genetic background. Importantly, we have detected an earlier onset of deficits than previously reported, possibly due to the age range assessed and the tests selected. Longitudinal examination of age-associated phenotypic features has enabled us to identify target ages in the SAMP8 strain for potential rejuvenating approaches. For instance, the age range of 5-7 months is of interest, as several deficits appear during this period, including impaired physical fitness and motor coordination, but there is still room for improvement. This study could be valuable for assessing or monitoring ageing-related interventions, such as drug therapies or lifestyle changes. In this respect, increased anxious behaviour emerges as a hallmark of ageing in the SAMP8 strain from an early age, and also occurs during natural ageing in the C57BL/6 strain.

1.2. *In vitro and ex vivo validation of novel molecular probes for senescent cell detection*

Assessing the rise of senescent cells in tissues with ageing is not a trivial task, both because of the phenotypic diversity of these cells and the limited methods for their detection. SA-β-Gal activity constitutes one of the most widespread biomarkers for senescent cell recognition. Given the extensive limitations of the classical X-gal histochemical reaction for *ex vivo* or *in vivo* functional analysis, molecular probes are emerging to fluorescently detect β-Gal activity in live cells. Our group has designed and developed several fluorogenic probes to identify senescent cells based on their enhanced β-Gal activity. These probes consist of a fluorescent dye conjugated to a galactose derivative and their mechanism of action employs an OFF/ON scheme. The molecular probes display a quenched fluorescence (OFF) until the β-Gal enzyme releases the dye by hydrolysis of an intramolecular O- or N-glycosidic bond. Once cleaved, the fluorophore emits fluorescence (ON). Hence, a greater amount of the highly fluorescent dye is released in cells with increased β-Gal levels (Lozano-Torres et al., 2017; 2023).

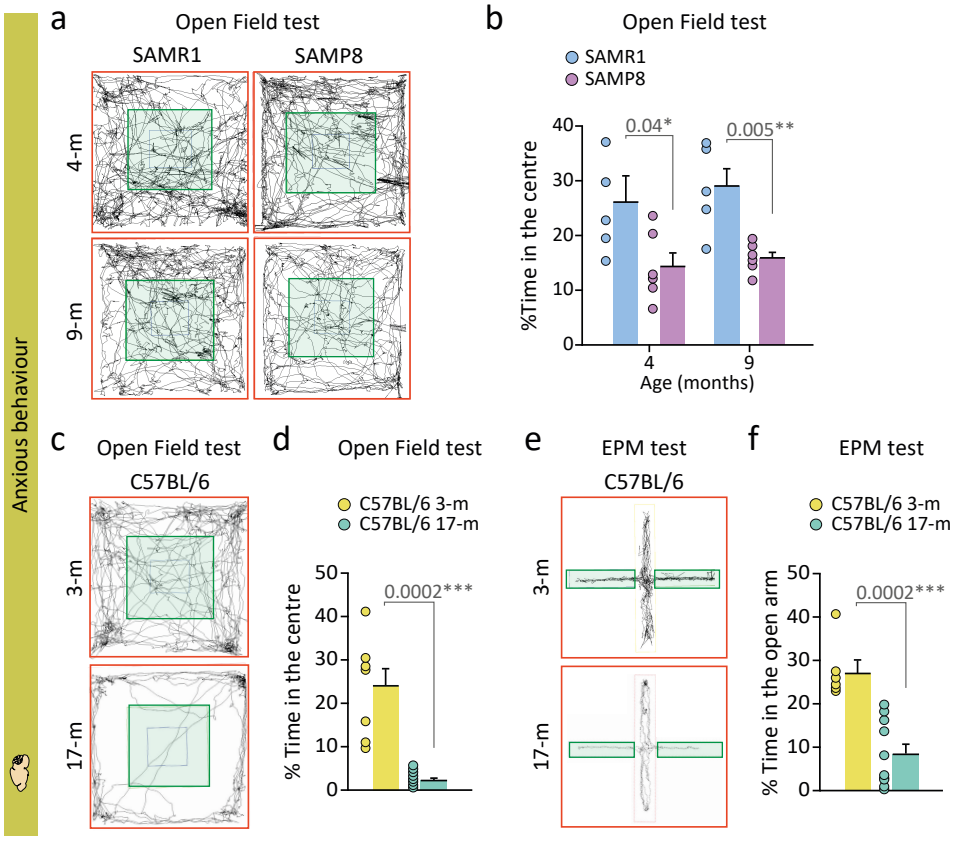

Figure 10. Evaluation of anxious-like behaviour during accelerated and natural ageing. a) Representative map of movement in the Open Field test comparing SAMR1 and SAMP8 mice at 4- and 9-m. **b**) Percentage of time that 4- and 9-m SAMR1 and SAMP8 mice spent in the centre of the open field (green area). Note that the avoidance of the central area, or thigmotaxis, of the SAMP8 mice is not due to differences in locomotion (**Figure 9**). **c**) Representative map of movement in the Open Field test of 3-m versus 17-m C57BL/6 mice. **d**) Percentage of time that 3- and 17-m C57BL/6 mice spent in the centre of the open field. Notice that older C57BL/6 mice exhibit significantly increased thigmotaxis in their behaviour during the test. **e**) Representative map of movement in the EPM test of 3-m versus 17-m C57BL/6 mice. **f**) Percentage of time that mice spent in the open arm during the EPM test. Observe that younger mice spent notably more time in this open area. The graphs show the mean ± SEM. Unpaired Student's t-test was used for statistical analysis. The exact p-values and the number of independent biological samples (represented as dots) used are indicated in the graphs.

To test the efficacy of these new fluorogenic probes against traditional methods, we first developed an *in vitro* model of cellular senescence with primary human ECs (hUVECs) through pharmacological intervention. We induced EC senescence with the drug palbociclib, which selectively inhibits CDKs 4 and 6. CDKs 4/6 can bind cyclin D1 leading to hyperphosphorylation of the retinoblastoma (Rb) protein and release of E2F1, which is essential to promote cell cycle progression from G1 phase to initiate DNA synthesis in S phase. However, the blockade of these CDKs leads to G1 arrest triggering a cellular response that can lead to a senescent fate mainly mediated by the p53-p21 pathway (Barr and McClelland, 2022). Palbociclib-treated cells exhibited a characteristic senescent profile. This included an enlarged shape, heightened β-Gal activity indicated by histochemical X-gal staining, reduced proliferation revealed by low Ki67 levels, upregulation of the cell cycle inhibitor p21, disrupted nuclear lamina and loss of Lamin B1, and the presence of DNA damage foci immunopositive for γH2AX. All these well-accepted markers validated this *in vitro* model of endothelial senescence (**Figure 11a-c**).

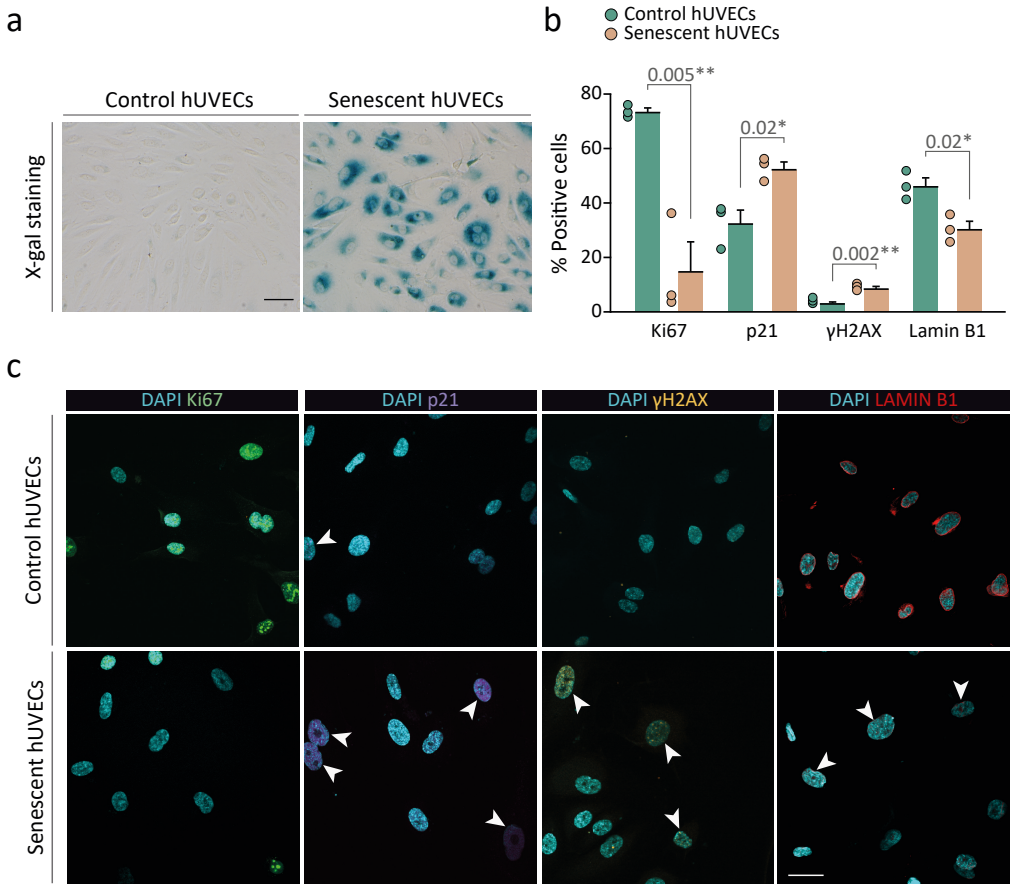

Figure 11. Characterisation of an *in vitro* model of senescence using hUVECs. a) Cytochemical X-gal staining for assessing β-Gal activity in cells treated with the senescence-inducing drug palbociclib, compared to untreated (control) cells. Note that palbociclib-treated cells exhibited not only higher levels of β-Gal activity, but also an elongated morphology. **b**) Immunofluorescence analysis of senescence-associated markers, comparing control and palbociclib-treated cells. **c**) Representative confocal images of control and senescent cells labelled with the senescence markers listed in graph *b*. The arrows indicate immune-positive cells in which fluorescence signal is not easily discernible. The graphs show the mean ± SEM. Unpaired Student's t-test was used for statistical analysis. The exact p-values and the number of independent biological samples (represented as dots) used are indicated in the graphs. Scale bars: 100 µm.

Subsequently, we used control and palbociclib-treated hUVECs to determine SA-β-Gal activity with our novel in-house fluorogenic probes AHGa, WOS-Cy7Gal and NBGal, each containing a dye displaying a different fluorescence emission range, green for the first one and red for the other two (Lozano-Torres et al., 2017; 2023; Rojas-Vázquez et al., submitted). The fluorophore released is retained cell lysosomes and exhibit a stippled pattern with a stronger fluorescent signal in senescent cells, as evidenced in confocal microscopy images (**Figure 12a-c**). The MFI can be quantified by FACS, with the advantage that the probe-associated fluorescence is measured in live cells and the labelling of senescent cells depends only on the activity of the enzyme, without relying on pH or fixation conditions as is the case for X-gal staining and other commercialised probes (Debacq-Chainiaux et al., 2009; Ogawa et al., 2021). The results revealed that palbociclib-treated cells show at least double the fluorescence intensity of untreated (or control) hUVECs (**Figure 12a-c**).

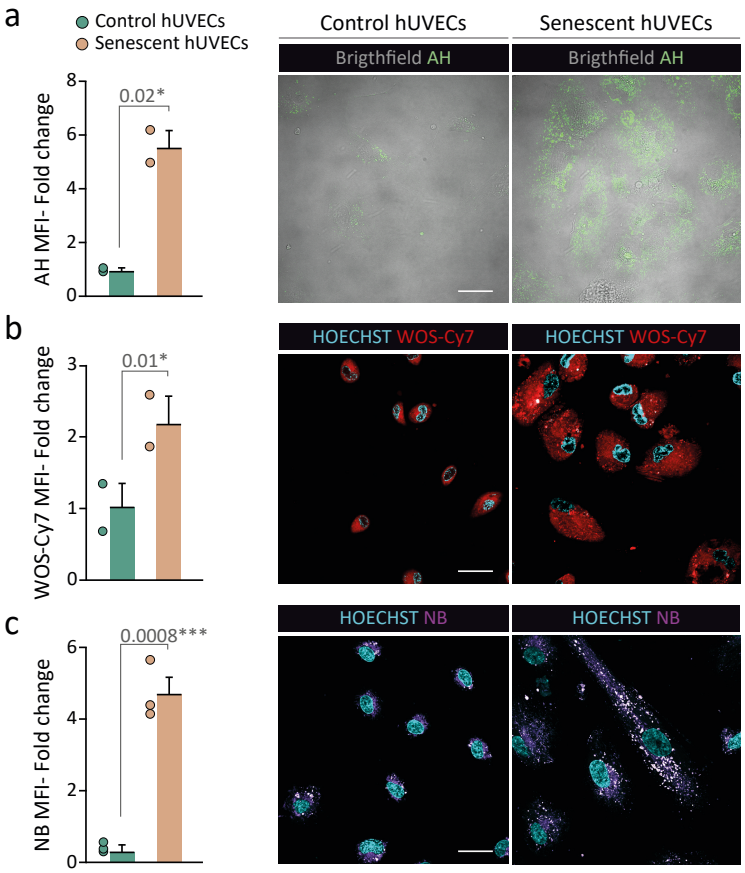

Figure 12. *In vitro* validation of new fluorogenic probes for SA-β-Gal detection. **a)** Analysis of the AHGa probe-associated fluorescence by flow cytometry, comparing the MFI of the AH dye between control and senescent hUVECs. Representative confocal images of control and senescent hUVECs labelled with this molecular probe on a brightfield background. **b**) Analysis of the WOS-Cy7Gal probe-associated fluorescence by flow cytometry, comparing the MFI of the WOS-Cy7 dye between control and senescent hUVECs. Representative confocal images of control and senescent hUVECs labelled with this molecular probe. **c**) Analysis of the NBGal probe-associated fluorescence by flow cytometry, comparing the MFI of the released NB dye between control and senescent hUVECs. Representative confocal images of control and senescent hUVECs labelled with this molecular probe. Hoechst is used for nuclei staining. Fold change is calculated relative to control hUVECs MFI. The graphs show the mean ± SEM. Unpaired Student's t-test was used for statistical analysis. The exact p-values and the number of independent biological samples (represented as dots) used are indicated in the graphs. Scale bars: 100 µm.

HUVECs are primary cells and can undergo senescence in culture after multiple passages (Ohori et al., 2021; Chala et al., 2021). To further explore the potential of these probes in a model of EC replicative senescence, we passaged hUVECs up to 29 times and compared them with cells at shorter passages (less than 10). In this model, cells at advanced passages showed clear senescent traits, such as increased p16 and γH2AX levels, as well as greater β-Gal activity, which was evidenced by the fluorogenic probe WOS-Cy7Gal and supported by classical X-gal staining (**Figure 13a-d**).

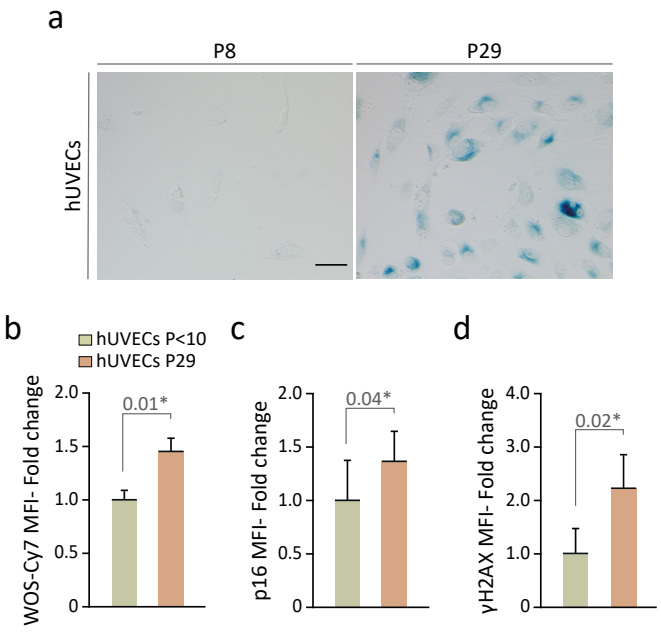

Figure 13. Evaluation of WOS-Cy7Gal efficiency for replicative senescence detection in hUVECs. **a**) Cytochemical X-gal staining for assessing β-Gal activity in hUVECs that have undergone 29 passages to induce replicative senescence, compared to hUVECs with less than 10 passages (control). **b**) Analysis of SA-β-Gal by flow cytometry using the WOS-Cy7Gal probe in long-passage versus short-passage hUVECs. **c**) Evaluation of p16 levels by flow cytometry in this model of replicative senescence. **d**) Assessment of γH2AX levels by flow cytometry in this model of replicative senescence. Fold change is calculated relative to short-passage hUVECs. The graphs show the mean ± SEM (n=3 for control and senescent cells). Paired Student's t-test was used for statistical analysis of hUVECs replicative senescence as cells proceeds from the same source. The exact p-values are indicated in the graphs. Scale bar: 100 µm.

Since we had observed clear signs of ageing in SAMP8 versus SAMR1 mice from an early age, we aimed to examine its correlation with the senescent cell burden. In this regard, we selected two representative organs to estimate the senescence load in 7-month-old mice of the two genetic backgrounds. In particular, we targeted liver and kidney, which are commonly associated with age-related accumulation of senescent cells and the development of senescence-induced disorders, such as liver cirrhosis or chronic kidney disease (Ogrodnik et al., 2017; Docherty et al., 2020). We measured the level of widely-accepted senescence markers by flow cytometry in both tissues, including p16, Lamin B1 and SA-β-Gal activity. We detected an increase of the cell cycle inhibitor p16 and a decrease of nuclear Lamin B1 levels in SAMP8 organs (**Figure 14a,b)**. To measure lysosomal β-Gal activity levels, we employed the fluorogenic probe WOS-Cy7Gal, which had demonstrated a reliable readout of β-Gal activity in both pharmacological and replicative-induced senescence models. The analysis revealed a higher β-Gal activity in SAMP8 compared to SAMR1 mice (**Figure 14c**). These findings confirm that there is a significant increase in the accumulation of senescent cells in the organs of SAMP8 mice as young as 7 months of age. This may account for the deficits we identified in our longitudinal study of ageing and further supports the efficiency of our probe in determining age-related senescence. Although this approach has enabled us to assess the senescent cell burden *ex vivo*, we sought for strategies to evaluate senescence *in vivo*, which would allow for longitudinal studies without the need to euthanize animals.

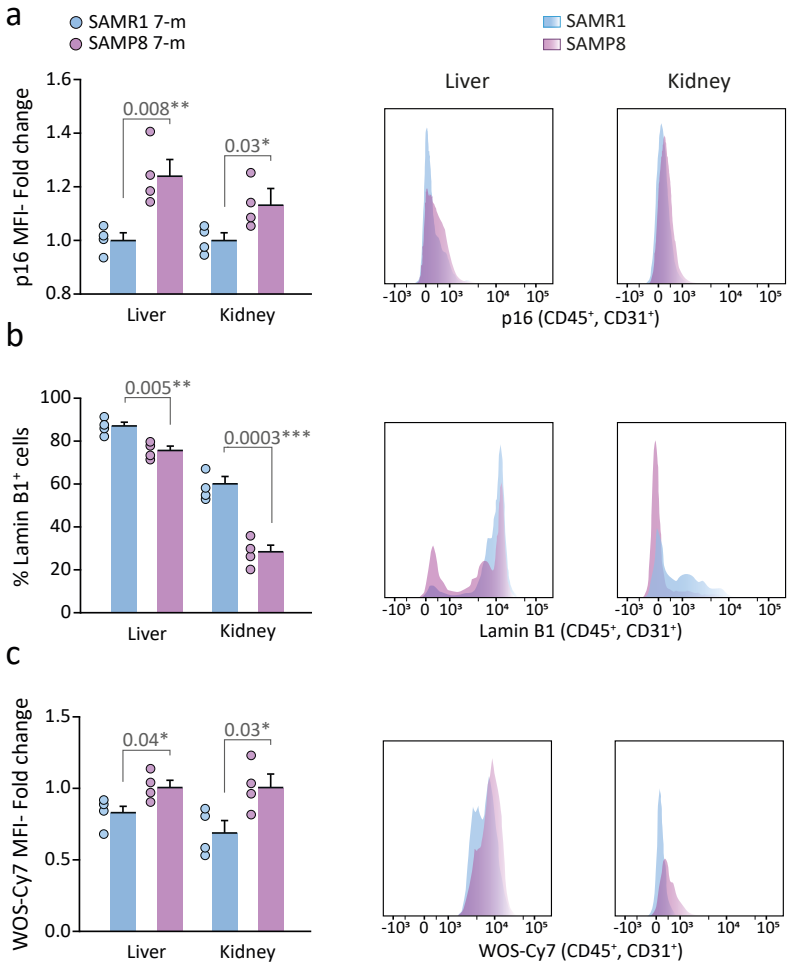

Figure 14. *Ex vivo* analysis of the senescent cell burden in SAMP8 and SAMR1 animals. a) *Ex vivo* flow cytometry analysis of p16 MFI in liver and kidney tissues of 7-m SAMP8 and SAMR1 mice. Representative FACS histogram. **b**) *Ex vivo* flow cytometry analysis of the percentage of lamin B1⁺ cells in liver and kidney tissues of SAMP8 and SAMR1 mice. Representative FACS histogram. **c**) *Ex vivo* flow cytometry analysis of SA-β-Gal activity, based on the measurement

(Figure 14. Continued) of WOS-Cy7Gal-associated MFI, in liver and kidney tissues from SAMR1 and SAMP8 mice. Representative FACS histogram. Fold change is calculated relative to SAMR1 mice organs for each senescence-associated marker. The graphs show the mean ± SEM. Unpaired Student's t-test was used for statistical analysis. The exact p-values and the number of independent biological samples (represented as dots) used are indicated in the graphs.

1.3. *Non-invasive monitoring of age-related senescent cell burden in vivo*

To meet the challenge of *in vivo* senescence detection, we decided to chemically modify the WOS-Cy7Gal probe to generate a new one that, following the same molecular logic, could be rapidly excreted and recovered in urine. For this purpose, we added two sulfonic groups to the fluorophore molecule (cyanine-7, Cy7), since the presence of negatively charged functional groups in the correct spatial position appears to favour diffusibility (**Figure 15a**) (Nishijima et al., 2010). From now on, we refer to the probe with sulfonic groups as Cy7Gal, as the previous one did not contain them and was named WOS (from "without sulfonic groups")-Cy7Gal. We first tested Cy7Gal in our well-characterised *in vitro* model of cell senescence with hUVECs treated with the drug palbociclib. We observed that the fluorescence signal is notably enhanced in senescent cells, again supporting the efficiency of the probe in SA-β-Gal detection (**Figure 15b**). Intriguingly, this signal acquires a diffuse pattern only a few minutes after the addition of the probe, which differs from the rigorously dotted one that we noticed in the same cell model with the WOS-Cy7Gal probe. This is compatible with a lower retention of the probe in cell lysosomes, suggesting that free Cy7 dye rapidly diffuses to other cellular compartments and outside the cell, in agreement with its recovery in urine in the intact animal (*vide infra*).

In order to verify that the renal clearance of Cy7Gal was indeed dependent on the sulfonic groups, we decided to inject this probe, in parallel with WOS-Cy7Gal, into 15-month-old SAMP8 animals and compare their fluorescence levels in urine and plasma. To this end, we injected mice i.p. with each of the probes or only DMEM (vehicle), and collected blood (from the submandibular vein) and urine samples 10 and 15 min after injection, respectively. Measurement of the free dye fluorescence in both fluids was performed in a fluorometer. SAMP8 mice that received the Cy7Gal probe showed a significant increase in fluorescence in urine samples, while in plasma it was more moderate. In contrast, SAMP8 mice injected with WOS-Cy7Gal or DMEM exhibited no detectable signal or difference between the two (**Figure 15c**). Importantly, in a scenario where there is presumably a heavy senescence burden in the organism, these results suggest that only the dye with sulfonic groups diffuses into the bloodstream, is cleared at kidneys, and rapidly accumulates in the bladder with urine.

Next, to validate Cy7Gal in an ageing context *in vivo*, we injected this probe in 7-month-old SAMP8 and SAMR1 mice, as in our previous *ex vivo* analysis. The Cy7 fluorescence readout in urine was higher in the SAMP8 mice, in line with an increased burden of senescence in these animals (**Figure 15d**). These data indicated a good correlation between the end-point measurement of cell senescence *ex vivo,* using different well-recognised markers, and the *in vivo* global detection of β-Gal activity with the Cy7Gal probe. Therefore, Cy7Gal represents a technological breakthrough for estimating the senescent cell burden non-invasively, simply by measuring fluorescence in urine, and with great potential for longitudinal studies. Such a tool would bring senescence-related therapies considerably closer to clinical use. Consequently, we decided to test Cy7Gal potential to monitor the effects of a senolytic treatment over time.

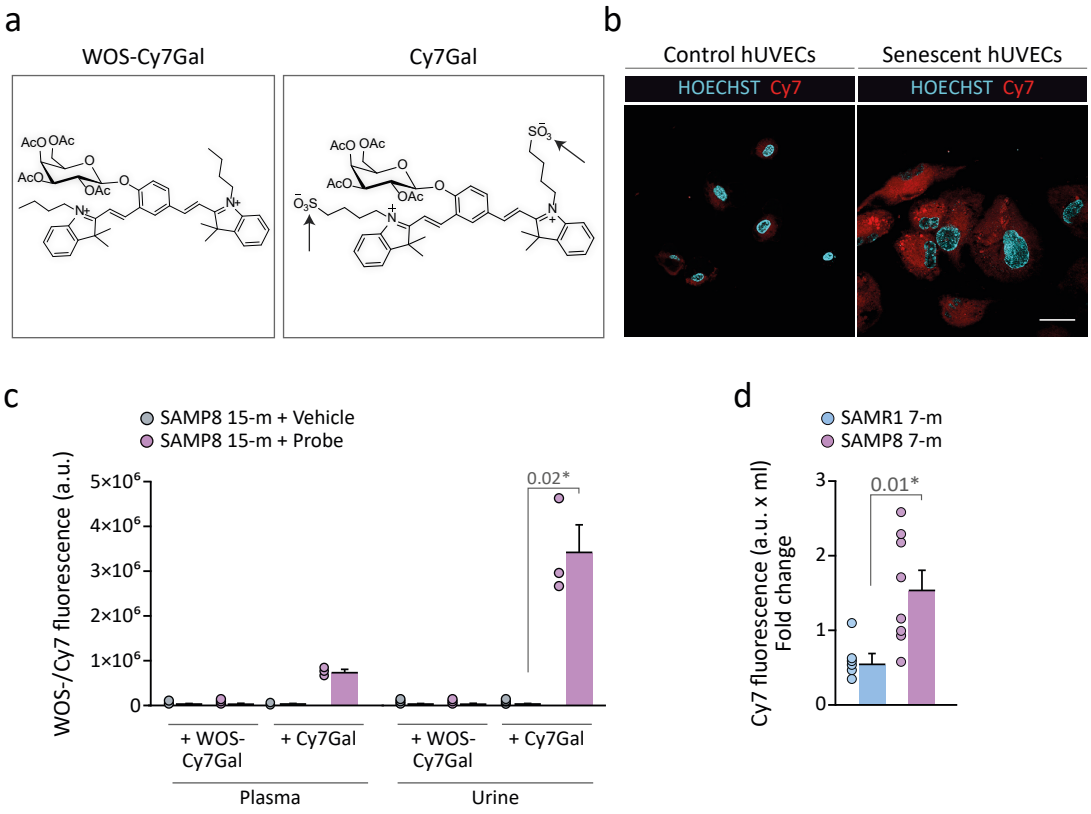

Figure 15. Cy7Gal, a new renally clearable fluorogenic probe for *in vivo* detection of β-Gal activity. a) Chemical structure of WOS-Cy7Gal and Cy7Gal. **b**) Confocal images of control and senescent (treated with palbociclib) hUVECs labelled with the Cy7Gal probe. Note that senescent cells exhibit a higher fluorescence signal, in line with a greater β-Gal activity, than control cells. **c**) Fluorescence levels in urine and plasma samples from 15-m SAMP8 mice injected with Cy7Gal, WOS-Cy7Gal, or DMEM as a control. Fluorescence measurement was performed using a fluorometer. **d**) Fluorometer measurement of Cy7 fluorescence in urine from 7-m SAMP8 and SAMR1 mice. The graph shows a.u. multiplied by the volume of urine recovered (a.u. x ml) to estimate the total amount of fluorophore in each urine sample. Fold change is calculated relative to SAMR1 mice values. The graphs show the mean ± SEM. Unpaired Student's t-test was used for statistical analysis. The number of independent biological samples (represented as dots) used and the exact p-values are indicated in the graphs. Scale bar: 100 µm.

1.4. *Longitudinal measurement of senescence and behaviour associated with accelerated ageing and its reversal by senolytics*

In our research, we had documented age-related deficits, as well as an increased senescence burden, in SAMP8 compared to SAMR1 mice at the age of 7 months. Accordingly, we targeted the same age for senolytic intervention. SAMP8 mice were treated orally for 5 weeks with the senolytic drug cocktail D+Q or with the vehicle (20% PEG-n400 and 0.9% NaCl) (**Figure 16a**). D is an inhibitor of several tyrosine-kinases used as an anti-neoplastic agent for the treatment of acute lymphocytic leukaemia, and Q is a flavonoid that acts as a BCL-XL inhibitor. Their combination has shown efficacy in counteracting mechanisms of apoptosis elusion in senescent cells, resulting in their selective elimination and consequent beneficial effects on aged organs. D+Q have been reported to alleviate age-related brain phenotypes and neurodegeneration, improving cognitive function and reducing anxiety (Zhang et al., 2019; Ogrodnik et al., 2019; Ota and Kodama, 2022; Wang et al., 2023). Based on this, anxious behaviour appears as a phenotypic trait potentially associated with the senescent cell burden. Of note, we had detected an exacerbated anxiety from 4 months of age in SAMP8 compared to SAMR1 mice.

As a correlate of the probe readout, we assessed the anxious behaviour of the mice using the Open Field test. This behavioural test revealed that the mice treated with the senolytic drugs were more predisposed to move around central areas of the open field (**Figure 16b**), exhibiting an alleviation of anxiety signs compared to untreated age-matched mice. Moreover, locomotion variables, such as total distance travelled or average speed of movement, were not affected by senolysis (**Figure 16c**). This means that the effect observed is not due to an increased hyperactivity, but to a reduced anxious perception of the open space. Relevantly, to demonstrate that these drugs are not anxiolytic *per se,* a 3-day treatment with the drugs combination did not change anxious behaviour of 3-month-old SAMR1 mice in the Open Field test (**Figure 16d**), sustaining that D+Q would not affect anxiety directly and its alleviation is a consequence of senescent cell clearance.

When we evaluated systemic cell β-Gal activity with Cy7Gal 21 days after senolytic treatment, D+Q significantly decreased Cy7 levels in urine, indicating a reduction in the burden of senescent cells in treated SAMP8 mice compared to the vehicle group (**Figure 16e**). However, when we assessed senescence more than 50 days post-treatment in the same animals, Cy7Gal indicated no differences between treated and vehicle mice, uncovering the transitory nature of these therapies (**Figure 16f**). To make sure that mice could still respond to senolysis, we decided to perform another cycle of treatment with D+Q in the same cohort of animals. After this second intervention, we found that the senolytic effects recovered, and treated mice showed markedly less Cy7Gal-associated fluorescence in urine than vehicles (**Figure 16g**). Remarkably, we identified a significant negative correlation between Cy7 fluorescence levels in urine and the time mice spent in the centre of the open field, but only in those cases where the senolytic effects were measured less than 3 weeks after the last drug administration (**Figure 16h,i**). These results reveal that treatment-induced reduction in senescence burden leads to decreased anxious behaviour in mice but, after a long period without senolytic intervention, there is a washout of drug effects.

Collectively, these data strongly suggest that the probe can be used to reliably monitor senescence *in vivo*. Hence, Cy7Gal would not only be useful for diagnosis or prognosis of senescence-associated diseases, but also for monitoring the effects of senolytic drugs that are transient and fade over time, in line with a treatment that kills senescent cells but does not eliminate the inducers of cell senescence. This opens up possibilities for longitudinal studies that are not currently feasible in humans or in experimental settings where cells cannot be extracted.

1.5. *Longitudinal measurement of senescence and behaviour associated with natural ageing and its reversal by senolytics*

With the aim of assessing age-related senescence also during natural ageing, we performed a longitudinal study with the Cy7Gal probe comparing 3- and 15-month-old C57BL/6 mice. As with the SAM model, we injected the probe and collected urine samples 15 min later. Although renal function may vary between mouse strains, the Cy7Gal readout in this animal model also reflected a significant rise in senescent cell burden in older mice, ratifying the sensitivity and versatility of this probe (**Figure 17a**). The rapid renal elimination of the Cy7Gal probe likely implies a short circulation time in the organism. This fact, despite the high β-Gal activity of senescent cells, would prevent total hydrolysis of the probe molecules. Nonetheless, the percentage of probe hydrolysis would rely mainly on the number of senescent cells. In line with this, we measured the percentage of probe molecules and free dye excreted in urine by HPLC. Almost 80% of the free dye (Cy7) was found in the urine of the older animals, while in the younger ones it was around 10%, as they excrete approximately 90% of the non-hydrolysed probe (Cy7Gal) (**Figure 17b**). These outcomes confirm that Cy7Gal is hydrolysed to a greater extent in older mice, meaning those with a higher senescence burden, and further support the fluorometer reading data of the Cy7 dye in urine.

Because we detected a marked increase in the whole-organism β-Gal activity in 15-month-old mice, we decided to initiate a senolytic treatment at this age in the same animals. For this purpose, these

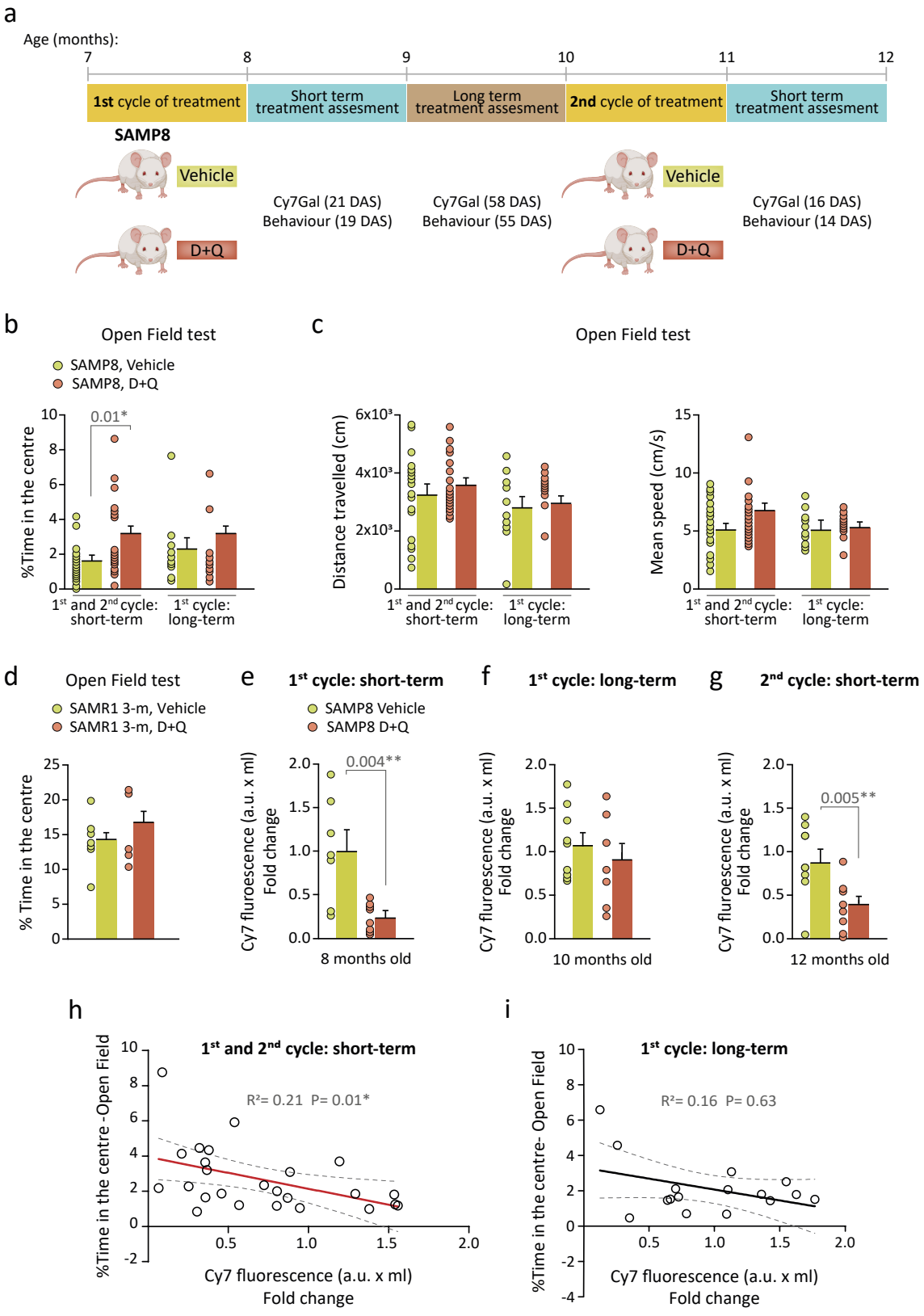

Figure 16. Monitoring of senolytic treatment during accelerated ageing. a) Timeline of the senolytic treatment and its monitoring in SAMP8 mice. SAMP8 7-m mice received an initial cycle of oral treatment with the senolytic drugs D+Q, or the vehicle. Anxious behaviour was evaluated using the Open Field test, and the senescence burden was assessed using Cy7Gal, shortly (15-21 days after senolysis or DAS; first cycle: short-term) and long after this treatment (55-58 DAS; first cycle: long-term). In addition, a second cycle was carried out at 10-m and Cy7Gal and behaviour were analysed 15-16 DAS (second cycle: short-term). **b**) Percentage of time that SAMP8 mice, treated

(Figure 16. Continued) with D+Q or vehicle, spent in the central area (green zone) of the open field. Note that a significant decrease in anxiety signs was observed in D+Q-treated mice, but only when anxious behaviour was assessed short-term after the treatment. **c**) Evaluation of locomotion-associated parameters in SAMP8 mice during the Open Field test, after senolysis. Observe that locomotion is not affected by the treatment, either when assessed in the short- or long-term after the senolytic intervention. **d**) Percentage of time that 3-m SAMR1 mice spent in the central area of the open field after 3 days receiving D+Q or vehicle. Note that D+Q senolytic drugs *per se* do not produce an anxiolytic effect. **e**) Cy7Gal-associated fluorescence in urine samples from SAMP8 mice administered with D+Q or vehicle, 21 days after the first treatment cycle. Fluorescence readout was performed on a fluorometer and measured in a.u. The graph shows a.u. multiplied by the volume of urine recovered (a.u. x ml). **f**) Cy7Gal-associated fluorescence in urine samples from SAMP8 mice treated or not with D+Q, 58 days after the first treatment cycle. **g**) Readout of Cy7Gal-associated fluorescence in urine samples from SAMP8 mice treated with D+Q or vehicle, 16 days after the second treatment cycle. **h**) Significant linear correlation found between the levels of Cy7 fluorescence in urine and the percentage of time in the centre of the open field of mice treated with D+Q or vehicle, when evaluated shortly after treatment. Observe that increased anxious behaviour corresponds to higher levels of Cy7 fluorescence in urine. **i**) No significant correlation was found between Cy7Gal and anxious behaviour when assessed in the long term after the senolytic intervention. Fold change is calculated relative to Cy7 fluorescence levels in the urine of vehicle-treated mice in all graphs. The graphs represent mean ± SEM. Unpaired Student's t-test was used for statistical analysis and a multiple linear regression to determine the equation of relationship between Cy7 fluorescence in urine and the time mice spent in the central area of the open field. Locomotor behaviour, in graphs *c*, was analysed with a two-way ANOVA, simultaneously comparing "treatment" and "evaluation term". Exact p-values and the number of independent biological samples (represented as dots) are shown in the graphs.

C57BL/6 mice were treated orally with D+Q for 5 weeks (**Figure 18a**). To determine whether reducing the senescence levels in treated mice has an anxiolytic effect in this model of natural ageing, we assessed anxious behaviour. Interestingly, D+Q treatment significantly improved the performance of the mice in the Open Field test, as they spent more time in the central zone than the age-matched vehicle-treated mice (**Figure 18b,c**). We observed no differences in locomotion (**Figure 18d**), again indicating that the perceived alleviation of anxiety is not driven by elevated hyperactivity. In parallel, we also assessed the anxious behaviour of these mice using the EPM test. In agreement with the Open Field test, the mice that received the senolytic treatment remained in the open arm longer than those treated with the vehicle, demonstrating that senolysis helps to reduce signs of anxiety-like behaviour in aged mice (**Figure 18e,f**).

Furthermore, we also controlled this pharmacological treatment with the Cy7Gal probe. To this end, we injected the probe in C57BL/6 mice 2 weeks after the senolytic intervention. As in SAMP8 mice, Cy7 fluorescence in urine was significantly reduced by the senolytic drugs (**Figure 18g**). Notably, we also identified a significant correlation between Cy7 fluorescence levels and anxious behaviour (**Figure 18h**,**i**). These combined results corroborate that senolytic treatment reduces the senescence burden, providing an anxiolytic effect. Considering the above, the Cy7Gal probe facilitates non-invasive monitoring of senescent cell accumulation and associated pathologies, as well as their reversal by senolytics, during both accelerated and natural ageing. Importantly, our data show that Cy7Gal is sensitive enough to predict age-related emotional behaviours, such as anxiety, further demonstrating that the removal of senescent cells ameliorates brain-associated disorders.

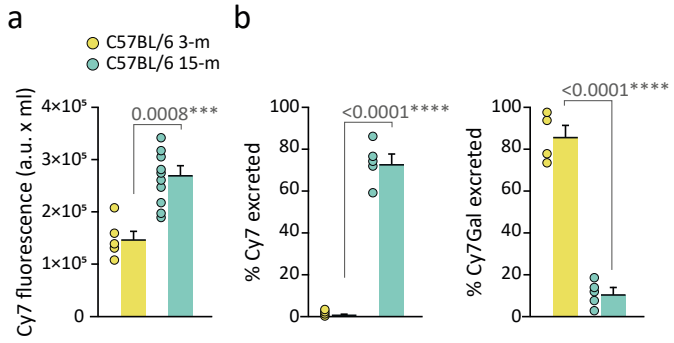

Figure 17. Cy7Gal-based detection of β-Gal activity *in vivo* during natural ageing. a) Fluorometer readout of Cy7Gal-associated fluorescence in urine samples from 3- and 15-m C57BL/6 mice. **b**) Measurement of the percentage of Cy7Gal probe or free Cy7 fluorophore excreted in the urine of 3- versus 15-m C57BL/6 mice by HPLC. The graphs show the mean ± SEM. Unpaired Student's t-test was used for statistical analysis. The number of independent biological samples (represented as dots) used and the exact p-values are indicated in the graphs.

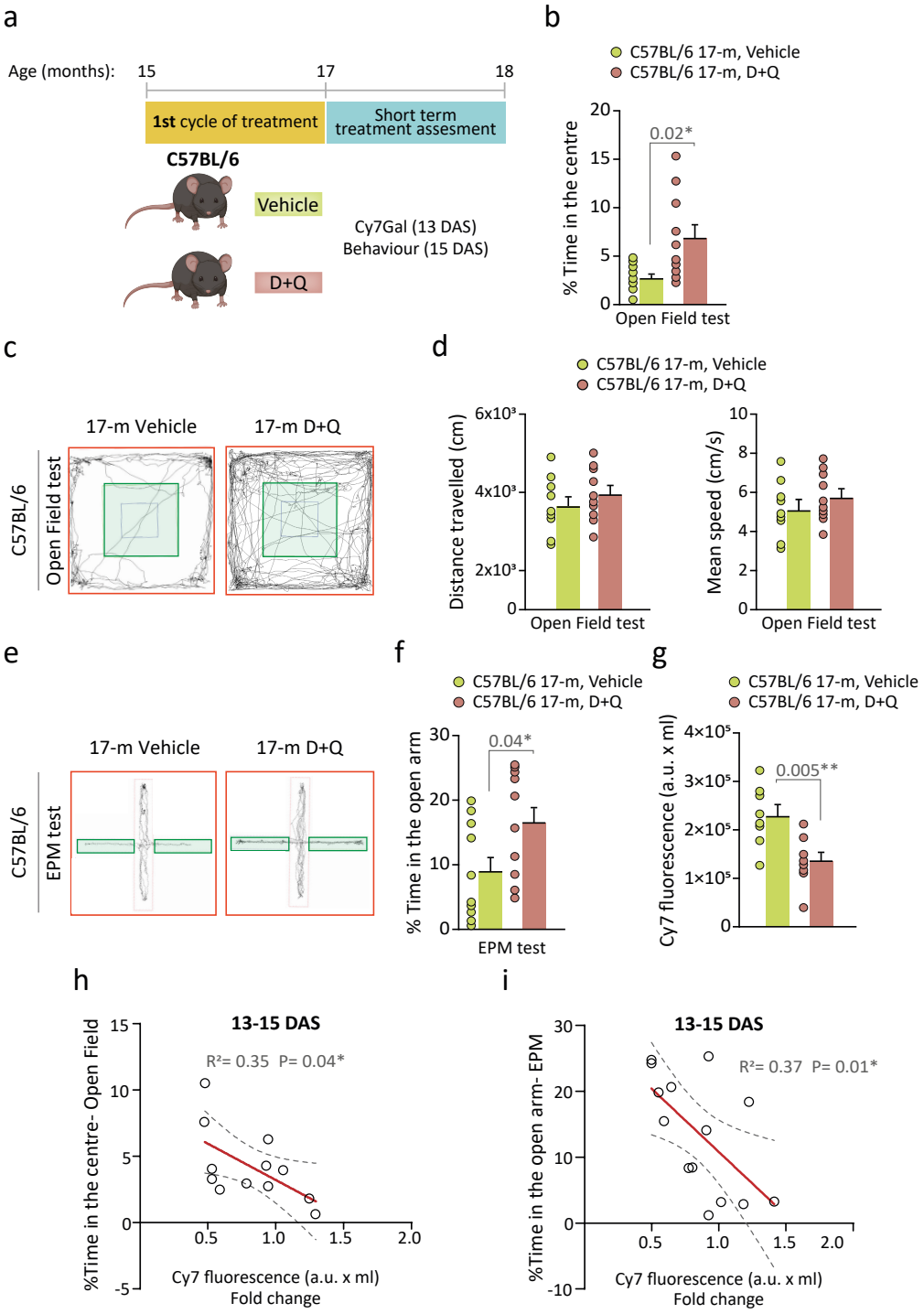

Figure 18. Monitoring of senolytic treatment during natural ageing. a) Timeline of the senolytic treatment and its monitoring in C57BL/6 mice. C57BL/6 15-m mice received the senolytic drugs D+Q or the vehicle for 5 weeks. Next, senescence burden was assessed with Cy7Gal 13 DAS and, 2 days later, anxious behaviour was examined. **b**) Percentage of time that mice spent in the central area (green zone) of the open field, treated with D+Q or vehicle. **c**) Representative map of movement during the Open Field test, comparing age-matched mice treated or not with senolytic drugs. **d**) Assessment of locomotion parameters during the Open Field test of C57BL/6 mice treated with D+Q or the vehicle. **e**) Representative map of movement during the EPM test, comparing age-matched C57BL/6 mice treated or not with senolytic drugs. **f**) Percentage of time that mice spent in the open arm of the EPM, after treatment with D+Q or vehicle. **g**) Measurement of Cy7Gal-associated fluorescence in urine samples from 17-m C57BL/6 treated with D+Q or vehicle. **h**) Significant linear correlation between the levels of Cy7 fluorescence in urine and the percentage of time spent in the centre of the open field of mice treated with senolytic drugs

(Figure 18. Continued) or vehicle. **i)** Significant linear correlation between Cy7 fluorescence in urine and the percentage of time in the open arm of the EPM of mice treated with D+Q or the vehicle. The fold change in graphs *h* and *i* refers to the Cy7 fluorescence levels in the urine of mice that received the vehicle. The graphs show the mean ± SEM. Unpaired Student's t-test was used for statistical analysis and a multiple linear regression to determine the equation of relationship between Cy7 fluorescence in urine and the time mice spent in the central area of the open field or the open arm of the EPM. The number of independent biological samples (represented as dots) used and the exact p-values are indicated in the graphs.

2. Characterisation of ageing-associated brain endothelial senescence and its impact on adult neurogenesis

The accumulation of senescent cells with increasing age can negatively affect brain tissue by contributing to neurodegeneration (Martínez-Cué and Rueda, 2020). Our findings also indicate that ageing and overall senescence burden are associated with specific behavioural alterations. Reports point out that naturally aged mice experience reduced neurogenesis due to deficits in NSC capacities. Classical birth dating studies have shown that the number of proliferative NSCs and their derived progeny decreases with ageing, resulting in reduced neurogenic production (Maslov et al., 2004; Luo et al., 2006; Molofsky et al., 2006; Ahlenius et al., 2009; Conover and Shook 2011; Shook et al., 2012). Moreover, the vascular niche also undergoes a structural remodelling with ageing that disrupts EC regulation on NSC behaviour and compromises neurogenesis (Rojas-Vázquez et al., 2021). If these age-related changes could be attributed to EC senescence is not known. In this regard, we set out to explore the specific effects that senescent BECs, and their released factors, may exert on NSC behaviour and neurogenesis.

2.1. *Paracrine effects of senescent ECs on NSC behaviour*

The SASP constitutes one of the main hallmarks of senescent cells, which release factors that can induce senescence in surrounding cells via paracrine manner (Coppé et al., 2010; Childs et al., 2017). Since BECs play an essential role in the extrinsic regulation of NSC activity (Rojas-Vázquez et al., 2021), we first investigated the potential impact of senescent ECs-secreted factors on these SCs, using *in vitro* systems. For this purpose, we disaggregated cells from the SEZ of young C57BL/6 mice and seeded them in culture medium containing the mitogens EGF and FGF. During the first week *in vitro*, differentiated cells die while NSCs begin to proliferate, generating floating spherical clones known as neurospheres. NSCs with proliferative potential maintain the culture through the consecutive passages (Belenguer et al., 2016). In order to explore how EC senescence may affect NSC activity, we collected the soluble fraction from the conditioned medium (CM) of control (C-CM) or palbociclib-induced senescent (S-CM) hUVECs that were seeded in neurosphere medium for 24 hours. Next, NSCs were cultured in each CM or in normal neurosphere medium (non-CM) and examined 4 days afterwards. A decrease in the size of the neurospheres was observed in C-CM, but this decrease was even more pronounced in S-CM and accompanied by an increased tendency of the neurospheres to slightly adhere to the culture plate surface (**Figure 19a**).

In addition, we assessed the proliferation dynamics of NSCs with a green fluorescent cell tracer known as DFFDA. Single neurosphere cells are passively loaded with this tracer that becomes subsequently diluted with each cell division during neurosphere formation. We have noticed that in about half of the neurospheres, the DFFDA tracer is completely diluted, as would be expected. However, the rest of the neurospheres contain cells that retain the dye, indicating that, at some early point during neurosphere formation, some cells switched to a slow mode of division (Belenguer et al., 2021). This strategy, therefore, allows the detection of a change in division pace within our cultures, where the most actively dividing

cells are classified as DFFDA^{low} and the least proliferating cells as DFFDA^{high}. The results showed that neurospheres grown in C-CM increased their percentage of DFFDA^{high} cells compared to non-CM, which is in agreement with previous reports of the lab showing that BECs can release quiescence-promoting factors (Delgado et al., 2014). Remarkably, factors released by senescent hUVECs produced a significant increase in the percentage of cells retaining the DFFDA tracer (**Figure 19b**). To determine whether senescent ECs were promoting quiescence or senescence via paracrine effects, we looked at the changes in Lamin B1 (Freund et al., 2012). We detected reduced levels of nuclear Lamin B1 in neurospheres grown in S-CM, but not in C-CM (**Figure 19c**). Taken together, the data suggest that, aside from the reported cytostatic effect of BECs on NSCs, senescent ECs induce senescence in NSCs in a paracrine manner.

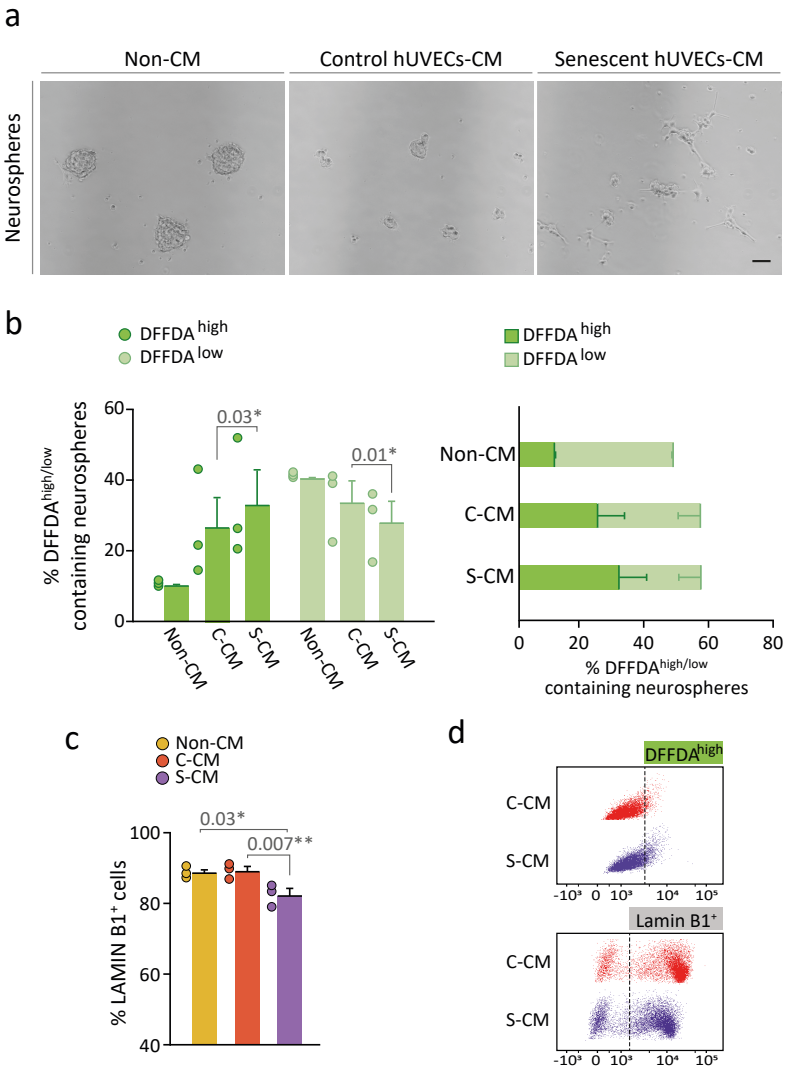

Figure 19. Evaluation of the paracrine effects of senescent hUVEC-secreted factors on NSCs *in vitro*. a) Brightfield images of neurospheres in culture non-conditioned (non-CM) or conditioned by control (C-CM) or senescent (S-CM) hUVEC-derived factors. **b**) Assessment of NSC proliferation with the cell division tracer DFFDA, targeting DFFDA^{high} (slowly proliferating) and DFFDA^{low} (highly proliferative) cells. Note that S-CM significantly arrests the self-renewal capacity of NSCs compared to NSCs exposed to C-CM. **c**) Flow cytometry analysis of the percentage of Lamin B1^{+} NSCs when conditioned by senescent or control hUVEC-derived factors or unconditioned. Notice that only senescent endothelial factors produce a reduction in the percentage of Lamin B1^{+} neurospheres. **d**) Dot plots showing the flow cytometry analysis of DFFDA^{high} and Lamin B1^{+} cells, comparing neurospheres conditioned by control or senescent EC-secreted factors. The graphs show the mean ± SEM. Paired Student's t-test was used for statistical analysis, as the same culture was exposed to different conditions. The exact p-values and the number of independent biological samples (represented as dots) are indicated in the graphs. Scale bar: 100 µm.

To further ascertain this possibility, we used a murine BEC line (bEnd.3 cells) and induced senescence by briefly exposing these cells to a pro-oxidant environment with H_2O_2. Elevated oxidative stress has been associated with vascular ageing as it promotes up-regulation of p16 through the p38-MAPK pathway (Rodriguez-Menocal et al., 2009; El Assar et al., 2013; Chandrasekaran et al., 2017; Izzo et al., 2021). We found exacerbated levels of p16 and SA-β-Gal activity in bEnd.3 cells exposed to this stress factor, compared to unexposed or control cells, via FACS (**Figure 20a,b**). This cellular model represents a closer approach to understanding the potential impact of endothelial senescence on NSC activity in the brain. Following the same experimental strategy described above, our results indicated that the proliferative arrest of neurospheres is significantly higher in those exposed to senescent bEnd.3 cells factors (**Figure**

20d). Moreover, phenotypic features typically associated with senescence, such as loss of Lamin B1 and increased β-Gal activity, were significantly more prominent in neurospheres seeded with S-CM (**Figure 20e,f**). These changes also correlated with greater levels of ROS, another marker of cell senescence, assessed using a mitoSOX™ probe (**Figure 20g**). Ultimately, our data demonstrate that soluble factors secreted by senescent BECs have a detrimental effect on NSC behaviour via paracrine signals, leading to a rise of senescence-associated markers and loss of growth in neurospheres. Importantly, this result makes EC senescence a key target in the study of brain ageing, as it can negatively influence NSC activity.

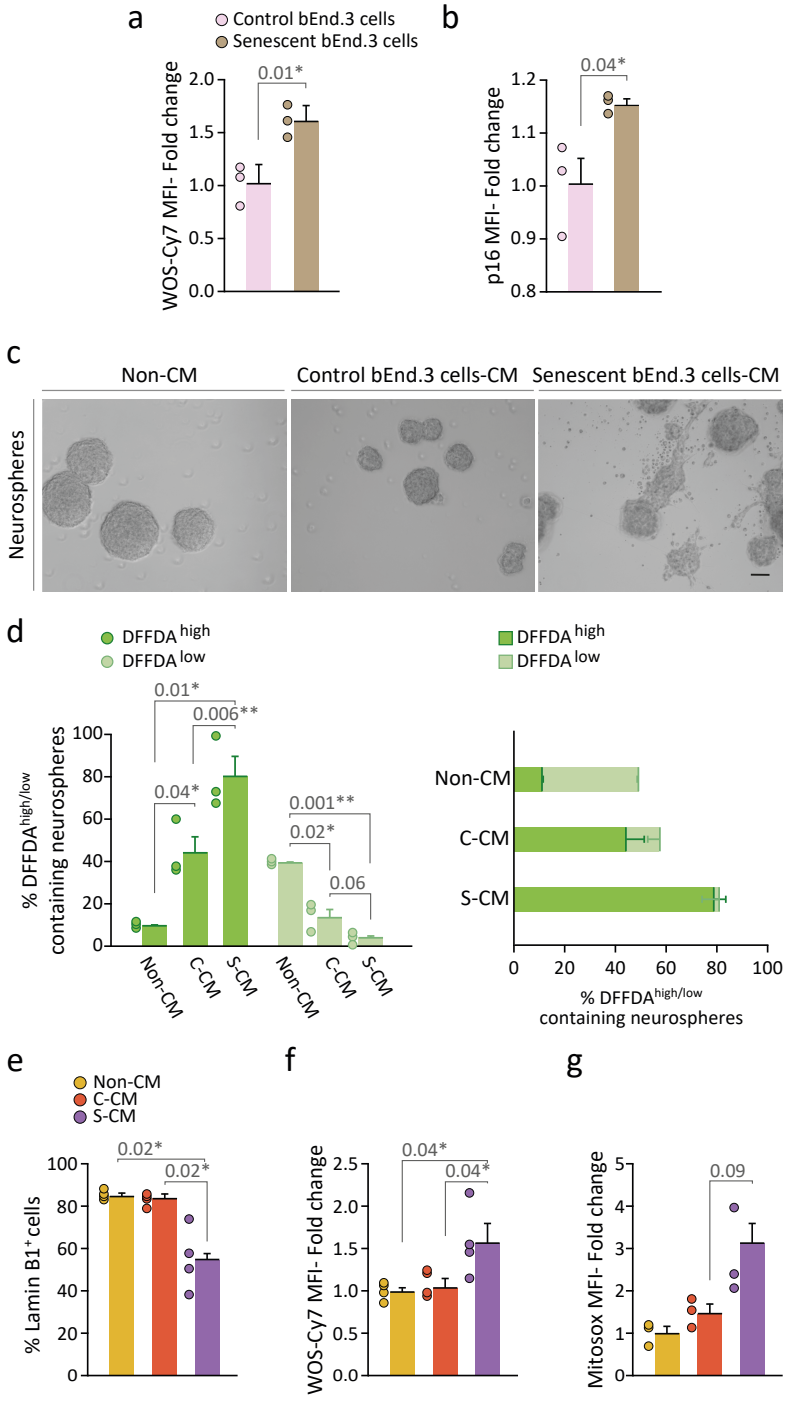

Figure 20. Evaluation of the paracrine effects of senescent BEC-secreted factors on NSCs *in vitro*. a) Evaluation of SA-β-Gal activity by flow cytometry, using the WOS-Cy7Gal probe, in bEnd.3 cells exposed (senescent) or not (control) to H_2O_2-induced oxidative stress. **b**) Evaluation of p16 levels by flow

(Figure 20. Continued) cytometry in bEnd.3 cells exposed or not to H_2O_2. **c**) Brightfield images of neurospheres in culture non-conditioned (non-CM) or conditioned by control (C-CM) or senescent (S-CM) bEnd.3 cells-derived factors. **d**) Assessment of NSC proliferation with the cell division tracer DFFDA, targeting $DFFDA^{high}$ (slowly proliferating) and $DFFDA^{low}$ (highly proliferative) cell subpopulations. Note that S-CM significantly arrest the self-renewal capacity of NSCs compared to C-CM. **c**) Flow cytometry analysis of the percentage of Lamin $B1^+$ NSCs with non-CM or C- or S-CM. Notice that only senescent endothelial factors produce a marked reduction in the percentage of Lamin $B1^+$ neurospheres. **e**) Analysis of β-Gal activity of NSC non-CM, C-CM or S-CM using the WOS-Cy7Gal probe, by flow cytometry. Observe that only S-CM significantly increases NSC β-Gal activity. **f**) Analysis of ROS production using the mitoSOX™ probe by flow cytometry. Note that the MFI for this probe is greater in NSC conditioned by senescent bEnd.3 cells-released factors. The graphs show the mean ± SEM. Unpaired Student's t-test was used for senescence analysis in bEnd.3 cells. For the analysis of the paracrine effects of BECs on NSCs, a paired Student's t-test was used, as the same cultures were exposed to different conditions. The exact p-values and the number of independent biological samples (represented as dots) used are indicated in the graphs. Scale bar: 100 µm.

2.2. *Correlative analysis of brain endothelial senescence and neurogenesis during ageing*

Our *in vitro* data showed that senescent ECs can exert paracrine effects on NSCs, potentially inducing their own senescence. Consequently, we aimed to evaluate the relationship between EC senescence and neurogenesis *in vivo*. Given that SAMP8 mice exhibited a higher burden of senescence at the age of 7 months, compared to their SAMR1 counterparts, we initiated our investigation into brain senescence at the same age. As a first approach, we isolated the SEZ from 7-month-old SAMP8 and SAMR1 mice as a whole-mount and performed traditional X-gal staining to examine the distribution and location of senescent cells in this neurogenic region. Interestingly, not only did we detect an increased number of blue-labelled cells in the SAMP8 SEZ, but the strongest labelled ones were delineating the path of blood vessels, reproducing a vascular pattern (**Figure 21a**). The data suggest that brain vasculature, perhaps due to its direct exposure to the systemic environment (Chen et al., 2020), may be particularly susceptible to senescence.

Next, we decided to perform a primary culture of BECs from SAMP8 and SAMR1 mice by the isolation of $CD31^+$ cells using antibody-bound magnetic beads. We obtained BECs from SAM mice at 4 months of age. Although older ages may provide more conclusive evidence as to whether BECs experience a senescent fate, we found that the yield of EC collected from brain tissue decreases with age. Despite being relatively young, our longitudinal study showed that SAMP8 mice already displayed pronounced signs of anxiety at 4 months. We used the AHGa fluorogenic probe to assess the SA-β-Gal activity (**Figure 21b**) of these cells *in vitro* and, in parallel, we examined other senescence phenotypic traits. According to the confocal microscopy images, the AHGa probe was hydrolysed more efficiently in SAMP8-derived BECs. Along with increased β-Gal activity, SAMP8 ECs also exhibited a decrease in proliferation (reduced percentage of $Ki67^+$ cells) and elevated levels of DNA damage (γH2AX-positive) foci and p21 protein (**Figure 21c,d**), all cell senescence features. These results suggest that senescent BECs begin to accumulate early in the SAMP8 mouse strain. However, these cells may also be more predisposed to acquiring a senescent profile when cultured *in vitro*, so we developed other more direct and refined strategies for the study of brain endothelial senescent cells.

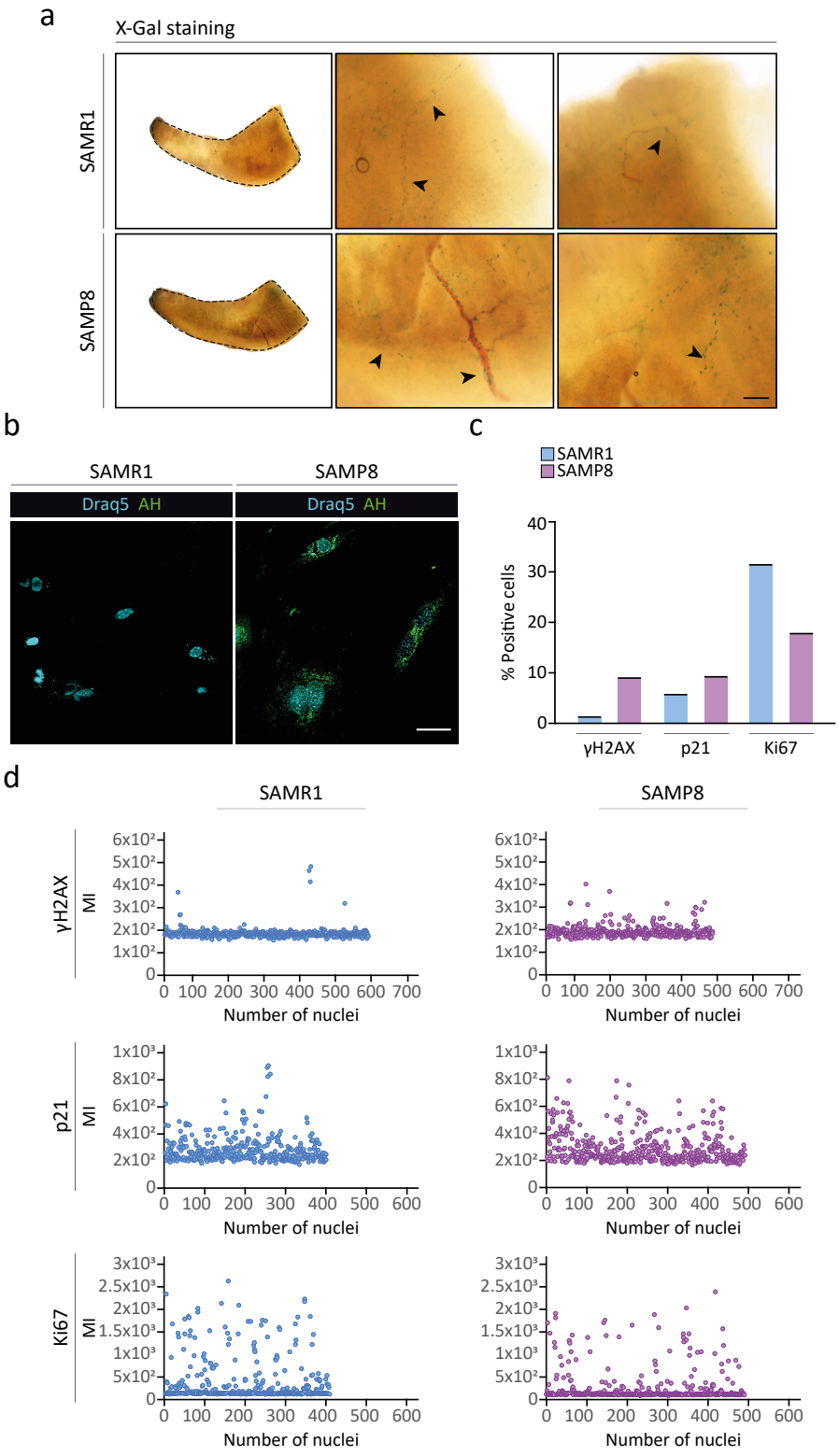

Figure 21. Initial assessment of cellular senescence in brain microvessels during accelerated ageing. **a**) Representative images of X-gal histochemical staining of SEZ wholemount preparations from 7-m SAMP8 and SAMR1 mice. Note the increased presence of blue-labelled cells resembling a vascular pattern in the SEZ of SAMP8 animals. **b**) Confocal images of primary cultured BECs from 4-m SAMP8 and SAMR1 mice labelled with the AHGa probe for SA-β-Gal assessment, and Draq5 for live cell nuclei staining. **c**) Evaluation of senescence-associated markers by image analysis. Note that there is a decrease in proliferation (Ki67), as well as an increase in p21 and γH2AX levels in SAMP8 BECs, which, together with the increased β-gal activity shown by the AHGa probe, supports a senescent profile in SAMP8

(Figure 21. Continued) BECs. **d**) Graphical representation of DAPI⁺ BECs and their mean fluorescence intensity (MI) for each of the markers analysed in graph *c*. Scale bars: 100 µm.

In order to further investigate age-related brain endothelial senescence closer to what is happening *in vivo*, we designed a flow cytometry strategy to phenotype senescent BECs. The pool of NSCs in SAMP8 mice is reportedly depleted by the age of 10 months (Soriano-Cantón et al., 2015) and we have also observed that there is a profound and generalised functional deterioration at this age. Hence, we assumed that endothelial senescence burden is augmented at this point. We obtained brain cell suspensions from 10-month-old SAMP8 and SAMR1 mice and selected CD31⁺ ECs to evaluate senescence-associated markers *ex vivo*. Importantly, we detected a significant increase in β-Gal activity in BECs from SAMP8 animals using the fluorogenic probe WOS-Cy7Gal. Furthermore, this result was accompanied by notably higher levels of the cell cycle inhibitor p16, elevated mitochondrial ROS production and a more complex cell morphology, thus defining a senescent profile in this cell population isolated from the brain of SAMP8 mice (**Figure 22a**).

Subsequently, we examined the SEZ aged phenotype using a newly-established FACS strategy, developed by our group, to assess the cellular components of the entire SEZ neurogenic lineage with higher resolution than conventional histological analyses. This FACS panel is a significant advantage in the field of adult neurogenesis, allowing for precise identification of potential changes in the neurogenic lineage due to specific treatments/mutations or, in this case, ageing. Phenotypic analysis by flow cytometry revealed a significant reduction in the proportions of NSCs and ENBs in SAMP8 versus SAMR1 mice at this age (**Figure 22b**), supporting a correlation between BEC senescence and reduced SEZ neurogenic potential.

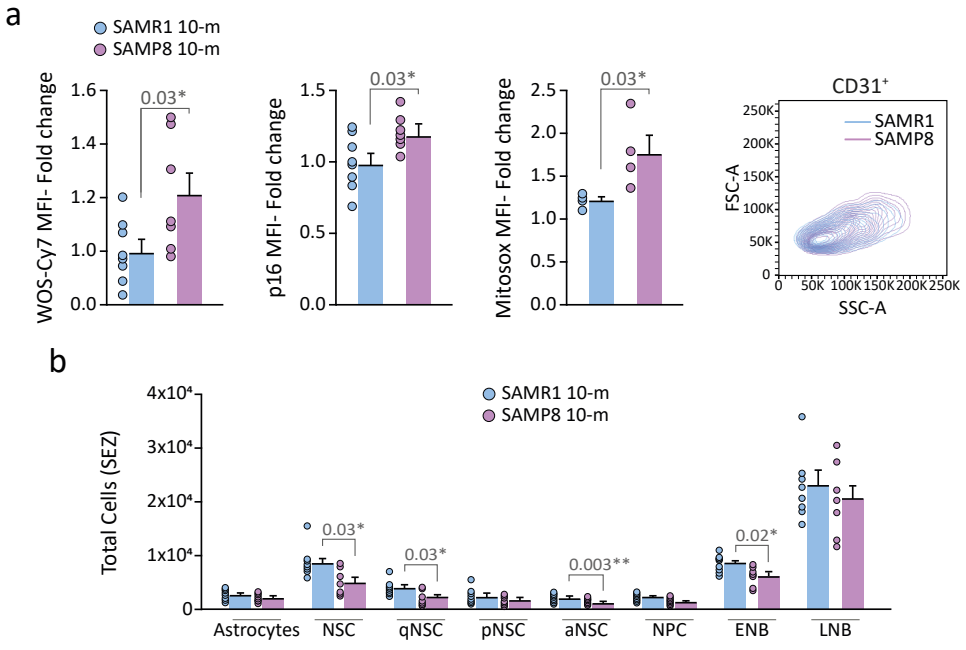

Figure 22. Detection of senescent BECs and analysis of SEZ neurogenesis during accelerated ageing. a) Analysis of senescence-associated markers in BECs by flow cytometry, comparing 10-m SAMP8 and SAMR1 mice. Note that SAMP8 BECs show senescent traits such as increased β-gal activity (measured with the WOS-Cy7Gal probe), higher levels of the cell cycle inhibitor p16, elevated ROS production and increased cellular complexity (FACS contour plot), compared to SAMR1 mice. **b**) Evaluation of the SEZ neurogenic lineage by flow cytometry of 10-m SAMP8 and SAMR1 mice. Observe that NSCs and ENB cell populations are significantly reduced in SAMP8 mice at this age. The graphs show the mean ± SEM. Unpaired Student's t-test was used for statistical analysis. The number of independent biological samples (represented as dots) used and the exact p-values are indicated in the graphs.

We also analysed BEC senescence traits in 24-month-old naturally aged C57BL/6 mice compared to 3-month-old ones by flow cytometry. Interestingly, we observed a significant increase in β-Gal activity using the NBGal probe, as well as a marked elevation of ROS-mediated cellular oxidative stress and a more complex morphology, in ECs isolated from the brain of old mice (**Figure 23a**). These results imply that BECs undergo senescence and accumulate in brain tissue during natural ageing. Additionally, a significant decrease in the pool of NSCs, NPCs and NBs, was observed in old versus young C57BL/6 mice (**Figure 23b**). Taken together, our data support that the age-related increase in EC senescence at the brain level is accompanied by a decrease in adult neurogenesis and a reduction in the number of NSCs.

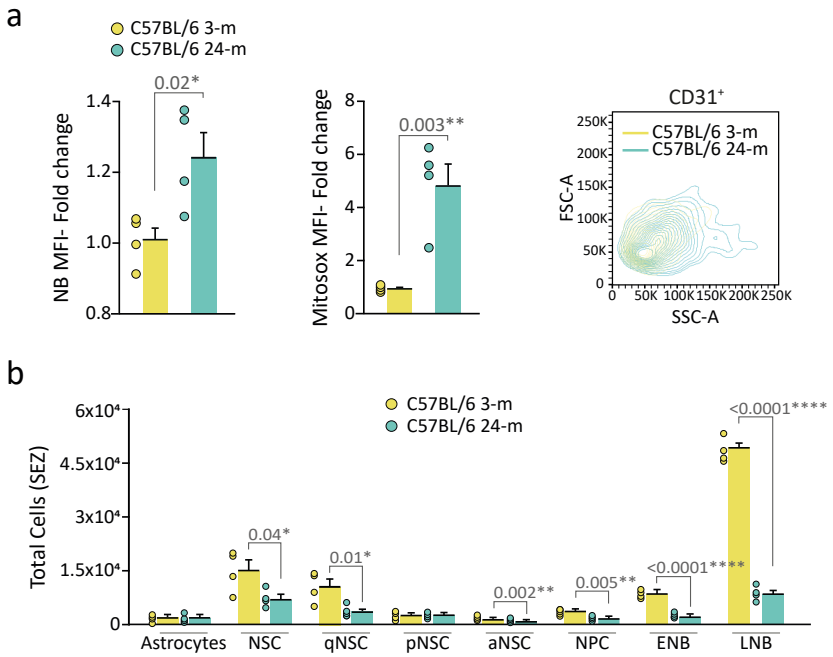

Figure 23. Detection of senescent BECs and analysis of SEZ neurogenesis during natural ageing. a) Analysis of senescence-associated markers in BECs by flow cytometry, comparing 24- and 3-m C57BL/6 mice. Note that BECs from older mice exhibit senescent traits such as increased β-gal activity (measured with the NBGal probe), elevated ROS production and increased cellular complexity (FACS contour plot). **b**) Evaluation of the SEZ neurogenic lineage in 2- versus 24-m C57BL/6 mice by flow cytometry. Observe that NSCs (qNSCs and aNSCs), NPCs and NBs (ENBs and LNBs) cell populations are significantly reduced in 24-m mice. The graphs show the mean ± SEM. Unpaired Student's t-test was used for statistical analysis. The number of independent biological samples (represented as dots) used and the exact p-values are indicated in the graphs.

2.3. *Correlative analysis of brain endothelial senescence and neurogenesis after senolytic intervention*

Aiming to improve our understanding of the associative link between increased BEC senescence and neurogenesis decline, we investigated if the treatment with D+Q senolytic drugs was capable of reversing this correlation. Following the same treatment timeline as previously described, i.e. after two cycles of 5 weeks each (**Figure 24a**), we analysed senescence-associated markers in BECs isolated from 12-month-old SAMP8 mice. We detected a significant decrease in β-Gal activity, as well as reduced levels of p16 protein and ROS production, in BECs from mice treated with D+Q compared to those treated with the vehicle (**Figure 24b**). These results indicated that the senolytic intervention effectively decreased endothelial senescence burden at the brain level. Moreover, we performed a phenotypic evaluation of the cell

components of the SEZ niche by flow cytometry. This study revealed that D+Q can restore the homeostasis of the neurogenic lineage and rescue, at least in part, the neurogenic potential of these cells (**Figure 24c**). Collectively, the findings suggest that alleviating EC senescence in the brain upon senolytic treatment has a beneficial effect on neurogenesis.

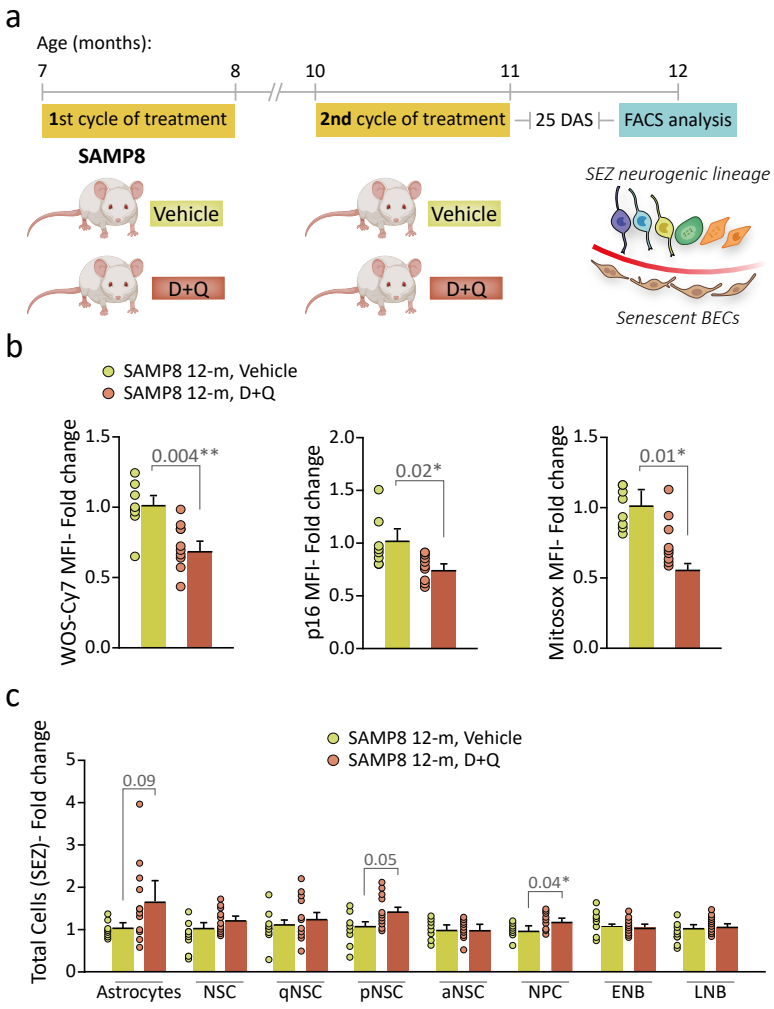

Figure 24. Evaluation of the impact of D+Q senolytic treatment on endothelial senescence and the SEZ neurogenic lineage. a) Time course schedule of D+Q senolytic treatment and analysises conducted. **b**) Flow cytometric analysis of senescence in BECs, regarding SA-β-Gal activity (WOS-Cy7Gal), p16 levels and mitochondrial ROS production (mitoSOX™). Note that these senescence-associated markers display a significantly reduced MFI in BECs from SAMP8 mice treated with D+Q. **c**) Flow cytometric evaluation of the SEZ neurogenic lineage in SAMP8 mice treated with senolytic drugs versus vehicle-treated ones. The graphs show the mean ± SEM. For statistical analysis, unpaired Student's t-test was applied. The number of independent biological samples (represented as dots) used and the exact p-values are indicated in the graphs.

The output of the brain neurogenic process is reportedly evaluated end-point by quantifying newly-generated neurons in the OB and the DG. Accordingly, to assess the impact of the senolytic treatment on global neurogenesis, we decided to conduct classical birth dating studies. To do so, we performed a 5-week cycle of treatment in 8-month-old SAMP8 mice and evaluated the effects of D+Q in BECs and neurogenesis (**Figure 25a**). Brain isolation of ECs and *ex vivo* readout of WOS-Cy7Gal showed a decrease in β-gal activity in D+Q-treated mice, compared to vehicle-treated ones. The treatment also resulted in a reduction of p16 levels and mitochondrial ROS generation in BECs, which confirmed the elimination of

senescent ECs by the senolytic drugs (**Figure 25b**)

To analyse the SEZ neurogenic process at the end-point and measure newly generated OB neurons, we injected BrdU i.p. into SAMP8 mice 5 days after the senolytic treatment. Mice that received the senolytic drugs or the vehicle were injected with 50 mg/kg of BrdU (10 mg/ml) twice daily, for 3 consecutive days, and euthanized 26 days later. Using this approach, only cells that abandon the cell cycle immediately after BrdU injections to terminally differentiate as OB interneurons are presumed to be labelled in the GL of the OB (Porlan et al., 2014). Interestingly, the number of BrdU⁺ newly generated neurons in this layer was higher in SAMP8 mice treated with D+Q (**Figure 25c-e**), indicating that acute senolytic treatment leads to enhanced olfactory neurogenesis. Furthermore, these results were supported by the improved odour discrimination capacity of treated mice detected during the Olfactory Habituation-Dishabituation test (**Figure 25f**). The findings showed that senolysis reduces endothelial senescence and boosts the generation of new olfactory neurons in SAMP8 mice, implying that cellular senescence has anti-neurogenic effects.

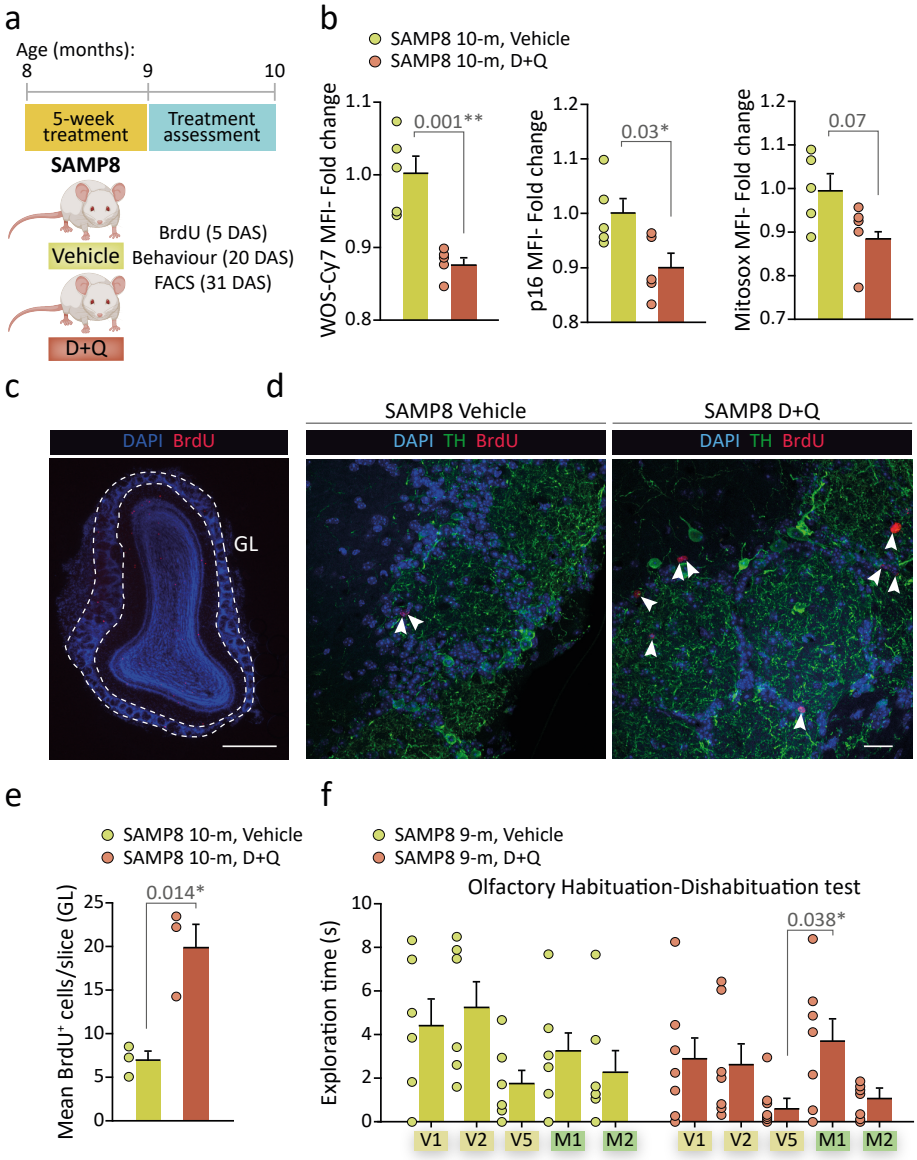

Figure 25. Evaluation of the impact of D+Q senolytic treatment on endothelial senescence and neurogenesis in the OB in SAMP8 mice. a) Time course schedule of D+Q senolytic treatment and analyses conducted. **b**) Flow cytometric analysis of senescence in BECs, regarding SA-β-Gal activity (WOS-Cy7Gal), p16 levels and mitochondrial ROS production (mitoSOX™). Note that these senescence-associated markers display a markedly reduced MFI in BECs from SAMP8 mice treated with D+Q. **c**) Panoramic image of BrdU staining in an OB slice. **d**) Representative confocal images

(Figure 25. Continued) of BrdU (red) and Tyrosine Hydroxylase (TH) (green) labelled cells in the GL of the OB. Arrows indicate BrdU⁺ cells. **e**) Immunohistochemical analysis and quantification of BrdU⁺ cells/slice *per* animal in the GL of the OB, after one cycle of senolytic treatment. Observe that SAMP8 mice that received D+Q senolytic drugs exhibit an increased number of BrdU⁺ cells, indicating an enhanced neurogenesis. **f**) Assessment of olfactory behaviour through odorant detection during an Habituation and Dishabituation test. The critical points of evaluation are contemplated in this graph. V1, V2 and V5 refer to vanilla odour in sticks 1, 2 and 5, while M1 and M2 correspond to stick 1 and 2 with mint aroma. The graphs show the mean ± SEM. For statistical analysis, unpaired Student's t-test was used except for the olfactory Habituation and Dishabituation test, which was analysed with a two-way ANOVA considering the variables "habituation process" and "treatment". The number of independent biological samples (represented as dots) used and the exact p-values are indicated in the graphs. Scale bars: *c* 500 µm, *d* 100 µm.

The BrdU regime applied allowed us to also evaluate hippocampal neurogenesis by quantifying the number of BrdU⁺ cells in the SGZ. As a result of the senolytic intervention, SAMP8-treated mice exhibited a significant increase in the number of BrdU⁺ cells in this region (**Figure 26a-c**). BrdU-label retaining cells in this structure include newly-generated granule neurons, but also hippocampal NSCs and NBs (Kempermann et al., 2003; Kunh et al., 2016). Still, the result is in line with beneficial effects of the senolytic treatment in the neurogenic activity of the SGZ. In addition, treated mice displayed improved performance in the NOR test, which assesses their ability to recognize and differentiate familiar and novel objects (**Figure 26d**). This test covers both exploration and memory, functions that rely on hippocampal neurogenesis, thereby reinforcing our previous result (Jessberger et al., 2009; Abrous and Wojtowicz, 2015; Lazarov and Holland, 2016; Kempermann, 2022). Based on these outcomes, reducing the senescent cell burden correlates with enhanced hippocampal neurogenic activity.

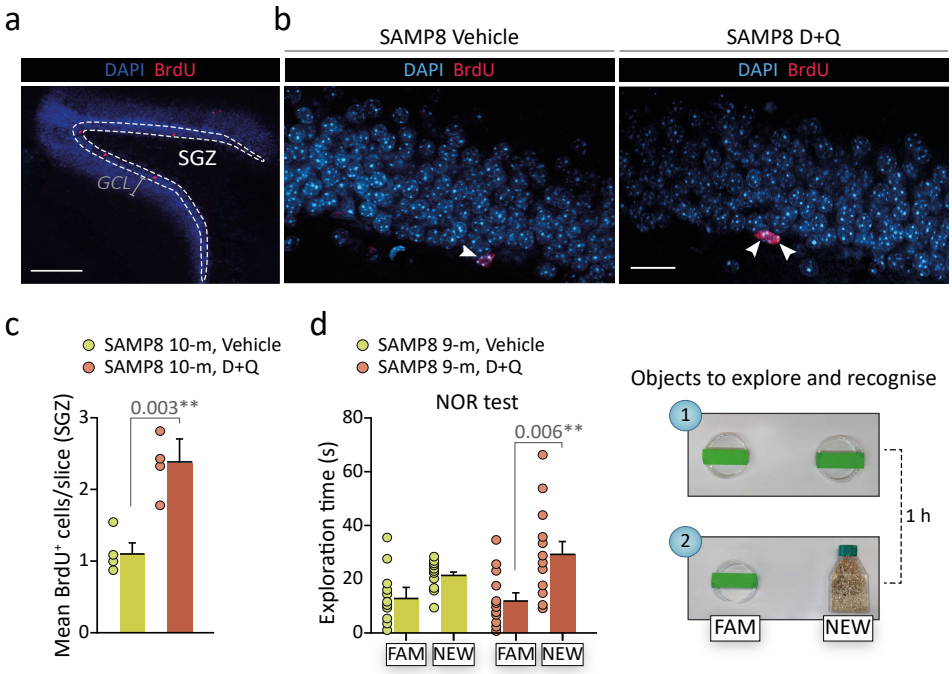

Figure 26. Evaluation of the impact of senolytic treatment on endothelial senescence and neurogenesis in the SGZ of SAMP8 mice. a) Panoramic image of BrdU staining in a DG slice. **b**) Representative confocal images of BrdU-labelled cells (red) in the hippocampal SGZ of SAMP8 mice treated with vehicle or D+Q. Arrows indicate BrdU⁺ cells. **c**) Immunohistochemical analysis of BrdU⁺ cells in the SGZ, after one cycle of senolytic treatment. Note that there is a significant increase of BrdU⁺ cells in SAMP8 mice treated with D+Q, indicating an increased neurogenic potential compared to vehicle-treated mice. **d**) Evaluation of NOR test, considering short-term memory. Observe that mice treated with senolytic drugs exhibit significantly increased interest for the new

(Figure 26. Continued) object, rather than the familiar one. The graphs show the mean ± SEM. Unpaired Student's t-test was used for statistical analysis. The number of independent biological samples (represented as dots) used and the exact p-values are indicated in the graphs. Scale bars: *a* 500 µm, *b* 100 µm.

Overall, oral treatment with the combination of D+Q reduces brain endothelial senescence and promotes neurogenesis. However, although the data showed an interesting correlation between vascular senescence and neurogenic activity, establishing a causal link between EC senescence and neurogenesis decline requires further experimentation.

2.4. *A novel genetic approach to induce senescence in BECs and its impact on neurogenesis*

Despite different types of glial cells and neurons reportedly exhibit cell senescence traits in the aged rodent brain, functional studies of the specific contribution of EC senescence to neurological performance are still missing, mainly due to the lack of appropriate animal models (Rojas-Vázquez et al., 2021). In this regard, our main objective was to investigate the specific contribution of BEC senescence to adult neurogenesis. To achieve this goal, it was necessary to develop a novel animal model in which senescence was induced exclusively in BECs, thereby minimizing potential confounding effects from other cell types. We decided to accomplish the task by overexpressing p16 *in vivo* using an adeno-associated virus vector (AAV) that was engineered to selectively target BECs.

An NRGTEWD peptide (also known as BR1) was identified in a screening of random ligand libraries displayed on AAV capsids for brain endothelium-targeting elements (Körbelin et al., 2016). With the aim to specifically induce senescence in BECs, we used an AAV2-BR1 carrying GFP and p16 genes (AAV2-BR1-p16-GFP) under the control of RSV and CAG promoters, respectively. This approach will enable us to determine the specificity of infection and transduction in our target, as only BECs are expected to preferentially display GFP-associated green fluorescence, as well as an overexpression of p16. According to our previous observations in *ex vivo* experiments, aged BECs increase their levels of p16 along with other senescence markers, suggesting that ageing-associated senescence may be mediated by this pathway in the brain endothelium. On the other hand, this system has the advantage of precisely targeting BECs through systemic i.v. administration, which neither locally restricts gene transfer near the injection site nor risks serious complications, such as haemorrhage and infection, that could profoundly alter the results.

As an initial step to evaluate the reliability of the strategy, we i.p. inoculated a young C57BL/6 mouse with the AAV2-BR1-p16-GFP, and another with PBS as a control. After 31 days, both mice were i.c. injected with tomato lectins (from *Lycopersicon esculentum*). This lectin is a fluorescently labelled glycoprotein that binds specifically to carbohydrates present on the surface of ECs, allowing for the visualisation of blood vessels through imaging techniques (Robertson et al., 2015). Afterwards, the SEZ was dissected as a whole-mount and incubated with the NBGal probe for 15 min to analyse SA-β-Gal activity in the vascular niche (**Figure 27a**). Relevantly, we observed a higher fluorescence intensity of the NB dye associated with blood vessels in the SEZ of the AAV-injected mouse compared to the PBS-injected one (**Figure 27b**). This suggested that our genetic approach affects the vascular niche in neurogenic regions.

To determine if there is a causal relationship between endothelial senescence and adult neurogenesis decline, we injected $1x10^{12}$ gc/mouse of AAV2-BR1-p16-GFP i.v. into the tail of 3-month-old C57BL/6 mice. As a control, PBS was i.v. injected into aged-matched mice, and both infected and non-infected mice were euthanized 31 days later (**Figure 28a**). We chose young mice to ensure that any detected effects on neurogenesis were caused exclusively by brain endothelial senescence and not by the accumulation of off-target senescent cells. For the analysis, we used our flow cytometry panel developed to phenotype senescent BECs, and a birth-dating protocol incorporating BrdU in order to evaluate neurogenesis in the OB and the hippocampal SGZ.

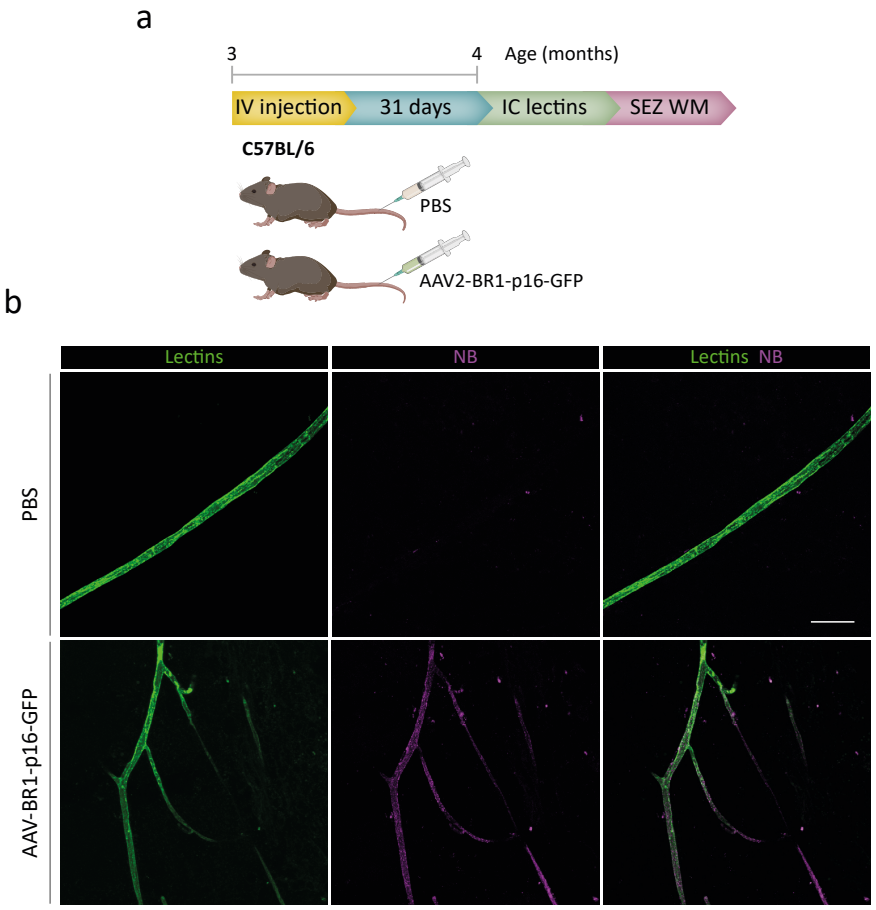

Figure 27. Imaging of SEZ blood vessels and β-Gal activity in AAV-BR1-p16-GFP-injected mice. a) Time course of the experimental procedure. After 31 days of PBS or vector i.v. inoculation, mice were i.c. injected with tomato lectin in order to label brain blood vessels. Subsequently, the SEZs were isolated as a whole-mount (WM) preparation for β-Gal activity assessment using the NBGal probe. **b**) Confocal microscopy images of blood vessels labelled with tomato lectins (green), and of β-Gal activity-based fluorogenic probe NBGal (magenta), in whole-mount preparations of the SEZ from mice injected with the adeno-associated vector or PBS. Scale bar: 100 µm.

Regarding EC senescence induction, we tested the specificity of infection by analysing brain versus liver tissue, focusing on vector GFP expression in the EC population of both organs. We observed that $CD31^+$ cells showed GFP-associated fluorescence only in the brain and exclusively in ECs, as other $CD31^-$ cell populations did not show any discernible GFP signal. Indeed, BECs from vector-injected mice exhibited around 20% GFP^+ cells compared to PBS-injected mice that were negative for GFP (**Figure 28b,c**). In addition, mice injected with the viral vector showed significantly increased levels of p16, which were higher in cells that displayed greater immunopositivity for GFP (GFP^{high}), indicating that transduction of the adeno-associated vector was efficient (**Figure 28d-f**). Notably, we did not find a rise in p16 in other cell populations in the brain, confirming the high selectivity of this genetic strategy (**Figure 28d**). To analyse senescence, we examined the levels of γH2AX, as well as the SA-β-Gal activity with the NBGal fluorogenic probe. We detected a significant increase in both markers in BECs isolated from mice injected with the AAV, compared to those injected with PBS. Moreover, the levels of these senescence-associated markers were also remarkably higher in GFP^{high} BECs (**Figure 28g-j**). Altogether, we concluded that senescence had been efficiently and specifically induced in ECs at the brain level.

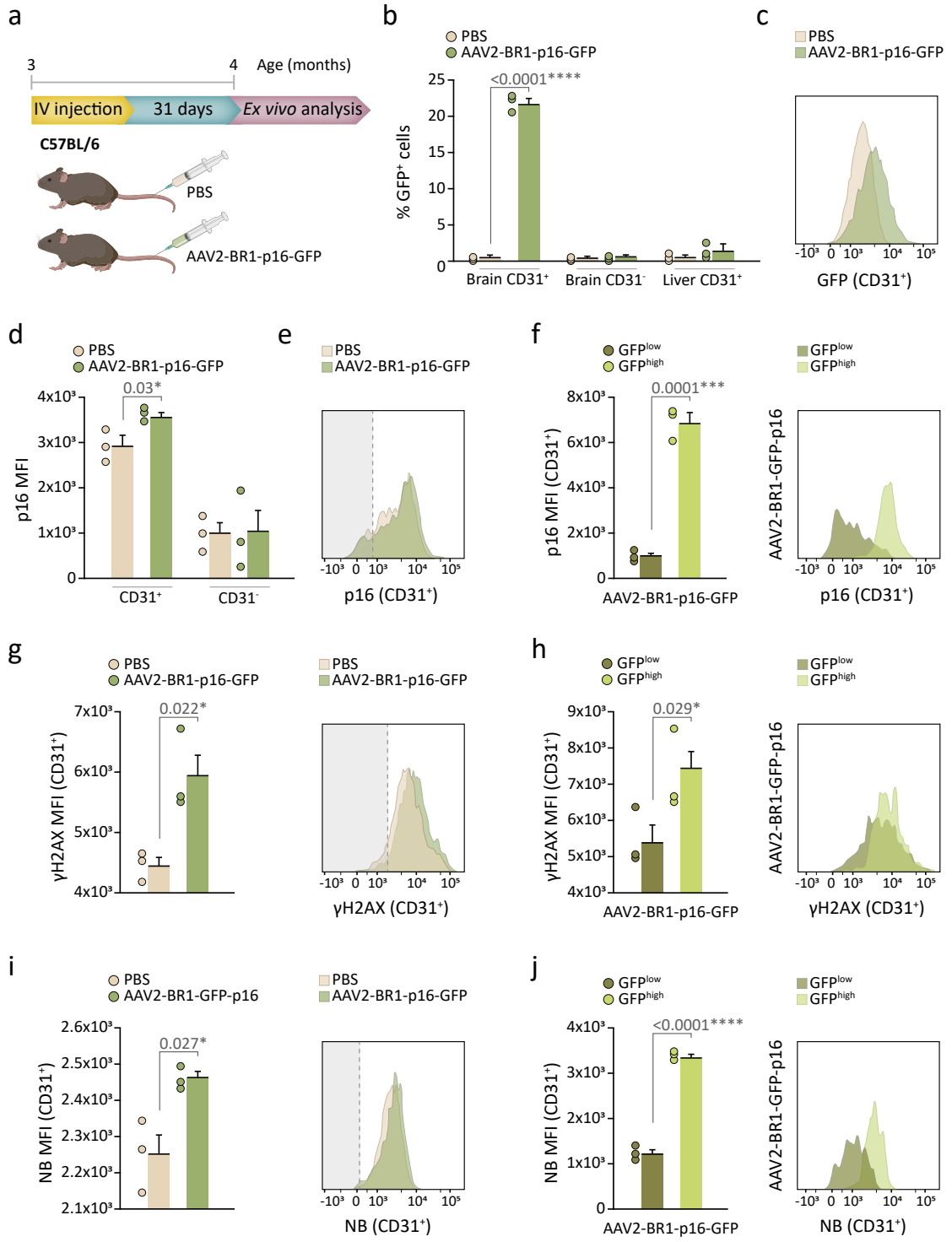

Figure 28. A genetic approach for selective induction of senescence in BECs. a) Schematic representation of the experimental design. Young C57BL/6 mice were injected with AAV2-BR1-p16-GFP for selective induction of senescence in BECs, and control mice were injected with PBS. After 31 days, mice were euthanized and processed for senescence detection by flow cytometry. **b**) FACS evaluation of vector transduction by analysing the percentage of GFP$^+$ cells within the CD31$^+$ cell population in brain (BECs), other brain cell populations (CD31$^-$) and in ECs in a different tissue, in this case liver. Note that only BECs from mice injected with the adeno-associated vector emit green fluorescence, indicating an efficient and selective transduction. **c**) Representative FACS histogram of GFP-associated fluorescence in BECs comparing animals injected with PBS or viral vector. **d**) Analysis of p16 MFI in CD31$^+$ and CD31$^-$ brain cell populations from mice that received either viral vector or PBS. Notice that p16 levels are significantly higher only in BECs isolated from mice injected with the modified AAV. **e**) Representative FACS histogram of p16-associated fluorescence in BECs

(Figure 28. Continued) comparing animals injected with PBS or viral vector. **f**) Evaluation of p16 MFI in mice injected with the viral vector comparing BECs positive (GFP^{high}) or negative (GFP^{low}) for GFP and representative FACS histogram illustration. Note that $CD31^{+}$ GFP^{high} cells showed significantly higher levels of p16. **g**) Analysis of γH2AX MFI in BECs from mice that received either viral vector or PBS, and representative FACS histogram of the results. **h**) Evaluation of γH2AX MFI in mice injected with the AAV, comparing BECs positive (GFP^{high}) or negative (GFP^{low}) for GFP, and representative FACS histogram illustration. Note that γH2AX levels are higher in GFP^{high} BECS population. **i**) Analysis of SA-β-Gal activity using the NBGal fluorogenic probe, assessing the MFI of the NB dye in BECs from mice injected with the viral vector versus PBS. Representative FACS histogram of NBGal-associated fluorescence in BECs, comparing mice that received the AAV with those that received PBS. **j**) Evaluation of SA-β-Gal activity in mice injected with the viral vector, comparing BECs positive (GFP^{high}) or negative (GFP^{low}) for GFP, and representative FACS histogram of the results. Observe that BECs with higher levels of GFP showed significantly greater β-Gal activity. The graphs show the mean ± SEM. Unpaired Student's t-test was used for statistical analysis. The exact p-values and the number of independent biological samples (represented as dots) used are indicated in the graphs.

For brain neurogenesis analysis, BrdU was injected i.p., twice daily, on days 14, 15, and 16 following adeno-associated virus inoculation (**Figure 29a**). We found fewer $BrdU^{+}$ cells in the GL of the OB in treated mice, indicating that senescent BECs have a strong impact on the neurogenic capacity of the SEZ (**Figure 29 b**). Furthermore, we analysed neurogenesis in the hippocampal SGZ, finding that there is a significant reduction in the number of $BrdU^{+}$ cells (**Figure 29c**). Therefore, the results revealed that senescent BECs alone can reduce the formation of new neurons in the adult brain.

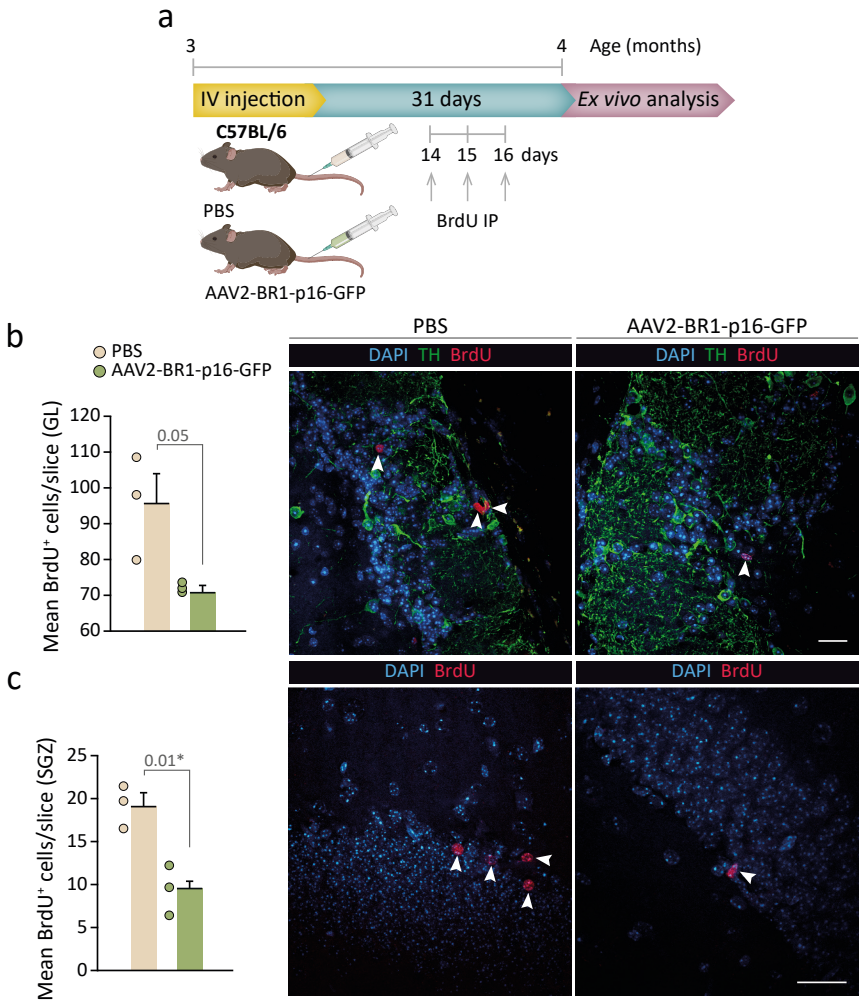

Figure 29. Assessment of the impact of selective genetic induction of senescence in BECs on adult neurogenesis. **a**) Experimental schedule for BrdU injections. Mice were i.p.-injected with BrdU, twice daily at an interval of 6 h, on days 14, 15 and 16 after i.v. injection of the viral vector or PBS. **b**) Analysis of neuron development by immunohistochemical detection of $BrdU^{+}$ cells in the GL of the OB, comparing mice injected with the viral vector versus PBS. **c**) Analysis of neuron development in the hippocampal DG by immunohistochemical detection of $BrdU^{+}$ cells in the SGZ, comparing mice injected with the viral vector versus PBS. The graphs show the mean ± SEM. Unpaired Student's t-test was used for statistical analysis. The exact p-values and the number of independent biological samples (represented as dots) used are indicated in the graphs. Scale bars: 100 µm.

Our work provides a valuable tool that opens up a range of possibilities for studying vascular senescence at the brain level and its currently unexplored effects. Importantly, using this genetic intervention, with the modified adeno-associated vector AAV2-BR1-p16-GFP, we have developed the first reported model of specific brain endothelial senescence induction. This strategy represents a promising approach for uncovering new potential therapeutic options, not only for promoting neurogenesis but also for addressing neurodegenerative disorders. Ultimately, our results indicate that senescent BECs play a significant role in the decline of adult neurogenesis.

Discussion

Ageing is characterised by a progressive functional decline in multiple organs leading to an alteration of systemic homeostasis and the concomitant development of age-related diseases. According to the World Health Organisation (WHO), the increasing life expectancy of the majority of the world's citizens will lead to doubling the population of people over 60 years of age by 2050, with far-reaching implications for health and social care costs. Neurological decline is a complex ageing-associated disorder with limited understanding that is emerging as one of the major public health challenges facing global society (Gorelick et al., 2017; Zheng and Chen, 2022). In fact, the WHO predicts that by 2040 neurodegenerative diseases will overtake cancer as the second leading cause of death, after cardiovascular diseases, in the ageing population. Therefore, it is imperative to elucidate the intricacies of brain deterioration to achieve healthy ageing, and this task requires addressing the mechanisms that lead to the loss of neurogenic activity over time.

One of the main features of ageing is the increased burden of senescence in the organism (López-Otín et al., 2013; 2023). Senescence is a state of irreversible cell cycle arrest in response to a variety of stressors that trigger a profound change in cell biology (Hernández-Segura et al., 2017). Senescent cells display DNA damage scars, morphological alterations, greatly increased levels of β-Gal activity and p16 and/or p21 CKI proteins (Herranz and Gil, 2018), among other disturbances. Characteristically, these cells also exhibit a rich SASP, whose components are mainly pro-oxidant and pro-inflammatory (Childs et al., 2017; van Deursen, 2014). Nonetheless, cellular senescence is a homeostatic process in which proliferative cessation conveniently prevents the spread of DNA damage to cell progeny. In this respect, senescent cells play a key role in tumour suppression, but they also have beneficial functions in optimising embryonic development, in tissue repair and regeneration, as well as in promoting cell reprogramming. However, while the short-term presence of senescent cells may be beneficial, their prolonged presence may be deleterious (Muñoz-Espín and Serrano, 2014; Huang et al., 2022).

The SASP promotes immune recruitment and elimination of senescent cells during younger ages, but senescent cells become resistant to extrinsic and intrinsic pro-apoptotic stimuli with increasing age (van Deursen, 2014). In fact, these cells have been reported to develop anti-apoptotic mechanisms that, together with a potential age-associated decline in immune function, contribute to incomplete elimination of senescent cells with ageing, resulting in their accumulation in tissues (Zhu et al., 2015; Yosef et al., 2016; Ovadya et al., 2018). In this context, chronic SASP can induce senescence in surrounding cells through paracrine signalling, leading to spread this cell fate, perpetuate an inflammatory environment, alter tissue function and structure, and potentially promote tumorigenesis and metastasis in a non-autonomous manner (Coppé et al., 2010; Campisi et al., 2011; Muñoz-Espín and Serrano, 2014; Bousset and Gil, 2022). When senescent cells are retained in tissues, resident SCs become exhausted in their attempt to repair tissue damage. Hence, senescence with advancing age leads to unstoppable tissue deterioration accompanied by the development of multiple age-related pathologies, including neurodegenerative diseases (Childs et al., 2017; Chinta et al., 2018; Zhang et al., 2019; Cué and Rueda, 2020; López-Otín et al., 2023). Given this overt dichotomy of senescent cells, it should be noted that this thesis always refers to senescence as a driver of ageing and its detrimental effects.

There is no single universal hallmark to detect senescent cells and, for this reason, it is always convenient to assess more than one (Hernández-Segura et al., 2018). Nevertheless, SA-β-Gal activity is one of the most accepted and widely used markers for senescent cell recognition. X-gal histochemical staining is the most commonly applied technique for the determination of the β-Gal enzyme, but its combination with other senescence indicators is severely limited, as it consists of a colorimetric reaction that requires cell fixation (Dimri et al., 1995; Debacq-Chainiaux et al., 2009). The development of new fluorogenic probes in the lab of Prof. Ramón Martínez-Máñez, such as AHGa, NBGal or WOS-Cy7Gal (Lozano-Torres et al., 2017; 2023; Rojas-Vázquez et al., submitted), has allowed us to detect SA-β-Gal activity in live cells under different senescent stimuli, as well as to phenotype senescent cells in combination with other senescence markers *ex vivo*. Recently, a new fluorogenic probe, called SPiDER-βGal (Dojindo, cat.

no. SG03-10), has been commercialised. It operates similarly to our probes, but is used together with bafilomycin A1, promising a more specific detection of senescent cells. Bafilomycin A1 is an inhibitor of the lysosomal proton pump, and causes pH alkalinisation in this compartment. However, bafilomycin A1 can also block mitochondrial ATP synthase, leading to mitochondrial uncoupling and subsequent energetic and metabolic dysfunction, thereby altering cell biology (Schüt et al., 2012; Redmann et al., 2017). The combination of β-Gal activity-based molecular probes with bafilomycin A1 may potentially compromise the accuracy of senescence characterization in conjunction with other senescence-associated markers, such as elevated ROS production. Furthermore, lysosomal pH alkalinisation fails to differentiate between age-related senescence and increased β-Gal activity caused by other factors, thus we did not consider it appropriate to apply this strategy.

The removal of senescent cells in tissues can appease the source of pro-inflammatory and stressful signals, allowing for better functionality of surrounding cells. In recent years, senolysis has emerged as a promising intervention for tissue rejuvenation. Killing these cells has been shown to help reduce inflammation and promote tissue renewal, offering beneficial effects in different age-related diseases (Xu et al., 2018; Ogrodnik et al., 2019). Still, replacing the removed cells to regenerate or repair tissue becomes very challenging when dealing with an aged environment in which the resident SCs are in an advanced state of exhaustion (Grosse et al., 2020). In this regard, it would be desirable to monitor age-associated senescence burden in order to initiate therapies (senolytic or senomorphic) at the right time for more lasting results (Ohtani, 2022). The absence of reagents to measure the senescent cell burden *in vivo* has not yet allowed a true correlation between senescence and age to be established (Blagosklonny, 2021). With the aim of developing a simple system for the *in vivo* detection of senescent cells, in this study we have devised a chemical strategy to promote the excretion in urine of a β-Gal activity-based fluorogenic probe. This method would enable the determination of systemic β-Gal activity in a non-invasive way, estimating the burden of senescence in the organism by simply measuring fluorescence in urine (Rojas-Vázquez et al., submitted).

To validate this innovative approach in an ageing context, we first used SAMP8 mice, which are prone to accelerated senescence, compared to SAMR1 mice, which are resistant to such senescence. Although these strains have been widely employed to study ageing-associated disorders, especially neurodegenerative ones, there is controversy in the literature about the onset of age-related phenotypic changes in the SAMP8 mice (Miyamoto et al, 1986; Butterfield and Poon, 2005; Yanai and Endo, 2016; Fernández et al., 2021). Therefore, to identify the age ranges in which there is a perceptible deterioration in SAMP8 mice, but still room for improvement in their health status, it was necessary to assess multiple physiological functions and behaviours at different chronological ages. On this basis, we conducted a longitudinal study covering various aspects related to ageing (physical, biochemical, motor and emotional) that allowed us to track the ageing process of male SAMP8 mice from 2- to 12-month-old, compared to their SAMR1 counterparts. Initially, we evaluated both males and females, but we realised that the rate of ageing was slower in females, as they performed better in tests until older ages (Flood et al., 1995). Consequently, we decided to conduct all our experiments only with males in order to avoid sex variability in our results. At the age of 7 months, we observed a generalised dysfunction in SAMP8 mice that was accentuated at older ages. Moreover, we identified increased anxious behaviour as a hallmark of functional ageing in this strain, which was also present during natural ageing in C57BL/6 mice, suggesting that anxiety could be a robust indicator of increasing age (Yanai and Endo, 2021; Vasilopoulou et al., 2021). To accurately associate age-related deficits with an increased senescence burden, we set out to measure global β-Gal levels at this age.

First, we examined the load of senescent cells *ex vivo* with recognized and widely used markers for cellular senescence detection such as p16, Lamin B1 and β-Gal activity (Hernández-Segura et al., 2018). For the assessment of SA-β-Gal activity, we used an in-house fluorogenic probe, WOS-Cy7Gal. We estimated the senescent cell burden by analysing these markers in two target tissues for senescent cell accumulation in the elderly, liver and kidney. Indeed, severe age-associated disorders triggered by a senescence process

have been described in both organs (Ogrodnik et al., 2017; Docherty et al., 2020). As expected, the results revealed a significantly heavier senescence burden in SAMP8 mice than in SAMR1 at 7 months. However, this approach still requires mice euthanasia and we were looking for strategies to address the senescent cell burden *in vivo*. Given the accuracy of WOS-Cy7Gal for the detection of senescent cells in consonance with other well-recognised markers during ageing, we decided to chemically modify this probe by the addition of two sulfonic groups in order to favour its excretion in urine (Rojas-Vázquez et al., submitted). Second, the modified probe, named Cy7Gal, was also administered to 7-month-old SAMP8 and SAMR1 animals. Consistent with the previous result, the Cy7Gal probe readout reaffirmed that the level of senescence is increased in SAMP8 mice at this age. To gain insight into the biodistribution of Cy7Gal, we measured the probe-associated fluorescence in plasma and urine samples from SAMP8 mice within 15 min, suggesting that the fluorophore rapidly diffuses from cells to blood stream and then is filtered at kidneys and accumulated in urine. Additionally, BALB/c mice of 2- and 14-month-old mice were injected with Cy7Gal to examine various organs, such as the bladder, brain, and lungs, through *ex vivo* IVIS imaging analysis (IVIS® spectrum, Perkin Elmer). We observed higher fluorescence levels in the older mice in all mentioned tissues. Notably, this probe has a wide distribution throughout the organism, and even seems to be able to reach the brain parenchyma, allowing us to obtain an estimated measure of the whole-organism burden of senescent cells (Rojas-Vázquez et al., submitted).

A marked increase in senescence burden and the onset of age-related disorders at the age of 7 months in SAMP8 mice, prompted us to target this age for a senolytic intervention with the combination of D+Q. These drugs act by inhibiting intrinsic anti-apoptotic pathways developed by senescent cells, promoting their elimination (Kirkland and Tchkonia, 2020). We used the Cy7Gal probe to measure systemic levels of β-Gal activity in order to monitor the load of senescence after the senolytic treatment. As we had evidenced that anxiety constitutes a phenotypic trait of accelerated and natural ageing, we examined the anxious behaviour of these animals as a correlate for the Cy7Gal probe readout. We found decreased Cy7 fluorescence levels in urine and reduced anxiety signs in SAMP8 mice treated with D+Q, compared to vehicle-treated mice, but only when evaluating shortly after the pharmacological intervention. Furthermore, we also identified a direct and significant correlation between the measurement of Cy7 fluorescence in urine and mouse anxious behaviour, demonstrating a connection between senescence and emotional alterations. In this sense, animals that received senolytic drugs showed decreased senescence levels and also performed better on anxious behaviour-related tests. Remarkably, upon evaluating long after treatment, we found no differences in either Cy7Gal-measured senescence levels or in anxious behaviour between D+Q and vehicle-treated mice. Senolytic treatment eliminates senescent cells but not the cause of their accumulation with age, hence it makes sense that these cells would reappear over time with the deleterious consequences of their accumulation in tissues. The discovery of the ephemeral nature of these treatments is not something trivial; until now, there was no clear evidence of this occurring *in vivo*, due to the shortage of tools for non-invasive detection of senescence-associated markers. In the SAMP8 mouse model the senolytic effects likely dissipate more quickly than in those of natural ageing, but this points out the need for monitoring of this type of therapies.

We also used the C57BL/6 mouse strain, as a model of natural ageing, to study age-associated increase in SA-β-Gal activity. In this mouse strain ageing-related changes are already extensively studied. In general, the greatest functional decline is reached after 20 months of age, manifested through several diseases that progressively leads to the death of the animal. Anxious-like behaviours become noticeable with increasing age and we indeed found a significant increase in anxiety signs in 15 versus 3-month-old C57BL/6 mice (Yanai and Endo, 2021). As with the SAMP8 strain, we targeted an age in the C57BL/6 strain at which there is still margin to alleviate some age-related disorders, and the selective removal of senescent cells is expected to lead to such improvement. Therefore, we initiated a D+Q senolytic treatment in 15-month-old C57BL/6 mice and found that age-associated anxious behaviour decreases with the reduction of senescence burden, as indicated by the Cy7Gal probe after the senolytic intervention. Interestingly, we also found a correlation between the levels of β-Gal activity assessed with the probe and the performance

of the animals during the anxious behaviour test. Thus, this molecular probe not only allows us to track the increased senescent cell burden with ageing, but it is also capable of predicting age-related behavioural traits, making it useful for measuring biological age.

We are aware of the limitation of this system, as there are other cells that exhibit high levels of the β-Gal enzyme and are not senescent at all (Yang et al., 2005). However, this is the first reported probe that collaborates to the detection of senescent cells non-invasively and has demonstrated a consistent senescence burden readout that is in agreement with other senescence-associated markers, age-related parameters and well-recognised senolytic drugs. The results highlight the value of this molecular probe for identifying target ages to implement personalised therapies at the most appropriate time point. These kinds of tools facilitate longitudinal studies and are readily transferable to humans, with the potential to be used for both diagnosis and prognosis of a range of diseases. Ultimately, Cy7Gal allowed us to associate a senescence marker with increasing age in naturally and accelerated ageing strains, establishing a correlation between an age-dependent emotional behaviour and senescence. This outcome supports that brain function is conditioned by senescent cells, as adult hippocampal neurogenesis is reportedly associated with anxiety-related behaviours (Revest et al., 2009).

Oxidative stress and neuroinflammation related to cellular senescence are major contributors to accelerated brain ageing, affecting neurogenesis and promoting neuronal degeneration (Chen et al., 2016; Kalamakis et al., 2019). NSCs in the two main adult neurogenic niches give rise to new neurons throughout life that are incorporated into pre-existing neural circuits (Silva-Vargas et al., 2013; Ruddy and Morshead, 2018; Obernier and Alvarez-Buylla, 2019). In the SEZ and the SGZ, NSCs coexist in a quiescent or non-proliferative state and in an active state that leads to self-renewal and differentiation (Urbán et al., 2019). Non-proliferation is also a characteristic of senescent cells, but quiescent cells can re-enter the cell cycle under physiological conditions. There is a great deal of diversity in NSCs based on their molecular signature. On their trajectory towards activity, qNSCs exhibit heterogeneous levels of quiescence. Accordingly, their transition to activation involves not only entry into the cell cycle but also profound changes in cell physiology (Dulken et al., 2017; Urbán et al., 2019; Ding et al., 2020). Long-lived proliferative cells benefit from quiescence, as it protects them from depletion of their proliferative potential and prevents the accumulation of replicative stress or damage that could lead to malignant transformation or senescence (Cheung and Rando, 2013). Indeed, there is evidence that a portion of aNSCs return to quiescence in both neurogenic niches, preserving the SC pool and extending neurogenesis (Obernier et al., 2018; Pilz et al., 2018; Urbán et al., 2019). Despite this, neurogenesis declines with age and NSCs and their neurogenic progeny fail to repair brain tissue in the elderly, for reasons that still remain unclear (Luo et al., 2006; Ahlenius et al., 2009; Ben-Abdallah et al., 2010; Lugert et al., 2010; Encinas et al., 2011; Conover and Shook, 2011; Shook et al., 2012; Kalamakis et al., 2019).

Recently, RNA sequencing analyses have revealed that there is a higher fraction of NSCs with a quiescence-related molecular profile in the elderly and that they become highly resistant to activation even in the presence of injury (Apostolopoulou et al., 2017; Ziebell et al., 2018; Kalamakis et al., 2019). Ageing drives numerous changes not only in NSCs, but also in the surrounding niche cells and in systemic signalling, making it difficult to pinpoint whether these changes are caused by cell-intrinsic or cell-extrinsic processes. Furthermore, it is unknown if qNSCs are susceptible to a senescent fate orchestrated by intrinsic age-related alterations. Functional studies on qNSCs are severely limited, as NSCs constitute a relatively small population in the brain, the niches environment are complex, methods to easily and reliably identify these cells are scarce, and qNSCs have not yet been successfully isolated and cultured *in vitro*. To date, only one population of SCs has been reported to undergo senescence *in vivo* caused by intrinsic variations: the geriatric SCs of skeletal muscle, or satellite SCs. Unlike NSCs, which reside in the niche in both quiescent and active states, the satellite SC population remains in reversible quiescence throughout life and only expands to regenerate tissue in case of injury. However, in the case of geriatric satellite SCs, regenerative functions are considerably diminished, as these old cells undergo a state of irreversible senescence caused

by p16 derepression. Prof. Pura Muñoz-Cánoves and her group found that ageing irreversibly affects muscle SCs, which cannot avoid their senescent fate even in young environments (Sousa-Victor et al., 2014). In contrast, geriatric subependymal NSCs have been shown to respond to extrinsic stimuli, such as physical exercise or a youthful environment in heterochronic parabiosis experiments, exhibiting similar levels of proliferation and differentiation as young NSCs (Ahlenius et al., 2009; Lugert et al., 2010; Katsimpardi et al., 2014). These results highlight the impact of extrinsic signals at this level and suggest that old NSCs mainly reflect the changes in their environment. Not least, NSCs are surrounded by multiple cellular elements responsible for regulating their activity, which may be affected by ageing and/or senescence (Silva-Vargas et al., 2013).

The ageing process affects the whole organism, causing alterations at the systemic level. In this context, the vasculature can be considered the largest and most ubiquitous organ in the body, reaching and connecting all tissues (Minami et al., 2019). The cellular components of blood vessels are directly exposed to circulating elements derived from different tissues, reflecting the general physiology at any time of life (Chen et al., 2020). Notably, vasculature plays an essential role in the CNS, meeting the high metabolic demand of the brain by providing a constant blood flow of nutrients and oxygen, as well as acting as a selective barrier for blood-borne molecules (Campos-Bedolla et al., 2014). At this level, the blood vessels adopt a specialised conformation, the BBB, where the ECs, lining the inner surface, are sealed by tight intercellular junctions that shield the brain parenchyma from the periphery and control the transfer of molecules. In neurogenic regions, the BBB is key for maintaining homeostasis and their privileged microenvironment (Tavazoie et al., 2008; Obermeier, et al., 2013). Interestingly, NSCs and NPCs have been found in close proximity to blood vessels, supporting that the brain vasculature exerts not only a structural but also a functional influence (Rojas-Vázquez et al., 2021).

Subependymal NSCs are exposed to signals derived from the vascular niche, either indirectly through the CSF conditioned by the highly vascularised CP, or through direct vascular interaction via their basal end. Particularly, the BBB in the SEZ niche lacks the astrocytic and pericyte envelope, which favours a direct interaction of NSCs with ECs (Tavazoie et al., 2008; Winkelman et al., 2021). As previously reviewed in the introduction of this thesis, NSCs and BECs are intimately linked. One of the main communication pathways between these two cell populations is mediated by diffusible local signals. EC-derived angiocrine factors constitute an important signalling source that converges on NSCs to tightly control their rates of activation, proliferation and differentiation, from postnatal development to old age (Rafii et al., 2016; Rojas-Vázquez et al., 2021). Moreover, BECs are highly exposed to circulating factors and small vesicles, which may trigger pro-ageing or pro-senescence effects at this level (Chen et al., 2020; Rojas-Vázquez et al., 2021). Disruption of the proper extrinsic regulation by BECs of NSC activity coud affect the proliferative capacity of these SCs. This makes endothelial senescence a potential driver of neurogenesis decline with ageing. Surprisingly, the relationship between BECs and NSCs has been poorly explored in the context of ageing. Although a connection between global vascular dysfunction and cognitive impairment and neurodegeneration has been described, the specific consequences of EC senescence in healthy brain ageing remain elusive (Rojas-Vázquez et al., 2021; Sikora et al., 2021). This is partly due to the lack of experimental models specially designed to study brain endothelial senescence and its effects. Given the crucial role of ECs in the regulation of NSC activity and the limited evidence of senescence in brain microvascular cells *in vivo*, we focused our study on brain endothelial senescence. In this regard, we have devoted our efforts to ascertain age-associated brain endothelial senescence and to explore its impact on neurogenesis.

As a first approach to study how BEC senescence may affect NSCs, the development of *in vitro* models of endothelial senescence, as well as the primary culture of murine SEZ NSCs, have been useful to explore the interaction between both populations in a precise and simple manner. The use of specific mitogens and the absence of serum protein in the culture medium prevents NSC differentiation and favours their self-renewal ability (Belenguer et al., 2016). Actually, the culture is sustained by NSCs with

proliferative potential (primed or activated) and can expand through several passages. As the most relevant intercellular signalling pathways of senescent cells are mediated by their secretome (SASP) (Fabián-Labora and O'Loghlen, 2020), we decided to investigate the paracrine effects of senescent EC-released factors on cultured NSCs. Our results suggest that soluble factors secreted by senescent BECs may exert a pro-senescence effect on NSCs *in vitro*. These cells exhibited a decreased proliferation index and low levels of Lamin B1, as well as increased β-gal activity and ROS production, all features of cellular senescence. However, we observed that the proliferative capacity of NSCs also decreases when exposed to control EC-secreted factors, as the percentage of DFFDA^{high} cells is significantly increased compared to unconditioned NSCs. An up-regulation of eNO followed by an enhanced release of NO (Govers et al., 2002) has been described in ECs when they are confluent in a monolayer, which may induce quiescence traits in NSCs (Carreira et al., 2014). In addition, ECs secrete the NT-3 factor, which promotes NCS quiescence by enhancing their self-production of NO. Thus, the cytostatic effect of control EC-derived factors was to be expected (Delgado et al., 2014). In the lab of Prof. Isabel Fariñas, it has also been observed that DFFDA^{high} cells show reminiscences of quiescent populations that largely coincide at the transcriptomic level with pNSCs (Belenguer et al., 2021). Although cellular senescence is characteristically associated with a decrease in eNOS activity (Yokoyama et al., 2014), senescent cell-derived factors lead to a more pronounced arrest of NSC self-renewal. Accordingly, senescent endothelial factors may involve other pathways that produce senescence or a deeper quiescence state in NSCs.

Our data show a significant difference in β-gal enzyme and Lamin B1 levels between non-conditioned NSCs and NSCs exposed to senescent endothelial factors, with no meaningful variations between non-conditioned NSCs and NSCs exposed to control endothelial factors. These results indicate that senescent BEC-derived molecules drive more complex changes in NSCs. Intriguingly, qNSCs share some features with senescent cells at the transcriptomic level, including a higher expression of *Glb1* mRNA (which codes for the β-gal enzyme), or a lower expression of *Lmbn1* (which codes for Lamin B1) (Leeman et al., 2018; Belenguer et al., 2021). Unfortunately, the current knowledge on qNSCs is mostly limited to transcriptomic analysis, making it difficult to unequivocally discern a senescent or a dormant fate in NSCs conditioned by endothelial senescent factors with our current data. Nonetheless, our findings suggest that endothelial senescence not only affects NSCs *in vivo* through structural changes, such as altered blood flow or impaired tight junctions, but also through a direct interaction mediated by senescent BEC-secretome. In order to uncover the molecular mechanisms that trigger this response in NSCs, we are currently conducting a proteomic study of the soluble molecules and sEVs secreted by ECs, which are considered key for spreading paracrine senescence (Borghesan et al., 2019; Fabían-Labora and O'Loghlen, 2020; Oh et al., 2022). Moreover, we intend to examine the transcriptomic profile of NSCs upon exposure to senescent EC-derived factors and vesicles, in an effort to enhance our understanding of the alterations incurred by these cells. On the other hand, it has been reported that NSCs in culture acquire a non-cycling quiescent profile in the presence of bone morphogenetic protein-4 (BMP4), which may be an interesting approach to investigate whether senescent EC factors affect qNSCs (Marques-Torrejon et al. 2021). Ultimately, we aim to identify potential therapeutic targets that contribute to extend NSC activity over time. Based on our results, it is evident that factors released by senescent BECs affect NSC behaviour. Therefore, we hypothesise that EC senescence in brain microvascular beds contribute to the age-related neurogenesis decline and impaired brain function. In this context, a deeper understanding of the global molecular mechanisms underlying brain endothelial senescence could be useful for devising interventions aimed at promoting healthier neurological ageing.

Although some work has reported an increase in senescent ECs with ageing in other tissues, and there are RNA sequencing studies that point to a senescent fate in BECs, protein expression levels of senescence-associated markers specifically in BECs have not yet been assessed *in vivo* (Zhan et al., 2010; Bhayadia et al., 2016; Regina et al., 2016; Jia et al., 2019; Kalamakis et al., 2019; Grosse et al., 2020; Kiss et al., 2020). In this regard, we have designed a FACS strategy applying our own molecular probes in combination with other senescence indicators to easily quantify the level of senescence in BECs *ex vivo*. Over the last few years, flow cytometry has emerged as a powerful tool to study population diversity

in the brain (Llorens-Bobadilla et al., 2015; Dulken et al., 2017; Belenguer et al., 2021). The use of more than three antibodies at the same time, in combination with better sensitivity and shorter analysis time, have overcome some of the limitations of traditional immunohistochemical techniques.

At the brain level, neurons exhibit physiologically elevated basal levels of the β-gal enzyme. In addition, it has been reported that these cells experience an increase in β-gal activity with age (Geng et al., 2010; Piechota et al., 2016). Neurons are highly susceptible to conventional enzymatic tissue dissociation methods. FACS strategies for neuron isolation often require fixation, a pool of several animals or tissue samples, genetically modified animal models and, also, their isolation is generally limited to the detection of nuclear epitopes. Furthermore, specific tissue disaggregation procedures are used to favour the enrichment of these cells (Lacar et al., 2016; Rubio et al., 2016; Martin et al., 2017; Eremenko et al., 2021). Considering all this, we decided to assess SA-β-Gal activity in brain endothelium by using the fluorogenic probes *ex vivo*. If administered *in vivo*, these probes are likely to cross the BBB and neurons could hoard the fluorescence, consequently masking age-related changes of the β-Gal enzyme in other cell populations, such as BECs. With our dissociation technique, we considerably reduce the number of neurons in the cell suspension in contact with the molecular probe. In this way, we are able to elucidate age-associated changes in SA-β-Gal activity in BECs, in a faithful manner to *in vivo*. Alongside the measurement of β-gal activity, we have analysed mitochondrial ROS production with a commercially available probe. Additionally, we have optimised the detection of well-accepted nuclear markers in the field of senescence, such as p16 and γH2AX. Using our BEC gating strategy and a combination of some of these markers in flow cytometry analysis, we confirmed that endothelial senescence increases with age at the brain level in both accelerated and naturally ageing animal models.

In parallel to the detection of the age-related accumulation of senescent BECs, we also used a unique flow cytometry protocol developed in the laboratory of Prof. Isabel Fariñas in which specific antibodies were used in combination to identify NSC populations and their neurogenic descendants in the SEZ niche (Belenguer et al., 2021). This FACS strategy confirmed that the increase in the levels of senescence-associated markers in BECs with ageing is also accompanied by a decline in the neurogenic potential of the SEZ. We found an *in vivo* correlation between brain endothelial senescence and decreased neurogenic activity that reinforces and supports our hypothesis that senescent BECs are a contributing factor to neurodegeneration.

Importantly, our senolytic treatment regimen has demonstrated beneficial effects on the CNS in mice models of natural and accelerated ageing. Indeed, we detected a decreased anxious-like behaviour in treated mice. D+Q drugs have been used in other studies demonstrating cognitive enhancement in mice, supporting that senescence plays a major role in brain ageing (Zhang et al., 2019; Krzystyniak et al., 2022; Ota and Kodama, 2022; Gonzales et al., 2022). Proper detection and elimination of senescent cells become reasonable targets for establishing a therapeutic approach to prevent brain deterioration. However, further research is needed to determine the specific effects of senolytic drugs on neurogenesis in aged mice. Venturing a bit further, we planned to test whether the correlation between increased brain endothelial senescence and impaired neurogenic function with ageing held in reverse, i.e., after senolytic intervention. In this regard, we assessed if senolysis reduces brain endothelial senescence burden and promotes neurogenesis recovery.

Following two cycles of senolytic treatment with D+Q in SAMP8 animals, we observed a decrease in senescence-associated markers in BECs and a potential recovery in the neurogenic activity of the SEZ lineage. Moreover, after just one cycle of treatment, we confirmed the reduction in the burden of senescent BECs and an increase in brain neurogenesis regarding the OB and the hippocampal DG. Treated SAMP8 mice showed increased number of $BrdU^+$ cells in the GL of the OB and the SGZ after a long chase injection protocol, compared to age-matched mice that received the vehicle. Interestingly, these mice also responded to different odorant stimuli more accurately, suggesting a higher production of neurons in the OB that tap into pre-existing circuits related to odour detection (Pérez-Villalba et al., 2015). In SAMP8

animals, a remarkable premature loss of NSCs has been described within the SEZ at the age of 10 months (Soriano-Cantón et al., 2015). In this context, senolytic treatment could prevent the rapid decline of NSCs by prolonging their neurogenic activity and the formation of new neurons through the reduction of anti-neurogenic signals. Furthermore, mice that received the senolytic drugs also showed better performance in tests assessing memory and emotional tasks, pointing to a more efficient neuronal circuitry at the hippocampal level than in vehicle-treated mice (Jessberger et al., 2009; Abrous and Wojtowicz, 2015; Kampermann, 2022; Bonds et al., 2023). These results suggest that senolysis may rescue, at least in part, the neurogenic function in elderly individuals or delay its deterioration, with a beneficial impact on ageing-associated brain disorders.

Not surprisingly, drugs that selectively induce apoptosis in senescent cells have become a prominent research topic in the field of ageing. However, at too advanced ages, the capacity of SCs to regenerate tissue and replace the removed senescent cells may be extremely impaired. In addition, the effects of these drugs are transient and their long-term use may be limited by adverse and off-target side effects (Ghosh et al., 2019; Ogrodnik et al., 2019). For this reason, it may also be interesting to look for therapies that not only eliminate senescent cells, but also promote tissue repair. In line with this idea, the combination of senolytic treatment and the administration of pro-youth factors could represent a promising strategy with more lasting results. For instance, the GDF11 factor stimulates SEZ vascular rejuvenation, which could contribute to restoring the proper extrinsic regulation that ECs exert on NSC behaviour and enhance neurogenesis. This circulating pro-youthful factor appears to promote neurogenic function through the restoration of vascular architecture that is accompanied by vessel remodelling, improved blood flow, and increased angiogenesis (Katsimpardi et al., 2014). This work suggested that the consequences of ageing on the brain vasculature contribute to neurodegeneration, which is consistent with our proposal of EC senescence as a driver of the age-related decline in neurogenic potential. Therefore, it appears desirable to target aged BECs in order to design therapies aimed at restoring adult neurogenesis. Ultimately, the goal is to repair damaged neural circuits and reduce the impact of age-associated neurodegenerative disorders or, at least, delay their development, rejuvenating brain tissue and extending brain health.

In our project, we approach ageing as a product of the accumulation of senescent cells, and senolytic agents have allowed us to evaluate the effects of the selective elimination of these cells. Our results indicate that the reduction of the senescent cell burden entails an enhancement in the generation of new neurons, but there are other studies that also report beneficial effects of senolysis at other levels, highlighting this strategy as an anti-ageing therapy. Not least, the D+Q senolytic drug combination is currently being tested in clinical trials (Hickson et al., 2019). Nevertheless, it is worth mentioning that there are other therapeutic approaches of great scientific interest under development. Although manipulation of dietary intake and physical exercise are among the best-studied interventions, a recent promising addition to anti-ageing strategies is cellular reprogramming (Ocampo et al., 2016; Simpson et al., 2021). Takahashi and Yamanaka demonstrated in 2006 that somatic cell identity can be rewritten (Takahashi and Yamanaka, 2006). They showed that overexpression of four transcription factors ("Yamanaka factors" or "OSKM" factors) reorganises the epigenetic map and converts somatic cells to a pluripotent state. Remarkably, induced pluripotency studies demonstrated that ageing-related cell phenotypes are not irreversible. However, the induction of pluripotency invariably leads to the appearance of tumours in mice (Wuputra et al., 2020). In this regard, "epigenetic rejuvenation" has been developed to make an old cell young again without loss of cell identity in order to avoid the risk of cancer. This intervention focuses on intermediate states during dedifferentiation, where old cells have started to change epigenetically but have not yet fully dedifferentiated. Transient cyclic reprogramming *in vivo* is one such example (Singh and Newman, 2018; Simpson et al., 2021; Chen et al., 2021; Wang et al., 2022). This strategy has been reported to have potential for ameliorating neurodegenerative diseases, but there is still a long way to optimise and implement this technique (Tamanini et al., 2018). Interestingly, senescent environments have been found to favour reprogramming *in vivo* due to certain cytokines derived from the secretome of senescent cells (Mosteiro et al., 2018). Additionally, some work suggests that these cells are also capable of rejuvenation,

but this deserves further investigation (Chiche et al., 2020).

Nonetheless, the technology used in this thesis has allowed us to achieve very important findings that represent a breakthrough in the fields of neurogenesis and senescence. Studies on vascular senescence in the brain are scarce, but much more limited when combined with the analysis of its impact on neurogenic niches. Relevantly, our data evidence the existence of a correlation between increased EC senescence and decreased neurogenesis during natural and accelerated ageing, which can be reversed by senolytic treatment. In fact, senolysis with D+Q drugs resulted in reduced endothelial senescence accompanied by increased neuronal development in the OB and the DG. Moreover, our observations from the primary culture of subependymal NSCs revealed that factors secreted by senescent BECs have a direct negative impact on these progenitor cells. However, increasing age is accompanied by an accumulation of senescent cells in various tissues, which may contribute to exerting an extrinsic pro-ageing effect on neurogenic niches independently of the vasculature. On the other hand, D+Q senolytic drugs act at the systemic level and can improve neurogenic function by a generalised decrease in the senescent cell burden, leading to a reduction of circulating pro-senescence factors. Although our *in vitro* study points to a cause-and-effect relationship between senescent endothelium and decreased NSC activity, it is worth noting that this model does not account for all *in vivo* stimuli mediated by different cellular components.

Therefore, we set out to investigate the cause-and-effect relationship between senescent BECs and neurogenesis decline in a deeper, more precise and refined manner. To do so, we designed a genetic approach using an adeno-associated AAV2-BR1 viral vector, whose capsid protein has been previously described to specifically target BECs (Körbelin et al., 2016). We included p16 genetic information in the vector to overexpress this cell cycle inhibitor and trigger a senescent fate in BECs *in vivo*. Indeed, a boost in p16 and senescence markers levels was exclusively noted in these cells by flow cytometry. As we used young mice, only brain endothelial senescence would be expected to have noticeable effects at the neurogenic level. With this strategy, we successfully induced selective senescence in BECs *in vivo* and also observed a marked decrease in neurogenesis in both the OB and the DG. These results confirm our hypothesis that a senescence process in ECs of the brain can strongly impact the neurogenic potential.

Accordingly, senescent BECs may actively contribute to the neurogenic dysfunction that accompanies neurodegenerative diseases in the elderly, becoming an attractive target to brain tissue rejuvenation. More importantly, our genetic strategy paves the way for further exploration of the underlying mechanisms behind the anti-neurogenic effect of senescent BECs and for identifying potential interventions for its reversal. Notably, through this work we have positioned endothelial senescence as a major driver of neurogenic decline, opening up an exciting new line of research to better understand brain ageing and for the development of innovative therapies aimed at promoting brain tissue regeneration, health and longevity.

Conclusions

1. Fluorogenic probes, specifically designed to be recovered in urine, allow for a systemic readout of β-Gal activity, leading to non-invasive estimation of senescence burden in longitudinal studies, either associated with ageing or senolytic therapies.

2. Longitudinal studies, correlating ageing-related anxiety and systemic β-Gal activity using urine-recovered fluorogenic probes, indicate that the effects of senolytic drugs are transient and fade over time.

3. Endothelial cells of the brain become senescent with ageing and this cell fate has a direct detrimental impact on neural stem cells and neurogenesis.

Summary

Introduction:

Ageing is a physiological process accompanied by a general decline in function and an increase in the burden of senescent cells in tissues (López-Otín et al., 2013; 2023). Cells exposed to stress factors generate a DNA damage response that can trigger a senescent fate, as an alternative to apoptosis. These stress factors can be of different nature, such as telomere shortening, DNA mutations, increased oxidative stress (reactive oxygen species, or ROS), among others. Cellular senescence is characterised by the increase of cell cycle inhibitors such as p16 or p21, and the irreversible loss of proliferative capacity that is also followed by other changes in cell biology (Herranz and Gil, 2018; Muñoz-Spín and Serrano, 2014). One of the most common phenotypic features of these cells is the high activity of the enzyme β-galactosidase (β-Gal or SA-β-Gal) due to the increase of the lysosomal compartment (Kurz et al., 2000). Additionally, senescent cells have a potent secretory phenotype (SASP), whereby they release pro-inflammatory and pro-oxidant factors that contribute to spreading senescence in tissues via paracrine manner (Childs et al., 2017; van Deursen, 2014).

Senescent cells develop anti-apoptotic mechanisms that favour their accumulation with age, potentiating a senescent environment (Zhu et al., 2015; Yosef et al., 2016; Ovadya et al., 2018). The persistence of SASP contributes to a pro-inflammatory environment that affects tissue function. In fact, the increase of senescence burden with ageing leads to the exhaustion of resident stem cells in the attempt to repair and recover tissue functionality. Although senescence, which stops cell growth, can act as a defence mechanism against tumours, it also promotes the development of various diseases during ageing, including cancer (Childs et al., 2017; Zhang et al., 2019). This is why when referred to senescence in an ageing context, essentially its negative effects are contemplated. The senescent cell burden is considered one of the main hallmarks of ageing and its adequate detection has become a priority for the development of therapeutic strategies (Muñoz-Spín and Serrano, 2014; López-Otín et al., 2023).

Unfortunately, there is no single universal marker for identifying senescent cells and, in addition, the phenotypic characteristics of these cells vary according to their origin, location and induction process (Hernández-Segura et al., 2018). However, measuring β-Gal activity represents one of the most widely used senescence markers in the field. Although this enzymatic activity has traditionally been determined by X-gal histochemical staining, this strategy has many limitations for use in combination with other senescence markers (Dimri et al., 1995; Debacq-Chainiaux et al., 2009). Currently, the development of fluorogenic probes for the detection of SA-β-Gal activity by fluorescence is emerging, which may be useful for the assessment of senescence *ex vivo* in conjunction with other markers (Lozano-Torres et al., 2017; 2023; Rojas-Vázquez et al., submitted). However, the association of age-related alterations with the senescent cell burden of the organism in longitudinal studies, has not yet been achieved. This type of strategy could be useful for the diagnosis of senescence-related diseases, as well as for the monitoring of therapies aimed at rejuvenating tissues (Rojas-Vázquez et al., submitted).

Progressive deterioration with age manifests itself with the onset of various pathologies that alter the well-being of the individual. In line with this, muscle strength, coordination and motor skills, as well as memory, cognition or emotion, among other aspects, begin to deteriorate, creating an imbalance in the health status between young and old animals that can be evaluated externally through specific tests (Yanai and Endo, 2021). Interestingly, senolytic strategies have demonstrated beneficial effects on the health of aged mice, improving physical function, reducing anxious behaviour and promoting healthy ageing (Xu et al., 2018; Ogrodnik et al., 2019; Ogrodnik et al., 2021). These results support that many of the changes that occur with increasing age are directly proportional to the prevalence of senescent cells in tissues.

The development of neurological disorders and neurodegenerative diseases is one of the primary concerns in the current socio-health landscape, as a result of the ageing population and the increasing incidence of these pathologies (Zheng and Chen, 2022). Research in this regard is progressing slowly due, in part, to the complexity of studying the ageing process at the brain level. In natural ageing mouse

models, such as the C57BL/6 strain, alterations at this level do not begin to manifest until at least 12 months of age (Yanai and Endo, 2021). Accelerated ageing animal models represent a good alternative in terms of cost and time. The senescence-prone (SAMP) or senescence-resistant (SAMR) mouse strains are among the most interesting models for gerontological studies (Takeda, 1999). In particular, SAMP8 mice are characterised by early deficits in memory and learning, as well as by sharing many features of human brain ageing, making them ideal models for the study of disorders such as Alzheimer's disease (Takeda, 2009; Ito, 2013; Akiguchi et al., 2017). The early deterioration of SAMP8 mice is a consequence of physiological ageing, whose incidence and severity increases with age. Therefore, studies using the SAM model, to clarify the mechanisms that lead to accelerated ageing, can give an idea of the fundamental mechanisms of natural ageing.

In the last years, it has been recognized that the exhaustion of adult stem cells in tissues triggers an unstoppable decline in organ function (Schultz and Sinclair, 2016; Rojas-Vázquez et al., 2021; López-Otín et al., 2023). Adult stem cells resident in specific tissues constitute a unique group of undifferentiated cells responsible for the maintenance of adult tissues in homeostasis and their potential regeneration in response to damage (Simons and Clevers, 2011). In relation to the adult brain of mammals, there are two main regions that harbour neural stem cells (NSCs) capable of generating new neurons destined for specific circuits: the subependymal zone (SEZ) and the subgranular zone (SGZ) of the dentate gyrus (DG) of the hippocampus. The SEZ is by far the most prolific niche in the mouse brain, generating millions of new neurons throughout life to be integrated into the olfactory bulb (OB) (Silva-Vargas et al., 2013; Ruddy and Morshead, 2018; Obernier and Alvarez-Buylla, 2019). However, adult neurogenesis experiences a great decline with ageing for reasons that are not yet well understood (Ben-Abdallah et al., 2010; Lugert et al., 2010; Encinas et al., 2011; Conover and Shook, 2011; Shook et al., 2012; Kalamakis et al., 2019).

NSCs in their niche environments coexist and interact with their progeny and other cell components, such as glial cells and vascular cells. Therefore, they are exposed to extrinsic stimuli that can influence their behaviour and play a role in the decline of neurogenic function with age (Silva-Vargas et al., 2013). Combining the use of specific markers with transcriptomic studies at the single cell level has enabled the development of strategies to detect subependymal NSCs, revealing significant heterogeneity in their proliferation dynamics. Thus, quiescent NSCs (qNSCs) and NSCs prone to activation or "primed" (pNSCs) coexist with proliferative or active NSCs (aNSCs). Maintaining homeostasis and proper neurogenic function requires a delicate balance between these states (Llorens-Bobadilla et al., 2015; Urbán et al., 2019; Belenguer et al., 2021). However, RNA sequencing studies in these stem cells over time point to a greater prevalence of qNSCs resistant to activation with increasing age (Kalamakis et al., 2019). Notably, old qNSCs recover some of their activity in response to certain pro-rejuvenation stimuli (Lugert et al., 2010; Katsimpardi et al., 2014). In this context, it is probable that the ageing environment, and extrinsic signals NSCs receive during ageing, inhibit the transition from quiescence to activation, contributing to the loss of the neurogenic activity.

The vasculature stands out as one of the key components of the neurogenic niches that has a significant impact on NSCs and their progeny. NSCs are in close contact with the blood vessels that make up the blood-brain barrier (BBB) in both the SEZ and the DG. The BBB plays an essential role in sustaining brain homeostasis, protecting the neural parenchyma and supplying nutrients and oxygen (Tavazoie et al., 2008; Shen et al., 2008; Rafii et al., 2016; Smith et al., 2018; Vicidomini et al., 2020). NSCs, in particular, maintain an intimate relationship with the endothelial cells (ECs) of the brain vessels, with which they interact actively and reciprocally. Angiocrine factors released by ECs have been shown to play a fundamental role in the proliferation, self-renewal and differentiation of NSCs (Delgado et al., 2014; Rojas-Vázquez et al., 2021). This communication pathway between the two populations seems to be actively involved in regulating NSC behaviour and, therefore, neurogenesis.

With age, the BBB also undergoes a profound transformation that compromises its integrity and

increases the exposure of these progenitor cells to circulating pro-ageing factors (Villeda et al., 2011; Obermeier et al., 2013; Segarra et al., 2021). Specifically, ECs undergo changes that alter their cellular function with age, affecting their regulatory role on NSC activity (Rojas-Vázquez et al., 2021). A senescent fate in these vascular cells could contribute to these deleterious events, but there are no functional studies on age-associated senescence in brain ECs (BECs) published yet. Despite this, phenotypic changes commonly associated with senescence have been observed in these cells with age, such as reduced proliferation, increased levels of p16 and p21, and metabolic disturbances (Rojas-Vázquez et al., 2021). At the transcriptomic level, changes have also been detected in old BECs compared to young ones, which include release of pro-inflammatory cytokines and generation of reactive oxygen species (Kalamakis et al., 2019; Kiss et al., 2020). In this scenario, BECs appear as an attractive target for studying the decay of neurogenic activity over time in both niches. However, determining the direct impact of endothelial senescence on neurogenesis in an aged organism is challenging due to the systemic accumulation of senescent cells, which can contribute to an anti-neurogenic effect through other means. According to the above, strategies are required to determine the specific role of endothelial senescence in the decline of neurogenesis. Nonetheless, this information highlights the potential of studying brain endothelium to understand brain ageing and develop therapeutic approaches for promoting brain health longevity.

In recent years, selective elimination of senescent cells (senolysis) has become one of the most promising strategies for tissue rejuvenation (see Rojas-Vázquez et al., 2021 for a review). Currently, the most promising senolytic drugs are those that target the anti-apoptotic mechanisms (SCAPs) that senescent cells are able to develop (Zhu et al., 2016; Hickson et al., 2019). In this regard, the combination of the drugs dasatinib and quercetin (D+Q) has been shown to effectively reduce senescence load *in vivo*, with minimal impact on other cells (Zhu et al., 2015). Intermittent treatment with these drugs in aged mice, or with certain senescence-related pathologies, has demonstrated positive effects on tissue regeneration and increased lifespan (Xu et al., 2018; Ogrodnik et al., 2019; Hickson et al., 2019; Ogrodnik et al., 2021). D and Q are able to cross the BBB and help reduce amyloid plaques or even enhance neurogenesis in the SEZ (Ogrodnik et al., 2019; Zhang et al., 2019). They have also been shown to improve the vasomotor function of aged mice (Roos et al., 2016). These results support that senolytic drugs can alleviate age-associated alterations in the brain, highlighting the close relationship between senescence and neurodegeneration. In this context, the detection and elimination of senescent cells could represent a novel therapeutic strategy for restoring neurogenesis and promoting long-term brain health, but still requires further investigation.

Objectives*:*

Ageing encompasses the development of several diseases that have been associated with an increased burden of senescence, such as neurodegenerative ones (Martínez-Cué and Rueda, 2020). Indeed, neurogenesis has been reported to decrease over time in the two main neurogenic niches of the mammalian brain, the SEZ and the SGZ (Encinas et al., 2011; Conover and Shook, 2011). However, it is unclear how senescence contributes to this end. Intriguingly, a definitive longitudinal correlation between ageing and senescence has yet to be established, due to the lack of tools for reliable detection of senescent cells *in vivo*. In this regard, our group is developing new strategies to identify senescent cells both *in vivo* and *ex vivo* with the aim of better understanding the impact of senescence on ageing in different organs, including the brain.

NSCs are exposed to multiple signals that extrinsically regulate their behaviour. The vasculature, especially BECs, exert a significant influence on NSC neurogenic function through diverse mechanisms (Rojas-Vázquez et al., 2021). The intimate relationship between BECs and NSCs makes the brain endothelium an attractive target of study. These vascular cells undergo functional alterations with ageing that may promote the loss of neurogenesis in the elderly. However, whether BECs can experience a senescent fate,

let alone whether this affects the neurogenic function of NSCs, has hardly been studied. In this context, our work is based on the hypothesis that ageing-associated senescence of BECs has deleterious effects on neurogenesis. To investigate this hypothesis, we have addressed two different primary objectives:

1. Development of novel strategies for longitudinally monitoring ageing-associated senescence *in vivo*.

2. Characterisation of ageing-associated brain endothelial senescence and its impact on adult neurogenesis.

Methods*:*

- Animal strains:

The mice were bred and housed in the animal facility of the University of Valencia (Servei Central de Suport a la Investigació Experimental, Burjassot) according to the guidelines of the European Union. In the experimental development, the SAMP8 mouse strain (as a model of accelerated ageing) and the SAMR1 strain (as its control) were used, as well as C57BL/6 (as a model of natural ageing) at different ages.

- Evaluation of the progression of ageing:

An in-depth study of the ageing process in SAMP8 mice (from 2 to 12 months of age) was carried out through the external evaluation of various age-associated phenotypic deficits, in comparison to the control strain SAMR1. Specific tests were carried out to evaluate physical, motor, metabolic, and emotional function. In this regard, we analysed the anxious behaviour of SAMP8 mice using the Open Field test. This emotional parameter was also evaluated during natural ageing, with the C57BL/6 strain.

- Validation of new fluorogenic probes for the detection of SA-β-Gal *in vitro* and *ex vivo*:

In the group led by Prof. Ramón Martínez-Máñez, new fluorogenic probes have been developed for the detection of β-Gal activity: AHGa, NBGal and WOS-Cy7Gal (Lozano-Torres et al., 2017; 2023; Rojas-Vázquez et al., submitted). Briefly, these probes consist of a fluorophore binding with a galactose derivative, and this bond can be hydrolysed by the lysosomal β-Gal enzyme. When the fluorophore is released, it emits high fluorescence allowing to identify those cells with higher β-Gal activity, i.e. senescent cells. Although the functional mechanism is similar to all, these probes differ mainly in the nature of the fluorophore.

An *in vitro* senescence model was developed with human ECs (hUVECs) treated with the inhibitor of CDKs 4 and 6 palbociclib. Senescence induction was tested by immunocytochemical analysis, using several markers associated with senescence: Ki67, Lamin B1, γH2Ax, p21. To do so, treated and untreated cells (controls) were fixed with 4% paraformaldehyde (PFA) and incubated with specific primary antibodies and fluorescently-labelled secondary antibodies. In addition, X-gal cytochemical staining was carried out following the instructions of the commercial Kit from Sigma-Aldrich (cat. no. CS0030-1KT). The labelled cells were photographed with a confocal microscope (Olympus FV10i) and the *Image J* software was used for image analysis.

Using this senescence model, we evaluated the signal associated with each of the fluorescent probes using confocal microscopy (Olympus FV-1000). To this end, we added the probe diluted in DMEM (10 µM AHGa, 2 µM NBGal and 20 µM WOS-Cy7Gal) and took images during the first hour of incubation. To quantify the difference in median fluorescence intensity (MFI) between control and senescent cells, we incubated the cells with each probe for 15 minutes. After centrifuging, we analysed the fluorescence associated with

each of the probes by flow cytometry (FACS) on a LSR-Fortessa (Becton Dickinson) cytometer.

In addition, the efficiency of the WOS-Cy7Gal probe has been tested in other *in vitro* senescence models, as well as in the *ex vivo* measurement of age-related senescence. *In vitro*, WOS-Cy7Gal has been used to measure β-Gal activity after replicative senescence induction in hUVECs or after exposure of bEnd.3 (mouse brain EC line) to oxidative stress (H_2O_2), in parallel with other senescence markers (p16, γH2AX). To do this, ECs were detached from the plate with a 0.05% trypsin/0.02% EDTA solution. A fraction of these cells was incubated with the probe for 15 minutes and the other was fixed and permeabilized, following the protocol detailed in the "Pharmingen™ Transcription-Factor Buffer Set" kit (BD-Biosciences), for subsequent incubation with specific primary antibodies and fluorescently-labelled secondary antibodies. The analysis was carried out by flow cytometry (LSR-Fortessa BD).

Regarding the detection of the senescent cell burden *ex vivo*, the WOS-Cy7Gal probe was used in conjunction with p16 and Lamin B1, to determine senescence levels in the liver and kidney of SAMP8 mice compared to SAMR1. To do so, the right kidney and a portion of the liver of 7-month-old SAMP8 and SAMR1 mice were extracted. Both tissues were enzymatically digested with collagenase/dispase and DNAse in an automatic dissociator (gentleMACS Octo Dissociator, Miltenyi) and filtered. Part of the sample was incubated with the WOS-Cy7Gal probe for 15 minutes. The other part was fixed and permeabilized for staining with specific primary antibodies and fluorescent secondary antibodies, following the protocol described in the "Pharmingen™ Transcription-Factor Buffer Set" kit (BD). The samples were analysed by flow cytometry (LSR-Fortessa BD).

- Culture of subependymal NSCs and evaluation of the paracrine effects of senescent ECs:

The methodological details and the culture media used for the establishment and propagation of NSC cultures can be consulted in the work published by our group in 2016 (Belenguer et al., 2016).

Concerning the experiments of NSCs conditioned by factors derived from senescent and control ECs, we used the senescence models established in hUVECs (using the drug palbociclib) and bEnd.3 cells (exposed to an oxidative stimulus). In both cases, control and senescent cells conditioned complete NSC medium without BSA for 24-48h. After this period, the soluble fraction of the medium was obtained by successive centrifugations (1,200 x*g*, 10 min and 10,000 x*g*, 60 min), filtration, and ultracentrifugation (100,000 x*g* 80 min). The NSCs were seeded with the media containing the soluble factors released by control or senescent ECs diluted 1/4, as well as with fresh NSC complete medium (unconditioned). A fraction of these cells were labelled with the cell division tracer Oregon Green 488 Carboxy-DFFDA-SE (DFFDA, ThermoFisher) before being seeded, in order to analyse the proliferation of these cells in the presence of senescent endothelial factors. After 4 days *in vitro*, the NSCs were dissociated with Acutase® and prepared for analysis. On the one hand, live cells were processed for the evaluation of DFFDA, β-Gal activity with the WOS-Cy7Gal probe, and ROS production with the commercial probe mitoSOX®-red (Invitrogen, refer to manufacturer's protocol). On the other hand, the NSCs were fixed, following the procedure described in the previous section for analysis of Lamin B1. All samples were analysed by flow cytometry (LSR-Fortessa BD).

- Phenotyping of senescent ECs in the brain using flow cytometry:

This procedure was carried out with the SAMP8, SAMR1, and C57BL/6 mouse strains. After euthanasia of the animal, the brain was extracted and bulbs and cerebellum were discarded. The tissue was enzymatically digested with collagenase/dispase and DNAse in an automatic dissociator (gentleMACS Octo Dissociator, Miltenyi). Then, it was filtered and processed to remove myelin (Debris Removal Solution, Miltenyi). For the analysis of BECs, CD45 antibody was used to exclude immune cells, and CD31 was used to select ECs (both from BD-Biosciences). The cells were incubated with these antibodies fluorescently labelled for 30 min at 4 °C. Then, the samples were divided for incubation with probes (WOS-Cy7Gal/NBGal and mitoSOX®) and for fixation-permeabilization (BD Pharmingen™ Transcription-Factor Buffer Set). The fixed

cells were incubated with specific primary antibodies (p16, γH2AX) and fluorescently-labelled secondary antibodies. The samples were analysed by flow cytometry (LSR-Fortessa BD).

- Phenotyping of the neurogenic lineage of the SEZ using flow cytometry:

In parallel to the phenotyping of endothelial senescence in the brain, the SEZ neurogenic lineage was analysed following the protocol detailed in the work published by our group in 2021 (Belenguer et al., 2021).

- Measurement of systemic β-Gal activity *in vivo*:

The WOS-Cy7Gal probe was chemically modified by adding two sulfonic groups to the fluorophore molecule, in order to make it more diffusible and able to be excreted in urine. This modified probe was named Cy7Gal. First, Cy7Gal was analysed by confocal microscopy in the same way as WOS-Cy7Gal, using the senescence model of palbociclib-treated hUVECs. Then, its biodistribution was studied in comparison to the WOS-Cy7Gal probe by intraperitoneal (i.p.) injection of both probes, or the vehicle (DMEM), in aged SAMP8 mice. After administration, the animals were anaesthetised by inhalation of isoflurane (2%) for 10 minutes. After this time, blood (submandibular vein) and urine samples were obtained. Blood was collected in heparinized tubes to obtain plasma (350 x*g*, 4 minutes). Plasma and urine samples were diluted (1/10 and 1/20 respectively) in 100 µl of distilled water prior to fluorescence analysis (Horiba Scientific Fluoromax-4 spectrofluorometer).

To measure systemic levels of β-Gal activity as a readout of senescence-associated ageing and/or senolytic treatments, the probe was injected i.p. in the experimental mice (140 mg/kg) and they were anaesthetised with isoflurane (2%) for 15 minutes. After this time, urine samples were collected and each one was diluted 1/20 in 100 µl of distilled water prior to the analysis in a fluorometer. To avoid variability in urination altering the results, the arbitrary units of fluorescence obtained were multiplied by the total volume of urine collected for each sample.

- Senolytic treatment:

The animals were treated orally with the combination of drugs D (5 mg/kg) + Q (50 mg/kg) (Xu et al., 2018). 7-month-old SAMP8 mice received this drug mixture for 5 consecutive weeks, alternating regimes of 5 or 1 day of treatment per week. The same group of animals received another cycle of treatment at 10 months. On the other hand, 15-month-old C57BL/6 mice received a D+Q regimen for 5 weeks with 2 doses per week.

- Immunohistochemical analysis of adult neurogenesis in the OB and the SGZ:

The mice were injected i.p. with a dose of 50 mg/kg of BrdU (10 mg/ml) twice a day, with a 6-hour interval, for 3 consecutive days. For BrdU immunohistochemical analysis, the injected animals were anaesthetised (with a mixture of medetomidine and ketamine, i.p.) and transcardiac perfused with 4% PFA. Mice under senolytic treatment were euthanized 26 days after BrdU injection, while mice treated with the AAV-BR1 were euthanized at 17 days. In the case of mice injected with the modified AAV-BR1, perfusion was not performed, and the bulb and hippocampus were dissected and post-fixed by immersion in 4% PFA for 24 hours. The brain/hippocampus and OBs were processed for sectioning on a vibratome. Subsequently, the detection of BrdU was carried out with specific primary antibody and fluorescently-labelled secondary antibody. The number of $BrdU^+$ cells in the glomerular layer (GL) of the OB, and in the SGZ, was counted manually under a Nikon ECLIPSE fluorescence microscope. The images were taken on a confocal microscope (Olympus FV10i).

- Analysis of the transduction of AAV2-BR1-GFP-p16 in BECs and its effect on neurogenesis:

Young C57BL/6 mice were injected intravenously (i.v.) with $1x10^{12}$ gc (genomic copies) of the AAV2-BR1-GFP-p16 adeno-associated vector into the tail vein (Körbelin et al., 2016). As a control, PBS was injected i.v. into mice of the same strain and age. On days 14, 15, and 16 after virus inoculation, BrdU was injected following the previously described protocol. After 31 days of the vector administration, the brain and a portion of the liver were extracted and processed, as previously described, for the identification of ECs and the analysis of senescence-associated markers such as SA-β-Gal (NBGal), p16, and γH2AX, using FACS. Additionally, GFP-associated fluorescence was evaluated in the liver and other brain cell populations to verify the specificity of virus infection. For the immunohistochemical analysis of neurogenesis in the OB and the SGZ, the procedure was followed as previously described.

Results and discussion*:*

The results of this thesis respond to the proposed objectives: from a more general study of senescence associated with ageing, to a more specific one focused on brain ageing by assessing endothelial senescence in the brain and its impact on adult neurogenesis.

1. Development of novel strategies for longitudinally monitoring ageing-associated senescence *in vivo*

In order to improve our understanding of ageing and its relationship with senescence, we first aimed to evaluate age-related phenotypic features in an animal model of accelerated ageing. To do this, we conducted a longitudinal study, evaluating a variety of easily measurable and age-related parameters (physical, biochemical, and emotional), which allowed us to characterise the ageing process in SAMP8 mice, compared to the SAMR1 strain. By assessing specific tests of different types and at different ages, we were able to discern the onset of typical age-associated deficits in SAMP8 mice. Surprisingly, we found that several signs of deterioration appeared earlier than described in the literature and this helped us to select target ages precisely to further assess the relationship between ageing and systemic senescence burden. Notably, SAMP8 mice exhibited particularly early emotional deterioration, only at 4 months of age, with evident signs of anxiety in the perception of open spaces (Open Field test). To clarify whether anxiety is a robust and useful marker to trace natural ageing, we also evaluated anxious behaviour in the C57BL/6 strain, comparing 3- and 17-month-old animals. The results obtained in the Open Field test indicated that 17-month-old animals experience a significant increase in anxiety levels with age.

With the purpose of investigating if these age-related phenotypic changes are associated with an increase in the senescent cell burden, fluorogenic probes based on the detection of SA-β-Gal activity were used to recognise senescent cells. First, these molecular probes (WOS-Cy7Gal, NBGal and AHGa) were validated in a well-characterised *in vitro* senescence model, hUVECs treated with the drug palbociclib. Through confocal microscopy and flow cytometry, it was found that cells treated with palbociclib exhibited a dotted pattern and higher fluorescence intensity than untreated cells (controls). This result correlates with the readout of other senescence-associated markers, indicating that the probes efficiently identify the increased lysosomal β-gal activity of senescent cells. Next, one of these probes was used to estimate the senescence levels in 7-month-old SAMP8 mice, compared to age-matched SAMR1 mice. Liver and kidney, two target organs for the accumulation of senescent cells, were processed for senescence analysis. β-Gal activity was assessed with the WOS-Cy7Gal probe, along with the levels of p16 and Lamin B1, two well-accepted markers in the field, by flow cytometry. Results indicate that there is a higher senescence burden in the SAMP8 strain at this age.

Given the efficiency of the WOS-Cy7Gal probe in measuring age-related senescence *ex vivo*, we decided to chemically modify it by including two sulfonic groups, in order to favour its excretion in urine. This modified probe, hereafter referred to as Cy7Gal, was injected into aged SAMP8 mice, compared to WOS-Cy7Gal, to analyse its biodistribution. Within 10 minutes of injection, urine and plasma samples were collected and then analysed for fluorescence levels. The probe with sulfonic groups was detected in both urine and plasma, while fluorescence levels in mice injected with WOS-Cy7Gal hardly differed from those administered with DMEM (vehicle). Based on these results, we infer that Cy7Gal diffuses rapidly from the cells into the blood and is filtered in the kidneys, accumulating in the urine. Next, we injected Cy7Gal in SAMP8 and SAMR1 animals at 7 months of age and, according to our *ex vitro* experiment, the fluorescence readout in urine indicated a higher systemic β-Gal activity in the SAMP8 mice. Therefore, the Cy7Gal probe appears as a valuable tool for the estimation of the burden of senescence *in vivo* and in a non-invasive way. In addition, we also tested the Cy7Gal probe in a natural ageing model with 3 and 15 month old C57BL/6 mice. The recorded fluorescence levels were significantly higher in the older mice, supporting the utility of this probe in measuring ageing-associated senescence in longitudinal studies. In this regard, we decided to test the efficacy of the probe as a monitoring tool in senolytic therapies.

First, we performed a senolytic treatment with D+Q in SAMP8 mice and analysed the effects of senolysis using the Cy7Gal probe and assessing anxious behaviour. In the short term after the senolytic treatment (20 days), we detected a decrease in signs of anxiety in the animals that received the drugs in correlation to a decrease in Cy7Gal-associated fluorescence in urine. Therefore, the probe indicates a reduction in senescent cell burden after treatment that has positive behavioural effects. On the other hand, when we evaluated the senolytic effects in the long term after treatment (over 50 days), we did not detect significant changes in either anxiety or the probe readout between treated and vehicle mice. This result shows that the effects of senolytic drugs *in vivo* are transient. To verify that the mice could respond again to the treatment, another cycle with D+Q was performed in the same animals. Interestingly, we detected a recovery in the effects of the senolytic drugs, with decreased signs of anxiety and reduced senescence burden in D+Q-treated mice. Furthermore, we identified a significant correlation between anxious behaviour and the probe readout when we evaluated the treatment in the short term. This result highlights that the probe is sensitive enough to predict an emotional age-related behaviour.

Second, we started senolytic treatment with D+Q on 15-month-old C57BL/6 mice. After the senolytic intervention, we detected the decrease in the senescence burden with Cy7Gal, as well as a reduction in anxious behaviour. Therefore, Cy7Gal allows for a reliable measurement of *in vivo* senescence burden and is a useful tool in longitudinal studies for diagnostic studies or for monitoring senolytic therapies. In addition, we found a significant correlation between anxiety and the probe readout, indicating that senescence has a strong detrimental impact at the brain level.

2. Characterisation of ageing-associated brain endothelial senescence and its impact on adult neurogenesis

In order to investigate whether BECs acquire a senescent fate with ageing in relation to a decrease in neurogenesis, we evaluated different senescence-associated markers in this vascular cells and analysed the SEZ neurogenic lineage. To do this, we developed a FACS strategy for phenotyping senescent BECs by evaluating β-Gal activity (with probes developed by our group), p16, and other markers such as γH2AX or ROS production (mitoSOX™). For the analysis of SEZ neurogenesis, we used the flow cytometry protocol published by our group (Belenguer et al., 2021). After applying these strategies in SAMP8 versus SAMR1 mice, as well as in young versus old C57BL/6 mice, the results showed that the levels of senescence-associated markers increase with ageing in BECs, while the neurogenic potential of the SEZ decreases.

To examine whether the correlation between increased endothelial senescence and reduced neurogenesis during ageing also remains under senolytic intervention, albeit inversely, we explored this connection in SAMP8 mice treated with D+Q. Alongside our FACs strategies, mice were injected with

BrdU for immunohistochemical analysis of neurogenesis in the OB and the DG. After pharmacological intervention, the results indicated a decrease in the levels of senescence-related markers in BECs and an increase the neurogenic potential of the SEZ, with notably more neurons generated in the OB in mice that received the senolytic drugs. Moreover, the number of BrdU+ cells in the SGZ was also markedly higher in SAMP8 mice treated with D+Q. These results demonstrate a consistency in the relationship between endothelial senescence and adult neurogenesis.

With the aim of analysing whether there is a cause-and-effect connection between brain endothelial senescence and decreased neurogenesis, we designed a model for the genetic induction of senescence in BECs, and studied its impact on adult neurogenesis. This strategy consists of an adeno-associated viral vector whose capsid protein is tropic for BECs (AAV-BR1) (Körbelin et al., 2016). In this vector, we have included genetic material for the overexpression of p16 in order to induce senescence in BECs. Additionally, we have incorporated GFP for easy analysis of virus transduction. Following i.v. injection of this modified vector or PBS (as a control) in C57BL/6 mice, BrdU was administered to analyse neurogenesis in the OB and the SGZ. The mice were euthanized 31 days after the inoculation of the adeno-associated vector, and we evaluated endothelial senescence in brain and liver by flow cytometry. Results showed that only BECs from virus-injected mice had significantly higher levels of GFP and p16, highlighting the specificity of the approach. This population also showed increased β-Gal activity and higher levels of γH2AX, confirming the induction of senescence. The immunohistochemical analysis revealed a decrease in the number of new neurons in both the OB and the DG in mice that received the virus compared to control ones. Thus, we conclude that endothelial senescence has a profound impact on adult neurogenesis, as it alone can reduce the number of new neurons created in the brain's main neurogenic niches. The results highlight the endothelial population as a key target for research in the study of brain ageing.

Conclusions*:*

1. Fluorogenic probes, specifically designed to be recovered in urine, allow for a systemic readout of β-Gal activity leading to non-invasive estimation of senescence burden in longitudinal studies, either associated with ageing or senolytic therapies.

2. Longitudinal studies, correlating ageing-related anxiety and systemic β-Gal activity using urine-recovered fluorogenic probes, indicate that the effects of senolytic drugs are transient and fade over time.

3. Endothelial cells of the brain become senescent with ageing and this cell fate has a direct detrimental impact on neural stem cells and neurogenesis.

Resumen

Impacto de la senescencia endotelial cerebral sobre la neurogénesis: aplicación de nuevas estrategias para la detección de senescencia asociada a la edad.

Introducción:

El envejecimiento es un proceso fisiológico que se acompaña de un deterioro funcional generalizado y de un aumento de la carga de células senescentes en los tejidos (López-Otín et al., 2013; 2023). Las células expuestas a factores estresantes generan una respuesta de daño en el ADN que puede desencadenar un destino senescente, alternativo a la apoptosis. Estos factores de estrés pueden ser de distinta índole, como el acortamiento de los telómeros, mutaciones en el ADN, aumento del estrés oxidativo (especies reactivas del oxígeno, o "ROS" por sus siglas en inglés), entre otros. La senescencia celular se caracteriza por el aumento de inhibidores del ciclo, como p16 o p21, y la pérdida irreversible de la capacidad proliferativa que, además, se acompaña de otros cambios en la biología de la célula (Herranz and Gil, 2018; Muñoz-Spín and Serrano, 2014). Uno de los rasgos fenotípicos más frecuentes en estas células es la alta actividad de la enzima β-Galactosidasa (β-Gal o SA-β-Gal) debido al aumento del compartimento lisosomal (Kurz et al., 2000). A su vez, las células senescentes poseen un potente fenotipo secretor ("SASP" por sus siglas en inglés) mediante el que liberan factores pro-inflamatorios y pro-oxidantes que contribuyen a la propagación de la senescencia en el tejido de forma paracrina (Childs et al., 2017; van Deursen, 2014).

Las células senescentes desarrollan mecanismos anti-apoptóticos que favorecen su acumulación con la edad, potenciando un entorno senescente (Zhu et al., 2015; Yosef et al., 2016; Ovadya et al., 2018). La persistencia del SASP promueve un ambiente pro-inflamatorio que afecta a la función tisular. El aumento de la carga de senescencia durante el envejecimiento conduce al agotamiento de las células madres residentes en su intento de reparar y recuperar la funcionalidad del tejido. De este modo, la senescencia, al detener el ciclo celular, puede actuar como mecanismo de defensa frente a tumores pero, durante el envejecimiento, esta promueve el desarrollo de diversas enfermedades, incluido el cáncer (Childs et al., 2017; Zhang et al., 2019). Es por esta dicotomía que, cuando se habla de senescencia crónica asociada a la edad, esencialmente se contempla el "lado oscuro" de este proceso celular que contribuye a la degeneración de los tejidos. Por tanto, la carga senescente se considera uno de los principales detonadores del envejecimiento y su efectiva detección se ha convertido en una prioridad para el desarrollo de estrategias terapéuticas (Muñoz-Spín and Serrano, 2014; López-Otín et al., 2023).

Desafortunadamente, no hay un único marcador universal para identificar células senescentes y, además, las características fenotípicas de estas células varían según su origen, ubicación y el proceso de inducción (Hernández-Segura et al., 2018). No obstante, la medida de la actividad β-Gal representa uno de los marcadores más empleados en el campo. Aunque esta actividad enzimática se ha determinado tradicionalmente mediante la tinción X-gal, este método presenta muchas limitaciones para su uso en combinación con otros marcadores de senescencia (Dimri et al., 1995; Debacq-Chainiaux et al., 2009). Actualmente, está emergiendo el desarrollo de sondas fluorogénicas para la determinación de la actividad β-Gal mediante fluorescencia, lo que puede ser útil para la detección de senescencia *ex vivo* junto a otros marcadores (Lozano-Torres et al., 2017; 2023; Rojas-Vázquez et al., submitted). Sin embargo, la asociación de alteraciones relacionadas con la edad y la carga senescente del organismo, de manera longitudinal, todavía no se ha conseguido. Este tipo de estrategia sería interesante para el diagnóstico de enfermedades relacionadas con senescencia y para monitorizar terapias que persigan el rejuvenecimiento de los tejidos (Rojas-Vázquez et al., submitted).

El deterioro progresivo con la edad se manifiesta con la aparición de diversas patologías que alteran el bienestar del individuo. En este sentido, la fuerza muscular, la coordinación motora, memoria, cognición y emoción, entre otros aspectos, empiezan a deteriorarse creando un desequilibrio en el estado de salud entre animales jóvenes y viejos que puede ser evaluado de forma

externa mediante test específicos (Yanai and Endo, 2021). Curiosamente, las intervenciones senolíticas han tenido efectos beneficiosos sobre la salud de ratones envejecidos, mejorando la función física, reduciendo el comportamiento ansioso y fomentando un envejecimiento saludable (Xu et al., 2018; Ogrodnik et al., 2019; Ogrodnik et al., 2021). Estos resultados sostienen que muchos de los cambios acaecidos con el aumento de la edad son directamente proporcionales a la prevalencia de las células senescentes en los tejidos.

El desarrollo de enfermedades neurodegenerativas representa una de las principales inquietudes del panorama socio-sanitario actual, debido al incremento de la población envejecida y de la incidencia de estas patologías (Zheng and Chen, 2022). Las investigaciones a este respecto avanzan lentamente debido, en parte, a la complejidad del estudio del proceso de envejecimiento a nivel cerebral. En modelos de ratón de envejecimiento natural, como la cepa C57BL/6, este tipo de alteraciones no comienzan a manifestarse hasta al menos los 12 meses de edad (Yanai and Endo, 2021). En este sentido, los modelos animales de envejecimiento acelerado representan una buena alternativa en términos de coste y tiempo. Los ratones de la cepa propensa a la senescencia acelerada (SAMP) o resistente a esta (SAMR) constituyen unos de los modelos más interesantes en el estudio gerontológico (Takeda, 1999). En concreto, los ratones SAMP8 se caracterizan por presentar déficits de memoria y aprendizaje tempranos, así como por compartir muchos rasgos del envejecimiento cerebral humano, convirtiéndolos en modelos de estudio de enfermedades como Alzheimer (Takeda, 2009; Ito, 2013; Akiguchi et al., 2017). El deterioro temprano de los ratones SAMP8 es consecuencia de la senectud fisiológica, cuya incidencia y severidad aumenta con la edad. Por tanto, los estudios llevados a cabo usando el modelo SAM para dilucidar los mecanismos que conducen al envejecimiento acelerado, pueden dar una idea de los mecanismos fundamentales del envejecimiento natural.

Recientemente, se ha establecido que el agotamiento de las células madre en los tejidos desencadena un imparable declive funcional en los órganos (Schultz and Sinclair, 2016; Rojas-Vázquez et al., 2021; López-Otín et al., 2023). Las células madre adultas residentes en tejidos específicos constituyen un grupo único de células indiferenciadas que es responsable del mantenimiento de los tejidos adultos en homeostasis y de su potencial regeneración en respuesta a daño (Simons and Clevers, 2011). En relación al cerebro adulto de los mamíferos, existen dos regiones principales que albergan células madre neurales (“NSCs” por sus siglas en inglés) capaces de generar nuevas neuronas destinadas a circuitos específicos: la zona subependimaria (“SEZ” por sus siglas en inglés) y la zona subgranular (“SGZ” por sus siglas en inglés) del giro dentado (“DG” por sus siglas en inglés) del hipocampo. La SEZ es el nicho más prolífico con diferencia en el cerebro de ratón, generando millones de nuevas neuronas a lo largo de la vida para que se integren en el bulbo olfatorio (“OB” por sus siglas en inglés) (Silva-Vargas et al., 2013; Ruddy and Morshead, 2018; Obernier and Alvarez-Buylla, 2019). Sin embargo, hay una pérdida de neurogénesis con el envejecimiento por razones que aún no se conocen bien (Encinas et al., 2011; Conover and Shook, 2011; Kalamakis et al., 2019).

Las NSCs en los nichos coexisten con células de su progenie y otros componentes celulares (células gliales, vasculares, …) y, por tanto, están expuestas a diferentes estímulos extrínsecos que modulan su comportamiento y pueden ser partícipes de la pérdida de actividad neurogénica que acontece con la edad (Silva-Vargas et al., 2013). El desarrollo de estrategias que permiten la detección de estas células mediante la combinación de marcadores específicos, y los estudios transcriptómicos a nivel de célula única, revelan que existe una gran heterogeneidad en las NSCs subependimarias en relación a su dinámica de proliferación. De este modo, se distinguen NSCs con distintos grados de quiescencia, que simplificamos en quiescentes (qNSCs) y propensas a la activación (“primed” en inglés) (pNSCs), que conviven con NSCs activadas (aNSCs). El equilibrio entre estos estados es necesario para mantener la homeostasis y la correcta función neurogénica (Llorens-Bobadilla et al., 2015; Urbán et al., 2019; Belenguer et al., 2021). Sin embargo, estudios de secuenciación de ARN en estas células madre a lo largo del tiempo, apuntan a una mayor prevalencia de qNSCs resistentes a la activación con la edad (Kalamakis et al., 2019). De forma llamativa, las qNSCs envejecidas recuperan parte de su actividad ante determinados estímulos pro-rejuvenecimiento (Lugert et al., 2010; Katsimpardi et al., 2014). En este contexto, parece que el entorno envejecido, y las señales extrínsecas que reciben

las NSCs durante el envejecimiento, pueden ser potenciales inhibidores de la transición del estado quiescente al activado y, por tanto, contribuir a la pérdida de la actividad neurogénica.

Entre aquellos componentes de los nichos neurogénicos que pueden ejercer mayor influencia en las NSCs y su descendencia, destaca la vasculatura. Las NSCs mantienen un contacto íntimo con los vasos sanguíneos que componen la barrera hematoencefálica ("BBB" por sus siglas en inglés) tanto en la SEZ como en el DG. La BBB desempeña un papel esencial en el mantenimiento de la homeostasis cerebral, protegiendo el parénquima neural y suministrando nutrientes y oxígeno (Tavazoie et al., 2008; Shen et al., 2008; Rafii et al., 2016; Smith et al., 2018; Vicidomini et al., 2020). Las NSCs, en concreto, guardan una estrecha relación con las células endoteliales de los vasos ("ECs" por sus siglas en inglés), con las que interaccionan de forma activa y recíproca. Los factores angiocrinos liberados por las ECs han demostrado jugar un rol fundamental en la proliferación, auto-renovación y diferenciación de las NSCs (Delgado et al., 2014; Rojas-Vázquez et al., 2021). Por tanto, esta vía de comunicación entre ambas poblaciones parece estar involucrada de forma activa en la regulación del comportamiento de las NSCs y, por ende, de la neurogénesis.

Con la edad, la BBB también experimenta una transformación profunda que compromete su integridad y aumenta la exposición de las células progenitoras neurales a factores circulantes pro-envejecimiento (Villeda et al., 2011; Obermeier et al., 2013; Segarra et al., 2021). Especialmente, las ECs sufren cambios que alteran su función celular con la edad y afectan a su papel regulador sobre la actividad de las NSCs (Rojas-Vázquez et al., 2021). Un destino senescente en estas células vasculares podría contribuir a estos acontecimientos deletéreos, pero aún no hay estudios funcionales publicados sobre la senescencia asociada a la edad en las ECs de cerebro. No obstante, se han descrito una serie de cambios fenotípicos en estas células con la edad, como una bajada en la proliferación, el aumento en los niveles de p16 y p21 o cambios a nivel metabólico, entre otros, que típicamente se asocian a un perfil senescente (Rojas-Vázquez et al., 2021). A nivel transcriptómico también se han detectado alteraciones, respecto a las ECs jóvenes, que incluyen liberación de citoquinas pro-inflamatorias y generación de especies reactivas del oxígeno (Kalamakis et al., 2019; Kiss et al., 2020). En este escenario, las ECs de cerebro aparecen como una diana interesante en el estudio del deterioro de la actividad neurogénica con la edad en ambos nichos. Sin embargo, determinar el impacto directo de la senescencia endotelial sobre la neurogénesis en un organismo envejecido es una ardua tarea, ya que la acumulación de células senescentes se produce a nivel sistémico y esta puede contribuir al efecto anti-neurogénico por otros medios. De acuerdo con lo anterior, se necesitan estrategias que permitan discernir el papel de la senescencia endotelial sobre el declive neurogénico. Con todo, esta información sitúa al endotelio cerebral como un punto de investigación prometedor para entender el envejecimiento cerebral y buscar enfoques terapéuticos que impulsen la longevidad de la salud cerebral.

En los últimos años, la eliminación selectiva de células senescentes (senolisis) se ha convertido en una de las estrategias con mayor interés para el rejuvenecimiento tisular (Rojas-Vázquez et al., 2021 para una revisión). Los fármacos senolíticos más prometedores en el panorama actual son aquellos dirigidos a inhibir los mecanismos anti-apoptóticos ("SCAPs" por sus siglas en inglés) que desarrollan las células senescentes (Zhu et al., 2016; Hickson et al., 2019). A este respecto, la combinación de los fármacos senolíticos dasatinib y quercetin (D+Q) ha demostrado reducir la carga senescente *in vivo* con efectos insignificantes sobre otras células (Zhu et al., 2015). El tratamiento intermitente con estos fármacos de ratones envejecidos, o con determinadas patologías asociadas a senescencia, ha conseguido efectos positivos en la renovación de tejidos dañados, así como en la esperanza de vida de estos animales (Xu et al., 2018; Ogrodnik et al., 2019; Hickson et al., 2019; Ogrodnik et al., 2021). D y Q son capaces de atravesar la BBB y favorecer la reducción de placas amiloides o incluso potenciar la neurogénesis en la SEZ (Ogrodnik et al., 2019; Zhang et al., 2019). Además, han demostrado mejorar la función vasomotora de ratones envejecidos (Roos et al., 2016). Estos resultados sostienen que los fármacos senolíticos pueden aliviar las alteraciones asociadas a la edad a nivel cerebral y demuestran la estrecha relación entre la senescencia y la

neurodegeneración. En este sentido, la detección y eliminación de células senescentes podría representar una nueva vía terapéutica para recuperar la neurogénesis y fomentar la salud del cerebro, pero esto aún requiere más investigación.

Objetivos:

El envejecimiento engloba el desarrollo de diversas enfermedades que se han asociado a una mayor carga de senescencia, como aquellas neurodegenerativas. De hecho, se ha descrito que la neurogénesis disminuye con el aumento de la edad tanto en la SEZ, como en la SGZ. Sin embargo, no está claro cómo contribuye la senescencia a este fin. Sorprendentemente, todavía no existe una verdadera correlación longitudinal entre el envejecimiento y la senescencia, debido a la falta de herramientas para la detección fiable de células senescentes *in vivo*. En este sentido, nuestro grupo está desarrollando nuevas estrategias para detectar células senescentes tanto *in vivo* como *ex vivo* que resulten útiles para comprender cómo contribuye la senescencia al envejecimiento en diferentes tejidos, incluido el cerebro.

Las NSCs están expuestas a múltiples señales que regulan extrínsecamente su comportamiento. De hecho, la vasculatura y, especialmente las ECs, ejercen una fuerte influencia sobre la función neurogénica de las NSCs mediante diversas vías. La íntima relación entre las ECs y las NSCs hace del endotelio cerebral una interesante diana de estudio. Las ECs sufren alteraciones funcionales con el envejecimiento que pueden contribuir a la pérdida de neurogénesis con la edad. No obstante, apenas se ha explorado si las ECs pueden sufrir un destino senescente, y mucho menos si esto afecta a la función neurogénica de las NSCs. En este contexto, nuestro trabajo se basa en la hipótesis de que la senescencia de las ECs de cerebro asociada al envejecimiento tiene efectos deletéreos sobre la neurogénesis. Para ello, hemos abordado los dos siguientes objetivos principales:

1. Desarrollo de estrategias novedosas para monitorizar longitudinalmente la senescencia asociada al envejecimiento *in vivo*.

2. Caracterización de la senescencia endotelial cerebral asociada al envejecimiento y su impacto en la neurogénesis adulta.

Material y métodos:

- Cepas animales:

Los ratones fueron criados y alojados en el animalario de la Universitat de València (Servei Central de Suport a la Investigació Experimental, Burjassot) según las directrices de la Unión Europea. En el desarrollo experimental se utilizaron las cepas de ratón SAMP8 (como modelo de envejecimiento acelerado) y SAMR1 (como su control), así como C57BL/6 (como modelo de envejecimiento natural), a diferentes edades.

- Evaluación externa de la progresión del envejecimiento:

Con ratones SAMP8 se llevó a cabo un estudio pormenorizado del proceso de envejecimiento (desde los 2 a los 12 meses de edad) mediante la evaluación externa de diversos cambios fenotípicos asociados a la edad, de forma comparativa a la cepa control SAMR1. De este modo, llevamos a cabo pruebas específicas para la evaluación de la función física, motora, metabólica, así como emocional. A este último respecto, analizamos el comportamiento ansioso de los animales SAMP8 con la prueba de Campo Abierto (“Open Field test” en inglés). Este parámetro emocional también se evaluó durante el envejecimiento natural, con

la cepa C57BL/6.

- Validación de nuevas sondas fluorogénicas para la detección de SA-β-Gal *in vitro* y *ex vivo*:

En el grupo liderado por el profesor Ramón Martínez-Máñez se han desarrollado nuevas sondas fluorogénicas para la detección de la actividad β-Gal (AHGa, NBGal y WOS-Cy7Gal) (Lozano-Torres et al., 2017; 2023; Rojas-Vázquez et al., submitted). Brevemente, estas sondas consisten en un fluoróforo asociado a un derivado de galactosa, mediante un enlace O- o N-glicosídico, susceptible de ser hidrolizado por la enzima β-Gal. Cuando el fluoróforo es liberado, emite una alta fluorescencia permitiendo identificar aquellas células con mayor actividad β-Gal, es decir, las senescentes. Aunque el mecanismo funcional es similar a todas, estas sondas difieren, principalmente, en la naturaleza del fluoróforo.

Con ECs humanas (hUVECs), se desarrolló un modelo de senescencia *in vitro* tras el tratamiento con el fármaco inhibidor de CDKs 4 y 6 palbociclib. La inducción fue testada mediante análisis inmunocitoquímico, con el uso de diversos marcadores asociados a senescencia: Ki67, Lamin B1, γH2Ax, p21. Para ello, las células tratadas y no tratadas (controles) se fijaron con paraformaldehido (PFA) 4% y se incubaron con anticuerpos primarios específicos y anticuerpos secundarios marcados fluorescentemente. Además, se llevó a cabo la tinción citoquímica X-gal siguiendo las instrucciones del Kit comercial de Sigma-Aldrich (CS0030-1KT). Las células marcadas fueron fotografiadas con un microscopio confocal (Olympus FV10i) y se utilizó el programa *Image J* para el análisis de imagen.

Utilizando este modelo de senescencia, se evaluó la señal asociada a cada una de las sondas fluorogénicas mediante microscopía confocal (Olympus FV-1000). Para este fin, se añadió la sonda diluida en DMEM (AHGa 10 µM, NBGal 2 µM y WOS-Cy7Gal 20 µM) y se tomaron imágenes durante la primera hora de incubación. Para cuantificar la diferencia en la mediana de intensidad de fluorescencia ("MFI" por sus siglas en inglés) entre células controles y senescentes, las células se incubaron con cada sonda durante 15 minutos. Tras centrifugar, analizamos la fluorescencia asociada a estas sondas mediante citometría de flujo (FACS) en un citómetro LSR-Fortessa (Becton Dickinson).

Además, la eficiencia de la sonda WOS-Cy7Gal ha sido testada en otros modelos *in vitro*, así como en la medida *ex vivo* de la senescencia asociada a la edad. *In vitro,* WOS-Cy7Gal se ha utilizado para medir la actividad β-Gal tras la inducción de senescencia replicativa en hUVECs o tras la exposición de células bEnd.3 (línea de ECs de cerebro de ratón) a estrés oxidativo (H_2O_2), en paralelo a otros marcadores como p16 y γH2AX. Con este fin, las ECs se despegaron de la placa con una solución de 0,05% tripsina/0,02% EDTA. Una fracción de estas células se incubó con la sonda durante 15 minutos y la otra se fijó y permeabilizó, siguiendo el protocolo detallado en el kit "Pharmingen™ Transcription-Factor Buffer Set" (BD-Biosciences), para su posterior incubación con anticuerpos primarios específicos y secundarios marcados fluorescentemente. El análisis se llevó a cabo por citometría de flujo (LSR-Fortessa BD).

Respecto a la detección de senescencia *ex vivo*, la sonda WOS-Cy7Gal se utilizó en paralelo a p16 y Lamin B1, para la determinación de los niveles de senescencia en hígado y riñón de ratones SAMP8 en comparación a SAMR1. Para este fin, se extrajo el riñón derecho y una porción de hígado de ratones SAMP8 y SAMR1 de 7 meses. Ambos tejidos se digirieron de forma enzimática con colagenasa/dispasa y ADNasa en un disociador automático (gentleMACS Octo Dissociator, Miltenyi) y se filtraron. Parte de la muestra se incubó con la sonda WOS-Cy7Gal durante 15 minutos. La otra parte, se fijó y permeabilizó para el marcaje con anticuerpos primarios específicos y secundarios fluorescentes, siguiendo el protocolo descrito en el kit "Pharmingen™ Transcription-Factor Buffer Set" (BD). Las muestras se analizaron por citometría de flujo (LSR-Fortessa BD).

- Cultivo de NSCs y evaluación de los efectos paracrinos de las ECs senescentes:

Los detalles metodológicos y los medios de cultivo empleados para el establecimiento y propagación

de cultivos de NSCs se pueden consultar en el trabajo publicado por nuestro grupo en 2016 (Belenguer et al., 2016).

Para el experimento de NSCs condicionadas por factores derivados de células endoteliales senescentes y controles, se utilizaron los modelos de senescencia establecidos en hUVECs (usando palbociclib) y células bEnd.3 (exponiendolas a un estímulo oxidativo). En ambos casos, las células controles y senescentes condicionaron el medio completo de NSCs desprovisto de BSA durante 24-48h. Tras este periodo, se obtuvo la fracción soluble del medio mediante sucesivas centrifugaciones (1.200 x*g*, 10 min y 10.000 x*g*, 60 min), filtración, y una ultracentrifugación (100.000 x*g* 80 min). Las NSCs se sembraron con los medios que contienen los factores solubles liberados por ECs controles o senescentes diluidos 1/4, así como con medio fresco (no condicionado). Una fracción de estas células fue marcada con el trazador de división celular Oregon Green 488 Carboxy-DFFDA-SE (DFFDA, ThermoFisher) antes de ser sembrada, con objeto de analizar la proliferación celular en presencia de factores endoteliales senescentes. A los 4 días *in vitro*, las NSCs se disociaron con Acutase® y se procesaron para su análisis. Por un lado, las células vivas se procesaron para el análisis de DFFDA, de la actividad β-Gal con la sonda WOS-Cy7Gal, y de la producción de ROS con la sonda comercial mitoSOX®-red (Invitrogen, consultar protocolo del fabricante). Por otro lado, las NSCs se fijaron, siguiendo el procedimiento descrito en el apartado anterior, para el análisis de Lamin B1. Todas las muestras fueron evaluadas por citometría de flujo (LSR-Fortessa BD).

- Fenotipado de ECs senescentes en cerebro mediante citometría de flujo:

Este procedimiento se ha llevado a cabo con las cepas murinas SAMP8, SAMR1 y C57BL/6. Tras la eutanasia del animal, se obtuvo el cerebro y se descartaron bulbos y cerebelo. El tejido se digirió enzimáticamente con colagenasa/dispasa y ADNasa en un disociador automático (gentleMACS Octo Dissociator, Miltenyi). Seguidamente, este se filtró y procesó para retirar la mielina (Debris Removal Solution, Miltenyi). Para el análisis de ECs de cerebro, se utilizaron los anticuerpos CD45 para la exclusión de células inmunes, y CD31 para la selección de ECs (ambos de BD-Biosciences). Las células se incubaron con estos anticuerpos (asociados a un fluoróforo) durante 30 min a 4 °C. A continuación, las muestras se dividieron para la incubación con sondas (WOS-Cy7Gal/NBGal y mitoSOX®) y para su fijación-permeabilización (BD Pharmingen™ Transcription-Factor Buffer Set). Las células fijadas fueron incubadas con anticuerpos primarios específicos (p16, γH2AX) y anticuerpos secundarios marcados fluorescentemente. Las muestras se analizaron mediante citometría de flujo (LSR-Fortessa BD).

- Fenotipado del linaje neurogénico de la SEZ mediante citometría de flujo:

En paralelo al fenotipado de la senescencia endotelial en cerebro, se analizó el linaje neurogénico de la SEZ siguiendo el protocolo detallado en el trabajo publicado por nuestro grupo en 2021 (Belenguer et al., 2021).

- Medida de la actividad β-Gal sistémica *in vivo*:

La sonda WOS-Cy7Gal fue químicamente modificada, mediante la adición de dos grupos sulfónicos a la molécula de fluoróforo, con el objetivo de hacerla más permeable y que pueda excretarse en orina. Esta sonda modificada recibió el nombre de Cy7Gal. Primero, Cy7Gal fue analizada mediante microscopía confocal del mismo modo que la WOS-Cy7Gal, con el modelo de senescencia de hUVECs tratadas con palbociclib. Seguidamente, se estudió su biodistribución en comparación a la sonda WOS-Cy7Gal mediante la inyección intraperitoneal (i.p.) de ambas sondas, o del vehículo (DMEM), en ratones SAMP8 de avanzada edad. Tras la administración, los animales fueron anestesiados vía inhalatoria con isoflurano durante 10 min. Pasado este tiempo, se obtuvieron muestras de sangre (vena submandibular) y orina. La sangre se recogió en tubos heparinizados para obtener plasma (350 x*g*, 4 min). Las muestras de plasma y orina se diluyeron (1/10 y 1/20 respectivamente) en 100 µl de agua destilada previo al análisis de fluorescencia (Horiba Scientific Fluoromax-4 spectrofluorometer).

Para la medida de los niveles sistémicos de actividad β-Gal como lectura de la carga senescente asociada al envejecimiento y/o a tratamientos senolíticos, la sonda fue inyectada i.p. en los ratones de experimentación (140 mg/kg) y estos se anestesiaron con isoflurano (2%) durante 15 minutos. Transcurrido este tiempo, se recogieron las muestras de orina y con cada una se realizó una dilución 1/20 en 100 µl de agua destilada previo a su análisis en el fluorímetro. Para evitar que la variabilidad en la micción altere los resultados, las unidades arbitrarias de fluorescencia obtenidas se multiplicaron por el volumen total de orina recogido para cada muestra.

- Tratamiento senolítico:

Los animales fueron tratados vía oral con la combinación de fármacos D (5 mg/kg) + Q (50 mg/kg) (Xu et al., 2018). Los ratones SAMP8 de 7 meses recibieron la mezcla de estos fármacos durante 5 semanas consecutivas, alternando regímenes de 5 o 1 día de tratamiento por semana. La misma cohorte de animales recibió otra ronda de tratamiento a los 10 meses siguiendo la misma pauta. Por otro lado, los ratones C57BL/6 de 15 meses recibieron una pauta de D+Q de 5 semanas con 2 dosis por semana.

- Análisis inmunohistoquímico de la neurogénesis adulta en el OB y la SGZ:

Los ratones fueron inoculados vía i.p. con una dosis de 50 mg/kg del análogo de timidina BrdU (10 mg/ml) dos veces al día, con un intervalo de 6 horas entre cada inyección, durante 3 días consecutivos. Para el análisis inmunohistoquímico de BrdU, los animales inyectados fueron anestesiados (con una mezcla de medetomidina y ketamina, i.p.) y sometidos a una perfusión transcardíaca con PFA 4%. En el caso de los ratones bajo tratamiento senolítico, la eutanasia se llevó a cabo 26 días después de la inyección de BrdU, mientras que en los infectados con AAV-BR1 se practicó a los 17 días. Con estos últimos, no se realizó perfusión, y bulbo e hipocampo fueron diseccionados y post-fijados por inmersión con PFA 4% durante 24 h. Cerebro/hipocampo y OBs fueron procesados para su corte en vibratomo. Posteriormente, la detección de BrdU y otros marcadores se llevó a cabo con anticuerpos primarios específicos y anticuerpos secundarios marcados fluorescentemente. El número de células $BrdU^+$ en la capa glomerular ("GL" por sus siglas en inglés) del OB, y en la SGZ del DG, se contó de forma manual bajo un microscopio de fluorescencia Nikon ECLIPSE. Las imágenes fueron tomadas en un microscopio confocal (Olympus FV10i).

- Análisis de la transducción de AAV2-BR1-GFP-p16 en ECs de cerebro y su efecto en neurogénesis:

Ratones C57BL/6 jóvenes fueron inyectados por vía intravenosa (i.v.) con $1x10^{12}$ gc (copias genómicas) del vector adenoasociado AAV2-BR1-GFP-p16 en la vena de la cola (Körbelin et al., 2016). Como control, se inyectó PBS i.v. en ratones de la misma cepa y edad. Los días 14, 15 y 16 tras la inoculación del virus se inyectó BrdU siguiendo el protocolo antes especificado. Tras 31 días de la administración del vector, se extrajo el cerebro y una porción del hígado y se procesaron, como se ha descrito previamente, para la identificación de ECs y el análisis de marcadores asociados a senescencia por FACS, como SA-β-Gal (NBGal), p16 y γH2AX. Además, se evaluó la fluorescencia asociada a GFP en ECs de hígado, y en otras poblaciones celulares de cerebro, para comprobar la especificidad en la transducción del vector. Para el análisis inmunohistoquímico de la neurogénesis en el OB y la SGZ, se procedió de forma semejante a la expuesta en el apartado anterior.

Resultados y discusión*:*

Los resultados de esta tesis responden a los objetivos planteados: pasando de un estudio más general de la senescencia asociada al envejecimiento, a otro más específico centrado en el envejecimiento cerebral mediante la evaluación de la senescencia endotelial en el cerebro y su impacto en la neurogénesis adulta.

1. Desarrollo de estrategias novedosas para monitorizar longitudinalmente la senescencia asociada al envejecimiento *in vivo*

Con objeto de mejorar nuestra comprensión sobre el envejecimiento y su relación con la senescencia, nos propusimos, en primera instancia, evaluar diversas características fenotípicas asociadas a la edad en un modelo animal de envejecimiento acelerado. Para ello, llevamos a cabo un estudio de carácter longitudinal, atendiendo a diversos parámetros fácilmente medibles y relacionados con la edad (físicos, bioquímicos, y emocionales), que nos permitió caracterizar el proceso de envejecimiento en los ratones SAMP8, en comparación a la cepa SAMR1. Gracias a la evaluación de pruebas específicas, de diversa índole y a distintas edades, pudimos discernir el comienzo de déficits típicamente relacionados con envejecimiento en los ratones SAMP8. Sorprendentemente, encontramos que varios signos de deterioro aparecían antes de lo descrito en la bibliografía y esto nos permitió seleccionar edades diana de forma precisa para relacionar el envejecimiento con la carga sistémica de senescencia. Cabe destacar que los ratones SAMP8 mostraron un deterioro emocional particularmente temprano, solo a 4 meses de edad, con evidentes signos de ansiedad en la percepción del espacio abierto (Open Field test). Para dilucidar si la ansiedad es una característica robusta y útil para trazar el envejecimiento natural, también evaluamos el comportamiento ansioso en la cepa C57BL/6, comparando animales de 3 y 17 meses. Los resultados obtenidos en la prueba de Open Field indicaron que los ratones de 17 meses también experimentan un aumento significativo en los niveles de ansiedad.

Con el propósito de estudiar si estos cambios con la edad se relacionan con un aumento de la carga senescente, empleamos sondas fluorogénicas basadas en la detección de la SA-β-Gal para la identificación de células senescentes. Primero, validamos estas sondas moleculares (WOS-Cy7Gal, NBGal y AHGa) en un modelo de senescencia *in vitro* bien caracterizado, hUVECs tratadas con el fármaco palbociclib. Mediante microscopía confocal y citometría de flujo comprobamos que, en aquellas células tratadas con palbociclib, las sondas exhibían un marcaje punteado y con mayor intensidad de fluorescencia que en las células no tratadas (controles). Este resultado se correlaciona con la lectura de otros marcadores asociados a senescencia, indicando que las sondas reconocen de forma eficiente la mayor actividad β-gal lisosomal de las células senescentes. Seguidamente, utilizamos una de estas sondas para estimar los niveles de senescencia de ratones SAMP8 de 7 meses, en comparación a ratones SAMR1 de la misma edad. Para ello, procesamos hígado y riñón, dos órganos diana para la acumulación de células senescentes. A continuación, analizamos la actividad β-Gal con la sonda WOS-Cy7Gal, junto a los niveles de p16 y Lamin B1 (dos marcadores altamente aceptados en el campo), por citometría de flujo. Los resultados indicaron que existe una mayor carga de células senescentes en la cepa SAMP8 a esta edad.

Dada la eficiencia de la sonda WOS-Cy7Gal en la lectura de senescencia asociada a la edad *ex vivo*, decidimos modificarla a nivel químico incluyendo dos grupos sulfónicos para favorecer su excreción en orina. Esta sonda modificada, de ahora en adelante denominada Cy7Gal, fue inyectada en ratones SAMP8 de avanzada edad, en comparación a la WOS-Cy7Gal, para analizar su biodistribución. A los 10 minutos de la inyección, se recogieron muestras de orina y plasma y, posteriormente, se analizaron los niveles de fluorescencia. La sonda con grupos sulfónicos fue detectada tanto en orina como en plasma, mientras que los niveles de fluorescencia en los animales inyectados con WOS-Cy7Gal apenas se diferenciaron de los animales administrados con DMEM (vehículo). En base a estos resultados, inferimos que Cy7Gal difunde rápidamente de las células a la sangre y se filtra en los riñones acumulándose en la orina. A continuación, inyectamos Cy7Gal en animales SAMP8 y SAMR1 de 7 meses de edad y, de acuerdo al experimento *ex vivo*, la lectura de fluorescencia en orina indicó una mayor actividad β-Gal sistémica en los ratones SAMP8. Por tanto, la sonda Cy7Gal aparece como una herramienta valiosa para la estimación de los niveles de senescencia *in vivo* y de forma no invasiva. Además, también testamos la sonda Cy7Gal en un modelo de envejecimiento natural con ratones C57BL/6 de 3 y 15 meses. Los niveles de fluorescencia registrados fueron significativamente más altos en los ratones más viejos, apoyando la utilidad de esta sonda en la medida de senescencia asociada a envejecimiento en estudios longitudinales. A este respecto, decidimos

testar la eficiencia de la sonda como herramienta de monitorización en terapias senolíticas.

Primero, llevamos a cabo un tratamiento senolítico con D+Q en ratones SAMP8 y analizamos los efectos de la senolisis con la lectura de la sonda Cy7Gal y con la evaluación del comportamiento ansioso. A corto plazo tras el tratamiento senolítico (20 días), detectamos una reducción en signos de ansiedad en los ratones que recibieron los fármacos en correlación a una disminución en los niveles de fluorescencia asociados a Cy7Gal en orina. Por tanto, la sonda nos indica una reducción en la carga senescente tras el tratamiento que, además, tiene efectos positivos a nivel de comportamiento. Por otro lado, cuando evaluamos los efectos senolíticos a más largo plazo tras el tratamiento (más de 50 días), no detectamos cambios significativos ni en el comportamiento ansioso, ni en la sonda entre ratones tratados y vehículos. Este resultado pone de manifiesto que los efectos de los fármacos senolíticos *in vivo* son transitorios. Para comprobar que los ratones podían responder de nuevo al tratamiento, se llevó a cabo otro ciclo con D+Q en los mismos animales. De forma interesante, detectamos una recuperación en los efectos de la senolisis, con signos de ansiedad disminuidos y carga senescente reducida en los ratones SAMP8 tratados. Además, cuando evaluamos el tratamiento a corto plazo, identificamos una correlación significativa entre el comportamiento ansioso y los resultados de la lectura de la sonda. Este resultado pone de relieve que la sonda es lo suficientemente sensible como para predecir un comportamiento emocional asociado a la edad.

Segundo, iniciamos el tratamiento senolítico con D+Q en ratones C57BL/6 de 15 meses. Tras la intervención senolítica, detectamos una bajada en los niveles de senescencia con la sonda Cy7Gal, así como una disminución en el comportamiento ansioso. Por tanto, Cy7Gal permite una medida fiable de la carga senescente *in vivo* y resulta una herramienta útil en estudios longitudinales diagnósticos o en la monitorización de terapias senolíticas. Además, encontramos una correlación significativa entre la ansiedad y la lectura de la sonda, lo que indica que la senescencia tiene un fuerte impacto deletéreo a nivel cerebral.

2. Caracterización de la senescencia endotelial cerebral asociada al envejecimiento y su impacto en la neurogénesis adulta

Con el objeto de investigar si las ECs de cerebro adquieren un destino senescente con la edad en relación a una disminución en la neurogénesis, evaluamos distintos marcadores asociados a senescencia en esta población vascular y analizamos el linaje neurogénico de la SEZ. Para este fin, desarrollamos un panel de FACS para el fenotipado de ECs senescentes de cerebro mediante el que evaluamos la actividad β-Gal (con las sondas desarrolladas por nuestro grupo), p16 y otros marcadores como γH2AX o la producción de ROS mitocondrial (mitoSOX). Para el análisis de la neurogénesis en la SEZ, empleamos el protocolo de citometría de flujo publicado por nuestro grupo (Belenguer et al., 2021). Tras aplicar estas estrategias en ratones SAMP8 versus SAMR1, así como en ratones C57BL/6 jóvenes versus viejos, los resultados obtenidos mostraron que en las ECs de cerebro aumentan los niveles de marcadores asociados a senescencia con la edad y que, además, el potencial neurogénico de la SEZ disminuye.

Para comprobar si la correlación entre senescencia endotelial y neurogénesis se mantenía bajo una intervención senolítica, analizamos esta conexión en ratones SAMP8 después del tratamiento con D+Q. Además de aplicar nuestros paneles de citometría, los ratones fueron inyectados con BrdU para el posterior análisis inmunohistoquímico de la neurogénesis en el OB y el DG. Los resultados indicaron una bajada en los niveles de marcadores asociados a senescencia en las ECs de cerebro y una recuperación en el potencial neurogénico de la SEZ de los SAMP8 tratados. Este se acompañó de un aumento en el número de nuevas neuronas que se integran en el OB. Además, la cantidad de células $BrdU^+$ en la SGZ también fue notablemente superior en los ratones tratados con los fármacos senolíticos. Estos resultados demuestran una consistencia en la relación entre la senescencia endotelial y la neurogénesis adulta.

Para analizar si existe una conexión causa-efecto entre la senescencia endotelial cerebral y la bajada en neurogénesis, diseñamos un modelo de inducción genética de senescencia en ECs de cerebro, y estudiamos su impacto en neurogénesis. Esta estrategia consiste en un vector viral adenoasociado cuyos péptidos de la cápside tienen tropismo por las ECs cerebrales (AAV-BR1) (Körbelin et al., 2016). En este vector incluimos material genético para la sobreexpresión de p16 en las ECs e inducción de senescencia. Además, también incluimos GFP para analizar de forma sencilla la transducción del virus. Tras la inyección i.v. de este vector o de PBS (como control) en ratones C57BL/6, administramos BrdU con objeto de analizar la neurogénesis en el OB y el DG. Los ratones fueron eutanasiados 31 días después de la inoculación del vector adenoasociado, y evaluamos la senescencia endotelial tanto en cerebro como en hígado, mediante citometría de flujo. Los resultados mostraron que solo las ECs de cerebro de los ratones inyectados con el virus exhibían niveles significativamente más altos de GFP y p16, resaltando la especificidad del abordaje. Además, esta población mostraba mayor actividad β-Gal y niveles más altos de γH2AX, confirmando la inducción de senescencia. El análisis inmunohistoquímico de la neurogénesis reveló un número menor de nuevas neuronas, tanto en el OB como en la SGZ, en los animales inyectados con el vector. De este modo, concluimos que la senescencia endotelial tiene un fuerte impacto en la neurogénesis adulta, y es suficiente para reducir el número de nuevas neuronas que se forman en los principales nichos neurogénicos del cerebro. En conjunto, los resultados apuntan a la población endotelial como una diana de investigación interesante en el estudio del envejecimiento cerebral.

Conclusiones*:*

1. Las sondas fluorogénicas, específicamente diseñadas para ser recuperadas en la orina, permiten una lectura de la actividad β-Gal sistémica, lo que posibilita la estimación de la carga de senescencia de forma no-invasiva en estudios longitudinales, ya sean asociados a envejecimiento o a tratamientos senolíticos.

2. Los estudios longitudinales, correlacionando la ansiedad asociada a la edad y los niveles de β-Gal sistémicos mediante sondas fluorogénicas que se recuperan en orina, indican que los efectos de los fármacos senolíticos son transitorios y desaparecen con el tiempo.

3. Las células endoteliales de cerebro entran en senescencia con la edad y este destino celular tiene un impacto perjudicial en las células madre neurales y en la neurogénesis.

Resum

Impacte de la senescència endotelial cerebral sobre la neurogènesi: aplicació de noves estratègies per a la detecció de senescència associada a l'edat

Introducció:

L'envelliment és un procés fisiològic que s'acompanya d'una deterioració funcional generalitzada i d'un augment de la càrrega de cèl·lules senescents en els teixits (López-Otín et al., 2013; 2023). Les cèl·lules exposades a factors estressants generen una resposta de mal en l'ADN que pot desencadenar un destí senescent, alternatiu a l'apoptosi. Aquests factors d'estrés poden ser de diferent índole, com l'escurçament dels telòmers, mutacions en l'ADN, augment de l'estrés oxidatiu (espècies reactives de l'oxigen, o "ROS" per les seues sigles en anglés), entre altres. La senescència cel·lular es caracteritza per l'augment d'inhibidors del cicle, com p16 o p21, i la pèrdua irreversible de la capacitat proliferativa que, a més, s'acompanya d'altres canvis en la biologia de la cèl·lula (Herranz and Gil, 2018; Muñoz-Spín and Serrano, 2014). Un dels trets fenotípics més freqüents en aquestes cèl·lules és l'alta activitat de l'enzim β-Galactosidasa (β-Gal o "SA-β-Gal" en anglés) a causa de l'augment del compartiment lisosòmic (Kurz et al., 2000). A més, les cèl·lules senescents posseeixen un potent fenotip secretor ("SASP" per les seues sigles en anglés) mitjançant el qual alliberen factors pro-inflamatoris i pro-oxidants que contribueixen a la propagació de la senescència en el teixit de forma paracrina (Childs et al., 2017; van Deursen, 2014).

Les cèl·lules senescents desenvolupen mecanismes anti-apoptòtics que contribueixen a la seua acumulació amb l'edat potenciant un entorn senescent (Zhu et al., 2015; Yosef et al., 2016; Ovadya et al., 2018). La persistència del SASP promou un ambient pro-inflamatori que afecta la funció tissular. De fet, l'augment de la càrrega de senescència durant l'envelliment comporta a l'esgotament de les cèl·lules mares residents en l'intent de reparar i recuperar la funcionalitat del teixit. D'aquesta manera, així com la senescència en detindre el cicle cel·lular pot actuar com a mecanisme de defensa enfront de tumors, durant l'envelliment aquesta promou el desenvolupament de diverses malalties, inclòs el càncer (Childs et al., 2017; Zhang et al., 2019). És per aquesta dicotomia que, quan es parla de senescència crònica associada a l'edat, essencialment es contempla el "costat fosc" d'aquest procés cel·lular que contribueix a la degeneració dels teixits. Així mateix, la càrrega senescent es considera una de les principals característiques de l'envelliment i la seua adequada detecció s'ha convertit en una prioritat per al desenvolupament d'estratègies terapèutiques (Muñoz-Spin and Serrano, 2014; López-Otín et al., 2023).

Desafortunadament, no hi ha un únic marcador universal per a identificar cèl·lules senescents i, a més, les característiques fenotípiques d'aquestes cèl·lules varien segons el seu origen, ubicació i el procés d'inducció (Hernández-Segura et al., 2018). No obstant això, la mesura de l'activitat β-Gal representa un dels marcadors de senescència més emprats en el camp. Encara que aquesta activitat enzimàtica s'ha determinat tradicionalment mitjançant tinció histoquímica X-gal, aquesta estratègia presenta moltes limitacions per al seu ús en combinació amb altres marcadors de senescència (Dimri et al., 1995; Debacq-Chainiaux et al., 2009). Actualment, està emergent el desenvolupament de sondes fluorogèniques per a la determinació de l'activitat SA-β-Gal mitjançant fluorescència, la qual cosa pot ser útil per a la detecció de senescència *ex vivo* al costat d'altres marcadors (Lozano-Torres et al., 2017; 2023; Rojas-Vázquez et al., submitted). No obstant això, l'associació d'alteracions relacionades amb l'edat amb la càrrega senescent de l'organisme, de manera longitudinal, és una cosa que encara no s'ha aconseguit. Aquest tipus d'estratègia seria interessant per al diagnòstic de malalties relacionades amb senescència, així com per a monitorar teràpies que perseguisquen el rejoveniment dels teixits (Rojas-Vázquez et al., submitted).

La deterioració progressiva amb l'edat es manifesta amb l'aparició de diverses patològiques que alteren el benestar de l'individu. En aquest sentit, la força muscular, la coordinació i habilitats motores, així com la memòria, cognició o emoció, entre altres aspectes, comencen a deteriorar-se creant un desequilibri en l'estat de salut entre animals joves i vells que pot ser avaluat de manera externa mitjançant test específics

(Yanai and Endo, 2021). Curiosament, les estratègies senilítiques han tingut efectes beneficiosos sobre la salut de ratolins envellits, millorant la funció física, reduint el comportament ansiós i fomentant un envelliment saludable (Xu et al., 2018; Ogrodnik et al., 2019; Ogrodnik et al., 2021). Aquests resultats sostenen que molts dels canvis esdevinguts amb l'augment de l'edat són directament proporcionals a la prevalença de les cèl·lules senescents en els teixits.

El desenvolupament de desordres neurològics i malalties neurodegeneratives representa una de les principals inquietuds del panorama sociosanitari actual, a causa de l'increment del a població envellida als països desenvolupats i de la incidència d'aquestes patologies (Zheng and Chen, 2022). Les investigacions referent a això avancen lentament degut, en part, a la complexitat de l'estudi del procés d'envelliment a nivell cerebral. En models de ratolí d'envelliment natural, com la soca C57BL/6, aquest tipus d'alteracions no comencen a manifestar-se fins almenys els 12 mesos d'edat. En aquest sentit, els models animals d'envelliment accelerat representen una bona alternativa en termes de cost i temps. Els ratolins de la soca propensa a la senescència accelerada (SAMP) o resistent a aquesta (SAMR) constitueixen uns dels models més interessants en l'estudi gerontològic (Takeda, 1999). En concret, els ratolins SAMP8 es caracteritzen per presentar dèficits de memòria i aprenentatge primerencs, així com per compartir molts trets de l'envelliment cerebral humà, convertint-los en models d'estudi de malalties com Alzheimer (Takeda, 2009; Ito, 2013; Akiguchi et al., 2017). La deterioració primerenca dels ratolins SAMP8 és conseqüència de la senectut fisiològica, la incidència i la severitat de la qual augmenta amb l'edat. Per tant, els estudis duts a terme usant el model SAM per a dilucidar els mecanismes que condueixen a l'envelliment accelerat, poden donar una idea dels mecanismes fonamentals de l'envelliment natural.

En els últims anys, s'ha reconegut que l'esgotament de les cèl·lules mare en els teixits desencadena un imparable declivi funcional en els òrgans (Schultz and Sinclair, 2016; Rojas-Vázquez et al., 2021; López-Otín et al., 2023). Les cèl·lules mare adultes residents en teixits específics constitueixen un grup únic de cèl·lules indiferenciades que és responsable del manteniment dels teixits adults en homeòstasis i de la potencial regeneració en resposta a mal (Simons and Clevers, 2011). En relació al cervell adult dels mamífers, existeixen dues regions principals que alberguen cèl·lules mare neurals ("NSCs" per les seues sigles en anglés) capaços de generar noves neurones destinades a circuits específics: la zona subependimària ("SEZ" per les seues sigles en anglés) i la zona subgranular ("SGZ" per les seues sigles en anglés) del gir dentat ("DG" per les seues sigles en anglés) de l'hipocamp. La SEZ és el nínxol més prolífic amb diferència en el cervell de ratolí, generant milions de noves neurones al llarg de la vida perquè s'integren en el bulb olfactori ("OB" per les seues sigles en anglés) (Silva-Vargas et al., 2013; Ruddy and Morshead, 2018; Obernier and Alvarez-Buylla, 2019). No obstant això, la neurogènesi adulta experimenta un gran declivi amb l'envelliment per raons que encara no es coneixen bé (Ben-Abdallah et al., 2010; Lugert et al., 2010; Alzines et al., 2011; Conover and Shook, 2011; Shook et al., 2012; Kalamakis et al., 2019).

Les NSCs en els nínxols coexisteixen amb cèl·lules de la seua progènie i altres components cel·lulars (cèl·lules glials, vasculars, …) i, per tant, estan exposades a diferents estímuls extrínsecs que modulen el seu comportament i poden ser partícips de la pèrdua d'activitat neurogènica que esdevé amb l'edat (Silva-Vargas et al., 2013). El desenvolupament d'estratègies que permeten la detecció d'aquestes cèl·lules mitjançant la combinació de marcadors específics, i els estudis transcriptòmics a nivell de cèl·lula única, revelen que existeix una gran heterogeneïtat en les NSCs subependimàries en relació a la seua dinàmica de proliferació. D'aquesta manera, es distingeixen NSCs amb diferents graus de quiescència, que simplifiquem en quiescents (qNSCs) i propenses a l'activació ("primed" en anglés), que conviuen amb NSCs proliferatives o actives (aNSCs). L'equilibri entre aquests estats és necessari per a mantindre l'homeòstasi i la correcta funció neurogènica (Llorens-Bobadilla et al., 2015; Urbán et al., 2019; Belenguer et al., 2021). No obstant això , estudis de seqüenciació d'ARN ("RNA-sequencing" en anglés) en aquestes cèl·lules mare al llarg del temps apunten a una major prevalença de qNSCs resistents a l'activació amb l'augment de l'edat (Kalamakis et al., 2019). De manera cridanera, les qNSCs envellides recuperen part de la seua activitat davant determinats estímuls pro-rejoveniment (Lugert et al., 2010; Katsimpardi et al., 2014). En aquest

context, sembla que l'entorn envellit, i els senyals extrínsecs que reben les NSCs durant l'envelliment, poden ser potencials inhibidors de la transició de l'estat quiescent a l'activat i, per tant, contribuir a la pèrdua de l'activitat neurogènica.

Entre aquells components dels nínxols neurogènics que poden exercir major influència en les NSCs, i la seua descendència, destaca la vasculatura. Les NSCs mantenen un contacte íntim amb els vasos sanguinis que componen la barrera hematoencefàlica ("BBB" per les seues sigles en anglés) tant en la SEZ com en el DG. La BBB exerceix un paper essencial en el manteniment de l'homeòstasi cerebral, protegint el parènquima neural i subministrant nutrients i oxigen (Tavazoie et al., 2008; Shen et al., 2008; Rafii et al., 2016; Smith et al., 2018; Vicidomini et al., 2020). Les NSCs, en concret, mantenen una estreta relació amb les cèl·lules endotelials dels gots ("ECs" per les seues sigles en anglés), amb les quals interaccionen de forma activa i recíproca. Els factors angiocrins alliberats per les ECs han demostrat jugar un rol fonamental en la proliferació, auto-renovació i diferenciació de les NSCs (Delgado et al., 2014; Rojas-Vázquez et al., 2021). Per tant, aquesta via de comunicació entre totes dues poblacions sembla estar involucrada de manera activa en la regulació del comportament de les NSCs i, per tant, de la neurogènesi.

Amb l'edat, la BBB també experimenta una transformació profunda que compromet la seua integritat i augmenta l'exposició de les cèl·lules progenitores neurals a factors circulants pro-envelliment (Villeda et al., 2011; Obermeier et al., 2013; Segarra et al., 2021). Especialment, les ECs pateixen canvis que alteren la seua funció cel·lular amb l'edat i afecten el seu paper regulador sobre l'activitat de les NSCs (Rojas-Vázquez et al., 2021). Un destí senescent en aquestes cèl·lules vasculars podria contribuir a aquests esdeveniments deleteris, però encara no hi ha estudis funcionals publicats sobre la senescència associada a l'edat en les ECs de cervell. No obstant això, s'han descrit una sèrie de canvis fenotípics en aquestes cèl·lules amb l'edat, com una baixada en la proliferació, l'augment en els nivells de p16 i p21 o canvis a nivell metabòlic, entre altres, que típicament s'associen a un perfil senescent (Rojas-Vázquez et al., 2021). A nivell transcriptòmic també s'han detectat canvis respecte a les ECs joves, que inclouen resposta a mal cel·lular, alliberament de citocines pro-inflamatòries i generació d'espècies reactives de l'oxigen (Kalamakis et al., 2019; Kiss et al., 2020). En aquest escenari, les ECs de cervell apareixen com una diana interessant en l'estudi de la deterioració de l'activitat neurogènica amb l'edat en tots dos nínxols. No obstant això, determinar l'impacte directe de la senescència endotelial sobre la neurogènesi en un organisme envellit és una àrdua tasca, ja que l'acumulació de cèl·lules senescents es produeix a nivell sistèmic i aquesta pot contribuir a aquest efecte anti-neurogènic per altres mitjans. D'acord amb l'anterior, es necessiten estratègies que permeten discernir el paper de la senescència endotelial sobre el declivi neurogènic. Amb tot, aquesta informació situa a l'endoteli cerebral com un punt de recerca prometedor per a entendre l'envelliment cerebral i buscar enfocaments terapèutics que impulsen la longevitat de la salut cerebral.

Recentment, l'eliminació selectiva de cèl·lules senescents (senilisi) s'ha convertit en una de les estratègies amb major interés per al rejoveniment tissular (Rojas-Vázquez et al., 2021). Els fàrmacs senilítics més prometedors en el panorama actual són aquells dirigits a inhibir els mecanismes anti-apoptòtics ("SCAPs" per les seues sigles en anglés) que desenvolupen les cèl·lules senescents (Zhu et al., 2016; Hickson et al., 2019). Referent a això, la combinació dels fàrmacs senilítics dasatinib i quercetin (D+Q) ha demostrat reduir la càrrega senescent *in vivo* amb efectes insignificants sobre altres cèl·lules (Zhu et al., 2015). El tractament intermitent amb aquests fàrmacs de ratolins envellits, o amb determinades patologies associades a senescència, ha demostrat efectes beneficiosos en la renovació de teixits danyats, així com en l'esperança de vida d'aquests animals (Xo et al., 2018; Ogrodnik et al., 2019; Hickson et al., 2019; Ogrodnik et al., 2021). D i Q són capaces de travessar la BBB i afavorir la reducció de plaques amiloides o fins i tot potenciar la neurogènesi en la SEZ (Ogrodnik et al., 2019; Zhang et al., 2019). A més, han demostrat millorar la funció vasomotora de ratolins envellits (Roos et al., 2016). Aquests resultats sostenen que els fàrmacs senilítics poden alleujar les alteracions associades a l'edat a nivell cerebral i demostren l'estreta relació entre la senescència i la neurodegeneració. En aquest sentit, la detecció i eliminació de cèl·lules senescents podria representar una nova estratègia terapèutica per a recuperar la neurogènesi.

Objectius*:*

El envelliment engloba el desenvolupament de diverses malalties que s'han associat a una major càrrega de senescència, com aquelles neurodegeneratives. De fet, s'ha descrit que la neurogènesi disminueix amb l'augment de l'edat tant en la SEZ, com en la SGZ. No obstant això, no és clar com contribueix la senescència a aquest efecte. Sorprenentment, encara no existeix una vertadera correlació longitudinal entre l'envelliment i la senescència, a causa de la falta d'eines per a la detecció fiable de cèl·lules senescents *in vivo*. En aquest sentit, el nostre grup està desenvolupant noves estratègies per a detectar cèl·lules senescents tant *in vivo* com *ex vivo* que resulten útils per a comprendre com contribueix la senescència a l'envelliment en diferents teixits, inclòs el cervell.

Les NSCs estan exposades a múltiples senyals que regulen extrínsecament el seu comportament. De fet, la vasculatura i, especialment les ECs, exerceixen una forta influència sobre la funció neurogènica de les NSCs mitjançant diverses vies. L'íntima relació entre les ECs i les NSCs fa de l'endoteli cerebral una interessant diana d'estudi. Les ECs pateixen alteracions funcionals amb l'envelliment que poden contribuir a la pèrdua de neurogènesi amb l'edat. No obstant això, gairebé no s'ha explorat si les ECs poden patir un destí senescent i, molt menys, si això afecta a la funció neurogènica de les NSCs. En aquest context, el nostre treball es basa en la hipòtesi que la senescència de les ECs de cervell associada a l'envelliment té efectes deleteris sobre la neurogènesi. Per a això, hem abordat els dos següents objectius:

1. Desenvolupament d'estratègies noves per a monitorar longitudinalment la senescència associada a l'envelliment *in vivo*.

2. Caracterització de la senescència endotelial cerebral associada a l'envelliment i el seu impacte en la neurogènesi.

Material i mètodes*:*

- Soques animals:

Els ratolins van ser criats i allotjats a l'animalari de la Universitat de València (Servei Central de Suport a la Investigació Experimental, Burjassot) segons les directrius de la Unió Europea. En el desenvolupament experimental es van utilitzar les soques de ratolí SAMP8 (com a model d'envelliment accelerat) i SAMR1 (com el seu control), així com C57BL/6 (com a model d'envelliment natural), a diferents edats.

- Avaluació externa de la progressió de l'envelliment:

Amb ratolins SAMP8 es va dur a terme un estudi detallat del procés d'envelliment (des dels 2 als 12 mesos d'edat) mitjançant l'avaluació externa de diversos canvis fenotípics associats a l'edat, de manera comparativa a la soca control SAMR1. D'aquesta manera, duem a terme proves específiques per a l'avaluació de la funció física, motora, metabòlica, així com emocional. A aquest últim respecte, analitzem el comportament ansiós dels animals SAMP8 amb la prova de Camp Obert ("Open Field test" en anglés). Aquest paràmetre emocional també es va avaluar durant l'envelliment natural, amb la soca C57BL/6.

- Validació de noves sondes fluorogèniques per a la detecció de SA-β-Gal *in vitro* i *ex vivo*:

En el grup liderat pel professor Ramón Martínez-Máñez s'han desenvolupat noves sondes fluorogèniques per a la detecció de l'activitat β-Gal: AHGa, NBGal i WOS-Cy7Gal (Lozano-Torcap de bestiar et al., 2017;

2023; Rojas-Vázquez et al., submitted). Breument, aquestes sondes consisteixen en un fluoròfor associat a un derivat de galactosa mitjançant un enllaç susceptible de ser hidrolitzat per l'enzim β-Gal. Quan el fluoròfor és alliberat, emet una alta fluorescència permetent identificar aquelles cèl·lules amb major activitat β-Gal, és a dir, les senescents. Encara que el mecanisme funcional és similar a totes, aquestes sondes difereixen, principalment, en la naturalesa del fluoròfor.

Amb ECs humanes (hUVECs), es va desenvolupar un model de senescència *in vitro* mitjançant el tractament amb el fàrmac inhibidor de CDKs 4 i 6 palbociclib. La inducció de senescència va ser testada mitjançant anàlisi immunocitoquímica, amb l'ús de diversos marcadors associats a senescència: Ki67, Lamin B1, γH2Ax, p21. Per a això, les cèl·lules tractades i no tractades (controls) es van fixar amb paraformaldehid (PFA) 4% i es van incubar amb anticossos primaris específics i anticossos secundaris marcats fluorescentment. A més, es va dur a terme la tinció citoquímica X-gal seguint les instruccions del Kit comercial de Sigma-Aldrich (ref.: CS0030-1KT). Les cèl·lules marcades van ser fotografiades amb un microscopi confocal (Olympus FV10i) i es va utilitzar el programa *Image J* per a l'anàlisi d'imatge.

Utilitzant aquest model de senescència, avaluem el senyal associat a cadascuna de les sondes fluorogèniques mitjançant microscòpia confocal (Olympus FV-1000). Per a aquest fi, afegim la sonda diluïda en DMEM (AHGa 10 µM, NBGal 2 µM i WOS-Cy7Gal 20 µM) i prenem imatges durant la primera hora d'incubació. Per a quantificar la diferència en la mitjana d'intensitat de fluorescència ("MFI" per les seues sigles en anglés) entre cèl·lules controles i senescents, incubem les cèl·lules amb cada sonda durant 15 minuts. Després de centrifugar, analitzem la fluorescència associada a aquestes sondes mitjançant citometria de flux (FACS) en un citòmetre LSR-Fortessa (Becton Dickinson).

A més, l'eficiència de la sonda WOS-Cy7Gal ha sigut testada en uns altres models de senescència *in vitro*, així com en la mesura *ex vivo* de la senescència associada a l'edat. *In vitro,* WOS-Cy7Gal s'ha utilitzat per a mesurar l'activitat β-Gal després de la inducció de senescència replicativa en hUVECs o després de l'exposició de cèl·lules bEnd.3 (línia de ECs de cervell murines) a estrés oxidatiu (H_2O_2), en paral·lel a altres marcadors de senescència (p16, γH2AX). A aquest efecte, les cèl·lules endotelials es van enlairar de la placa amb una solució de 0,05% tripsina/0,02% EDTA. Una fracció d'estes cèl·lules es va incubar amb la sonda durant 15 minuts i l'altra es va fixar i permeabilitzar, seguint el protocol detallat en el kit "Pharmingen™ Transcription-Factor Buffer Set" (BD-Biosciences), per a la seua posterior incubació amb anticossos primaris específics i secundaris marcats fluorescentment. L'anàlisi es va dur a terme per citometria de flux (LSR-Fortessa BD).

Respecte a la detecció de senescència *ex vivo*, la sonda WOS-Cy7Gal es va utilitzar en paral·lel a p16 i Lamin B1, per a la determinació dels nivells de senescència en fetge i ronyó de ratolins SAMP8 en comparació a SAMR1. Per a aquest fi, es va extraure el ronyó dret i una porció de fetge de ratolins SAMP8 i SAMR1 de 7 mesos. Tots dos teixits es van digerir de manera enzimàtica amb col·lagenasa/dispasa i ADNasa en un dissociador automàtic (gentleMACS Octo Dissociator, Miltenyi) i es van filtrar. Part de la mostra es va incubar amb la sonda WOS-Cy7Gal durant 15 minuts. L'altra part, es va fixar i permeabilització per al marcatge amb anticossos primaris específics i secundaris fluorescents, seguint el protocol descrit en el kit "Pharmingen™ Transcription-Factor Buffer Set" (BD). Les mostres es van analitzar per citometria de flux (LSR-Fortessa BD).

- Cultiu de NSCs i avaluació dels efectes paracrins de les ECs senescents:

Els detalls metodològics i els medis de cultiu emprats per a l'establiment i propagació de cultius de NSCs es poden consultar en el treball publicat pel nostre grup en 2016 (Belenguer et al., 2016).

Per a l'experiment de NSCs condicionades per factors derivats de cèl·lules endotelials senescents i controls, es van utilitzar els models de senescència establerts en hUVECs (usant palbociclib) i cèl·lules bEnd.3 (exposant-les a un estímul oxidatiu). En tots dos casos, les cèl·lules control i senescents van

condicionar el mitjà complet de NSCs desproveït de BSA durant 24-48h. Després d'aquest període, es va obtindre la fracció soluble del mitjà mitjançant successives centrifugacions (1.200 x*g*, 10 min i 10.000 x*g*, 1 h), filtració, i una ultracentrifugació (100.000 x*g* 1.20 h). Les NSCs es van sembrar amb els mitjans que contenen els factors solubles alliberats per ECs controls o senescents diluïts 1/4, així com amb medi fresc (no condicionat). Una fracció d'aquestes cèl·lules van ser marcades amb el traçador de divisió cel·lular Oregon Green 488 Carboxy-DFFDA-ES (DFFDA, ThermoFisher) abans de ser sembrades, a fi d'analitzar la proliferació d'aquestes cèl·lules en presència de factors endotelials senescents. Als 4 dies *in vitro*, les NSCs es van dissociar amb Acutase® i es van processar per a la seua anàlisi· D›una banda, les cèl·lules vives es van processar per a l›anàlisi de DFFDA, de l›activitat β-Gal amb la sonda WOS-Cy7Gal, i de la producció de ROS amb la sonda comercial mitoSOX®-xarxa (Invitrogen, consultar protocol del fabricant). D'altra banda, les NSCs es van fixar, seguint el procediment descrit en l'apartat anterior, per a l'anàlisi de Lamin B1. Totes les mostres van ser analitzades per citometria de flux (LSR-Fortessa BD).

- Fenotipat de ECs senescents en cervell mitjançant citometria de flux:

Aquest procediment s'ha dut a terme amb les soques murines SAMP8, SAMR1 i C57BL/6. Després de l'eutanàsia de l'animal, es va obtindre el cervell i es van descartar bulbs i cerebel. El teixit es va digerir enzimàticament amb col·lagenasa/dispasa i ADNasa en un dissociador automàtic (gentleMACS Octo Dissociator, Miltenyi). Seguidament, aquest es va filtrar, i va processar per a retirar la mielina (Debris Removal Solution, Miltenyi). Per al anàlisi de ECs de cervell, es van utilitzar els anticossos CD45 per a l'exclusió de cèl·lules immunes, i CD31 per a la selecció de ECs (tots dos de BD-Biosciences). Les cèl·lules es van incubar amb aquests anticossos associats a un fluoròfor durant 30 min a 4 °C. Seguidament, les mostres es van dividir per a la incubació amb sondes (WOS-Cy7Gal/NBGal i mitoSOX®) i per a la seua fixació-permeabilització (BD Pharmingen™ Transcription-Factor Buffer Set). Les cèl·lules fixades van ser incubades amb anticossos primaris específics (p16, γH2AX) i anticossos secundaris marcats fluorescentment. Les mostres es van analitzar mitjançant citometria de flux (LSR-Fortessa BD).

- Fenotipat del llinatge neurogènic de la SEZ mitjançant citometria de flux:

En paral·lel al fenotipat de la senescència endotelial en cervell, es va analitzar el llinatge neurogènic de la SEZ seguint el protocol detallat en el treball publicat pel nostre grup en 2021 (Belenguer et al., 2021).

- Mesura de l'activitat β-Gal sistèmica *in vivo*:

La sonda WOS-Cy7Gal va ser químicament modificada, mitjançant l'addició de dos grups sulfònics a la molècula de fluoròfor, amb l'objectiu de fer-la més difusible i que puga excretar-se en orina. Aquesta sonda modificada va rebre el nom de Cy7Gal. Primer, Cy7Gal va ser analitzada mitjançant microscòpia confocal de la mateixa manera que la WOS-Cy7Gal, amb el model de senescència de hUVECs tractades amb palbociclib. Seguidament, es va estudiar la seua biodistribució en comparació a la sonda WOS-Cy7Gal mitjançant la injecció intraperitoneal (i.p.) de totes dues sondes, o del vehicle (DMEM), en ratolins SAMP8 d'avançada edat. Després de l'administració, els animals van ser anestesiats via inhalatòria amb isoflurà durant 10 min. Passat aquest temps, es van obtindre mostres de sang (vena submandibular) i orina. La sang es va recollir en tubs heparinizats per a obtindre plasma (350 x*g*, 4 min). Les mostres de plasma i orina es van diluir (1/10 i 1/20 respectivament) en 100 µl d'aigua destil·lada previ a l'anàlisi de fluorescència (Horiba Scientific Fluoromax-4 spectrofluorometer).

Per a la mesura dels nivells sistèmics d'activitat β-Gal com a lectura de la càrrega senescent associada a l'envelliment i/o a tractaments senilítics, la sonda va ser injectada i.p. en els ratolins d'eexperimentació (140 mg/kg) i aquests es van anestesiar amb isoflurà (2%) durant 15 minuts. Transcorregut aquest temps, es van recollir les mostres d'orina i amb cadascuna es va realitzar una dilució 1/20 en 100 µl d'aigua destil·lada prèviament a la seua anàlisi en el fluorímetre. Per tal d'evitar que la variabilitat en la micció altere els resultats, les unitats arbitràries de fluorescència obtingudes es van multiplicar pel volum total

d'orina recollit per a cada mostra.

- Tractament senilític:

Els animals van ser tractats via oral amb la combinació de fàrmacs D (5 mg/kg) + Q (50 mg/kg) (Xu et al., 2018). Els ratolins SAMP8 de 7 mesos van rebre la mescla d'aquests fàrmacs durant 5 setmanes consecutives, alternant règims de 5 o 1 dia de tractament per setmana. La mateixa cohort de animals va rebre una altra ronda de tractament als 10 mesos seguint la mateixa pauta. D'altra banda, els ratolins C57BL/6 de 15 mesos van rebre una pauta de D+Q de 5 setmanes amb 2 dosi per setmana.

- Anàlisi immunohistoquímica de la neurogènesi adulta en el OB i la SGZ:

Els ratolins van ser inoculats via i.p. amb una dosi de 50 mg/kg de l'anàleg de timidina BrdU (10 mg/ml) dues vegades al dia, amb un interval de 6 hores entre cada injecció, durant 3 dies consecutius. Per a l'anàlisi immunohistoquímica de BrdU, els animals injectats van ser anestesiats (amb una mescla de medetomidina i ketamina, i.p.) i sotmesos a una perfusió transcardíaca amb PFA 4% entre 17 i 26 dies després de la inoculació. En el cas dels ratolins inoculats amb el AAV-BR1 modificat no es va realitzar perfusió i bulb i hipocamp van ser disseccionats i post-fixats per immersió amb PFA 4% durant 24 h. Cervell/hipocamp i OBs van ser processats per a la seua cort en vibratom. Posteriorment, la detecció de BrdU i altres marcadors es va dur a terme amb anticossos primaris específics i anticossos secundaris marcats fluorescentment. El nombre de cèl·lules $BrdU^+$ en la capa glomerular del OB i en la SGZ es va comptar de manera manual sota un microscopi de fluorescència Nikon ECLIPSE. Les imategsvan ser preses en un microscopi confocal (Olympus FV10i).

- Anàlisi de la transducció d'AAV2-BR1-GFP-p16 en ECs de cervell i el seu efecte en neurogènesi:

En la cua de ratolins C57BL/6 joves es van injectar per via intravenosa (i.v.) $1x10^{12}$ gc (còpies genòmiques) del vector adenoassociat AAV2-BR1-GFP-p16 (Körbelin et al., 2016). Com a control, es va injectar PBS i.v. en ratolins de la mateixa soca i edat. Els dies 14, 15 i 16 després de la inoculació del virus es va injectar BrdU seguint el protocol abans especificat. Després de 31 dies de l'administració del vector, es va extraure el cervell i una porció del fetge i es van processar, com s'ha descrit prèviament, per a la identificació de ECs i l'anàlisi de marcadors associats a senescència, com a SA-β-Gal (NBGal), p16 i γH2AX, mitjançant FACS. A més, es va avaluar la fluorescència associada a GFP en fetge i en altres poblacions cel·lulars de cervell per a comprovar l'especificitat d'infecció del virus. Per a l'anàlisi immunohistoquímica de la neurogènesi en el OB i la SGZ, es va procedir de manera similar a l'exposada en l'apartat anterior.

Resultats i discussió*:*

Els resultats d'aquesta tesi responen als objectius plantejats: passant d'un estudi més general de la senescència associada a l'envelliment, a altre més específic centrat en l'envelliment cerebral, mitjançant l'avaluació de la senescència endotelial en el cervell i el seu impacte en la neurogènesi adulta.

1. Desenvolupament d'estratègies noves per a monitorar longitudinalment la senescència associada a l'envelliment *in vivo*

A fi de millorar la nostra comprensió sobre l'envelliment i la seua relació amb la senescència, ens vam proposar, en primera instància, avaluar diverses característiques fenotípiques associades a l'edat en un model animal d'envelliment accelerat. Per fer-ho, vam dur a terme un estudi de caràcter longitudinal,

atenent diversos paràmetres fàcilment mesurables i relacionats amb l'edat (físics, bioquímics, i emocionals), el qual ens va permetre caracteritzar el procés d'envelliment en els ratolins SAMP8, en comparació a la soca SAMR1. Gràcies a l'avaluació de proves específiques, de diversa índole i a diferents edats, vam poder discernir el començament de dèficits típicament relacionats amb envelliment en els ratolins SAMP8. Sorprenentment, vam trobar que diversos signes de deterioració apareixien abans d'allò descrit en la bibliografia i això ens va permetre seleccionar edats diana de forma apurada (rang de 5-7 mesos), per a relacionar l'envelliment amb la càrrega sistèmica de senescència. A destacar, els ratolins SAMP8 van exhibir un deteriorament emocional particularment d'hora, només a 4 mesos d'edat, amb evidents signes d'ansietat en la percepció d'un espai obert (Open Field test). Per a dilucidar si l'ansietat és una característica robusta i útil per a traçar l'envelliment natural, també vam avaluar el comportament ansiós en la soca C57BL/6, comparant animals de 3 i 17 mesos. Els resultats obtinguts en la prova d'Open Field van indicar que els animals de 17 mesos experimenten un augment significatiu en els nivells d'ansietat amb l'edat.

Amb el propòsit d'estudiar si aquests canvis amb l'edat es relacionen amb un augment de la càrrega senescent, vam emprar sondes fluorogèniques basades en la detecció de la SA-β-Gal per a la detecció de cèl·lules senescents. Primer, vam validar aquestes sondes moleculars (WOS-Cy7Gal, NBGal i AHGa) en un model de senescència *in vitro* ben caracteritzat, hUVECs tractades amb el fàrmac palbociclib. Mitjançant microscòpia confocal i citometria de flux vam comprovar que, en aquelles cèl·lules tractades amb palbociclib, les sondes exhibien un marcatge puntejat i amb major intensitat de fluorescència que en les cèl·lules no tractades (controls). Aquest resultat es correlaciona amb la lectura d'altres marcadors associats a senescència, indicant que les sondes identifiquen de manera eficient la major activitat β-gal de les cèl·lules senescents. Seguidament, vam utilitzar una d'aquestes sondes per a estimar els nivells de senescència de ratolins SAMP8 de 7 mesos, en comparació a ratolins SAMR1 de la mateixa edat. Per a això, vam processar fetge i ronyó, dos òrgans diana per a l'acumulació de cèl·lules senescents, i vam analitzar l'activitat β-Gal amb la sonda WOS-Cy7Gal, al costat dels nivells de p16 i Lamin B1 (dos marcadors altament acceptats en el camp), per citometria de flux. Els resultats van indicar que existeix una major càrrega de cèl·lules senescents en la soca SAMP8 a aquesta edat.

Donada l'eficiència de la sonda WOS-Cy7Gal en la lectura de senescència associada a l'edat *ex vivo*, vam decidir modificar-la a nivell químic incloent dos grups sulfònics per afavorir la seua excreció en orina. Aquesta sonda modificada, d'ara en avant denominada Cy7Gal, va ser injectada en ratolins SAMP8 d'avançada edat, en comparació a la WOS-Cy7Gal, per a analitzar la seua biodistribució. Pocs minuts després de la injecció, es van recollir mostres d'orina i plasma i es van analitzar els nivells de fluorescència. La sonda amb grups sulfònics va ser detectada tant en orina com en plasma, mentre que els nivells de fluorescència en els animals injectats amb WOS-Cy7Gal a penes es van diferenciar dels animals administrats amb DMEM (vehicle). Sobre la base d'aquests resultats, inferim que Cy7Gal difon ràpidament de les cèl·lules a la sang i es filtra en els ronyons acumulant-se en l'orina. A continuació, vam injectar Cy7Gal en animals SAMP8 i SAMR1 de 7 mesos d'edat i, d'acord amb l'experiment *ex vivo*, la lectura de fluorescència en orina va indicar una major activitat β-Gal sistèmica en els ratolins SAMP8. Per tant, la sonda Cy7Gal apareix com una eina interessant per a l'estimació dels nivells de senescència *in vivo* i de forma no invasiva. A més, també vam testar la sonda Cy7Gal en un model d'envelliment natural amb ratolins C57BL/6 de 3 i 15 mesos. Els nivells de fluorescència registrats van ser significativament més alts en els ratolins més vells, donant suport a la utilitat d'aquesta sonda en la mesura de senescència associada a envelliment en estudis longitudinals. Referent a això, decidim testar l'eficiència de la sonda com a eina de monitoratge en teràpies senilítiques.

Primer, vam dur a terme un tractament senilític amb D+Q en ratolins SAMP8 i vam avaluar els efectes de la senilisi amb la lectura de la sonda Cy7Gal i amb l'avaluació del comportament ansiós. A curt termini després del tractament senilític (20 dies), vam detectar una reducció en signes d'ansietat en els animals que van rebre els fàrmacs en correlació amb una disminució en els nivells de fluorescència associats a Cy7Gal en orina. Per tant, la sonda ens indica una reducció en la càrrega senescent després del tractament que, a més, té efectes positius a nivell de comportament. D'altra banda, quan vam avaluar els efectes

senilítics a més llarg termini després del tractament (més de 50 dies), no vam detectar canvis significatius ni en el comportament ansiós, ni en la sonda entre ratolins tractats i vehicles. Aquest resultat posa de manifest que els efectes dels fàrmacs senilítics *in vivo* són transitoris. Per a comprovar que els ratolins podien respondre de nou al tractament, es va dur a terme altre cicle amb D+Q en els mateixos animals. De manera interessant, vam detectar una recuperació en els efectes de la senilisi, amb signes d'ansietat disminuïts i càrrega senescent reduïda en els ratolins SAMP8 tractats. A més, quan vam avaluar el tractament a curt termini, vam identificar una correlació significativa entre el comportament ansiós i els resultats de la lectura de la sonda. Aquest resultat posa en relleu que la sonda és prou sensible com per a predir un comportament associat a l'edat.

Segon, vam iniciar el tractament senilític amb D+Q en ratolins C57BL/6 de 15 mesos. Després de la intervenció senilítica, vam detectar una baixada en els nivells de senescència amb la sonda Cy7Gal, així com una disminució en el comportament ansiós. Per tant, Cy7Gal permet una lectura fiable de la càrrega senescent *in vivo* i resulta una eina útil en estudis longitudinals diagnòstics o en el monitoratge de teràpies senilítiques. A més, vam trobar una correlació significativa entre l'ansietat i la lectura de la sonda, la qual cosa indica que la senescència té un fort impacte deleteri a nivell cerebral.

2. Caracterització de la senescència endotelial cerebral associada a l'envelliment i el seu impacte en la neurogènesi

A fi d'investigar si les ECs de cervell adquireixen un destí senescent amb l'edat en relació a una disminució en la neurogènesi, vam avaluar diferents marcadors associats a senescència en aquesta població vascular i vam analitzar el llinatge neurogènic de la SEZ en ratolins SAMP8 front a SAMR1, així com en ratolins C57BL/6 joves front a vells. Amb aquest propòsit, vam desenvolupar un panell de FACS per al fenotipat de ECs senescents de cervell mitjançant el qual podem avaluar l'activitat β-Gal (amb les sondes desenvolupades pel nostre grup), p16 i altres marcadors com γH2AX o la producció de ROS (mitoSOX). Per a l'anàlisi de la neurogènesi en la SEZ, vam emprar el protocol de citometria de flux publicat pel nostre grup (Belenguer et al., 2021). Els resultats obtinguts amb tots dos models animals van demostrar que en les ECs de cervell augmenten els nivells de marcadors associats a senescència amb l'envelliment i que, a més, el potencial neurogènic de la SEZ disminueix.

Per a comprovar si la correlació entre senescència endotelial i neurogènesi es mantenia sota una intervenció senolítica, analitzem aquesta connexió en ratolins SAMP8 després del tractament amb D+Q. A més d'aplicar els nostres panells de citometria, els ratolins van ser injectats amb BrdU per a la posterior anàlisi immunohistoquímica de la neurogènesi en el OB i el DG. Els resultats van indicar una baixada en els nivells de marcadors associats a senescència en les ECs de cervell i una recuperació en el potencial neurogènic de la SEZ dels SAMP8 tractats. Aquest es va acompanyar d'un augment en el nombre de noves neurones que s'integren en el OB. A més, la quantitat de cèl·lules $BrdU^+$ en la SGZ també va ser notablement superior en els ratolins tractats amb els fàrmacs senolíticos. Aquests resultats demostren una consistència en la relació entre la senescència endotelial i la neurogènesi adulta.

Per a analitzar si existeix una relació causa-efecte entre la senescència endotelial cerebral i la baixada en neurogènesi, vam dissenyar un model per a la inducció genètica de senescència, de manera selectiva, en ECs de cervell, i vam estudiar el seu impacte en neurogènesi. Aquesta estratègia consisteix en un vector viral adenoassociat la proteïna de la càpsida del qual té tropisme per les ECs cerebrals (AAV-BR1) (Körbelin et al., 2016). En aquest vector vam incloure material genètic per a la sobreexpresió de p16 en les ECs i inducció de senescència. A més, també vam incloure GFP per a analitzar de manera senzilla la transducció del virus. Després de la injecció i.v. d'aquest vector, o de PBS com a control, en ratolins C57BL/6, vam administrar BrdU a fi d'analitzar la neurogènesi en el OB i la SGZ. Els ratolins van ser eutanasiats 31 dies després de la inoculació del vector adenoassociat, i vam avaluar la senescència endotelial tant en cervell com

en fetge, mitjançant citometria de flux. Els resultats van mostrar que només les ECs de cervell dels ratolins injectats amb el virus exhibien nivells significativament més alts de GFP i p16, ressaltant l'especificitat de l'estratègia. A més, aquesta població mostrava major activitat β-Gal i alts nivells de γH2AX, confirmant la inducció de senescència. L'anàlisi immunohistoquímica de la neurogènesi va revelar un nombre menor de noves neurones tant en el OB com en l'hipocamp en els animals injectats amb el vector, en comparació als injectats amb PBS. D'aquesta manera, concloem que la senescència endotelial té un fort impacte en la neurogènesi adulta i és suficient per a reduir el nombre de noves neurones que es formen en els principals nínxols neurogènics del cervell. En conjunt, els resultats apunten a la població endotelial com una diana d'investigació interessant en l'estudi de l'envelliment cerebral.

Conclusions*:*

1. Les sondes fluorogèniquess, específicament dissenyades per a ser recuperades en l'orina, permeten una lectura de l'activitat β-Gal sistèmica, la qual possibilita l'estimació de la càrrega de cèl·lules senescents en estudis longitudinals associats a envelliment, i/o tractaments senilítics, de forma no invasiva.

2. Els estudis longitudinals, correlacionant l'ansietat associada a l'edat i els nivells de β-Gal sistèmics, indiquen que els efectes dels fàrmacs senilítics són transitoris.

3. Les cèl·lules endotelials de cervell entren en senescència amb l'edat i aquest destí cel·lular té un impacte perjudicial en les cèl·lules mare neurals i en la neurogènesi.

Bibliography

Abrous, D. N., & Wojtowicz, J. M. (2015). Interaction between Neurogenesis and Hippocampal Memory System: New Vistas. Cold Spring Harbor Perspectives in Biology, 7(6), 1–24.

Acosta, J. C., Banito, A., Wuestefeld, T., Georgilis, A., Janich, P., Morton, J. P., Athineos, D., Kang, T. W., Lasitschka, F., Andrulis, M., Pascual, G., Morris, K. J., Khan, S., Jin, H., Dharmalingam, G., Snijders, A. P., Carroll, T., Capper, D., Pritchard, C., … Gil, J. (2013). A complex secretory program orchestrated by the inflammasome controls paracrine senescence. Nature Cell Biology, 15(8), 978.

Ahlenius, H., Visan, V., Kokaia, M., Lindvall, O., & Kokaia, Z. (2009). Neural Stem and Progenitor Cells Retain Their Potential for Proliferation and Differentiation into Functional Neurons Despite Lower Number in Aged Brain. Journal of Neuroscience, 29(14), 4408–4419.

Akiguchi, I., Pallàs, M., Budka, H., Akiyama, H., Ueno, M., Han, J., Yagi, H., Nishikawa, T., Chiba, Y., Sugiyama, H., Takahashi, R., Unno, K., Higuchi, K., & Hosokawa, M. (2017). SAMP8 mice as a neuropathological model of accelerated brain aging and dementia: Toshio Takeda's legacy and future directions. Neuropathology: Official Journal of the Japanese Society of Neuropathology, 37(4), 293–305.

Anacker, C., & Hen, R. (2017). Adult hippocampal neurogenesis and cognitive flexibility — linking memory and mood. Nature Reviews Neuroscience 2017 18:6, 18(6), 335–346.

Andreu-Agulló, C., Morante-Redolat, J. M., Delgado, A. C., & Fariñas, I. (2009). Vascular niche factor PEDF modulates Notch-dependent stemness in the adult subependymal zone. Nature Neuroscience 2009 12:12, 12(12), 1514–1523.

Apostolopoulou, M., Kiehl, T. R., Winter, M., Cardenas De La Hoz, E., Boles, N. C., Bjornsson, C. S., Zuloaga, K. L., Goderie, S. K., Wang, Y., Cohen, A. R., & Temple, S. (2017). Non-monotonic Changes in Progenitor Cell Behavior and Gene Expression during Aging of the Adult V-SVZ Neural Stem Cell Niche. Stem Cell Reports, 9(6), 1931–1947.

Apple, D. M., & Kokovay, E. (2017). Vascular niche contribution to age-associated neural stem cell dysfunction. American Journal of Physiology. Heart and Circulatory Physiology, 313(5), H896–H902.

Artegiani, B., Lyubimova, A., Muraro, M., van Es, J. H., van Oudenaarden, A., & Clevers, H. (2017). A Single-Cell RNA Sequencing Study Reveals Cellular and Molecular Dynamics of the Hippocampal Neurogenic Niche. Cell Reports, 21(11), 3271–3284.

Banks, W. A., Farr, S. A., Morley, J. E., Wolf, K. M., Geylis, V., & Steinitz, M. (2007). Anti-amyloid beta protein antibody passage across the blood-brain barrier in the SAMP8 mouse model of Alzheimer's disease: an age-related selective uptake with reversal of learning impairment. Experimental Neurology, 206(2), 248–256.

Barinda, A. J., Ikeda, K., Nugroho, D. B., Wardhana, D. A., Sasaki, N., Honda, S., Urata, R., Matoba, S., Hirata, K. ichi, & Emoto, N. (2020). Endothelial progeria induces adipose tissue senescence and impairs insulin sensitivity through senescence associated secretory phenotype. Nature Communications 2020 11:1, 11(1), 1–13.

Barr, A. R., & McClelland, S. E. (2022). Cells on lockdown: long-term consequences of CDK4/6 inhibition. The EMBO Journal, 41(6), e110764.

Bayram, B., Nikolai, S., Huebbe, P., Ozcelik, B., Grimm, S., Grune, T., Frank, J., & Rimbach, G. (2013). Biomarkers of oxidative stress, antioxidant defence and inflammation are altered in the senescence-accelerated mouse prone 8. Age, 35(4), 1205.

Beckervordersandforth, R., Tripathi, P., Ninkovic, J., Bayam, E., Lepier, A., Stempfhuber, B., Kirchhoff, F., Hirrlinger, J., Haslinger, A., Lie, D. C., Beckers, J., Yoder, B., Irmler, M., & Götz, M. (2010). In vivo fate mapping and expression analysis reveals molecular hallmarks of prospectively isolated adult neural stem cells. Cell Stem Cell, 7(6), 744–758.

Belenguer, G., Domingo-Muelas, A., Ferrón, S. R., Morante-Redolat, J. M., & Fariñas, I. (2016). Isolation, culture and analysis of adult subependymal neural stem cells. Differentiation; Research in Biological Diversity, 91(4–5), 28–41.

Belenguer, G., Duart-Abadia, P., Domingo-Muelas, A., Morante-Redolat, J. M., & Fariñas, I. (2021). Cell population analysis of the adult murine subependymal neurogenic lineage by flow cytometry. STAR Protocols, 2(2).

Belenguer, G., Duart-Abadia, P., Jordán-Pla, A., Domingo-Muelas, A., Blasco-Chamarro, L., Ferrón, S. R., Morante-Redolat, J. M., & Fariñas, I. (2021). Adult Neural Stem Cells Are Alerted by Systemic Inflammation through TNF-α Receptor Signaling. Cell Stem Cell, 28(2), 285-299.e9.

Ben Abdallah, N. M. B., Slomianka, L., Vyssotski, A. L., & Lipp, H. P. (2010). Early age-related changes in adult hippocampal neurogenesis in C57 mice. Neurobiology of Aging, 31(1), 151–161.

Bhayadia, R., Schmidt, B. M. W., Melk, A., & Hömme, M. (2016). Senescence-Induced Oxidative Stress Causes Endothelial Dysfunction. The Journals of Gerontology. Series A, Biological Sciences and Medical Sciences, 71(2), 161–169.

Blagosklonny, M. V. (2021). The hyperfunction theory of aging: three common misconceptions. Oncoscience, 8, 103–107.

Bonds, J. A., Tunc-Ozcan, E., Dunlop, S. R., Rawat, R., Peng, C. Y., & Kessler, J. A. (2023). Why Some Mice Are Smarter than Others: The Impact of Bone Morphogenetic Protein Signaling on Cognition. ENeuro, 10(1).

Borghesan, M., Fafián-Labora, J., Eleftheriadou, O., Carpintero-Fernández, P., Paez-Ribes, M., Vizcay-Barrena, G., Swisa, A., Kolodkin-Gal, D., Ximénez-Embún, P., Lowe, R., Martín-Martín, B., Peinado, H., Muñoz, J., Fleck, R. A., Dor, Y., Ben-Porath, I., Vossenkamper, A., Muñoz-Espin, D., & O'Loghlen, A. (2019). Small Extracellular Vesicles Are Key Regulators of Non-cell Autonomous Intercellular Communication in Senescence via the Interferon Protein IFITM3. Cell Reports, 27(13), 3956-3971.e6.

Bousset, L., & Gil, J. (2022). Targeting senescence as an anticancer therapy. Molecular Oncology, 16(21), 3855–3880.

Bussian, T. J., Aziz, A., Meyer, C. F., Swenson, B. L., van Deursen, J. M., & Baker, D. J. (2018). Clearance of senescent glial cells prevents tau-dependent pathology and cognitive decline. Nature 2018 562:7728, 562(7728), 578–582.

Butterfield, D. A., Howard, B. J., Yatin, S., Allen, K. L., & Carney, J. M. (1997). Free radical oxidation of brain proteins in accelerated senescence and its modulation by N-tert-butyl-alpha-phenylnitrone. Proceedings of the National Academy of Sciences of the United States of America, 94(2), 674–678.

Butterfield, D. A., & Poon, H. F. (2005). The senescence-accelerated prone mouse (SAMP8): a model of age-related cognitive decline with relevance to alterations of the gene expression and protein abnormalities in Alzheimer's disease. Experimental Gerontology, 40(10), 774–783.

Campisi, J. (2013). Aging, Cellular Senescence, and Cancer. Annual Review of Physiology, 75, 685.

Campisi, J., Andersen, J. K., Kapahi, P., & Melov, S. (2011). Cellular senescence: a link between cancer and age-related degenerative disease? Seminars in Cancer Biology, 21(6), 354–359.

Campos-Bedolla, P., Walter, F. R., Veszelka, S., & Deli, M. A. (2014). Role of the blood-brain barrier in the nutrition of the central nervous system. Archives of Medical Research, 45(8), 610–638.

Capilla-Gonzalez, V., Cebrian-Silla, A., Guerrero-Cazares, H., Garcia-Verdugo, J. M., & Quiñones-Hinojosa, A. (2014). Age-related changes in astrocytic and ependymal cells of the subventricular zone. Glia, 62(5), 790–803.

Carreira, B. P., Morte, M. I., Santos, A. I., Lourenço, A. S., Ambrósio, A. F., Carvalho, C. M., & Araújo, I. M.

(2014). Nitric oxide from inflammatory origin impairs neural stem cell proliferation by inhibiting epidermal growth factor receptor signaling. Frontiers in Cellular Neuroscience, 8, 343.

Chaib, S., Tchkonia, T., & Kirkland, J. L. (2022). Cellular senescence and senolytics: the path to the clinic. Nature Medicine 2022 28:8, 28(8), 1556–1568.

Chaker, Z., Codega, P., & Doetsch, F. (2016). A mosaic world: puzzles revealed by adult neural stem cell heterogeneity. Wiley Interdisciplinary Reviews. Developmental Biology, 5(6), 640–658.

Chala, N., Moimas, S., Giampietro, C., Zhang, X., Zambelli, T., Exarchos, V., Nazari-Shafti, T. Z., Poulikakos, D., & Ferrari, A. (2021). Mechanical Fingerprint of Senescence in Endothelial Cells. Nano Letters, 21(12), 4911–4920.

Chandrasekaran, A., Idelchik, M. del P. S., & Melendez, J. A. (2017). Redox control of senescence and age-related disease. Redox Biology, 11, 91.

Chang, J., Wang, Y., Shao, L., Laberge, R. M., Demaria, M., Campisi, J., Janakiraman, K., Sharpless, N. E., Ding, S., Feng, W., Luo, Y., Wang, X., Aykin-Burns, N., Krager, K., Ponnappan, U., Hauer-Jensen, M., Meng, A., & Zhou, D. (2016). Clearance of senescent cells by ABT263 rejuvenates aged hematopoietic stem cells in mice. Nature Medicine, 22(1), 78.

Changarathil, G., Ramirez, K., Isoda, H., Sada, A., & Yanagisawa, H. (2019). Wild-type and SAMP8 mice show age-dependent changes in distinct stem cell compartments of the interfollicular epidermis. PLOS ONE, 14(5), e0215908.

Chapman, J., Fielder, E., & Passos, J. F. (2019). Mitochondrial dysfunction and cell senescence: deciphering a complex relationship. FEBS Letters, 593(13), 1566–1579.

Chen, H., Zhou, X., Emura, S., & Shoumura, S. (2009). Site-specific bone loss in senescence-accelerated mouse (SAMP6): a murine model for senile osteoporosis. Experimental Gerontology, 44(12), 792–798.

Chen, M. B., Yang, A. C., Yousef, H., Lee, D., Chen, W., Schaum, N., Lehallier, B., Quake, S. R., & Wyss-Coray, T. (2020). Brain Endothelial Cells Are Exquisite Sensors of Age-Related Circulatory Cues. Cell Reports, 30(13), 4418-4432.e4.

Chen, W. W., Zhang, X., & Huang, W. J. (2016). Role of neuroinflammation in neurodegenerative diseases (Review). Molecular Medicine Reports, 13(4), 3391–3396.

Chen, Y., Lüttmann, F. F., Schoger, E., Schöler, H. R., Zelarayán, L. C., Kim, K. P., Haigh, J. J., Kim, J., & Braun, T. (2021). Reversible reprogramming of cardiomyocytes to a fetal state drives heart regeneration in mice. Science, 373(6562), 1537–1540.

Cheung, T. H., & Rando, T. A. (2013). Molecular regulation of stem cell quiescence. Nature Reviews Molecular Cell Biology 2013 14:6, 14(6), 329–340.

Chia, C. W., Egan, J. M., & Ferrucci, L. (2018). Age-Related Changes in Glucose Metabolism, Hyperglycemia, and Cardiovascular Risk. Circulation Research, 123(7), 886–904.

Chiche, A., Chen, C., & Li, H. (2020). The crosstalk between cellular reprogramming and senescence in aging and regeneration. Experimental Gerontology, 138, 111005.

Childs, B. G., Durik, M., Baker, D. J., & Van Deursen, J. M. (2015). Cellular senescence in aging and age-related disease: from mechanisms to therapy. Nature Medicine, 21(12), 1424.

Childs, B. G., Gluscevic, M., Baker, D. J., Laberge, R. M., Marquess, D., Dananberg, J., & Van Deursen, J. M. (2017). Senescent cells: an emerging target for diseases of ageing. Nature Reviews. Drug Discovery, 16(10), 718.

Chinta, S. J., Woods, G., Demaria, M., Rane, A., Zou, Y., McQuade, A., Rajagopalan, S., Limbad, C., Madden,

D. T., Campisi, J., & Andersen, J. K. (2018). Cellular Senescence Is Induced by the Environmental Neurotoxin Paraquat and Contributes to Neuropathology Linked to Parkinson's Disease. Cell Reports, 22(4), 930–940.

Chirivella, L., Kirstein, M., Ferrón, S. R., Domingo-Muelas, A., Durupt, F. C., Acosta-Umanzor, C., … Fariñas, I. (2017). Cyclin-Dependent Kinase 4 Regulates Adult Neural Stem Cell Proliferation and Differentiation in Response to Insulin. Stem Cells (Dayton, Ohio), 35(12), 2403–2416.

Chou, A. H., Yeh, T. H., Ouyang, P., Chen, Y. L., Chen, S. Y., & Wang, H. L. (2008). Polyglutamine-expanded ataxin-3 causes cerebellar dysfunction of SCA3 transgenic mice by inducing transcriptional dysregulation. Neurobiology of Disease, 31(1), 89–101.

Codega, P., Silva-Vargas, V., Paul, A., Maldonado-Soto, A. R., DeLeo, A. M., Pastrana, E., & Doetsch, F. (2014). Prospective Identification and Purification of Quiescent Adult Neural Stem Cells from Their in Vivo Niche. Neuron, 82(3), 545–559.

Cohen, J., & Torres, C. (2019). Astrocyte senescence: Evidence and significance. Aging Cell, 18(3).

Conover, J. C., & Shook, B. A. (2011). Aging of the Subventricular Zone Neural Stem Cell Niche. 2(1), 49–63.

Coppé, J. P., Patil, C. K., Rodier, F., Sun, Y., Muñoz, D. P., Goldstein, J., Nelson, P. S., Desprez, P. Y., & Campisi, J. (2008). Senescence-Associated Secretory Phenotypes Reveal Cell-Nonautonomous Functions of Oncogenic RAS and the p53 Tumor Suppressor. PLoS Biology, 6(12).

Coppé, J.-P., Desprez, P.-Y., Krtolica, A., & Campisi, J. (2010). The Senescence-Associated Secretory Phenotype: The Dark Side of Tumor Suppression.

Costa, V., Lugert, S., & Jagasia, R. (2015). Role of adult hippocampal neurogenesis in cognition in physiology and disease: pharmacological targets and biomarkers. Handbook of Experimental Pharmacology, 228, 99–155.

Crouch, E. E., Liu, C., Silva-Vargas, V., & Doetsch, F. (2015). Regional and stage-specific effects of prospectively purified vascular cells on the adult V-SVZ neural stem cell lineage. The Journal of Neuroscience: The Official Journal of the Society for Neuroscience, 35(11), 4528–4539.

Crozier, L., Foy, R., Mouery, B. L., Whitaker, R. H., Corno, A., Spanos, C., Ly, T., Cook, J. G., & Saurin, A. T. (2022). CDK4/6 inhibitors induce replication stress to cause long-term cell cycle withdrawal. The EMBO Journal, 41(6), e108599.

Czupalla, C. J., Yousef, H., Wyss-Coray, T., & Butcher, E. C. (2018). Collagenase-based Single Cell Isolation of Primary Murine Brain Endothelial Cells Using Flow Cytometry. Bio-Protocol 8(22), e3092.

Dagher, O., Mury, P., Thorin-Trescases, N., Noly, P. E., Thorin, E., & Carrier, M. (2021). Therapeutic Potential of Quercetin to Alleviate Endothelial Dysfunction in Age-Related Cardiovascular Diseases. Frontiers in Cardiovascular Medicine, 8, 220.

Daynac, M., Morizur, L., Chicheportiche, A., Mouthon, M. A., & Boussin, F. D. (2016). Age-related neurogenesis decline in the subventricular zone is associated with specific cell cycle regulation changes in activated neural stem cells. Scientific Reports 2016 6:1, 6(1), 1–10.

Deacon, R. M. J. (2013). Measuring the Strength of Mice. Journal of Visualized Experiments: JoVE, 76, 2610.

Debacq-Chainiaux, F., Erusalimsky, J. D., Campisi, J., & Toussaint, O. (2009). Protocols to detect senescence-associated beta-galactosidase (SA-βgal) activity, a biomarker of senescent cells in culture and in vivo. Nature Protocols, 4(12), 1798–1806.

Del Valle, J., Duran-Vilaregut, J., Manich, G., Camins, A., Pallàs, M., Vilaplana, J., & Pelegrí, C. (2009). Time-course of blood-brain barrier disruption in senescence-accelerated mouse prone 8 (SAMP8) mice. International Journal of Developmental Neuroscience: The Official Journal of the International Society for De-

velopmental Neuroscience, 27(1), 47–52.

Delgado, A. C., Ferrón, S. R., Vicente, D., Porlan, E., Perez-Villalba, A., Trujillo, C. M., D'Ocón, P., & Fariñas, I. (2014). Endothelial NT-3 delivered by vasculature and CSF promotes quiescence of subependymal neural stem cells through nitric oxide induction. Neuron, 83(3), 572–585.

Dimri, G. P., Lee, X., Basile, G., Acosta, M., Scott, G., Roskelley, C., Medrano, E. E., Linskens, M., Rubelj, I., Pereira-Smith, O., Peacocke, M., & Campisi, J. (1995). A biomarker that identifies senescent human cells in culture and in aging skin in vivo. Proceedings of the National Academy of Sciences of the United States of America, 92(20), 9363–9367.

Ding, W. Y., Huang, J., & Wang, H. (2020). Waking up quiescent neural stem cells: Molecular mechanisms and implications in neurodevelopmental disorders. PLoS Genetics, 16(4).

Docherty, M. H., Baird, D. P., Hughes, J., & Ferenbach, D. A. (2020). Cellular Senescence and Senotherapies in the Kidney: Current Evidence and Future Directions. Frontiers in Pharmacology, 11.

Doetsch, F., Caille, I., Lim, D. A., Garcia-Verdugo, J. M., & Alvarez-Buylla, A. (1999). Subventricular zone astrocytes are neural stem cells in the adult mammalian brain. Cell, 97(6), 703–716.

Dulken, B. W., Leeman, D. S., Boutet, S. C., Hebestreit, K., & Brunet, A. (2017). Single-Cell Transcriptomic Analysis Defines Heterogeneity and Transcriptional Dynamics in the Adult Neural Stem Cell Lineage. Cell Reports, 18(3).

Ehret, F., Vogler, S., & Kempermann, G. (2015). A co-culture model of the hippocampal neurogenic niche reveals differential effects of astrocytes, endothelial cells and pericytes on proliferation and differentiation of adult murine precursor cells. Stem Cell Research, 15(3), 514–521.

El Assar, M., Angulo, J., & Rodríguez-Mañas, L. (2013). Oxidative stress and vascular inflammation in aging. Free Radical Biology & Medicine, 65, 380–401.

Encinas, J. M., Michurina, T. V., Peunova, N., Park, J. H., Tordo, J., Peterson, D. A., Fishell, G., Koulakov, A., & Enikolopov, G. (2011). Division-coupled astrocytic differentiation and age-related depletion of neural stem cells in the adult hippocampus. Cell Stem Cell, 8(5), 566–579.

Eremenko, E., Golova, A., Stein, D., Einav, M., Khrameeva, E., & Toiber, D. (2021). FACS-based isolation of fixed mouse neuronal nuclei for ATAC-seq and Hi-C. STAR Protocols, 2(3).

Estepa-Fernández, A., Alfonso, M., Morellá-Aucejo, Á., García-Fernández, A., Lérida-Viso, A., Lozano-Torres, B., Galiana, I., Soriano-Teruel, P. M., Sancenón, F., Orzáez, M., & Martínez-Máñez, R. (2021). Senolysis Reduces Senescence in Veins and Cancer Cell Migration. Advanced Therapeutics, 4(10), 2100149.

Fabián-Labora, J. A., & O'Loghlen, A. (2020). Classical and Nonclassical Intercellular Communication in Senescence and Ageing. Trends in Cell Biology, 30(8), 628–639.

Fernagut, P. O., Chalon, S., Diguet, E., Guilloteau, D., Tison, F., & Jaber, M. (2003). Motor behaviour deficits and their histopathological and functional correlates in the nigrostriatal system of dopamine transporter knockout mice. Neuroscience, 116(4), 1123–1130.

Fernández, A., Quintana, E., Velasco, P., Moreno-Jimenez, B., de Andrés, B., Gaspar, M. L., Liste, I., Vilar, M., Mira, H., & Cano, E. (2021). Senescent accelerated prone 8 (SAMP8) mice as a model of age dependent neuroinflammation. Journal of Neuroinflammation 2021 18:1, 18(1), 1–20.

Ferrón, S. R., Andreu-Agulló, C., Mira, H., Sánchez, P., Ángeles Marqués-Torrejón, M., & Fariñas, I. (2007). A combined ex/in vivo assay to detect effects of exogenously added factors in neural stem cells. Nature Protocols, 2(4), 849–859.

Ferrón, S. R., Marqués-Torrejón, M. Á., Mira, H., Flores, I., Taylor, K., Blasco, M. A., & Fariñas, I. (2009). Telomere shortening in neural stem cells disrupts neuronal differentiation and neuritogenesis. The Journal

of Neuroscience: The Official Journal of the Society for Neuroscience, 29(46), 14394–14407.

Ferrón, S., Mira, H., Franco, S., Cano-Jimenez, M., Bellmunt, E., Ramírez, C., Fariñas, I., & Blasco, M. A. (2004). Telomere shortening and chromosomal instability abrogates proliferation of adult but not embryonic neural stem cells. Development, 131(16), 4059–4070.

Fielder, E., Wan, T., Alimohammadiha, G., Ishaq, A., Low, E., Weigand, B. M., Kelly, G., Parker, C., Griffin, B., Jurk, D., Korolchuk, V. I., von Zglinicki, T., & Miwa, S. (2022). Short senolytic or senostatic interventions rescue progression of radiation-induced frailty and premature ageing in mice. ELife, 11, 75492.

Fleming, S. M., Salcedo, J., Fernagut, P. O., Rockenstein, E., Masliah, E., Levine, M. S., & Chesselet, M. F. (2004). Early and Progressive Sensorimotor Anomalies in Mice Overexpressing Wild-Type Human α-Synuclein. The Journal of Neuroscience, 24(42), 9434.

Flood, J. F., Farr, 1. Susan A., Kaiser, F. E., & Morley, J. E. (1995). Age-related impairment in learning but not memory in SAMP8 female mice. Pharmacology, Biochemistry and Behavior, 50(4), 661–664.

Flor, A. C., Wolfgeher, D., Wu, D., & Kron, S. J. (2017). A signature of enhanced lipid metabolism, lipid peroxidation and aldehyde stress in therapy-induced senescence. Cell Death Discovery 2017 3:1, 3(1), 1–12.

Freund, A., Laberge, R. M., Demaria, M., & Campisi, J. (2012). Lamin B1 loss is a senescence-associated biomarker. Molecular Biology of the Cell, 23(11), 2066–2075.

Fuentealba, L. C., Rompani, S. B., Parraguez, J. I., Obernier, K., Romero, R., Cepko, C. L., & Alvarez-Buylla, A. (2015). Embryonic Origin of Postnatal Neural Stem Cells. Cell, 161(7), 1644–1655.

Fülöp, T., Nagy, J. T., Worum, I., Fóris, G., Mudri, K., Varga, P., & Udvardy, M. (1987). Glucose intolerance and insulin resistance with aging--studies on insulin receptors and post-receptor events. Archives of Gerontology and Geriatrics, 6(2), 107–115.

Furutachi, S., Miya, H., Watanabe, T., Kawai, H., Yamasaki, N., Harada, Y., Imayoshi, I., Nelson, M., Nakayama, K. I., Hirabayashi, Y., & Gotoh, Y. (2015). Slowly dividing neural progenitors are an embryonic origin of adult neural stem cells. Nature Neuroscience, 18(5), 657–665.

Geng, Y. Q., Guan, J. T., Xu, X. H., & Fu, Y. C. (2010). Senescence-associated beta-galactosidase activity expression in aging hippocampal neurons. Biochemical and Biophysical Research Communications, 396(4), 866–869.

Ghosh, A. K., O'Brien, M., Mau, T., Qi, N., & Yung, R. (2019). Adipose Tissue Senescence and Inflammation in Aging is Reversed by the Young Milieu. The Journals of Gerontology. Series A, Biological Sciences and Medical Sciences, 74(11), 1709–1715.

Goldsworthy, M. E., & Potter, P. K. (2014). Modelling age-related metabolic disorders in the mouse. Mammalian Genome, 25(9), 487.

Gomez-Cabrera, M. C., Garcia-Valles, R., Rodriguez-Mañas, L., Garcia-Garcia, F. J., Olaso-Gonzalez, G., Salvador-Pascual, A., Tarazona-Santabalbina, F. J., & Viña, J. (2017). A New Frailty Score for Experimental Animals Based on the Clinical Phenotype: Inactivity as a Model of Frailty. The Journals of Gerontology. Series A, Biological Sciences and Medical Sciences, 72(7), 885–891.

Gómez-Gaviro, M. V., Scott, C. E., Sesay, A. K., Matheu, A., Booth, S., Galichet, C., & Lovell-Badge, R. (2012). Betacellulin promotes cell proliferation in the neural stem cell niche and stimulates neurogenesis. Proceedings of the National Academy of Sciences of the United States of America, 109(4), 1317–1322.

Gonzales, M. M., Garbarino, V. R., Marques Zilli, E., Petersen, R. C., Kirkland, J. L., Tchkonia, T., Musi, N., Seshadri, S., Craft, S., & Orr, M. E. (2022). Senolytic Therapy to Modulate the Progression of Alzheimer's Disease (SToMP-AD): A Pilot Clinical Trial. The Journal of Prevention of Alzheimer's Disease, 9(1), 22–29.

González-Gualda, E., Baker, A. G., Fruk, L., & Muñoz-Espín, D. (2021). A guide to assessing cellular senes-

cence in vitro and in vivo. The FEBS Journal, 288(1), 56–80.

Gonzalez-Meljem, J. M., Apps, J. R., Fraser, H. C., & Martinez-Barbera, J. P. (2018). Paracrine roles of cellular senescence in promoting tumourigenesis. British Journal of Cancer 2018 118:10, 118(10), 1283–1288.

Gorelick, P. B., Furie, K. L., Iadecola, C., Smith, E. E., Waddy, S. P., Lloyd-Jones, D. M., Bae, H. J., Bauman, M. A., Dichgans, M., Duncan, P. W., Girgus, M., Howard, V. J., Lazar, R. M., Seshadri, S., Testai, F. D., van Gaal, S., Yaffe, K., Wasiak, H., & Zerna, C. (2017). Defining Optimal Brain Health in Adults: A Presidential Advisory From the American Heart Association/American Stroke Association. Stroke, 48(10), e284–e303.

Govers, R., Bevers, L., de Bree, P., & Rabelink, T. J. (2002). Endothelial nitric oxide synthase activity is linked to its presence at cell–cell contacts. Biochemical Journal, 361(2), 193–201.

Graber, T. G., Ferguson-Stegall, L., Kim, J. H., & Thompson, L. D. V. (2013). Editor's choice: C57BL/6 Neuromuscular Healthspan Scoring System. The Journals of Gerontology Series A: Biological Sciences and Medical Sciences, 68(11), 1326.

Graves, S. I., & Baker, D. J. (2020). Implicating endothelial cell senescence to dysfunction in the ageing and diseased brain. Basic & Clinical Pharmacology & Toxicology, 127(2), 102–110.

Grosse, L., Wagner, N., Emelyanov, A., Molina, C., Lacas-Gervais, S., Wagner, K. D., & Bulavin, D. V. (2020). Defined p16High Senescent Cell Types Are Indispensable for Mouse Healthspan. Cell Metabolism, 32(1), 87-99.e6.

Guo, A. Y., Leung, K. S., Siu, P. M. F., Qin, J. H., Chow, S. K. H., Qin, L., … Cheung, W. H. (2015). Muscle mass, structural and functional investigations of senescence-accelerated mouse P8 (SAMP8). Experimental Animals, 64(4), 425.

Guyenet, S. J., Furrer, S. A., Damian, V. M., Baughan, T. D., la Spada, A. R., & Garden, G. A. (2010). A Simple Composite Phenotype Scoring System for Evaluating Mouse Models of Cerebellar Ataxia. Journal of Visualized Experiments: JoVE, 39.

Han, D., Li, F., Zhang, H., Ji, C., Shu, Q., Wang, C., Ni, H., Zhu, Y., & Wang, S. (2021). Mesencephalic astrocyte-derived neurotrophic factor restores blood–brain barrier integrity of aged mice after ischaemic stroke/reperfusion through anti-inflammation via TLR4/MyD88/NF-κB pathway. Journal of drug targeting 30(4), 430-441.

Hayashi, T., Matsui-Hirai, H., Miyazaki-Akita, A., Fukatsu, A., Funami, J., Ding, Q. F., Kamalanathan, S., Nation, Y., Ignarro, L. J., & Iguchi, A. (2006). Endothelial cellular senescence is inhibited by nitric oxide: implications in atherosclerosis associated with menopause and diabetes. Proceedings of the National Academy of Sciences of the United States of America, 103(45), 17018–17023.

Hernandez-Segura, A., de Jong, T. V., Melov, S., Guryev, V., Campisi, J., & Demaria, M. (2017). Unmasking Transcriptional Heterogeneity in Senescent Cells. Current Biology: CB, 27(17), 2652-2660.e4.

Hernandez-Segura, A., Nehme, J., & Demaria, M. (2018). Hallmarks of Cellular Senescence. Trends in Cell Biology, 28(6), 436–453.

Herranz, N., & Gil, J. (2018). Mechanisms and functions of cellular senescence. The Journal of Clinical Investigation, 128(4), 1238–1246.

Hickson, L. T. J., Langhi Prata, L. G. P., Bobart, S. A., Evans, T. K., Giorgadze, N., Hashmi, S. K., Herrmann, S. M., Jensen, M. D., Jia, Q., Jordan, K. L., Kellogg, T. A., Khosla, S., Koerber, D. M., Lagnado, A. B., Lawson, D. K., LeBrasseur, N. K., Lerman, L. O., McDonald, K. M., McKenzie, T. J., … Kirkland, J. L. (2019). Senolytics decrease senescent cells in humans: Preliminary report from a clinical trial of Dasatinib plus Quercetin in individuals with diabetic kidney disease. EBioMedicine, 47, 446–456.

Hidalgo-Lanussa, O., Baez-Jurado, E., Echeverria, V., Ashraf, G. M., Sahebkar, A., Garcia-Segura, L. M.,

Melcangi, R. C., & Barreto, G. E. (2020). Lipotoxicity, neuroinflammation, glial cells and oestrogenic compounds. JOURNAL OF NEUROENDOCRINOLOGY, 32(1), 1–15.

Hosokawa, M., Kasai, R., Higuchi, K., Takeshita, S., Shimizu, K., Hamamoto, H., Honma, A., Irino, M., Toda, K., Matsumura, A., Matsushita, M., & Takeda, T. (1984). Grading score system: a method for evaluation of the degree of senescence in senescence accelerated mouse (SAM). Mechanisms of Ageing and Development, 26(1), 91–102.

Hu, L., Li, H., Zi, M., Li, W., Liu, J., Yang, Y., Zhou, D., Kong, Q. P., Zhang, Y., & He, Y. (2022). Why Senescent Cells Are Resistant to Apoptosis: An Insight for Senolytic Development. Frontiers in Cell and Developmental Biology, 10, 246.

Huang, W., Hickson, L. T. J., Eirin, A., Kirkland, J. L., & Lerman, L. O. (2022). Cellular senescence: the good, the bad and the unknown. Nature Reviews. Nephrology, 18(10), 611–627.

Huang, Y., Wu, B., Shen, D., Chen, J., Yu, Z., & Chen, C. (2021). Ferroptosis in a sarcopenia model of senescence accelerated mouse prone 8 (SAMP8). International Journal of Biological Sciences, 17(1), 151–162.

Ito, K. (2013). Frontiers of model animals for neuroscience: two prosperous aging model animals for promoting neuroscience research. Experimental Animals, 62(4), 275–280.

Izzo, C., Vitillo, P., Di Pietro, P., Visco, V., Strianese, A., Virtuoso, N., Ciccarelli, M., Galasso, G., Carrizzo, A., & Vecchione, C. (2021). The Role of Oxidative Stress in Cardiovascular Aging and Cardiovascular Diseases. Life, 11(1), 1–42.

Jessberger, S., Clark, R. E., Broadbent, N. J., Clemenson, G. D., Consiglio, A., Lie, D. C., Squire, L. R., & Gage, F. H. (2009). Dentate gyrus-specific knockdown of adult neurogenesis impairs spatial and object recognition memory in adult rats. 16(2).

Jia, G., Aroor, A. R., Jia, C., & Sowers, J. R. (2019). Endothelial cell senescence in aging-related vascular dysfunction. Biochimica et Biophysica Acta. Molecular Basis of Disease, 1865(7), 1802–1809.

Jong, H. L., Mustafa, M. R., Vanhoutte, P. M., AbuBakar, S., & Wong, P. F. (2013). MicroRNA 299-3p modulates replicative senescence in endothelial cells. Physiological Genomics, 45(7), 256–267.

Jurk, D., Wang, C., Miwa, S., Maddick, M., Korolchuk, V., Tsolou, A., Gonos, E. S., Thrasivoulou, C., Jill Saffrey, M., Cameron, K., & von Zglinicki, T. (2012). Postmitotic neurons develop a p21-dependent senescence-like phenotype driven by a DNA damage response. Aging Cell, 11(6), 996–1004.

Kalamakis, G., Brüne, D., Ravichandran, S., Bolz, J., Fan, W., Ziebell, F., Stiehl, T., Catalá-Martinez, F., Kupke, J., Zhao, S., Llorens-Bobadilla, E., Bauer, K., Limpert, S., Berger, B., Christen, U., Schmezer, P., Mallm, J. P., Berninger, B., Anders, S., … Martin-Villalba, A. (2019). Quiescence Modulates Stem Cell Maintenance and Regenerative Capacity in the Aging Brain. Cell, 176(6), 1407-1419.e14.

Karakatsani, A., Shah, B., & Ruiz de Almodovar, C. (2019). Blood Vessels as Regulators of Neural Stem Cell Properties. Frontiers in Molecular Neuroscience, 12.

Katsimpardi, L., Litterman, N. K., Schein, P. A., Miller, C. M., Loffredo, F. S., Wojtkiewicz, G. R., Chen, J. W., Lee, R. T., Wagers, A. J., & Rubin, L. L. (2014). Vascular and neurogenic rejuvenation of the aging mouse brain by young systemic factors. Science (New York, N.Y.), 344(6184), 630.

Katsimpardi, L., & Lledo, P. M. (2018). Regulation of neurogenesis in the adult and aging brain. In Current Opinion in Neurobiology (Vol. 53, pp. 131–138). Elsevier Ltd.

Katsuumi, G., Shimizu, I., Yoshida, Y., & Minamino, T. (2018). Vascular Senescence in Cardiovascular and Metabolic Diseases. Frontiers in Cardiovascular Medicine, 5, 18.

Kempermann, G. (2022). What Is Adult Hippocampal Neurogenesis Good for? 16, 487.

Kempermann, G., Gast, D., Kronenberg, G., Yamaguchi, M., & Gage, F. H. (2003). Early determination and long-term persistence of adult-generated new neurons in the hippocampus of mice. Development, 130(2), 391–399.

Kempermann, G., Song, H., & Gage, F. H. (2015). Neurogenesis in the Adult Hippocampus. Cold Spring Harbor Perspectives in Biology, 7(9), a018812.

Kim, D. W., & Choi, J. H. (2000). Effects of age and dietary restriction on animal model SAMP8 mice with learning and memory impairments. Journal of Nutrition, Health and Aging, 4(4), 233–238.

Kirkland, J. L., & Tchkonia, T. (2020). Senolytic drugs: from discovery to translation. Journal of Internal Medicine, 288(5), 518.

Kiss, T., Nyúl-Tóth, Á., Balasubramanian, P., Tarantini, S., Ahire, C., DelFavero, J., Yabluchanskiy, A., Csipo, T., Farkas, E., Wiley, G., Garman, L., Csiszar, A., & Ungvari, Z. (2020). Single-cell RNA sequencing identifies senescent cerebromicrovascular endothelial cells in the aged mouse brain. GeroScience, 42(2), 429–444.

Kokovay, E., Goderie, S., Wang, Y., Lotz, S., Lin, G., Sun, Y., Roysam, B., Shen, Q., & Temple, S. (2010). Adult SVZ lineage cells home to and leave the vascular niche via differential responses to SDF1/CXCR4 signaling. Cell Stem Cell, 7(2), 163–173.

Komatsu, M., Waguri, S., Chiba, T., Murata, S., Iwata, J. I., Tanida, I., Ueno, T., Koike, M., Uchiyama, Y., Kominami, E., & Tanaka, K. (2006). Loss of autophagy in the central nervous system causes neurodegeneration in mice. Nature, 441(7095), 880–884.

Körbelin, J., Dogbevia, G., Michelfelder, S., Ridder, D. A., Hunger, A., Wenzel, J., Seismann, H., Lampe, M., Bannach, J., Pasparakis, M., Kleinschmidt, J. A., Schwaninger, M., & Trepel, M. (2016). A brain microvasculature endothelial cell-specific viral vector with the potential to treat neurovascular and neurological diseases. EMBO Molecular Medicine, 8(6), 609.

Krzystyniak, A., Wesierska, M., Petrazzo, G., Gadecka, A., Dudkowska, M., Bielak-Zmijewska, A., Mosieniak, G., Figiel, I., Wlodarczyk, J., & Sikora, E. (2022). Combination of dasatinib and quercetin improves cognitive abilities in aged male Wistar rats, alleviates inflammation and changes hippocampal synaptic plasticity and histone H3 methylation profile. Aging, 14(2), 572–595.

Kumari, R., & Jat, P. (2021). Mechanisms of Cellular Senescence: Cell Cycle Arrest and Senescence Associated Secretory Phenotype. Frontiers in Cell and Developmental Biology, 9.

Kuhn, H. G., Eisch, A. J., Spalding, K., & Peterson, D. A. (2016). Detection and Phenotypic Characterization of Adult Neurogenesis. Cold Spring Harbor Perspectives in Biology, 8(3).

Kurz, D., Decary, S., Hong, Y., & Erusalimsky, J. (2000). Senescence-associated *β*-galactosidase reflects an increase in lysosomal mass during replicative ageing of human endothelial cells. Journal of cell science,113 (Pt 20):3613-22.

Lacar, B., Linker, S. B., Jaeger, B. N., Krishnaswami, S., Barron, J., Kelder, M., Parylak, S., Paquola, A., Venepally, P., Novotny, M., O'Connor, C., Fitzpatrick, C., Erwin, J., Hsu, J. Y., Husband, D., McConnell, M. J., Lasken, R., & Gage, F. H. (2016). Nuclear RNA-seq of single neurons reveals molecular signatures of activation. Nature Communications 2016 7:1, 7(1), 1–13.

Lalonde, R., & Strazielle, C. (2011). Brain regions and genes affecting limb-clasping responses. Brain Research Reviews, 67(1–2), 252–259.

Lazarov, O., & Hollands, C. (2016). Hippocampal neurogenesis: learning to remember. Progress in Neurobiology, 138–140, 1.

Lee, S. Y., Abel, E. D., & Long, F. (2018). Glucose metabolism induced by Bmp signaling is essential for murine skeletal development. Nature Communications 2018 9:1, 9(1), 1–11.

Leeman, D. S., Hebestreit, K., Ruetz, T., Webb, A. E., McKay, A., Pollina, E. A., Dulken, B. W., Zhao, X., Yeo, R. W., Ho, T. T., Mahmoudi, S., Devarajan, K., Passegué, E., Rando, T. A., Frydman, J., & Brunet, A. (2018). Lysosome activation clears aggregates and enhances quiescent neural stem cell activation during aging. Science (New York, N.Y.), 359(6381), 1277–1283.

Lehtinen, M. K., Bjornsson, C. S., Dymecki, S. M., Gilbertson, R. J., Holtzman, D. M., & Monuki, E. S. (2013). The choroid plexus and cerebrospinal fluid: emerging roles in development, disease, and therapy. The Journal of Neuroscience: The Official Journal of the Society for Neuroscience, 33(45), 17553–17559.

Liu, H. W., Chan, Y. C., Wei, C. C., Chen, Y. A., Wang, M. F., & Chang, S. J. (2017). An alternative model for studying age-associated metabolic complications: Senescence-accelerated mouse prone 8. Experimental Gerontology, 99, 61–68.

Llanos, S., Megias, D., Blanco-Aparicio, C., Hernández-Encinas, E., Rovira, M., Pietrocola, F., & Serrano, M. (2019). Lysosomal trapping of palbociclib and its functional implications. Oncogene 2019 38:20, 38(20), 3886–3902.

Llorens-Bobadilla, E., Zhao, S., Baser, A., Saiz-Castro, G., Zwadlo, K., & Martin-Villalba, A. (2015). Single-Cell Transcriptomics Reveals a Population of Dormant Neural Stem Cells that Become Activated upon Brain Injury. Cell Stem Cell, 17(3), 329–340.

López-Otín, C., Blasco, M. A., Partridge, L., Serrano, M., & Kroemer, G. (2013). The hallmarks of aging. Cell, 153(6), 1194.

López-Otín, C., Blasco, M. A., Partridge, L., Serrano, M., & Kroemer, G. (2023). Hallmarks of aging: An expanding universe. Cell, 186(2), 243–278.

Lozano-Torres, B., Galiana, I., Rovira, M., Garrido, E., Chaib, S., Bernardos, A., Muñoz-Espín, D., Serrano, M., Martínez-Máñez, R., & Sancenón, F. (2017). An OFF-ON Two-Photon Fluorescent Probe for Tracking Cell Senescence in Vivo. Journal of the American Chemical Society, 139(26), 8808–8811.

Lozano-Torres, B., García-Fernández, A., Domínguez, M., Sancenón, F., Blandez, J. F., & Martínez-Máñez, R. (2023). β-Galactosidase-Activatable Nile Blue-Based NIR Senoprobe for the Real-Time Detection of Cellular Senescence. Analytical Chemistry, 95(2).

Lueptow, L. M. (2017). Novel Object Recognition Test for the Investigation of Learning and Memory in Mice. Journal of Visualized Experiments: JoVE, 2017(126), 55718.

Lugert, S., Basak, O., Knuckles, P., Haussler, U., Fabel, K., Götz, M., Haas, C. A., Kempermann, G., Taylor, V., & Giachino, C. (2010). Quiescent and active hippocampal neural stem cells with distinct morphologies respond selectively to physiological and pathological stimuli and aging. Cell Stem Cell, 6(5), 445–456.

Luo, J., Daniels, S. B., Lennington, J. B., Notti, R. Q., & Conover, J. C. (2006). The aging neurogenic subventricular zone. Aging Cell, 5(2), 139–152.

Luo, J., Shook, B. A., Daniels, S. B., & Conover, J. C. (2008). Subventricular Zone-Mediated Ependyma Repair in the Adult Mammalian Brain. The Journal of Neuroscience, 28(14), 3804.

Malaquin, N., Tu, V., & Rodier, F. (2019). Assessing functional roles of the senescence-associated secretory phenotype (SASP). Methods in Molecular Biology, 1896, 45–55.

Mao, G., & Xu, X. (2020). Exosomes Derived From Senescent Cells Promote Cellular Senescence. Innovation in Aging, 4(Suppl 1), 132.

Maranzana, E., Barbero, G., Falasca, A. I., Lenaz, G., & Genova, M. L. (2013). Mitochondrial Respiratory Supercomplex Association Limits Production of Reactive Oxygen Species from Complex I. Antioxidants & Redox Signaling, 19(13), 1469.

Marqués-Torrejón, M. Á., Porlan, E., Banito, A., Gómez-Ibarlucea, E., Lopez-Contreras, A. J., Fernández-Ca-

petillo, Ó., Vidal, A., Gil, J., Torres, J., & Fariñas, I. (2013). Cyclin-dependent kinase inhibitor p21 controls adult neural stem cell expansion by regulating Sox2 gene expression. Cell Stem Cell, 12(1), 88–100.

Marqués-Torrejón, M. Á., Williams, C. A. C., Southgate, B., Alfazema, N., Clements, M. P., Garcia-Diaz, C., Blin, C., Arranz-Emparan, N., Fraser, J., Gammoh, N., Parrinello, S., & Pollard, S. M. (2021). LRIG1 is a gatekeeper to exit from quiescence in adult neural stem cells. Nature Communications 2021 12:1, 12(1), 1–15.

Martin, D., Xu, J., Porretta, C., & Nichols, C. D. (2017). Neurocytometry: Flow Cytometric Sorting of Specific Neuronal Populations from Human and Rodent Brain. ACS Chemical Neuroscience, 8(2), 356–367.

Martínez, P., & Blasco, M. A. (2017). Telomere-driven diseases and telomere-targeting therapies. The Journal of Cell Biology, 216(4), 875–887.

Martínez-Cué, C., & Rueda, N. (2020). Cellular Senescence in Neurodegenerative Diseases. 14, 16.

Maslov, A. Y., Barone, T. A., Plunkett, R. J., & Pruitt, S. C. (2004). Neural stem cell detection, characterization, and age-related changes in the subventricular zone of mice. The Journal of Neuroscience: The Official Journal of the Society for Neuroscience, 24(7), 1726–1733.

Matsushita, H., Chang, E., Glassford, A. J., Cooke, J. P., Chiu, C. P., & Tsao, P. S. (2001). eNOS activity is reduced in senescent human endothelial cells: Preservation by hTERT immortalization. Circulation Research, 89(9), 793–798.

Matsuura, K., Kabuto, H., Makino, H., & Ogawa, N. (1997). Pole test is a useful method for evaluating the mouse movement disorder caused by striatal dopamine depletion. Journal of Neuroscience Methods, 73(1), 45–48.

Meeker, H. C., Chadman, K. K., Heaney, A. T., & Carp, R. I. (2013). Assessment of social interaction and anxiety-like behavior in senescence-accelerated-prone and -resistant mice. Physiology & Behavior, 118, 97–102.

Menn, B., Garcia-Verdugo, J. M., Yaschine, C., Gonzalez-Perez, O., Rowitch, D., & Alvarez-Buylla, A. (2006). Origin of oligodendrocytes in the subventricular zone of the adult brain. The Journal of Neuroscience : The Official Journal of the Society for Neuroscience, 26(30), 7907–7918.

Mich, J. K., Signer, R. A. J., Nakada, D., Pineda, A., Burgess, R. J., Vue, T. Y., Johnson, J. E., & Morrison, S. J. (2014). Prospective identification of functionally distinct stem cells and neurosphere-initiating cells in adult mouse forebrain. ELife, 3(3).

Minami, T., Muramatsu, M., & Kume, T. (2019). Organ/Tissue-Specific Vascular Endothelial Cell Heterogeneity in Health and Disease. Biological and Pharmaceutical Bulletin, 42(10), 1609–1619.

Minamino, T., Miyauchi, H., Yoshida, T., Ishida, Y., Yoshida, H., & Komuro, I. (2002). Endothelial cell senescence in human atherosclerosis: role of telomere in endothelial dysfunction. Circulation, 105(13), 1541–1544.

Mirzadeh, Z., Merkle, F. T., Soriano-Navarro, M., Garcia-Verdugo, J. M., & Alvarez-Buylla, A. (2008). Neural stem cells confer unique pinwheel architecture to the ventricular surface in neurogenic regions of the adult brain. Cell Stem Cell, 3(3), 265–278.

Miyamoto, M. (1997). Characteristics of age-related behavioral changes in senescence-accelerated mouse SAMP8 and SAMP10. Experimental Gerontology, 32(1–2), 139–148.

Miyamoto, M., Kiyota, Y., Yamazaki, N., Nagaoka, A., Matsuo, T., Nagawa, Y., & Takeda, T. (1986). Age-related changes in learning and memory in the senescence-accelerated mouse (SAM). Physiology & Behavior, 38(3), 399–406.

Molofsky, A. V., Slutsky, S. G., Joseph, N. M., He, S., Pardal, R., Krishnamurthy, J., Sharpless, N. E., & Morrison, S. J. (2006). Increasing p16INK4a expression decreases forebrain progenitors and neurogenesis during

ageing. Nature, 443(7110), 448–452.

Montecino-Rodriguez, E., Berent-Maoz, B., & Dorshkind, K. (2013). Causes, consequences, and reversal of immune system aging. The Journal of Clinical Investigation, 123(3), 958.

Morante-Redolat, J. M., & Porlan, E. (2019). Neural Stem Cell Regulation by Adhesion Molecules Within the Subependymal Niche. Frontiers in Cell and Developmental Biology, 7(JUN).

Morley, J. E., Armbrecht, H. J., Farr, S. A., & Kumar, V. B. (2012). The senescence accelerated mouse (SAMP8) as a model for oxidative stress and Alzheimer's disease. 1822(5), 650–656.

Mosteiro, L., Pantoja, C., de Martino, A., & Serrano, M. (2018). Senescence promotes in vivo reprogramming through p16INK4a and IL-6. Aging Cell, 17(2).

Moya-Pérez, A., Perez-Villalba, A., Benítez-Páez, A., Campillo, I., & Sanz, Y. (2017). Bifidobacterium CECT 7765 modulates early stress-induced immune, neuroendocrine and behavioral alterations in mice. Brain, Behavior, and Immunity, 65, 43–56.

Mühleder, S., Fernández-Chacón, M., Garcia-Gonzalez, I., & Benedito, R. (2021). Endothelial sprouting, proliferation, or senescence: tipping the balance from physiology to pathology. Cellular and Molecular Life Sciences, 78(4), 1329.

Muñoz-Espín, D., & Serrano, M. (2014). Cellular senescence: from physiology to pathology. 15(7), 482–496.

Murayama, A., Matsuzaki, Y., Kawaguchi, A., Shimazaki, T., & Okano, H. (2002). Flow cytometric analysis of neural stem cells in the developing and adult mouse brain. Journal of Neuroscience Research, 69(6), 837–847.

Nelson, G., Wordsworth, J., Wang, C., Jurk, D., Lawless, C., Martin-Ruiz, C., & von Zglinicki, T. (2012). A senescent cell bystander effect: senescence-induced senescence. Aging Cell, 11(2), 345–349.

Nishijima, K., Shinkawa, T., Yamashita, Y., Sato, N. K., Nishida, H., Kato, K., … Miyano, S. (2010). Synthesis and Diuretic Activity of 2,3-Dihydro-4(1H)-quinolinone 4-Oxime-O-sulfonic Acid Derivatives. ChemInform, 29(37), 6.

Nishikawa, T., Takahashi, J. A., Fujibayashi, Y., Fujisawa, H., Zhu, B., Nishimura, Y., Ohnishi, K., Higuchi, K., Hashimoto, N., & Hosokawa, M. (1998). An early stage mechanism of the age-associated mitochondrial dysfunction in the brain of SAMP8 mice; an age-associated neurodegeneration animal model. Neuroscience Letters, 254(2), 69–72.

Obermeier, B., Daneman, R., & Ransohoff, R. M. (2013). Development, maintenance and disruption of the blood-brain barrier. Nature Medicine, 19(12), 1584–1596.

Obernier, K., & Alvarez-Buylla, A. (2019). Neural stem cells: Origin, heterogeneity and regulation in the adult mammalian brain. In Development (Cambridge) (Vol. 146, Issue 4). Company of Biologists Ltd.

Obernier, K., Cebrian-Silla, A., Thomson, M., Parraguez, J. I., Anderson, R., Guinto, C., Rodas Rodriguez, J., Garcia-Verdugo, J. M., & Alvarez-Buylla, A. (2018). Adult Neurogenesis Is Sustained by Symmetric Self-Renewal and Differentiation. Cell Stem Cell, 22(2), 221-234.e8.

Ocampo, A., Reddy, P., & Belmonte, J. C. I. (2016). Anti-Aging Strategies Based on Cellular Reprogramming. Trends in Molecular Medicine, 22(8), 725–738.

Ogawa, N., Hirose, Y., Ohara, S., Ono, T., & Watanabe, Y. (1985). A simple quantitative bradykinesia test in MPTP-treated mice. Research Communications in Chemical Pathology and Pharmacology, 50(3), 435–441.

Ogawa, S., Kubo, H., Murayama, Y., Kubota, T., Yubakami, M., Matsumoto, T., Yamamoto, Y., Morimura, R., Ikoma, H., Okamoto, K., Kamiya, M., Urano, Y., & Otsuji, E. (2021). Rapid fluorescence imaging of human hepatocellular carcinoma using the β-galactosidase-activatable fluorescence probe SPiDER-βGal. Scientific

Reports, 11(1), 17946.

Ogrodnik, M., Evans, S. A., Fielder, E., Victorelli, S., Kruger, P., Salmonowicz, H., Weigand, B. M., Patel, A. D., Pirtskhalava, T., Inman, C. L., Johnson, K. O., Dickinson, S. L., Rocha, A., Schafer, M. J., Zhu, Y., Allison, D. B., von Zglinicki, T., LeBrasseur, N. K., Tchkonia, T., … Jurk, D. (2021). Whole-body senescent cell clearance alleviates age-related brain inflammation and cognitive impairment in mice. Aging Cell, 20(2).

Ogrodnik, M., Miwa, S., Tchkonia, T., Tiniakos, D., Wilson, C. L., Lahat, A., Day, C. P., Burt, A., Palmer, A., Anstee, Q. M., Grellscheid, S. N., Hoeijmakers, J. H. J., Barnhoorn, S., Mann, D. A., Bird, T. G., Vermeij, W. P., Kirkland, J. L., Passos, J. F., Von Zglinicki, T., & Jurk, D. (2017). Cellular senescence drives age-dependent hepatic steatosis. Nature Communications 2017 8:1, 8(1), 1–12.

Ogrodnik, M., Zhu, Y., Langhi, L. G. P., Tchkonia, T., Krüger, P., Fielder, E., Victorelli, S., Ruswhandi, R. A., Giorgadze, N., Pirtskhalava, T., Podgorni, O., Enikolopov, G., Johnson, K. O., Xu, M., Inman, C., Palmer, A. K., Schafer, M., Weigl, M., Ikeno, Y., … Jurk, D. (2019). Obesity-Induced Cellular Senescence Drives Anxiety and Impairs Neurogenesis. Cell Metabolism, 29(5), 1233.

Oh, C., Koh, D., Jeon, H. Bin, & Kim, K. M. (2022). The Role of Extracellular Vesicles in Senescence. Molecules and Cells, 45(9), 603.

Ohori, M., Nakayama, Y., Ogasawara-Shimizu, M., Toyoshiba, H., Nakanishi, A., Aparicio, S., & Araki, S. (2021). Gene regulatory network analysis defines transcriptome landscape with alternative splicing of human umbilical vein endothelial cells during replicative senescence. BMC Genomics, 22(1), 1–14.

Ohtani, N. (2022). The roles and mechanisms of senescence-associated secretory phenotype (SASP): can it be controlled by senolysis? 42(1), 1–8.

Okatani, Y., Wakatsuki, A., & Reiter, R. J. (2002). Melatonin protects hepatic mitochondrial respiratory chain activity in senescence-accelerated mice. Journal of Pineal Research, 32(3), 143–148.

Olofsson, J. K., Ekström, I., Larsson, M., & Nordin, S. (2021). Olfaction and Aging: A Review of the Current State of Research and Future Directions. I-Perception, 12(3), 1–24.

Orasan, M. S., Roman, I. I., Coneac, A., Muresan, A., & Orasan, R. I. (2016). Hair loss and regeneration performed on animal models. Clujul Medical, 89(3), 327.

Ota, H., & Kodama, A. (2022). Dasatinib plus quercetin attenuates some frailty characteristics in SAMP10 mice. Scientific Reports, 12(1).

Ottone, C., Krusche, B., Whitby, A., Clements, M., Quadrato, G., Pitulescu, M. E., Adams, R. H., & Parrinello, S. (2014). Direct cell-cell contact with the vascular niche maintains quiescent neural stem cells. Nature Cell Biology, 16(11), 1045–1056.

Ottone, C., & Parrinello, S. (2015). Multifaceted control of adult SVZ neurogenesis by the vascular niche. Cell cycle, 14(14), 2222-5.

Ouellette, J., & Lacoste, B. (2021). Isolation and functional characterization of primary endothelial cells from mouse cerebral cortex. STAR Protocols, 2(4), 101019.

Ovadya, Y., Landsberger, T., Leins, H., Vadai, E., Gal, H., Biran, A., Yosef, R., Sagiv, A., Agrawal, A., Shapira, A., Windheim, J., Tsoory, M., Schirmbeck, R., Amit, I., Geiger, H., & Krizhanovsky, V. (2018). Impaired immune surveillance accelerates accumulation of senescent cells and aging. Nature Communications 2018 9, 1, 9(1), 1–15.

Pačesová, A., Holubová, M., Hrubá, L., Strnadová, V., Neprašová, B., Pelantová, H., … Maletínská, L. (2022). Age-related metabolic and neurodegenerative changes in SAMP8 mice. Aging, 14(18), 7300–7327.

Palmer, T. D., Willhoite, A. R., & Gage, F. H. (2000). Adult Neurogenesis in the Mammalian Brain. J Comp Neurol, 425(4), 479–494.

Pastrana, E., Cheng, L. C., & Doetsch, F. (2009). Simultaneous prospective purification of adult subventricular zone neural stem cells and their progeny. Proceedings of the National Academy of Sciences of the United States of America, 106(15), 6387–6392.

Pastrana, E., Silva-Vargas, V., & Doetsch, F. (2011). Eyes wide open: a critical review of sphere-formation as an assay for stem cells. Cell Stem Cell, 8(5), 486–498.

Patel, R. C., & Larson, J. (2009). Impaired olfactory discrimination learning and decreased olfactory sensitivity in aged C57Bl/6 mice. Neurobiology of Aging, 30(5), 829–837.

Pedro, P. F., Tsakmaki, A., & Bewick, G. A. (2020). The Glucose Tolerance Test in Mice. Methods in Molecular Biology (Clifton, N.J.), 2128, 207–216.

Pelegrí, C., Canudas, A. M., del Valle, J., Casadesus, G., Smith, M. A., Camins, A., … Vilaplana, J. (2007). Increased permeability of blood–brain barrier on the hippocampus of a murine model of senescence. Mechanisms of Ageing and Development, 128(9), 522–528.

Perez-Villalba, A., Palop, M., Perez-Sanchez, F., & Fariñas, I. (2015). Assessment of Olfactory Behavior in Mice: Odorant Detection and Habituation-Dishabituation Tests. BIO-PROTOCOL, 5(13).

Perez-Villalba, A., Sirerol-Piquer, M. S., Belenguer, G., Soriano-Cantón, R., Muñoz-Manchado, A. B., Villadiego, J., … Fariñas, I. (2018). Synaptic Regulator α-Synuclein in Dopaminergic Fibers Is Essentially Required for the Maintenance of Subependymal Neural Stem Cells. Journal of Neuroscience, 38(4), 814–825.

Piechota, M., Sunderland, P., Wysocka, A., Nalberczak, M., Sliwinska, M. A., Radwanska, K., & Sikora, E. (2016). Is senescence-associated β-galactosidase a marker of neuronal senescence? Oncotarget, 7(49), 81099.

Piedra, J., Ontiveros, M., Miravet, S., Penalva, C., Monfar, M., & Chillon, M. (2015). Development of a rapid, robust, and universal picogreen-based method to titer adeno-associated vectors. Human Gene Therapy Methods, 26(1), 35–42.

Pilz, G. A., Bottes, S., Betizeau, M., Jörg, D. J., Carta, S., Simons, B. D., … Jessberger, S. (2018). Live imaging of neurogenesis in the adult mouse hippocampus. Science (New York, N.Y.), 359(6376), 658.

Pole, A., Dimri, M., Dimri, G. P., Pole, A., Dimri, M., & Dimri, G. P. (2016). Oxidative stress, cellular senescence and ageing. AIMS Molecular Science 2016 3:300, 3(3), 300–324.

Pombero, A., Garcia-Lopez, R., Estirado, A., & Martinez, S. (2018). Vascular pattern of the dentate gyrus is regulated by neural progenitors. Brain Structure and Function, 223(4), 1971–1987.

Ponti, G., Obernier, K., Guinto, C., Jose, L., Bonfanti, L., & Alvarez-Buylla, A. (2013). Cell cycle and lineage progression of neural progenitors in the ventricular-subventricular zones of adult mice. Proceedings of the National Academy of Sciences of the United States of America, 110(11).

Porlan, E., Martí-Prado, B., Morante-Redolat, J. M., Consiglio, A., Delgado, A. C., Kypta, R., … Fariñas, I. (2014). MT5-MMP regulates adult neural stem cell functional quiescence through the cleavage of N-cadherin. Nature Cell Biology, 16(7), 629–638.

Porlan, E., Perez-Villalba, A., Delgado, A. C., & Ferrón, S. R. (2013). Paracrine regulation of neural stem cells in the subependymal zone. Archives of Biochemistry and Biophysics, 534(1–2), 11–19.

Radulescu, C. I., Cerar, V., Haslehurst, P., Kopanitsa, M., & Barnes, S. J. (2021). The aging mouse brain: cognition, connectivity and calcium. Cell Calcium, 94, 102358.

Rafii, S., Butler, J. M., & Ding, B. Sen. (2016). Angiocrine functions of organ-specific endothelial cells. Nature 2016 529:7586, 529(7586), 316–325.

Ramírez-Castillejo, C., Sánchez-Sánchez, F., Andreu-Agulló, C., Ferrón, S. R., Aroca-Aguilar, J. D., Sánchez,

P., … Fariñas, I. (2006). Pigment epithelium-derived factor is a niche signal for neural stem cell renewal. Nature Neuroscience, 9(3), 331–339.

Rayess, H., Wang, M. B., & Srivatsan, E. S. (2012). Cellular senescence and tumor suppressor gene p16. International Journal of Cancer. Journal International Du Cancer, 130(8), 1715.

Rea, I. M., Gibson, D. S., McGilligan, V., McNerlan, S. E., Denis Alexander, H., & Ross, O. A. (2018). Age and Age-Related Diseases: Role of Inflammation Triggers and Cytokines. Frontiers in Immunology, 9(APR).

Rebo, J., Mehdipour, M., Gathwala, R., Causey, K., Liu, Y., Conboy, M. J., & Conboy, I. M. (2016). A single heterochronic blood exchange reveals rapid inhibition of multiple tissues by old blood. Nature Communications 2016 7:1, 7(1), 1–11.

Recasens, A., Dehay, B., Bové, J., Carballo-Carbajal, I., Dovero, S., Pérez-Villalba, A., … Vila, M. (2014). Lewy body extracts from Parkinson disease brains trigger α-synuclein pathology and neurodegeneration in mice and monkeys. Annals of Neurology, 75(3), 351–362.

Redmann, M., Benavides, G. A., Berryhill, T. F., Wani, W. Y., Ouyang, X., Johnson, M. S., … Zhang, J. (2017). Inhibition of autophagy with bafilomycin and chloroquine decreases mitochondrial quality and bioenergetic function in primary neurons. Redox Biology, 11, 73.

Regina, C., Panatta, E., Candi, E., Melino, G., Amelio, I., Balistreri, C. R., … Ruvolo, G. (2016). Vascular ageing and endothelial cell senescence: Molecular mechanisms of physiology and diseases. Mechanisms of Ageing and Development, 159, 14–21.

Revest, J. M., Dupret, D., Koehl, M., Funk-Reiter, C., Grosjean, N., Piazza, P. V., & Abrous, D. N. (2009). Adult hippocampal neurogenesis is involved in anxiety-related behaviors. Molecular Psychiatry, 14(10), 959–967.

Reynolds, B. A., & Rietze, R. L. (2005). Neural stem cells and neurospheres--re-evaluating the relationship. Nature Methods, 2(5), 333–336.

Reynolds, B. A., & Weiss, S. (1992). Generation of neurons and astrocytes from isolated cells of the adult mammalian central nervous system. Science (New York, N.Y.), 255(5052), 1707–1710.

Rhea, E. M., & Banks, W. A. (2017). The SAMP8 mouse for investigating memory and the role of insulin in the brain. Experimental Gerontology, 94, 64.

Riquelme, J. A., Takov, K., Santiago-Fernández, C., Rossello, X., Lavandero, S., Yellon, D. M., & Davidson, S. M. (2020). Increased production of functional small extracellular vesicles in senescent endothelial cells. Journal of Cellular and Molecular Medicine, 24(8), 4871.

Robbins, P. D., Jurk, D., Khosla, S., Kirkland, J. L., Lebrasseur, N. K., Miller, J. D., … Niedernhofer, L. J. (2021). Senolytic Drugs: Reducing Senescent Cell Viability to Extend Health Span. Annual Review of Pharmacology and Toxicology, 61, 779.

Robertson, R. T., Levine, S. T., Haynes, S. M., Gutierrez, P., Baratta, J. L., Tan, Z., … Longmuir, K. J. (2015). Use of labeled tomato lectin for imaging vasculature structures. Histochemistry and Cell Biology, 143(2), 225–234.

Rodriguez-Menocal, L., Pham, S. M., Mateu, D., St-Pierre, M., Wei, Y., Pestana, I., … Vazquez-Padron, R. I. (2009). Aging increases p16 INK4a expression in vascular smooth-muscle cells. Bioscience Reports, 30(1), 11–18.

Rojas-Vázquez, S., Blasco-Chamarro, L., López-Fabuel, I., Martínez-Máñez, R., & Fariñas, I. (2021). Vascular Senescence: A Potential Bridge Between Physiological Aging and Neurogenic Decline. Frontiers in Neuroscience, 15.

Rojas-Vázquez, Sara; Lozano-Torres, Beatriz; García-Fernández, Alba; Galiana, Irene; Perez-Villalba, Ana;

Martí-Rodrigo, Pablo; Palop, M. José; Orzáez, Mar; Sancenón, Félix; Blandez, Juan F.; Fariñas, Isabel and Martínez-Máñez, R. (n.d.). A renal clearable fluorogenic probe for the in vivo detection of cellular senescence. Nature Aging. Submitted.

Roos, C. M., Zhang, B., Palmer, A. K., Ogrodnik, M. B., Pirtskhalava, T., Thalji, N. M., … Miller, J. D. (2016). Chronic senolytic treatment alleviates established vasomotor dysfunction in aged or atherosclerotic mice. Aging Cell, 15(5), 973–977.

Rubio, F. J., Li, X., Liu, Q. R., Cimbro, R., & Hope, B. T. (2016). Fluorescence Activated Cell Sorting (FACS) and Gene Expression Analysis of Fos-expressing Neurons from Fresh and Frozen Rat Brain Tissue. Journal of Visualized Experiments: JoVE, 2016(114), 54358.

Ruddy, R. M., & Morshead, C. M. (2018). Home sweet home: the neural stem cell niche throughout development and after injury. Cell and Tissue Research. Springer Verlag, 371(1), 125-141.

Sabbatinelli, J., Prattichizzo, F., Olivieri, F., Procopio, A. D., Rippo, M. R., & Giuliani, A. (2019). Where Metabolism Meets Senescence: Focus on Endothelial Cells. Frontiers in Physiology, 10, 1523.

Salazar, G. (2018). NADPH Oxidases and Mitochondria in Vascular Senescence. International Journal of Molecular Sciences, 19(5).

Schafer, M. J., Zhang, X., Kumar, A., Atkinson, E. J., Zhu, Y., Jachim, S., … LeBrasseur, N. K. (2020). The senescence-associated secretome as an indicator of age and medical risk. JCI Insight, 5(12).

Schindelin, J., Arganda-Carreras, I., Frise, E., Kaynig, V., Longair, M., Pietzsch, T., … Cardona, A. (2012). Fiji: an open-source platform for biological-image analysis. Nature Methods 2012 9:7, 9(7), 676–682.

Schmitt, C. A., Wang, B., & Demaria, M. (2022). Senescence and cancer — role and therapeutic opportunities. Nature Reviews Clinical Oncology 2022 19:10, 19(10), 619–636.

Schmidt, U., Weigert, M., Broaddus, C., & Myers, G. (2018). Cell Detection with Star-convex Polygons. Lecture Notes in Computer Science (Including Subseries Lecture Notes in Artificial Intelligence and Lecture Notes in Bioinformatics), 11071 LNCS, 265–273.

Schultz, M. B., & Sinclair, D. A. (2016). When stem cells grow old: phenotypes and mechanisms of stem cell aging. Development (Cambridge, England), 143(1), 3–14.

Schütt, F., Aretz, S., Auffarth, G. U., & Kopitz, J. (2012). Moderately Reduced ATP Levels Promote Oxidative Stress and Debilitate Autophagic and Phagocytic Capacities in Human RPE Cells. Investigative Ophthalmology & Visual Science, 53(9), 5354–5361.

Segarra, M., Aburto, M. R., & Acker-Palmer, A. (2021). Blood-Brain Barrier Dynamics to Maintain Brain Homeostasis. Trends in Neurosciences, 44(5), 393–405.

Shen, J., Wang, D., Wang, X., Gupta, S., Ayloo, B., Wu, S., … Ge, S. (2019). Neurovascular Coupling in the Dentate Gyrus Regulates Adult Hippocampal Neurogenesis. Neuron, 103(5), 878-890.e3.

Shen, Q., Wang, Y., Kokovay, E., Lin, G., Chuang, S. M., Goderie, S. K., … Temple, S. (2008). Adult SVZ stem cells lie in a vascular niche: a quantitative analysis of niche cell-cell interactions. Cell Stem Cell, 3(3), 289–300.

Shi, Z., Geng, Y., Liu, J., Zhang, H., Zhou, L., Lin, Q., … Sun, Y. E. (2018). Single-cell transcriptomics reveals gene signatures and alterations associated with aging in distinct neural stem/progenitor cell subpopulations. Protein & Cell, 9(4), 351–364.

Shin, J., Berg, D. A., Zhu, Y., Shin, J. Y., Song, J., Bonaguidi, M. A., … Song, H. (2015). Single-Cell RNA-Seq with Waterfall Reveals Molecular Cascades underlying Adult Neurogenesis. Cell Stem Cell, 17(3), 360–372.

Shoji, H., Takao, K., Hattori, S., & Miyakawa, T. (2016). Age-related changes in behavior in C57BL/6J mice

from young adulthood to middle age. Molecular Brain, 9(1).

Shook, B. A., Manz, D. H., Peters, J. J., Kang, S., & Conover, J. C. (2012). Spatiotemporal changes to the subventricular zone stem cell pool through aging. Journal of Neuroscience, 32(20), 6947–6956.

Short, S., Fielder, E., Miwa, S., & von Zglinicki, T. (2019). Senolytics and senostatics as adjuvant tumour therapy. EBioMedicine, 41, 683–692.

Sikora, E., Bielak-Zmijewska, A., Dudkowska, M., Krzystyniak, A., Mosieniak, G., Wesierska, M., & Wlodarczyk, J. (2021). Cellular Senescence in Brain Aging. Frontiers in Aging Neuroscience, 13.

Silva-Vargas, V., Crouch, E. E., & Doetsch, F. (2013). Adult neural stem cells and their niche: A dynamic duo during homeostasis, regeneration, and aging. Current Opinion in Neurobiology, 23(6), 935–942.

Silva-Vargas, V., Maldonado-Soto, A. R., Mizrak, D., Codega, P., & Doetsch, F. (2016). Age-Dependent Niche Signals from the Choroid Plexus Regulate Adult Neural Stem Cells. Cell Stem Cell, 19(5), 643–652.

Simons, B. D., & Clevers, H. (2011). Strategies for homeostatic stem cell self-renewal in adult tissues. Cell, 145(6), 851–862.

Simpson, D. J., Olova, N. N., & Chandra, T. (2021). Cellular reprogramming and epigenetic rejuvenation. Clinical Epigenetics 2021 13:1, 13(1), 1–10.

Singh, P. B., & Newman, A. G. (2018). Age reprogramming and epigenetic rejuvenation. Epigenetics & Chromatin, 11(1).

Sirerol-Piquer, M. S., Belenguer, G., Morante-Redolat, J. M., Duart-Abadia, P., Perez-Villalba, A., & Fariñas, I. (2019). Physiological Interactions between Microglia and Neural Stem Cells in the Adult Subependymal Niche. Neuroscience, 405, 77–91.

Smith, L. K., He, Y., Park, J. S., Bieri, G., Snethlage, C. E., Lin, K., … Villeda, S. A. (2015). β2-microglobulin is a systemic pro-aging factor that impairs cognitive function and neurogenesis. Nature Medicine, 21(8), 932–937.

Smith, L. K., White, C. W., & Villeda, S. A. (2018). The systemic environment: at the interface of aging and adult neurogenesis. Cell and Tissue Research, 371(1), 105–113.

Sohn, J., Orosco, L., Guo, F., Chung, S. H., Bannerman, P., Ko, E. M., … Pleasure, D. (2015). The Subventricular Zone Continues to Generate Corpus Callosum and Rostral Migratory Stream Astroglia in Normal Adult Mice. Journal of Neuroscience, 35(9), 3756–3763.

Soriano-Cantón, R., Perez-Villalba, A., Morante-Redolat, J. M., Marqués-Torrejón, M. Á., Pallás, M., Pérez-Sánchez, F., & Fariñas, I. (2015). Regulation of the p19(Arf)/p53 pathway by histone acetylation underlies neural stem cell behavior in senescence-prone SAMP8 mice. Aging Cell, 14(3), 453–462.

Sousa-Victor, P., Gutarra, S., García-Prat, L., Rodriguez-Ubreva, J., Ortet, L., Ruiz-Bonilla, V., … Muñoz-Cánoves, P. (2014). Geriatric muscle stem cells switch reversible quiescence into senescence, 506(7488), 316–321.

Srinivas, U. S., Tan, B. W. Q., Vellayappan, B. A., & Jeyasekharan, A. D. (2019). ROS and the DNA damage response in cancer. Redox Biology, 25.

Stabenow, L. K., Zibrova, D., Ender, C., Helbing, D. L., Spengler, K., Marx, C., … Heller, R. (2022). Oxidative Glucose Metabolism Promotes Senescence in Vascular Endothelial Cells. Cells, 11(14), 1–18.

Stevic, R., Zivkovic, T. B., Erceg, P., Milosevic, D., Despotovic, N., & Davidovic, M. (2007). Oral glucose tolerance test in the assessment of glucose-tolerance in the elderly people. Age and Ageing, 36(4), 459–462.

Stoll, E. A., Cheung, W., Mikheev, A. M., Sweet, I. R., Bielas, J. H., Zhang, J., … Horner, P. J. (2011). Aging neu-

ral progenitor cells have decreased mitochondrial content and lower oxidative metabolism. The Journal of Biological Chemistry, 286(44), 38592–38601.

Sun, J., Zhou, W., Ma, D., & Yang, Y. (2010). Endothelial cells promote neural stem cell proliferation and differentiation associated with VEGF activated Notch and Pten signaling. Developmental Dynamics: An Official Publication of the American Association of Anatomists, 239(9), 2345–2353.

Sureda, F. X., Gutierrez-Cuesta, J., Romeu, M., Mulero, M., Canudas, A. M., Camins, A., … Pallàs, M. (2006). Changes in oxidative stress parameters and neurodegeneration markers in the brain of the senescence-accelerated mice SAMP-8. Experimental Gerontology, 41(4), 360–367.

Takahashi, K., & Yamanaka, S. (2006). Induction of pluripotent stem cells from mouse embryonic and adult fibroblast cultures by defined factors. Cell, 126(4), 663–676.

Takasugi, M. (2018). Emerging roles of extracellular vesicles in cellular senescence and aging. Aging Cell, 17(2), e12734.

Takeda, T. (1999). Senescence-accelerated mouse (SAM): A biogerontological resource in aging research. Neurobiology of Aging, 20(2), 105–110.

Takeda, T. (2009). Senescence-accelerated mouse (SAM) with special references to neurodegeneration models, SAMP8 and SAMP10 mice. Neurochemical Research, 34(4), 639–659.

Takeda, T., Hosokawa, M., Takeshita, S., Irino, M., Higuchi, K., Matsushita, T., … Yamamuro, T. (1981). A new murine model of accelerated senescence. Mechanisms of Ageing and Development, 17(2), 183–194.

Tamanini, S., Comi, G. P., & Corti, S. (2018). In Vivo Transient and Partial Cell Reprogramming to Pluripotency as a Therapeutic Tool for Neurodegenerative Diseases. Molecular Neurobiology, 55(8), 6850–6862.

Tavazoie, M., Van der Veken, L., Silva-Vargas, V., Louissaint, M., Colonna, L., Zaidi, B., … Doetsch, F. (2008). A specialized vascular niche for adult neural stem cells. Cell Stem Cell, 3(3), 279–288.

Tchkonia, T., Zhu, Y., Van Deursen, J., Campisi, J., & Kirkland, J. L. (2013). Cellular senescence and the senescent secretory phenotype: therapeutic opportunities. The Journal of Clinical Investigation, 123(3), 966.

Tominaga, K., & Suzuki, H. I. (2019). TGF-β Signaling in Cellular Senescence and Aging-Related Pathology. International Journal of Molecular Sciences, 20(20).

Treiber, N., Maity, P., Singh, K., Ferchiu, F., Wlaschek, M., & Scharffetter-Kochanek, K. (2012). The role of manganese superoxide dismutase in skin aging. Dermato-Endocrinology, 4(3), 232.

Tucker, L. B., & McCabe, J. T. (2021). Measuring Anxiety-Like Behaviors in Rodent Models of Traumatic Brain Injury. Frontiers in Behavioral Neuroscience, 15, 264.

Urbán, N., Blomfield, I. M., & Guillemot, F. (2019). Quiescence of Adult Mammalian Neural Stem Cells: A Highly Regulated Rest. Neuron, 104(5), 834–848.

Van Der Loo, B., Labugger, R., Skepper, J. N., Bachschmid, M., Kilo, J., Powell, J. M., … Lüscher, T. F. (2000). Enhanced peroxynitrite formation is associated with vascular aging. The Journal of Experimental Medicine, 192(12), 1731–1743.

Van Deursen, J. M. (2014). The role of senescent cells in ageing. Nature, 509(7501), 439–446.

Vasilopoulou, F., Companys-Alemany, J., Canudas, A.-M., Palomera-Ávalos, V., Ortuño-Sahagún, D., Pallàs, M., & Griñán-Ferré, C. (2021). Anxiety, Impaired Social and Aggressive Behaviour Correlates With Cognitive Decline Accompanied by Molecular Alterations in Older SAMP8 Males.

Vicidomini, C., Guo, N., & Sahay, A. (2020). Communication, Cross Talk, and Signal Integration in the Adult Hippocampal Neurogenic Niche. Neuron, 105(2), 220–235.

Villeda, S. A., Luo, J., Mosher, K. I., Zou, B., Britschgi, M., Bieri, G., … Wyss-Coray, T. (2011). The ageing systemic milieu negatively regulates neurogenesis and cognitive function. Nature, 477(7362), 90–96.

Wang, C., Kang, Y., Liu, P., Liu, W., Chen, W., Hayashi, T., … Ikejima, T. (2023). Combined use of dasatinib and quercetin alleviates overtraining-induced deficits in learning and memory through eliminating senescent cells and reducing apoptotic cells in rat hippocampus. Behavioural Brain Research, 440, 114260.

Wang, F., Chen, H., Sun, X. J., & Ke, Z. J. (2014). Improvement of cognitive deficits in SAMP8 mice by 3-n-butylphthalide. Neurological Research, 36(3), 224–233.

Wang, K., Liu, H., Hu, Q., Wang, L., Liu, J., Zheng, Z., … Liu, G. H. (2022). Epigenetic regulation of aging: implications for interventions of aging and diseases. Signal Transduction and Targeted Therapy 2022 7:1, 7(1), 1–22.

Winkelman, M. A., Koppes, A. N., Koppes, R. A., & Dai, G. (2021). Bioengineering the neurovascular niche to study the interaction of neural stem cells and endothelial cells. APL Bioengineering, 5(1).

Wojtowicz, J. M., & Kee, N. (2006). BrdU assay for neurogenesis in rodents. Nature Protocols, 1(3), 1399–1405.

Wu, Y., Shen, S., Shi, Y., Tian, N., Zhou, Y., & Zhang, X. (2022). Senolytics: Eliminating Senescent Cells and Alleviating Intervertebral Disc Degeneration. Frontiers in Bioengineering and Biotechnology, 10.

Wuputra, K., Ku, C. C., Wu, D. C., Lin, Y. C., Saito, S., & Yokoyama, K. K. (2020). Prevention of tumor risk associated with the reprogramming of human pluripotent stem cells. Journal of Experimental & Clinical Cancer Research 2020 39:1, 39(1), 1–24.

Xu, M., Pirtskhalava, T., Farr, J. N., Weigand, B. M., Palmer, A. K., Weivoda, M. M., … Kirkland, J. L. (2018). Senolytics Improve Physical Function and Increase Lifespan in Old Age. Nature Medicine, 24(8), 1246.

Yagi, H., Katoh, S., Akiguchi, I., & Takeda, T. (1988). Age-related deterioration of ability of acquisition in memory and learning in senescence accelerated mouse: SAM-P/8 as an animal model of disturbances in recent memory. Brain Research, 474(1), 86–93.

Yanai, S., & Endo, S. (2016). Early onset of behavioral alterations in senescence-accelerated mouse prone 8 (SAMP8). Behavioural Brain Research, 308, 187–195.

Yanai, S., & Endo, S. (2021). Functional Aging in Male C57BL/6J Mice Across the Life-Span: A Systematic Behavioral Analysis of Motor, Emotional, and Memory Function to Define an Aging Phenotype. Frontiers in Aging Neuroscience, 13, 457.

Yang, J., Liu, M., Hong, D., Zeng, M., & Zhang, X. (2021). The Paradoxical Role of Cellular Senescence in Cancer. Frontiers in Cell and Developmental Biology, 9, 722205.

Yang, N. C., & Hu, M. L. (2005). The limitations and validities of senescence associated-β-galactosidase activity as an aging marker for human foreskin fibroblast Hs68 cells. Experimental Gerontology, 40(10), 813–819.

Yokoyama, M., Okada, S., Nakagomi, A., Moriya, J., Shimizu, I., Nojima, A., … Minamino, T. (2014). Inhibition of endothelial p53 improves metabolic abnormalities related to dietary obesity. Cell Reports, 7(5), 1691–1703.

Yosef, R., Pilpel, N., Tokarsky-Amiel, R., Biran, A., Ovadya, Y., Cohen, S., … Krizhanovsky, V. (2016). Directed elimination of senescent cells by inhibition of BCL-W and BCL-XL. Nature Communications, 7.

Zhan, H., Suzuki, T., Aizawa, K., Miyagawa, K., & Nagai, R. (2010). Ataxia telangiectasia mutated (ATM)-mediated DNA damage response in oxidative stress-induced vascular endothelial cell senescence. The Journal of Biological Chemistry, 285(38), 29662–29670.

Zhang, L., Pitcher, L. E., Prahalad, V., Niedernhofer, L. J., & Robbins, P. D. (2022). Targeting cellular senescence with senotherapeutics: senolytics and senomorphics. The FEBS Journal.

Zhang, L., Liu, M., Li, Q., Shen, B., Hu, C., Fu, R., … Wang, Y. (2019). Identification of differential gene expression in endothelial cells from young and aged mice using RNA-Seq technique. American Journal of Translational Research, 11(10), 6553–6560.

Zhang, P., Kishimoto, Y., Grammatikakis, I., Gottimukkala, K., Cutler, R. G., Zhang, S., … Mattson, M. P. (2019). Senolytic therapy alleviates Aβ-associated oligodendrocyte progenitor cell senescence and cognitive deficits in an Alzheimer's disease model. Nature Neuroscience, 22(5), 719–728.

Zhang, Y., Unnikrishnan, A., Deepa, S. S., Liu, Y., Li, Y., Ikeno, Y., … Richardson, A. (2017). A new role for oxidative stress in aging: The accelerated aging phenotype in Sod1−/− mice is correlated to increased cellular senescence. Redox Biology, 11, 30.

Zheng, J. C., & Chen, S. (2022). Translational Neurodegeneration in the era of fast growing international brain research. Translational Neurodegeneration, 11(1), 1–2.

Zhu, C., Mahesula, S., Temple, S., & Kokovay, E. (2019). Heterogeneous Expression of SDF1 Retains Actively Proliferating Neural Progenitors in the Capillary Compartment of the Niche. Stem Cell Reports, 12(1), 6–13.

Zhu, X. Y., & Lerman, L. O. (2022). Senomorphic, senolytic, and rejuvenation therapies. Regenerative Nephrology, 405–417.

Zhu, Y., Tchkonia, T., Fuhrmann-Stroissnigg, H., Dai, H. M., Ling, Y. Y., Stout, M. B., … Kirkland, J. L. (2016). Identification of a novel senolytic agent, navitoclax, targeting the Bcl-2 family of anti-apoptotic factors. Aging Cell, 15(3), 428–435.

Zhu, Y., Tchkonia, T., Pirtskhalava, T., Gower, A. C., Ding, H., Giorgadze, N., … Kirkland, J. L. (2015). The Achilles' heel of senescent cells: from transcriptome to senolytic drugs. Aging Cell, 14(4), 644.

Ziebell, F., Dehler, S., Martin-Villalba, A., & Marciniak-Czochra, A. (2018). Revealing age-related changes of adult hippocampal neurogenesis using mathematical models. Development (Cambridge), 145(1).

Zolotukhin, S., Byrne, B. J., Mason, E., Zolotukhin, I., Potter, M., Chesnut, K., … Muzyczka, N. (1999). Recombinant adeno-associated virus purification using novel methods improves infectious titer and yield. Gene Therapy, 6(6), 973–985.

Annex I

Annex I. Antibodies

Table 1: List of primary antibodies.

Primary antibodies	Host	Dilution	Provider	Cat. no.	Application
BrdU	rat	1:800	Abcam	Ab6326	IHC
GFP	chicken	1:200	Aveslab	GFP-1020	FC
Ki67	rabbit	1:300	Abcam	A15580	IHC/ICC
Lamin B1	rabbit	1:100	Abcam	Ab16048	ICC/FC
p16	rabbit	1:100	Abcam	Ab211542	FC
p21	mouse	1:100	Abcam	Ab109520	ICC
TH	rabbit	1:800	Novus Bio.	NB300-120	IHC
γH2Ax	mouse	1:100	Millipore	05-636-I	ICC/FC

IHC: immunohistochemistry

ICC: immunocytochemistry

FC: flow cytometry

Table 2: List of secondary antibodies.

Secondary antibodies	Dilution	Provider	Cat. no.	Application
Alexa Fluor™ 488 Donkey anti-rabbit	1:500/1:400	Invitrogen	A21206	ICC/FC
Alexa Fluor™ 488 Donkey anti-rabbit	1:600	JacksonIR	711-547-003	IHC
Alexa Fluor™ 488 Donkey anti-mouse	1:400	Invitrogen	A21202	FC
Alexa Fluor™ 488 Donkey anti-chicken	1:600	JacksonIR	703-606-155	IHC
Alexa Fluor™ 647 Donkey anti-rabbit	1:400	Invitrogen	A31573	FC
Alexa Fluor™ 555 Donkey anti-mouse	1:500/1:400	Invitrogen	A31570	ICC/FC
Cy3 Donkey anti-rat	1:600	JacksonIR	712-165-153	IHC

JakcsonIR: JacksonImmunoResearch

Table 3: List of flow cytometry antibodies.

Flow cytometry antibodies	Dilution	Clone	Provider	Cat. no.
DAPI*	0.1 µg/ml		Sigma	D9542
CD31 BV421	1:100	Rat 390	BD-Biosciences	563356
CD31 BV395	1:100	Rat 390	BD-Biosciences	740239
CD45 BV421	1:100	Rat 30-F11	BD-Biosciences	563890
CD45 BV395	1:100	Rat 30-F11	BD-Biosciences	565967
TER-119 BV395	1:200	Rat Ter-119	BD-Biosciences	566206
O4 AF405	1:50	Mouse O4	R&D	FAB1326V
CD24 PerCP-Cy5.5	1:300	Rat M1/69	BD-Biosciences	562360
CD9 APC-VIO770	1:20	Rat MZ3	Miltenyi	130-102-384
GLAST-APC	1:50	Mouse ACSA1	Miltenyi	130-095-814
GLAST-PE	1:50	Mouse ACSA1	Miltenyi	130-118-344
EGF-A488	1:300		Invitrogen	E13345

Annex II

Annex II. Culture media and buffers

Table 1: Washing medium.

Reagents	Working concentration	Stock concentration	Provider	Cat. no.
DMEM F12 (+ L-Glutamine)	1X	1X	Gibco	11320-074
L-Glutamine	2 mM	200mM	Panreac	141341
Sodium bicarbonate	0.1%	7,5%	Biowest	L0680-500
HEPES	5 mM	1 M	Biowest	L180-100
Antibiotic/antimycotic	1X	100X	Gibco	15240-062
BSA	0.4 mg/ml	Powder	Sigma	B4287

Table 2: Neurosphere control medium.

Reagents	Working concentration	Stock concentration	Provider	Cat. no.
DMEM F12 (+ L-Glutamine)	1X	1X	Gibco	11320-074
L-Glutamine	2 mM	200mM	Panreac	141341
Sodium bicarbonate	0.1%	7,5%	Biowest	L0680-500
HEPES	5 mM	1 M	Biowest	L180-100
Antibiotic/antimycotic	1X	100X	Gibco	15240-062
Hormone mix*	1X	10X	Homemade*	
Heparin sodium salt	0.7 U/ml	350 U/ml	Sigma	H3149

**Hormone mix recipe*:

Reagents	Working concentration	Stock concentration	Provider	Cat. no.
DMEM F12 (w/o L-Glutamine)	1X	1X	Biowest	M500N9
Sodium bicarbonate	0.1%	7,5%	Biowest	L0680-500
HEPES	5 mM	1 M	Biowest	L180-100
Apo-transferrin	1 mg/ml	Powder	Sigma	T2252
Bovine Insulin	0.05 mg/ml	8.3 mg/ml	Sigma	I6634
Putrescine	160 µg/ml	96.5 mg/ml	Sigma	P7505
Progesterone	0.2 nM	2 µM	Sigma	P6149
Sodium selenite	0.3 µM	3 mM	Sigma	*S9133*
BSA	0.5 mg/ml	75 mg/ml	Sigma	B4287

Table 3: Neurosphere complete medium.

Reagents	Working concentration	Stock concentration	Provider	Cat. no.
Neurosphere control medium	1X	1X		
EGF	20 ng/ml	4 µg/ml	Gibco	53003-018
bFGF	10 ng/ml	25 µg/ml	Sigma	F0291

Table 4: HUVECs medium.

Reagents	Working concentration	Stock volume (kit)	Provider	Cat. no.
EndoGRO-LS basal medium	1X	475 ml	Sigma	SCME001
EndoGRO-LS supplement	0.2%	1 ml	Sigma	SCME001
rhEGF	5 ng/ml	0.5 ml	Sigma	SCME001
Ascorbic acid	50 µg/mL	0.5 ml	Sigma	SCME001
Heparin sulfate	0.75 U/ml	0.5 ml	Sigma	SCME001
Hydrocortisone hemissucinate	1 µg/ml	0.5 ml	Sigma	SCME001
L-Glutamine	10 mM	25 ml	Sigma	SCME001
FBS	2%	10 ml	Sigma	SCME001
Antibiotic/antymicotic*	1X	100X	Gibco	15240-062
*not in the kit				

Table 5: BEnd.3 cells medium.

Reagents	Working concentration	Stock concentration	Provider	Cat. no.
DMEM F12 (+ L-Glutamine)	1X	1X	Gibco	11320-074
FBS	10%	100%	Labclinics	S181B-500
Antibiotic/antimitotic	1X	100X	Gibco	15240-062

Table 6: BECs primary culture medium.

Reagents	Working concentration	Stock concentration	Provider	Cat. no.
Growth medium MV2	1X	1X	Promocell	C-22022
Supplement mix	5,4X	100X	Promocell	C-22022
Antibiotic/antimycotic	1X	100X	Gibco	15240-062

Table 7: FACS buffer/ FACS blocking buffer.

Reagents	Working concentration	Stock concentration	Provider	Cat. no.
HBSS (w/o Ca^{2+} and Mg^{2+})	1X	10X	Gibco	14185052
HEPES	10 mM	1 M	Biowest	L0189-100
EDTA	2 mM	20 mM	Sigma	E6511
BSA	0.5%	Powder	Sigma	B4287

Table 8: ECs blocking buffer.

Reagents	Working concentration	Stock concentration	Provider	Cat. no.
HBSS (+ Ca^{2+} and Mg^{2+})	1X	10X	Fisher	14025-050
D(+)-Glucose	0,6%	30%	Panreac	L0642-500
Sodium pyruvate	1 mM	100 mM	Biowest	E6511
Sterile distilled H_2O	1X	1X		

Annex III

Annex III. Genetic map of AAV2-NRGTEWD (BR1) capsid protein (Körbelin et al., 2016)

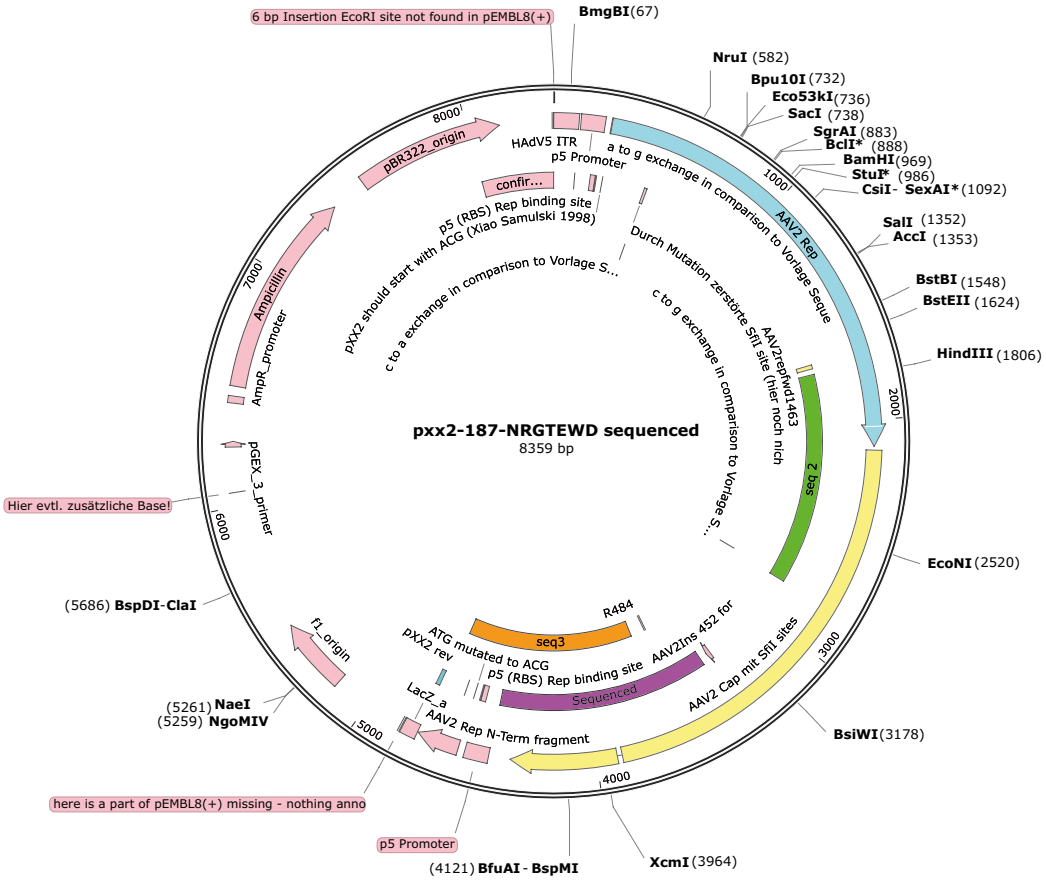

Annex IV

Submitted publication (Rojas-Vázquez et al., submitted).

A renal clearable fluorogenic probe for the in vivo detection of β-galactosidase activity during aging and senolysis

Sara Rojas-Vázquez[1,3,5*], Beatriz Lozano-Torres[1-4*], Alba García-Fernández[1-4], Irene Galiana[1-4], Ana Perez-Villalba[6,7], Pablo Martí-Rodrigo[5,7], M. José Palop[5,7], Marcia Domínguez[1,3], Mar Orzáez[2,8], Félix Sancenón[1-4], Juan F. Blandez[1-4], Isabel Fariñas[5,7] and Ramón Martínez-Máñez[1-4]

[1]Instituto Interuniversitario de Investigación de Reconocimiento Molecular y Desarrollo Tecnológico (IDM), Universitat Politècnica de València-Universitat de València, Spain.

[2]Unidad Mixta UPV-CIPF de Investigación en Mecanismos de Enfermedades y Nanomedicina, Universitat Politècnica de València, Centro de Investigación Príncipe Felipe, Valencia, Spain.

[3]CIBER de Bioingeniería, Biomateriales y Nanomedicina (CIBER-BBN), Spain.

[4]Unidad Mixta de Investigación en Nanomedicina y Sensores. Universitat Politècnica de València, IIS La Fe, Valencia, Spain.

[5]Instituto de Biotecnología y Biomedicina (BIOTECMED), Universitat de València, Spain.

[6]Laboratory of Animal Behavior Phenotype (L.A.B.P.). Facultad de Psicología. Universidad Católica de Valencia, Spain.

[7]Centro de Investigación Biomédica en Red de Enfermedades Neurodegenerativas (CIBERNED), Spain.

[8]Centro de Investigación Príncipe Felipe, Valencia, Spain.

* Equal contribution

Addresses for correspondence:

Ramón Martínez-Máñez: rmaez@qim.upv.es

Isabel Fariñas: isabel.farinas@uv.es

Abstract

The accumulation of senescent cells with advancing age reflects deterioration in cell repair mechanisms and in the capacity of the immune system to clear damaged cells. An increased burden of senescent cells results in tissue functional decline and leads aging and age-related diseases. Reliable detection of senescent cells *in vivo* still constitutes a major challenge in aging research. Here we describe the design and synthesis of a renal clearable fluorogenic probe (Cy7Gal) based on a Cy7 fluorophore skeleton modified with sulfonic groups and conjugated to a galactose derivative to serve as a substrate for the β-galactosidase **enzyme *in vivo*. Upon administration of the probe to animals,** β-galactosidase **activity cleaves the O-glycosidic bond, releasing the renal clearable Cy7 fluorophore that can be quantitated in urine. We provide evidence of the reliability of the Cy7Gal probe to monitor an experimentally controlled load of cellular senescence *in vivo*. We also show that the fluorophore intensity in urine correlates with age-associated anxiety in mice during natural and accelerated aging and during senolytic treatment. Interestingly, the probe read-out and correlated behavioral tests indicate that senolytic treatments have non-lasting effects that disappear if the treatment is not maintained. Our strategy may serve as a basis for the development of fluorogenic platforms aimed at easy longitudinal follow-ups of aging and senolysis in biofluids.**

Introduction

The design and development of new cost-effective and of easy implementation diagnostic tools is an important goal in health[1]. In this context, diagnostic systems capable of detecting target biomarkers in readily accessible biofluids constitute a potential solution for non-invasive longitudinal studies[2]. An approach that fulfills these characteristics is the design of probes that can be specifically transformed by the action of certain biomarkers in cells and tissues and have a rapid renal clearance thus allowing detection in the urine. A few reports have described the use of multiplexed protease-responsive nanoparticles that, in response to proteolytic cleavage in disease environments, release small reporter probes that can be detected in urine by mass spectrometry or immunoassays[3,4]. This approach has been elegantly exploited to detect acute kidney injury with fluorescent and chemiluminescent derivatives equipped with a (2-hydroxypropyl)-β-cyclodextrin (HPβCD) moiety that allowed a renal clearance of the probes[5,6]. Another example describes a nanosensor based on ultra-small renally removable nanoparticles able to recognize deregulated proteases in cells. In this case, a colorimetric signal is indirectly detected by measuring the ability of the urine-recovered nanoparticles to oxidize a chromogenic peroxidase substrate in the presence of hydrogen peroxide[7]. These systems, however, rely on the application of complex techniques, expensive analytical assays, or use nanoparticles which could result in undesired accumulation or side effects[8]. A reasonable alternative could be based on the use of a dye or fluorophore in an OFF state whose turning ON is dependent on the presence of a specific biomarker, such as an enzyme, that interacts with the probe at the site of the disease and that is chemically designed to favor its diffusion out of the cells and its filtration by the kidney into the urine. However, such a simple idea has not been widely exploited.

Aging is characterized by a progressive and generalized functional decline and by the concomitant development of age-related diseases[9]. One of the hallmarks of aging is a rise in the frequency of senescent cells in most organs. Cells undergo senescence in response to several stressors, entering an irreversible cell cycle arrest that is accompanied by an increase in heterochromatin and in foci of DNA damage-responsive proteins, or DNA scars, increased levels of cyclin-dependent kinase (CDK) inhibitor proteins $p16^{INK4a}$ (p16) and/or $p21^{CIP1}$ (p21), and reduced levels of lamin B1. They also exhibit larger cell size and an augmented

lysosomal compartment, with highly increased levels of the enzyme β-galactosidase (β-Gal)[10]. Senescent cells also display an intense secretory activity which appears to be involved in the pathophysiology of many aging related diseases through paracrine effects on neighbor healthy cells[11-13]. Senolysis, or the selective pharmacological killing of senescent cells, is thus being explored as a potentially promising intervention to promote tissue rejuvenation and health[14-16]. However, new strategies aimed at the detection of senescent cells and their monitoring during aging or after senolytic interventions are still required[17-19]. Although the quantification of cell senescence in biopsies from different human tissues is an active area of research, non-invasive procedures to monitor cellular senescence *in vivo* have not yet been developed[17,20].

Here we report the design and synthesis of a cyanine-7-based probe (Cy7Gal) and its ability to act as an *in vivo* read-out of β-Gal activity. Upon *in vivo* administration, the non-emissive Cy7Gal probe becomes hydrolyzed by β-Gal in cells to release the highly fluorescent dye Cy7[21]. Subsequently, the Cy7 fluorophore diffuses out of the cells and is quickly cleared at the kidneys, allowing its detection and quantitation in the urine. We show that the probe can be used to detect cell senescence in mice non-invasively and that it provides read-outs during aging and senolytic intervention that correlate with age-associated anxious behavior. Interestingly, our *in vivo* studies reveal the transient nature of senolytic treatments. The rapid optical readout of overall β-Gal activity through a simple urine measurement represents an attractive alternative to other procedures and enables longitudinal studies, i.e. in aging research. Our results also indicate that the same strategy could be used to generate fluorogenic probes to monitor the activity of disease-related enzymes in easily collectable biological fluids in experimental animals and, eventually, in humans.

Results and Discussion

Design and synthesis of a probe to monitor β-Gal *in vivo*

Fluorescent probes that are turned ON from an OFF state by the hydrolysis of an intramolecular O- or N-glycosidic bond by β-Gal at lysosomes have been previously generated by our group and others for detecting senescent cells[19,22]. Building on this work, we decided to develop a probe in which the addition of sulfonic groups to the releasable fluorophore would promote its diffusion out of the cells and its recovery in the urine when injected *in vivo*[23]. Because the incorporation of the sulfonic groups should result in a more diffusible fluorophore, we first synthesized the probe without this modification to assess its value as a specific detector for β-Gal activity in senescent cells. The probe without sulfonic groups (WOS)-Cy7Gal was prepared following a two-step synthetic procedure shown in **Fig. 1a**. First, 2,3,4,6-tetra-O-acetyl-α-D-galactopyranosyl bromide was reacted with 4-hydroxyisophthalaldehyde in anhydrous acetonitrile yielding compound **1**. Then, a Knoevenagel condensation between **1** and 1-butyl-2,3,3-trimethyl-3H-indol-1-ium iodide (**2**) yielded the WOS-Cy7Gal probe. The WOS-Cy7 fluorophore was synthesized by protecting the hydroxyl group of 4-hydroxyisophthalaldehyde with *t*-butyldimethylsilyl chloride followed by a Knoevenagel condensation with **2** and the subsequent deprotection of the hydroxyl group. WOS-Cy7Gal and WOS-Cy7 were fully characterized by ^{1}H-NMR, ^{13}C-NMR, and HRMS (see **Methods**). PBS (pH 7) solutions of the WOS-Cy7 fluorophore showed an intense emission at ca. 660 nm ($\Phi_{WOS\text{-}Cy7}$ = 0.48) when excited at 580 nm, whereas PBS solutions of the WOS-Cy7Gal probe were poorly emissive at the same excitation wavelength ($\Phi_{WOS\text{-}Cy7Gal}$ = 0.0076).

In order to validate the ability of WOS-Cy7Gal to monitor cell senescence, we tested the probe in cultures of primary venous endothelial cells obtained from the human umbilical cord (hUVECs) treated with 1 μM palbociclib, a CDK4/6 inhibitor that reportedly induces cell cycle arrest and senescence[24]. Treatment with the drug for 7 days resulted in increased cell size and adherence, in agreement with morphological

features described for senescent phenotypes[25]. The induction of cell senescence was corroborated by increased β-Gal activity in the X-Gal histochemical reaction (**Fig. 1b**). Treated cells ceased proliferation (Ki67-negative) and exhibited increased levels of DNA damage (γH2AX-positive foci) and p21 protein and lower levels of lamin B1, all cell senescence features[10] (**Fig. 1c**). Pharmacologically-induced senescent hUVECs were strongly positive for WOS-Cy7-emission after 10 min in the presence of the probe (**Fig. 1d**). Likewise, we could detect the emission of the probe when these cells reached replicative senescence after 29 passages (**Extended Data Fig. 1a,b**)**.** Our results indicated that WOS-Cy7Gal is an appropriate probe to monitor senescence in cells.

Subsequently, we set out to correlate the probe detection with well-established markers of cell senescence at the single cell level. Given that the β-Gal enzyme is still active after fixation, we formaldehyde-fixed palbociclib-treated and untreated hUVECs before the immunostaining for p16 and lamin B1. Next, we applied WOS-Cy7Gal and monitored its emission signal after only 10 min. Increased levels of emission from punctate structures resembling lysosomes in the senescent cells were found to co-label with apparently lower lamin B1 levels and higher p16 levels (**Fig. 1e,f**). To establish a quantitative correlation between p16 and probe-related fluorescent levels, we first immunostained fixed cells with antibodies to p16 and then exposed the cells to WOS-Cy7Gal for 10 min. Both fluorescent emissions were monitored 15 min afterwards by flow cytometry. We observed that the cells with higher levels of p16 were also brighter for the WOS-Cy7 emission (**Fig. 1g,h**), indicating that the WOS-Cy7Gal probe can be a reliable indicator of senescence-associated β-Gal activity.

We next synthesized the same probe with sulfonic groups added (Cy7Gal). Basically, 2,3,4,6-tetra-O-acetyl-α-D-galactopyranosyl bromide was reacted with 4-hydroxyisophthalaldehyde in anhydrous acetonitrile yielding compound **1**. Again, a Knoevenagel condensation between **1** and, in this case, 2,3,3-trimethyl-1-(4-sulfobutyl)indolium salt (**3**) yielded the Cy7Gal probe (**Fig. 2a**). The Cy7 fluorophore was synthesized by protecting the hydroxyl group of 4-hydroxyisophthalaldehyde with *t*-butyldimethylsilyl chloride followed by a Knoevenagel condensation with **3** and the subsequent deprotection of the hydroxyl group. Cy7Gal and Cy7 were fully characterized by ^{1}H-NMR, ^{13}C-NMR, and HRMS (see **Methods**). PBS (pH 7) solutions of the Cy7 fluorophore showed an intense broad emission band centered at ca. 660 nm (Φ_{Cy7} = 0.43) when excited at 580 nm, whereas PBS solutions of the Cy7Gal probe were poorly fluorescent at the same excitation wavelength (Φ_{Cy7Gal} = 0.0062) (**Extended Data Fig. 2a**). The fluorescence emission intensity of Cy7 fluorophore remained unchanged in the 5-10 pH range (**Extended Data Fig. 2b,c**). The hydrolysis of Cy7Gal in PBS solutions in the presence of the β-Gal enzyme was studied by HPLC. The chromatograms showed the disappearance of the Cy7Gal peak and the appearance of Cy7 if the enzyme was present (**Extended Data Fig. 2d**). The specificity and selectivity of the probe for β-Gal were further tested by incubation of Cy7Gal with different enzymes and with interfering species, such as cations, anions, and small peptides (**Extended Data Fig. 2e**). Only β-Gal induced a marked emission enhancement at ca. 660 nm due to the hydrolysis of Cy7Gal. Interestingly, an emission enhancement was observed when Cy7Gal was incubated in the presence of both esterase and β-Gal, but not esterase alone (**Extended Data Fig. 2e**). The increased emission is likely due to the hydrolysis of the acetate moieties in Cy7Gal by esterases prior to the rupture of the O-glycosidic bond by β-Gal, a sequence that is expected to happen intracellularly. Both Cy7Gal and WOS-Cy7Gal yielded brighter emission in naturally senescent *vs*. replication-competent hUVECs in culture but, as expected, the signal upon treatment with Cy7Gal exhibited a more diffuse cellular pattern that was compatible with lower retention in lysosomes (**Extended Data Fig. 3f**).

In order to evaluate whether Cy7Gal could provide a reliable readout in urine of induced cell senescence *in vivo*, we used it in mice in which the senescent cell burden could be experimentally controlled. To this end, we generated grafts of cells of the 4T1 mouse mammary tumor cell line, a murine cellular model of triple

negative-breast cancer, that are sensitive to palbociclib-induced senescence[26-28]. We first corroborated that 4T1 cells enter senescence *in vitro* when treated with 5 μM palbociclib for 2 weeks. The treatment resulted in increased SA-β-Gal activity in the X-Gal histochemical reaction and increased levels of β-Gal protein in immunoblots (**Extended Data Fig. 3a**). Subsequently, control, and senescent 4T1 cells were incubated with 20 μM Cy7Gal and analyzed by confocal microscopy 2 h post-incubation (**Extended Data Fig. 3a**). Neither control nor palbociclib-treated 4T1 cells exhibited any noticeable fluorescence signal in the absence of the probe when excited at 580 nm. After exposure to Cy7Gal, control 4T1 cells still displayed poor fluorescence emission, whereas senescent 4T1 cells showed a 2.4-fold higher red emission, that could be significantly reduced (ca. 60%) if cells were pre-incubated for 30 min with the β-Gal specific inhibitor D-galactose at 5 mM (**Extended Data Fig. 3b**). A marked reduction in the intensity was also found when the expression of *Glb1*, the gene that encodes lysosomal β-Gal, was interfered with a specific *Glb1* siRNA (**Extended Data Fig. 3c,d**), indicating that β-Gal is responsible for the emission. Finally, viability assays indicated that the probe was innocuous for both normal and senescent cells (**Extended Data Fig. 3e**).

We next implanted orthotopic grafts of $1x10^6$ 4T1 cells into the left mammary fat pad of BALB/cByJ young female mice that were subsequently treated by daily oral gavage with 0, 10, 50, or 100 mg/kg palbociclib for 7 days to induce different degrees of cell senescence in the grafts. Tumors from mice treated with 10 mg/kg of palbociclib grew similarly to those in untreated mice, while tumors in mice treated with 50 or 100 mg/kg palbociclib displayed a significant reduction in volume, measured with a caliper (**Extended Data Fig. 4a**). Histological analyses indicated a progressively reduced proportion of Ki67-positive cells as the palbociclib dose increased, in line with its reported induction of cell senescence[29,30], and increased β-Gal activity in the tumors, but not in organs such as liver or kidney (**Extended Data Fig. 4b-d**), providing us with a model of controlled cell senescence load *in vivo*. Next, mice bearing 4T1 tumors and treated with palbociclib at the different concentrations were anesthetized and 2.5 μmol of Cy7Gal was intraperitoneally (i.p.) administered to each mouse. Fluorescence analysis *in vivo* using an IVIS® Spectrum 15 min after Cy7Gal administration clearly showed fluorescence accumulation in the tumors and the bladder that became more intense with increasing palbociclib dosage (**Fig. 2b** and **Extended Data Fig. 5a**). The emission in urine, collected after mice recovered from anesthesia and quantitated in IVIS® as fluorescence arbitrary units, was higher in mice treated with increasing amounts of palbociclib (**Fig. 2c** and **Extended Data Fig. 5b**). The amount in μmoles of Cy7 recovered in the urine was also quantified by using a fluorometer and a calibration curve (**Fig. 2d**) and showed a clear correlation with the cell senescent burden and with the Cy7 signal within the tumors, determined by IVIS® imaging *ex vivo* in organs collected from the same animals at the end of the experiment (**Extended Data Fig. 6a,b**). In parallel, the same amount (2.5 μmol) of the WOS-Cy7Gal probe was also i.p. administered to BALB/cByJ mice bearing 4T1 tumors and treated with 100 mg/kg palbociclib. We could not detect fluorescence accumulation in the bladder or in the urine collected 15 min after the injection of WOS-Cy7Gal neither in untreated nor in palbociclib-treated mice (**Fig. 2b,c**).

In agreement with a renal clearance of the Cy7 fluorophore in animals injected with the Cy7Gal probe, we found a detectable amount of Cy7 in the urine (ca. 2.34 μmol) while the presence in plasma was significantly lower (0.33 μmol). In contrast, the WOS-Cy7 fluorophore was basically undetectable in plasma (0.02 μmol) or urine (0.01 μmol) in animals injected with the WOS-Cy7Gal probe (**Fig. 2e**). A simple mass balance of the amount of Cy7Gal injected and that of Cy7 in urine allows calculating that, on average, ca 95% of injected Cy7Gal was excreted through urine as Cy7 in palbociclib treated mice (100 mg/kg) while the excretion of WOS-Cy7 from WOS-Cy7Gal was negligible (1%). In autopsy samples, both probes gave a strong positive signal in the tumors (**Fig. 2f,g**), in accordance with their capacity to detect senescent cells. Again, we could only detect a signal in the bladder and urine of Cy7Gal-injected mice. (**Fig. 2f,g**), indicating

that sulfonic acid moieties are responsible for the rapid renal clearance of the Cy7 fluorophore.

The Cy7Gal probe is a reliable urine detector for the aging-associated increase in β-Gal activity

We next aimed to test the potential of the Cy7Gal probe for monitoring overall β-Gal activity in healthy young and old individuals. For this purpose, 2- and 14-month-old (m) BALB/cJyB mice were i.p. injected with the Cy7Gal probe. IVIS® images of the anesthetized mice 15 min post-injection revealed fluorescence accumulation in the bladder of 14-m, but not 2-m mice (**Fig. 3a**). The fluorescent signal detected by IVIS imaging in the urine collected from elderly mice was 5.2-fold stronger than from young mice (**Fig. 3b**), in agreement with an expected higher systemic β-Gal activity in old animals[11]. After euthanasia, the bladder, brain and lungs were studied by IVIS imaging. Quantification of the emission intensity revealed an increase of also 5.2 in the bladder of aged *vs*. young mice. We also observed increases of 2.3 and 3-fold for brain and lungs, respectively, in aged mice when compared to young animals (**Extended Data Fig. 7a-c**). The latter is in agreement with increases in cell senescence incidence in lungs reported with aging[31]. In the brain, β-Gal activity is not a specific marker of senescence, as many healthy neurons have large lysosomal compartments[32]. Interestingly, senescent-like neurons and glial cells have been identified in mouse models of neurodegeneration and in neuropathological human tissue[33,34]. The apparent capacity of the probe to permeate the blood-brain barrier (BBB), however, opens the possibility to study global β-Gal activity, including that of the brain. Furthermore, aging-associated endothelial cell senescence can increase BBB permeability[35] potentially contributing to the use of the probe for studies in brain aging and neurodegeneration. Because renal function can vary depending on the mouse strain[36], we also tested the Cy7Gal probe in mice of the C57BL/6 strain and found again higher fluorescence in the urine of old 15-m animals relative to 3-m younger counterparts by fluorimeter-based detection (**Fig. 3c**). Direct measurement of the relative levels of the probe and the released fluorophore in the urine by HPLC indicated that most of the Cy7Gal probe is excreted intact in young animals (ca. 80%) whereas the Cy7 fluorophore is the major species excreted in aged mice (ca. 75%) (**Fig. 3d**). These results were indicative of the potential of the Cy7Gal probe to monitor aging.

We decided to also use senescence accelerated mouse (SAM) strains which exhibit premature aging traits. Inbreeding of AKR/J mice and selection for the early appearance of features such as hair loss, skin coarseness, and short life span, led to the isolation of senescence-prone (P) and senescence-resistant (R) series of mice which were crossed separately to establish the inbred SAMP and SAMR strains. Relative to their genetic background-controls (SAMR1 mice), SAMP8 mice exhibit several aging traits at earlier physiological ages[37] and are, therefore, widely used in aging research to study immune dysfunction[38], osteoporosis[39] or brain atrophy[40]. Injection of the Cy7Gal and WOS-Cy7Gal probes in 15-m mice of the SAMP8 background also resulted in the detection of Cy7 in urine, and in plasma to a lesser extent, in animals treated with the renal-clearable probe (**Fig. 3e**).

Because the age-related phenotypic differences between SAMP8 and SAMR1 mice begin to be evident after approximately 6 months of age[41-43], we injected 7-m SAMR1 and SAMP8 mice with Cy7Gal and found a stronger fluorescent signal in the urine of SAMP8 *vs*. SAMR1 mice (**Fig. 3f**). We next decided to test whether the Cy7Gal probe could indeed be providing an *in vivo* readout of cell senescence, by comparing urine fluorescence with markers of senescence at the cell level in SAM mice. After euthanasia, we extracted the kidneys and livers, and their isolated cells were incubated *ex vivo* with the cell-trapped WOS-Cy7Gal probe or intracellularly immunostained for p16 or lamin B1 prior to their analysis by flow cytometry. In agreement with the levels of fluorescence in the urine of the animals, we found higher levels of β-Gal activity in SAMP8 *vs*. SAMR1 mice with the WOS-Cy7Gal probe (**Fig. 4a**). Likewise, we could observe higher proportions of cells with detectable levels of p16 and reduced levels of lamin B1 in homogenates from the organs of SAMP8 mice (**Fig. 4b,c**). These data indicated a good correlation between the end-

point measurement of cell senescence with well-accepted markers and the *in vivo* global detection of β-Gal activity with the Cy7Gal probe in urine.

The use of the Cy7Gal probe reveals that senolytic effects are transient

As the urine excretion of the Cy7 fluorophore enables longitudinal studies, we next set out to determine whether the Cy7Gal probe could be used to reliably monitor the effects of a senolytic treatment. Combination of dasatinib (D), an inhibitor of several tyrosine-kinases used as an anti-neoplastic agent for the treatment of acute lymphocytic leukemia, and quercetin (Q), a flavonoid that acts as an anti-apoptotic BCL-XL protein inhibitor, has shown efficacy in counteracting mechanisms of apoptosis evasion in senescent cells resulting in their selective elimination and subsequent beneficial effects in aged organs[14,44]. In our senolytic experiment, 15-m C57BL/6 mice were treated by oral gavage with two doses of D (5 mg/kg) + Q (50 mg/ml) or vehicle (20% PEG-n400 in saline solution) *per* week for 5 weeks and, 13 days after the end of the treatment, they were injected with the Cy7Gal probe (**Fig. 5a**). We could observe lower fluorescence in the urine of treated *vs*. untreated mice (**Fig. 5b**).

The selected senolytic treatment reportedly alleviates brain phenotypes associated with aging and neurodegeneration[45,46]. Therefore, as another non-invasive measure of the senolytic treatment, we decided to perform parallel behavioral tests that reportedly correlate with age-related declines in mice. Because an increase in anxiety is associated with aging and frailty, we used the open field and the elevated plus maze (EPM) tests to evaluate anxiety-related behavior. The open field test measures overall locomotor activity but also anxiety-like behavior as anxious mice typically avoid the lit central area and spend more time at the periphery of the open box, close to the walls. In the EPM, mice are confronted with the decision to spend time exploring the closed arms or the anxiety-generating open arms of an elevated maze[47,48]. As expected, the time spent in the central area of the open field or in the open arms is significantly reduced in 17-m C57BL/6 mice when compared to young 3-m mice of the same strain (**Fig. 5c-f**). In the senolytic experiment, the animals were tested for their performance in the open field and EPM tests 2 days after the measurement of the probe level in urine (**Fig. 5a**). The treatment resulted in improved performance of the elderly mice in both behavioral tests (**Fig. 5c-f**; a group of 3-m mice was included as behavioral controls) without changes in general locomotion (**Extended Data Fig. 8**), reflecting lower anxiety after D+Q treatment. Importantly, we found a significant negative correlation between Cy7 fluorescent levels in urine and time spent in the central area of the open field or in the open arms of the EPM (**Fig. 5g,h**), indicating that animals with an organismal lower β-Gal read-out have a less anxious behavior. Interestingly, senescent cell clearance also alleviates obesity-induced anxiety-like behavior[49]. These data suggested that Cy7Gal is sensitive enough to predict an age-related behavior and, more importantly, that this probe can be used to monitor senolytic treatments at the organismal level.

Next, we decided to test whether our probe could monitor intermittent senolytic treatment. Because in comparison with aged SAMR1 mice, the aged SAMP8 mice also show increased anxious behavior in the open field at ages when they still exhibit normal locomotion (i.e., 4 and 9-m) (**Extended Data Fig. 9a-c**)[37,50], we exposed 7-m SAMP8 mice to the D+Q treatment for 5 weeks and evaluated fluorophore recovery in urine 21 days after cessation of the treatment (**Fig. 6a**). As before, we found that the treatment efficaciously decreased Cy7 levels in the urine (**Fig. 6b**; first cycle, short-term). A 3-day treatment with the drug combination did not change the behavior of 3-m SAMR1 control mice in the open field test, indicating that the D+Q drug combination *per se* does not affect anxiety (**Extended Data Fig. 9d**); however, we observed a decrease in anxious behavior when we assessed the animals at short-term after the senolytic treatment (**Extended Data Fig. 9e,f**), in line with the reduced Cy7 levels in the urine. We then repeated the measurements at 58 days post-treatment and found no differences in anxiety (**Extended Data Fig. 9e**) or urine fluorescence between animals treated with vehicle or with D+Q (**Fig. 6c**; first cycle, long-term),

suggesting that transient senolysis does not result in permanent alleviating effects. To make sure that the animals could still respond to senolysis, we treated again the same animals and analyzed them 16 days after the treatment and found again the reduction in urine fluorescence (**Fig. 6d;** second cycle, short-term). As with naturally aged mice of the C57BL/6 strain, we could find a significant negative correlation between levels of Cy7 fluorescence in urine and the time that SAMP8 mice spent in the central area of the open field test, only in those short-term cases, i.e. in which the effect was measured less than 3 weeks after senolytic administration (**Fig. 6e,f**). Our data indicates that the Cy7Gal probe can reliably and non-invasively monitor senolysis and that effects of D+Q wash off with time, in line with a treatment that eliminates senescent cells but does not eliminate inductors of cell senescence.

Conclusions

Precision medicine aims to guide healthcare decisions toward the most effective treatment for a certain patient to improve care quality[51]. One attractive approach in this area is to detect biomarkers from readily accessible biofluids using detection systems as simple as possible[52,53]. One approach pursues the design of fluorogenic probes (in an OFF state) that can be transformed by the action of certain biomarkers (i.e. an enzyme) in cells and tissues to give a final fluorescent product (in an ON highly emissive state) that can diffuse out of the cells and has a rapid renal clearance thus allowing its detection in the urine using a simple fluorimeter[54]. Based on this concept, we report herein the case of detection of lysosomal β-Gal using the fluorogenic probe Cy7Gal. We show that cell-entrapped (WOS-Cy7Gal) and diffusible (Cy7Gal) forms of this probe produce a brighter emission in cells undergoing replicative or induced senescence. We provide evidence of the reliability of the Cy7Gal probe to monitor an experimentally controlled load of cellular senescence *in vivo* by using BALB/cByJ mice bearing breast cancer tumors treated with senescence-inducing chemotherapy. We also show that the fluorophore intensity in urine correlates with age progression and age-associated anxiety in mice during natural and accelerated aging. In addition, the probe allows a non-invasive monitoring of the effects of senolytic treatment. Interestingly, our data reveals that senolytic treatments based on the pharmacological use of agents that eliminate senescent cells are transient. Our findings demonstrate that renal clearable fluorogenic probes are a versatile modular tool that opens new opportunities to develop simple diagnoses in urine for a variety of diseases where abnormal enzymatic activity is a biomarker. We anticipate that this technology can also be applied in the monitoring of therapeutic treatments. Such adaptive detection platform could also be applicable in low-resource environments and might democratize access to advanced and sensitive diagnoses.

Methods

Synthesis and characterization of fluorophore and probes.

WOS-Cy7Gal: 4-hydroxyisophthalaldehyde (Tokyo Chemical Industry Co. Ltd.; 75 mg, 0.5 mmol), α-acetobromogalactose (Sigma-Aldrich; 607 mg, 1.5 mmol) and potassium carbonate (Sigma-Aldrich; 400 mg, 4 mmol) were mixed in a round bottom flask under argon atmosphere and dissolved in 30 mL of anhydrous acetonitrile (Acros Organics). The reaction mixture was heated to 70 ºC and stirred for 4 hours under argon atmosphere and the solvent was removed under vacuum. The residue was purified by column chromatography on silica gel (hexane-ethyl acetate 2:1 v/v as eluent) to obtain product **1** as a yellow solid (230 mg, 0.46 mmol, 92.6% yield). Then, product **1** (90 mg, 0.17 mmol) 1-butyl-2,3,3trimethyl-3H-indol-1-ium iodide (**2**, 120 mg, 0.35 mmol) and sodium acetate (47.80 mg, 0.35 mmol) were mixed in a Schlenk flask under argon atmosphere and dissolved in 2 mL of acetic anhydride. The reaction mixture was heated to 70 ºC and stirred under argon atmosphere. After 4 hours, the solvent was removed under vacuum and

the crude product was purified in a silica flash column using diethyl ether as eluent. WOS-Cy7Gal was obtained as red-brown oil (50 mg, 0.05 mmol, 33% yield).

^{1}H NMR (400 MHz, $CDCl_3$) δ 7.60 – 7.51 (m, 2H), 7.20 – 7.14 (m, 4H), 7.08 (dd, J = 21.5, 6.2 Hz, 2H), 6.97 (t, J = 7.4 Hz, 2H), 6.71 (d, J = 7.7 Hz, 2H), 6.38 (bs, 1H), 5.70 (d, J = 8.3 Hz, 1H), 5.50 (d, J = 1.3 Hz, 1H), 5.43 (d, J = 2.5 Hz, 1H), 5.08 (dd, J = 10.4, 3.4 Hz, 1H), 4.34 (t, J = 6.4 Hz, 1H), 4.14 (t, J = 6.6 Hz, 2H), 4.10 (dd, J = 6.7, 4.0 Hz, 1H), 4.08 – 4.03 (m, 1H), 3.61 (t, J = 7.6 Hz, 4H), 2.04 (s, 3H), 2.02 (s, 3H), 2.01 (s, 3H), 2.00 (s, 3H), 1.72 (s, 12H), 1.66 (dd, J = 13.9, 6.1 Hz, 4H), 1.62 – 1.55 (m, 4H), 0.99 (t, J = 7.3 Hz, 6H). ^{13}C NMR (101 MHz, $CDCl_3$) δ 193.44 (2C), 170.49 (1C), 170.26 (1C), 170.00 (1C), 169.50 (1C), 169.05 (1C), 147.19 (1C), 143.36 (1C), 142.18 (1C), 140.38 (1C), 139.41 (1C), 136.17 (1C), 135.60 (1C), 127.66 (1C), 127.46 (1C), 124.58 (1C), 124.10 (1C), 122.50 (1C), 122.29 (1C), 122.01 (1C), 121.95 (1C), 119.23 (1C), 119.21 (1C), 114.19 (1C), 108.44 (1C), 107.75 (2C), 93.69 (1C), 71.83 (1C), 68.89 (1C), 67.94 (1C), 67.54 (1C), 61.37 (1C), 48.31 (2C), 42.61 (2C), 31.56 (1C), 30.31 (1C), 29.82 (4C), 24.58 (1C), 22.81 (1C), 21.01 (1C), 20.93 (1C), 20.77 (1C), 20.73 (1C), 20.67 (1C), 20.47 (1C).

HRMS: calculated for $C_{52}H_{64}N_2O_{10}$ ($M+H^+$) 876.459 m/z; measured 876.7992 m/z ($M+H^+$).

Cy7Gal: 4-hydroxyisophthalaldehyde (Tokyo Chemical Industry Co. Ltd.; 75 mg, 0.5 mmol), α-acetobromogalactose (Sigma-Aldrich; 607 mg, 1.5 mmol) and potassium carbonate (Sigma-Aldrich; 400 mg, 4 mmol) were mixed in a round bottom flask under argon atmosphere and dissolved in 30 mL of anhydrous acetonitrile (Acros Organics). The reaction mixture was heated to 70 ºC and stirred for 4 hours under argon atmosphere and the solvent was removed under vacuum. The residue was purified by column chromatography on silica gel (hexane-ethyl acetate 2:1 v/v as eluent) to obtain product **1** as yellow solid (230 mg, 0.46 mmol, 92.6% yield). Then, compound **1** (90 mg, 0.17 mmol), 1-(4sulfobutyl)-2,3,3-trimethylindolium inner salt (**3**) (Sigma-Aldrich; 100 mg, 0.35 mmol) and sodium acetate (Sigma-Aldrich; 47.80 mg, 0.35 mmol) were dissolved in 2 ml of acetic anhydride (Sigma-Aldrich) in a Schlenk flask under an argon atmosphere. The reaction mixture was heated to 70 ºC and stirred for 4 hours under argon atmosphere and solvent was eliminated under vacuum. The crude was purified by reverse phase column chromatography (dicholoromethane-methanol 10:1 v/v as eluent) to obtain Cy7Gal as a red-brown solid. (120 mg, 0.116 mmol, 68.1% yield).

^{1}H NMR (400 MHz, $CDCl_3$) δ = 7,72 – 7,62 (m, 1H), 7,53 (dd, J = 7,5; 1,6 Hz, 1H), 7,49 – 7,43 (m, 2H), 7,42 – 7,32 (m, 2H), 7,00 (d, J = 7,3 Hz, 2H), 6,79 (t, J = 7,2 Hz, 1H), 6,69 (t, J = 7,3 Hz, 1H), 6,37 (d, J = 1,7 Hz, 1H), 5,69 (d, J = 8,3 Hz, 1H), 5,49 (d, J = 1,3 Hz, 1H), 5,42 (dd, J = 3,4; 0,9 Hz, 1H), 5,34 – 5,32 (m, 2H), 5,24 (s, 1H), 5,07 (dd, J = 10,4; 3,4 Hz, 1H), 4,17 – 4,04 (m, 4H), 3,48 (s, 4H), 2,91 (s, 4H), 2,03 (s, 12H), 1,93 (s, 4H), 1,82 (s, 4H), 1,58 (s, 12H) ppm.

^{13}C NMR (400 MHz, $CDCl_3$) δ 193.63 (2C), 170.52 (1C), 170.28 (1C), 170.15 (1C), 169.80 (1C), 169.07 (1C), 144.10 (1C), 143.12 (1C), 140.70 (2C), 140.11 (2C), 139.11 (1C), 130.30 (1C), 130.21 (1C), 129.96 (1C), 129.88 (1C), 127.64 (1C), 124.61 (1C), 124.50 (1C), 121.86 (1C), 121.61 (1C), 115.77 (1C), 114.70 (1C), 114.19 (1C), 112.51 (1C), 108.17 (1C), 92.29 (1C), 70.97 (1C), 68.89 (1C), 67.55 (1C), 66.57 (1C), 61.15 (1C), 53.56 (2C), 52.87 (2C), 48.15 (2C), 32.27 (1C), 31.56 (1C), 29.82 (4C), 23.34 (2C), 21.02 (1C), 20.94 (1C), 20.78 (1C), 20.67 (1C) ppm.

HRMS: calculated for $C_{52}H_{63}N_2O_{16}S_2$ ($M+H^+$) 1035.3619 m/z; measured 1035.3606 m/z ($M+H^+$), 1051.3546 ($M+H_2O-2H^+$).

Cy7: 4-hydroxyisophthalaldehyde (1.5 g, 9.9 mmol) and imidazole (1.7 g, 25 mmol) were dissolved in 100 mL of anhydrous dichloromethane. Tertbutyldimethylsilyl chloride (1.8 g, 12 mmol) was then added dropwise to the solution. The reaction was stirred at room temperature (RT) overnight. Afterwards, the mixture was washed with brine (2 x 100 ml) and the organic phase was dried with $MgSO_4$. The solvent was

removed under vacuum and the crude was purified by silica column using a mixture hexane:ethyl acetate (10:1) as eluent. Hydroxyl-protected product was obtained as colorless oil (2.48 g, 9.39 mmol, 94.8% yield). Subsequently, hydroxyl-protected product (79.24 mg, 0.3 mmol) was added in a Schlenk tube with sodium acetate (83.9 mg, 1.02 mmol) and 2,3,3-trimethyl-1-(4-sulfobutyl)-indolium inner salt (**3**). The mixture was dissolved in acetic anhydride under argon atmosphere. The reaction was stirred at 80 ºC for 4 hours. Acetic anhydride was removed under vacuum and treated with dichloromethame and the solvent was eliminated again under vacuum. Finally, deprotection of hydroxyl group was assessed by stirring the obtained product in a solution of $KF{\cdot}2H_2O$ (47 mg, 0.5 mmol) in acetonitrile (2 ml) for 2 h at RT. Then, the mixture was treated with saturated $NaHCO_3$ water solution (1 ml) and extracted with CH_2Cl_2 (3 x 20 ml). The organic layer was washed with brine and dried with $MgSO_4$. The crude was purified by reverse phase column chromatography (dicholoromethane-methanol 8:1 v/v as eluent). Cy7 was obtained as brown-green solid (85 mg, 0.120 mmol, 40 % yield).

^{1}H NMR (400 MHz, $CDCl_3$) δ 7.60 – 7.45 (m, 4H), 7.35 (d, J = 2.5 Hz, 2H), 7.28 (d, J = 2.0 Hz, 1H), 7.15 – 6.96 (m, 3H), 6.84 – 6.69 (m, 1H), 5.81 (ddt, J = 16.9, 10.2, 6.7 Hz, 1H), 5.37 (dt, J = 9.1, 4.1 Hz, 1H), 5.02 – 4.90 (m, 2H), 2.04 (dd, J = 14.9, 7.3 Hz, 4H), 1.77 (d, J = 4.7 Hz, 4H), 1.67 (dt, J = 15.4, 7.6 Hz, 4H), 1.45 (dd, J = 14.8, 7.5 Hz, 4H), 1.37 (s, 12H) ppm.

^{13}C NMR (101 MHz, $CDCl_3$) 174.97 (2C), 160.73 (1C), 154.00 (1C), 149.87 (1C), 140.72 (2C), 140.08 (2C), 130.71(1C), 130.12 (1C), 128.89 (1C), 128.44 (2C), 125.20 (2C), 124.39 (1C), 123.17 (2C), 117.05 (1C), 114.61 (2C), 109.08 (1C), 107.48 (1C), 53.97 (2C), 48.90 (2C), 42.15 (2C), 28.67 (2C), 26.23 (2C), 19.29 (2C) ppm.

HRMS: calculated for $C_{38}H_{44}N_2O_7S_2$ ($M+H^+$) 705,269 m/z; measured 705,2673 m/z ($M+H^+$).

WOS-Cy7: 4-hydroxyisophthalaldehyde (500 mg, 3.3 mmol) and imidazole (567 mg, 8.3 mmol) were dissolved in 100 mL of anhydrous dichloromethane. Tertbutyldimethylsilyl chloride (603 mg, 4 mmol) was then added dropwise to the solution. The reaction was stirred at room temperature overnight. Afterwards, the mixture was washed with brine (2 x 100 ml) and the organic phase was dried with $MgSO_4$. The solvent was removed under vacuum and the crude was purified by silica column using a mixture of hexane-ethyl acetate (10:1 v/v) as eluent. The hydroxyl-protected product was obtained as colorless oil (806 mg, 3.05 mmol, 92.5% yield). Then, the hydroxyl-protected product (90 mg, 0.17 mmol), 1-butyl-2,3,3-trimethyl-3H-indolium, iodide (**2**, 120 mg, 0.35 mmol) and sodium acetate (47.80 mg, 0.35 mmol) were mixed in a Schlenk flask under argon atmosphere and dissolved in 2 mL of acetic anhydride. The reaction mixture was heated to 70 ^{o}C and stirred under argon atmosphere. After 4 hours, the solvent was removed under vacuum and the crude product was purified in a silica flash column using diethyl ether as eluent. **WOS-Cy7** was obtained as red-brown oil (61 mg, 0.06 mmol, 36 % yield).

^{1}H NMR (400 MHz, $CDCl_3$) δ 7.43-7.41 (m, 4H), 7.31 – 7.27 (m, 2H), 7.26 (d, J = 2.5 Hz, 1H), 7.24 (d, J = 2.0 Hz, 1H), 7.02 (d, J = 7.6 Hz, 1H), 6.96 – 6.92 (m, 2H), 5.64 (dt, J = 7.9, 1.0 Hz, 1H), 5.30 (d, J = 14.5 Hz, 1H), 4.50 (s, 1H), 4.35 (d, J = 7.1 Hz, 1H), 4.06 (d, J = 7.2 Hz, 2H), 2.11 (s, 2H), 2.04 (s, 2H), 1.46 (s, 12H), 1.40 (s, 1H), 1.37 – 1.32 (m, 4H), 1.26 (s, 1H), 1.19 (d, J = 2.3 Hz, 6H) ppm.

^{13}C NMR (101 MHz, $CDCl_3$) δ 172.83 (2C), 162.18 (1C), 155.32 (1C), 141.66 (1C), 141.35 (1C), 139.75 (2C), 130.17 (1C), 129.18 (1C), 128.53 (2C), 125.22 (2C), 122.53 (1C), 120.26 (2C), 118.80 (1C), 113.10 (2C), 111.96 (1C), 98.96 (1C), 53.35 (2C), 48.21 (2C), 42.72 (2C), 28.82 (2C), 27.45 (2C), 20.78 (2C), 14.68 (2C) ppm.

HRMS: calculated for $C_{38}H_{45}N_2O$ ($M+H^+$) 546.3560 m/z; measured 546.4042 m/z ($M+H^+$).

All obtained products were characterized by ^{1}H and ^{13}C NMR spectra on a Bruker FT-NMR Avance 400 (Ettlingen, Germany) spectrometer at 300 K, using TMS as internal standard and by high resolution

mass spectrometry (HRMS) with a TRIPLETOF T5600 (ABSciex, USA) spectrometer. Fluorescence was characterized in a JASCO FP-8500 fluorescence spectrophotometer. To study the hydrolysis of Cy7Gal by β-Gal, 2 µl of human β-Gal enzyme (Biotechne) were added to PBS (pH 7) solutions of Cy7Gal (10^{-5} M). Chromatograms of Cy7Gal, Cy7 and Cy7Gal+β-Gal after 30 min were obtained by reversed-phase liquid chromatography using a KromasilC18 column as the stationary phase, a mixture water-acetonitrile under gradient conditions (flow: 0.8 ml/min, initial condition 90:10 vol. %, final condition 10:90 vol. %) as mobile phase and a photodiode array detector. To study the specificity and selectivity of the probe to β-Gal, fluorescence intensity of solutions of Cy7Gal (20 µM, PBS, pH 7.4) was measured in the presence of cations (150 µM), anions (150 µM), small peptides (150 µM), proteins (150 µg/ml) and enzymes (150 µg/ml) at 37 °C after 30 min in a JASCO FP-8500 fluorescence spectrophotometer (λ_{ex} = 580 nm; λ_{em} = 665 nm).

Cell culture, immunocytochemistry and imaging. The 4T1 mouse mammary tumor cell line was obtained from the American Type Culture Collection (ATCC), cultured in DMEM supplemented with 10% FBS (Sigma) and penicillin-streptomycin and maintained in 5% CO_2 at 37 °C. For senescence induction, 4T1 cells were treated with 5 µM palbociclib (Eurodiagnostico) for 14 days. Cellular senescence was assessed by the senescence β-Galactosidase KIT acquired from Cell Signaling. 4T1 control and senescent cells were seeded in a clear flat bottom 96-well plate at a density of 3,000 and 4,000 cell *per* well, respectively. After 24 h cells were incubated with Cy7Gal (20 µM in DMEM with 10% FBS and 0.1% DMSO). For competition experiments with D-Galactose, a total of 200,000 control or 500,000 senescent 4T1 cells were seeded *per* well in a clear glass 6-well plate. The following day, cells were pre-incubated or not with D-Galactose (5 mM) for 30 min and then treated with Cy7Gal. Confocal images were acquired after 2 h in a Leica TCS SP8 AOBS confocal microscope (λ_{exc}= 552 nm; λ_{em}= 574-765 nm) and analyzed with the Image J software. For the *in vitro* cytotoxicity studies, 4T1 cells were plated in 96 well plates (4,000 control and 6,000 senescent cells *per* well) and allowed to adhere. At 24 h post-seeding, the cells were incubated with varying concentrations of the Cy7Gal probe (diluted in DMEM) for 24 h. The cell viability was evaluated using the cellTiter-Glo® Luminnescent Cells assay (Promega). Luminescence was collected in a VICTOR Multilabel Plate Reader (Pelkin Elmer). Human endothelial cells (hUVECs) were obtained from EndoGRO™ (Sigma-Aldrich), cultured in a specific medium (EndoGRO-LS supplemented medium from Sigma-Aldrich) and maintained at 37 °C and 5% CO_2. For experimental set-ups, cells were seeded in 60 mm cell culture plates at a density of 500,000 cells *per* plate for pharmacological induction of senescence and half for control (untreated) cells. Senescence induction was carried out by treating the cells with 1 µM palbociclib for 7 days. For the analysis of WOS-Cy7Gal in live hUVECs, senescent and control cells were seeded in a specific chamber for optical imaging (8-well Ibidi® chamber) at a density of 20,000 and 10,000 cells, respectively. Once the cells were adhered to the plate, nuclei were labelled with 10 µg/ml Hoechst 33342 (Invitrogen) for 30 min. After careful washing of the cells, 20 µM of WOS-Cy7Gal in DMEM was added and images were obtained with an Olympus FV10i confocal microscope (using a 60x objective) within the first 10 min of incubation with the probe. The same procedure was followed using WOS-/Cy7Gal in hUVECs entering replicative senescence after being passaged 29 times. For traditional SA-β-Gal activity detection, the Sigma-Aldrich kit for X-Gal histochemical staining was used. To detect by immunofluorescence senescence-associated markers, control and palbociclib-treated hUVECs were seeded in 48-well plates at a density of 12,500 and 25,000 cells/cm^2, respectively, on round glass coverslips. After 24 h, the cells were fixed with 2% paraformaldehyde (PFA) for 15 min and washed thoroughly with 0.1M PBS. Prior to antigen-specific detection with primary antibodies, potential non-specific sites were blocked by incubating the cells in blocking buffer (10% horse serum and 0.1% Triton™ X-100 in 0.1 M PBS) for 1 h at RT. Cells were then incubated with primary antibodies to Ki67 (Abcam, ab15580; diluted 1:50), p21 (Abcam Ab109520; diluted 1:100), lamin B1 (Abcam, Ab16048; diluted 1:100) and γH2AX (Millipore, 05-636-I; diluted 1:100) overnight at 4 °C. After several washes, cells were labelled with fluorescent secondary antibodies (Molecular Probes, diluted 1:600) for 1 h at RT.

Finally, nuclei were stained with 4′,6-diamidino-2-phenylindole (DAPI, 1 µg/ml in distilled water) for 4 min and the glass coverslips containing labelled cells were mounted with FlourSave™ reagent (Calbiochem, 345789) for image acquisition with an Olympus FV10i confocal microscope. Quantitative analysis was performed using Image J software. Similarly, senescent and control hUVECs were fixed with 2% PFA for co-localization of p16 and lamin B1 with WOS-Cy7Gal in a 8-well Ibidi® chamber. The probe was added at 20 µM in DMEM and incubated with the immunostained cells for 10 min at 37 ºC. After washing the cells, images were immediately captured using an Olympus FV10i confocal microscope.

Knock-down experiments. For transient downregulation of *Glb1*, a total of 20,000 control or 50,000 senescent 4T1 cells were seeded *per* well in 24-well plate. After 24 h, cells were transfected with TriFECTa® Kit DsiRNA Duplex siRNAs (Integrated DNA Technologies) hs.Ri.GLB1.13.3 or scrambled siRNA, using lipofectamine RNAiMAX reagent (Thermo Fisher Scientific) as *per* manufacturer's instructions. At 48 h after transfection, cells were washed with PBS and fixed for 10 min with SA-β-Gal staining kit fixative. Then, cells were stained overnight using the SA-β-Gal staining kit (Cell Signaling) following manufacturer's instructions. The following day, cells were thoroughly washed with PBS and imaged using a colored bright field microscope. Other knock-down cells were treated with 20 µM Cy7Gal and imaged as before.

Immunoblot. To determine the levels of β-Gal protein in control and senescent 4T1 cells, whole-cell extracts were obtained by using lysis buffer (25 mM Tris-HCl pH 7.4, 1 mM EDTA, 1% SDS, plus protease and phosphatase inhibitors). Cell lysates were resolved by SDS-PAGE, transferred to nitrocellulose membranes, blocked with 5% nonfat milk and incubated overnight with antibodies to β-Gal (E2U2I; rabbit mAb #27198; Cell Signaling) and to GAPDH (#14C10; Cell Signaling) as a loading control. Then, membranes were washed and probed with secondary antibodies conjugated to horseradish peroxidase that were detected with an enhanced chemiluminescence detection kit (Amersham Pharmacia Biotech).

Mouse strains, treatments, IVIS® imaging and fluorometer measurements. BALB/cByJ mice were acquired from Charles River laboratories (France) and maintained at the Centro de Investigación Príncipe Felipe (CIPF). SAMR1 and SAMP8 mice, as well as C57BL/6 mice, were housed at the Universitat de València (UV). All mice were bred and housed, under 12 h periods of light/darkness, room temperature of 20-22 °C, and free accessible diet of pellets and water following European Union 2010/63/UE and Spanish RD-53/2013 guidelines and under official veterinary supervision. All animal procedures were approved by the CIPF and UV Ethics Committees for Research and Animal Welfare (CEBA) and conducted in accordance with the recommendations of the Federation of European Laboratory Animal Science Associations (FELASA). For senolytic treatment, a combination of dasatinib (D) and quercetin (Q) was orally administered at different regimens to each mouse model. D (5 mg/kg) and Q (50 mg/ml) were dissolved with 20% PEG-n400 and 0.9% sodium chloride (Xu et al., 2018). 15-m C57BL/6 mice received a 5-week treatment cycle with 2 doses *per* week and were tested for Cy7Gal and behavioral monitoring 15 days after the end of the treatment. On the other hand, 7-m SAMP8 mice received the same drug mixture for consecutive 5 weeks, alternating a regime of 5 or 1 administrations *per* week. In this case, Cy7Gal and behavior monitoring were evaluated in the first 21 and 58 days after the end of treatment. The same cohort of animals received another round of treatment at 10 months of age and were tested only within the first 21 days after the completion of this second cycle of treatment. Breast 4T1 tumors were established by using 4T1 cells in BALB/cByJ mice. Cells were trypsinized, counted with a LUNA™ Automated Cell Counter, and 0.5 x 10^6 cells in a volume of 100 µl were injected subcutaneously in the left mammary fat pad of 28- to 34-week-old BALB/cByJ female mice. Palbociclib dissolved in 50 mM sodium lactate (pH 4) was administered at different doses by daily oral gavage for 7 days. Tumor volume was measured every two days with a caliper and calculated as $V = (a \times b^2)/2$, where a is the longest and b is the shortest of two perpendicular diameters. Mice were anesthetized by inhalation of 2% isoflurane and intraperitoneally (i.p.) injected with Cy7Gal (23.3 mg/ml; 100 µl, 2.5 µmol

per mice) or WOS-Cy7Gal (19.7 mg/ml; 100 µl, 2.5 µmol *per* mice) and maintained in an IVIS® spectrum (Perkin Elmer) for 15 min taking photographs every 2 min (λ_{exc}= 535 nm; λ_{em}= 640 nm; exposure time: 10s). Urine was collected after mice recovered from anesthesia in an Eppendorf tube and analyzed directly by IVIS® (λ_{exc}= 535 nm; λ_{em}= 640 nm; exposure time: 1s). Radiant efficiency quantification in images obtained from whole animals was performed in the regions of interest (ROIs) manually delimited using the software of Live Imaging from Caliper Life Sciences. Moreover, urine fluorescence was analyzed with a fluorometer (JASCO FP-8500). For this purpose, 5 µl of urine was diluted in 95 µl of distilled water and fluorescence was recorded at (λ_{exc}= 535 nm; λ_{em}= 560 nm). The amount of Cy7 fluorophore excreted in urine was calculated through a calibration curve. For the calibration curve, a stock solution of Cy7 in blank urine from mouse was prepared. Serial dilutions were prepared with the same urine and 5 µl of each Cy7 urine solutions was added to 95 µl of distilled water and measured in the fluorometer under the same conditions. In order to assess the biodistribution of the fluorophores from the Cy7Gal and WOS-Cy7Gal probes, fluorescence was measured in urine and plasma. Plasma samples were obtained 10 min after the probe or vehicle injection by submandibular puncture of mice with a 25G needle. Blood was collected in heparinized tubes and, subsequently, these samples were centrifuged at 350 g for 4 min and the supernatant (plasma) was collected. From each plasma sample 10 µl was diluted in 90 µl of distilled water and fluorescence reading was performed in the fluorometer (λ_{exc}= 535 nm; λ_{em}= 560 nm). For the calibration curve, a stock solution of Cy7 in blank plasma from mouse was prepared. Serial dilutions were prepared in the same plasma and 10 µl of each Cy7 urine solution was added to 90 µl of distilled water and measured in the fluorimeter under the same condition. Mice were immediately euthanized after collecting the urine by CO_2 exposure, and tumors and organs (lungs, liver, kidney, spleen, brain and bladder) were immediately harvested and freshly analyzed by IVIS® (λ_{exc}= 535 nm; λ_{em}= 640 nm; exposure time: 1s). Fluorescence images were taken on an IVIS® spectrum imaging system and analyzed and quantified by establishing ROIs and measuring the radiant efficiency associated to each one using the Live Imaging software from Caliper Life Sciences. On the other hand, when analyzing mice of different age and strain, the dose of Cy7Gal administered was adjusted to the body weight of each animal (140 mg/kg). After injection, all animals were anesthetized with isoflurane for 15 min and, upon awakening, urine samples were collected individually. Because the volume of micturition may vary between young and old animals, we measured in a fluorometer (Horiba Scientific Fluoromax-4) the counts *per* second (CPS or arbitrary units) of a 1/20 dilution in distilled water of 5 µl of the collected urine and the resulting units were multiplied by the total volume of urine collected in each sample

HPLC-MS. HPLC-MS measurements were obtained using an eluent gradient method from H2O-methanol (100:0 v/v) to H_2O-methanol (0:100 v/v) at 10 min with a flow rate of 0.5 ml/min with a kromasil C18 column. Mass spectroscopy chromatograms were recorded with an Agilent Ultivo mass spectrometer equipped with a triple Q-TOF detector using a dual selected ion monitoring (SIM) function at 1034 m/z and 705 m/z simultaneously, corresponding to the Cy7Gal and Cy7 fluorophores, respectively. The calibration curve was obtained by measuring known concentrations of the Cy7Gal probe and Cy7 fluorophore in H_2O using the dual SIM method. The amount of Cy7Gal and Cy7 fluorophore excreted was calculated by measuring 5 µl of urine sample diluted in 500 µl H_2O and multiplying the corresponding concentration, obtained with the calibration curve, by the volume of urine collected for each sample. The percentage of probe or dye excreted in the urine was obtained by relating it to the amount of Cy7Gal injected.

Histology. Tumors were fixed with 4% PFA in PBS for 4 h, embedded in paraffin, sectioned at 5 µm and mounted onto pre-coated slides. Sections were dewaxed, incubated with the primary antibody Ki67 (Cell Signaling, at 1:800) and then with the corresponding peroxidase-conjugated secondary antibody in an automated immunostaining platform (Leica Microsistems Bond RXm). After the peroxidase detection, the sections were counterstained with hematoxylin, dehydrated, and coverslipped. In some animals, tumors together with kidneys and liver were extracted at the endpoint and snap-frozen in liquid nitrogen. Next, the

samples were embedded in OCT and sectioned with a cryostat at 7 µm thickness. Sections were used for the detection of SA-β-Gal with the X-Gal histochemical reaction as previously reported[55].

Cytometry. For *ex vivo* assessment of senescence burden, 7-m SAMP8 and SAMR1 mice were euthanized by cervical dislocation and the right kidney and a piece of the right lobe of the liver were extracted. These tissues were subjected to enzymatic digestion with a mixture of 1 mg/ml collagenase/dispase (Roche) and 0.2 mg/ml DNAse (Labclinics) diluted in 2 ml RPMI *per* sample. Tissue enzymatic dissociation was performed using a gentleMACS™ Octo Dissociator with heaters (Miltenyi). Next, the digested tissue pieces were mechanically dissociated and filtered through a 40 µm nylon filter to obtain a single cell suspension. In order to avoid the auto-fluorescence noise of some cells and to target cell populations that are found in many organs, cells were incubated with CD31 and CD45 antibodies (BD Bioscience, BUV-395 and BUV-421, respectively) to label endothelial and immune cells. Thus, the results obtained are the product of the analysis of senescence markers in both populations. For SA-β-Gal detection, a proportion of live cells was incubated with 20 µM of WOS-Cy7Gal for 15 min prior to the flow cytometry assay (BD LSR-Fortessa cytometer) together with 0.1 µg/ml DAPI to exclude dead cells. The remaining cells were fixed and permeabilized using BD Pharmingen™ Transcription-Factor Buffer Set for detection of intranuclear senescent markers. Cells were first incubated with the primary rabbit antibodies to p16 (Abcam, ab211542) or lamin B1 (Abcam, ab16048) and then with secondary anti-rabbit antibodies labeled with Alexa Fluor™ (Invitrogen) and analyzed in LSR-Fortessa cytometer. Similarly, for *in vitro* assessment of senescence, senescent and control hUVECs were permeabilized and fixed, using the same kit, for subsequent immunostaining to p16 and lamin B1 antibodies. Following incubation of cells with secondary antibodies, 20 uM WOS-Cy7Gal was added for 10 min. The cells were then centrifuged and resuspended in blocking buffer (10% Hank's Balance Salt Solution, 10% EDTA, 1% HEPES, sterile H_2O), and the fluorescence levels were evaluated in the LSR-Fortessa flow cytometer. Flow cytometry analysis was carried out with FlowJo_v10.8.1 software.

Behavioral tests. Anxious behavior and general locomotor activity was measured in the open field test using a grey squared Plexiglas open box (50 cm^2) (Panlab, S.L.). Briefly, mice were gently introduced in the open field and videotaped for 10 min in a dim light room to which they have been previously habituated. Periphery/center areas were automatically established by the Smart video tracking software (Panlab, Harvard Apparatus). Trajectory of movement and motor behavior were analyzed. Anxious behavior was also evaluated with a grey Plexiglas elevated plus maze (30 cm L x 5 cm W x 40 cm H) for 5 min as described previously[56].

Statistical analyses. All the statistical analyses were conducted in GraphPad 5.0 (Prism) software. All the sample sizes and statistical tests are specified in the figure legends. The Rout method (Q=5%) was used to identify and exclude outliers. Unpaired two-tailed t-test, one-way or two-way ANOVA were used when appropriate. For each animal experiment, groups were established before tumorigenesis or treatment with Cy7Gal or WOS-Cy7Gal, and therefore no randomization was used in the allocation of groups. Investigators were not blinded to the groups and treatments during the experiments, with the exception of the probe read-out and behavioral tests performance.

Acknowledgments

We acknowledge the support of the Servicio Central de Soporte a la Investigación Experimental of the Universitat de València (SCSIE-UVEG). We are grateful to Biorender.com for the illustrations of mice used in the temporal scheme of the senolytic treatment in figures 5 and 6. We thank Dr. D. Muñoz-Espín for providing us with siRNAs for knock-down experiments and Dr. S. Gil for his assistance in NMR analysis.

Work in the laboratory of R. M.-M was supported by grants from the Spanish Government (RTI2018-100910-B-C41) and the Generalitat Valenciana (PROMETEO 2018/024). Work in the laboratory of I.F. was supported by grants from the Spanish Government (PID2020-117937GB-I00 and CIBERNED) and Generalitat Valenciana (PROMETEO/2021/028). We also acknowledge the financial support from the Spanish Government (SAF2017-84689-R project MINECO/AEI/FEDER, UE) and the Generalitat Valenciana (project PROMETEO/2019/065) to M. O. A.P.V. was also founded by CITSAM (2021-283-001). S. R.-V. (FPU 16/03714) and B.L.-T. (FPU15/02707) have been the recipients FPU predoctoral fellowships from the Spanish Ministerio de Educación; J.F.B. is the recipient of a postdoctoral contract of the Universitat Politècnica de València (PAID-10-17).

Author Contributions

S. R.-V., B. L.-T., J. F. B., F. S., I. F., and R. M.-M. conceived and designed the research. B. L.-T. and J. F. B. synthesized and characterized all organic molecules. J. F. B. performed HPLC studies. S. R.-V. and B. L.-T. carried out all *in vitro* and *in vivo* studies and analyzed the data. A. G.-F., I. G., and M.J. P. assisted with the *in vitro* and *in vivo* experiments. M. O. helped in designing the *in vivo* experiment in the chemotherapy-induced 4T1 breast cancer model. S. R.-V. and A. P.-V. carried out the behavioral analyses, S.R.-V. and P. M.-R. performed the cytometry studies. I.F. and R. M.-M. wrote the manuscript with feedback from all the authors.

Competing Interest Statement

B. L.-T., A. G.-F., I. G., M. O., R. M.-M., F. S, and J. F. B. have filed a patent application related to this research with the “Oficina Española de Patentes y Marcas”. R.M.-M. is co-founder of Senolytic Therapeutics, Inc. (USA) and Senolytic Therapeutics, S.L. (Spain)

Data availability statement

The authors declare that the data supporting the findings of this study are available within the paper and its supplementary information files.

References

1. Urdea, M. et al. Requirements for high impact diagnostics in the developing world. *Nature* 23, 444 (2006).
2. Warrena, A. D., Kwonga, G. A., Woodc, D. K, Linb, K. Y. & Bhatiaa, S. N. Point-of-care diagnostics for noncommunicable diseases using synthetic urinary biomarkers and paper microfluidics. *PNAS* 111(10), 3671-3676 (2014).
3. Kwong, G. A., et al. Mass-encoded synthetic biomarkers for multiplexed urinary monitoring of disease. *Nat. Biotech.* 31 (1), 63-71 (2013).
4. Lin, K. Y., Kwong, G. A., Warren, A. D., Wood, D. K. & Bhatia, S. N. Nanoparticles that sense thrombin activity as synthetic urinary biomarkers of thrombosis. *ACS Nano* 7, 9001-9009 (2013).
5. Huang, J. Li, J. Lyu, Y. Miao, Q. & Pu, K. Molecular optical imaging probes for early diagnosis of drug-induced acute kidney injury. *Nat. Mater.* 18, 1133-1143 (2019).
6. Choi, H. et al. Renal clearance of quantum dots. *Nat. Biotechnol.* 25, 1165-1170 (2007).
7. Loynachan, C. N., et al. Renal clearable catalytic gold nanoclusters for in vivo disease monitoring. *Nat. Nanotech.* 14, 883–890 (2019).
8. Wolfram, J., et al. Safety of nanoparticles in medicine. *Curr. Drug. Targets* 16(14): 1671–1681 (2015).
9. López-Otín, C., Blasco, M. A., Partridge, L., Serrano, M. & Kroemer, G. The hallmarks of aging. *Cell* 153(6), 1194-217 (2013).

10. Herranz, N. & Gil, J. Mechanisms and functions of cellular senescence. *J. Clin. Invest.* 128(4), 1238–1246 (2018).

11. van Deursen, J. M. The role of senescent cells in ageing. *Nature* 509(7501), 439–446 (2014).

12. Muñoz-Espín, D. & Serrano, M. Cellular senescence: from physiology to pathology. *Nat. Rev. Mol. Cell Biol.* 15(7), 482-496 (2014).

13. He, S. & Sharpless, N.E. Senescence in Health and Disease. *Cell* 169(6), 1000-1011 (2017).

14. Xu, M. et al. Senolytics improve physical function and increase lifespan in old age. *Nat. Med*. 24(8), 1246-1256 (2018).

15. Soto-Gamez, A. & Demaria, M. Therapeutic interventions for aging: The case of cellular senescence. *Drug Discov. Today* 22(5), 786-795 (2017).

16. Páez-Ribes, M., González-Gualda, E., Doherty, G. J. & Muñoz-Espín, D. Targeting senescent cells in translational medicine. *EMBO Mol. Med.* 11, e10234 (2019).

17. Lozano-Torres, B. et al. The Chemistry of Senescence. *Nat. Rev. Chem*. 3, 426-441 (2019).

18. González-Gualda, E., Baker, A.G., Fruk, L. & Muñoz-Espín, D. A guide to assessing cellular senescence in vitro and in vivo. *FEBS J*. 288(1), 56-80 (2021).

19. Lozano-Torres, B., et al. An OFF–ON two-photon fluorescent probe for tracking cell senescence *in vivo*. *J. Am. Chem. Soc.* 139, 8808-8811 (2017).

20. Ferrucci, L. et al. Measuring biological aging in humans: A quest. *Aging Cell* 19(2), e13080 (2020).

21. Karton-Lifshin, N. et al. A unique paradigm for a turn-on near-infrared cyanine-based probe: Non-invasive intravital optical imaging of hydrogen peroxide. *J. Am. Chem. Soc.* 133, 10960-10965 (2011).

22. Lozano-Torres, B., Blandez, J.F., Sancenón, F. & Martínez-Máñez, R. Chromo-Fluorogenic Probes for β-Galactosidase Detection. *Anal. Bioanal. Chem* 413(9), 2361–88. (2021).

23. Nishijima, K. et al. Synthesis and diuretic activity of 2,3-dihydro-4(1H)-quinolinone 4-oxime-O-sulfonic acid derivatives. *Eur. J. Med. Chem.* 33 (4), 267-277 (1998).

24. Estepa-Férnandez, A. et al. Senolysis reduces senescence in veins and cancer cell migration. *Adv. Ther*. 4(10), 2100149 (2021).

25. Belsky, D. W. et al. Quantification of biological aging in young adults. *PNAS* 112(30), 4104-4110 (2015).

26. Galiana, I. et al. Preclinical antitumor efficacy of senescence-inducing chemotherapy combined with a nanoSenolytic. *JCR*. 323, 624-634 (2020).

27. Bollard, J. et al. Palbociclib (PD-0332991), a selective CDK4/6 inhibitor, restricts tumour growth in preclinical models of hepatocellular carcinoma. Gut. 66(7), 1286–1296 (2017).

28. Childs, B. G., Durik, M., Baker, D. J. & van Deursen, J. M. Cellular senescence in aging and age-related disease: from mechanisms to therapy. *Nat Med.* 21(12), 1424–1435 (2015).

29. Whittaker, S. R., Mallinger, A., Workman, P. & Clarke, P. A. Inhibitors of cyclin-dependent kinases as cancer therapeutics. *Pharmacol. Ther.* 173, 83-105 (2017).

30. Jost, T., Heinzerling, L., Fietkau, R., Hecht, M. & Distel, L.V. Palbociclib induces senescence in melanoma and breast cancer cells and leads to additive growth arrest in combination with irradiation. *Front Oncol.* 11, 740002 (2021).

31. Aghali, A., Koloko Ngassie, M.L., Pabelick, C.M., Prakash, Y.S. Cellular Senescence in Aging Lungs and Diseases. *Cells* 11(11), 1781 (2022).

32. Piechota, M. et al. Is senescence-associated β-galactosidase a marker of neuronal senescence? *Oncotarget* 7(49), 81099-81109 (2016)

33. Guerrero, A., De Strooper, B. & Arancibia-Cárcamo, I.L. Cellular senescence at the crossroads of

inflammation and Alzheimer's disease. *Trends Neurosci.* 44(9), 714-727 (2021).

34. Rojas-Vázquez, S., Blasco-Chamarro, L., López-Fabuel, I., Martínez-Máñez, R. & Fariñas, I. Vascular Senescence: A Potential Bridge Between Physiological Aging and Neurogenic Decline. *Front Neurosci*. 15, 666881 (2021).

35. Yamazaki, Y. et al. Vascular Cell Senescence Contributes to Blood-Brain Barrier Breakdown. *Stroke* 47(4), 1068-1077 (2016).

36. Meneton, P., Ichikawa, I., Inagami, T. & Schnermann, J. Renal physiology of the mouse. *Am J Physiol Renal Physiol*. 278(3), F339-351 (2000).

37. Yanai, S. & Endo, S. Early onset of behavioral alterations in senescence-accelerated mouse prone 8 (SAMP8). Behav Brain Res. 15(308), 187-195 (2016).

38. Abe, Y., Yuasa, M., Kajiwara, Y. & Hosono, M. Defects of immune cells in the senescence-accelerated mouse: a model for learning and memory deficits in the aged. *Cell. Immunol.* 157(1), 59-69 (1994).

39. Zhang, N., Chow, S. K. H., Leung, K. S., Lee, H. H. & Cheung, W. H. An animal model of co-existing sarcopenia and osteoporotic fracture in senescence accelerated mouse prone 8 (SAMP8). *Exp Gerontol.* 15(97), 1-8 (2017).

40. Akiguchi I. et al. SAMP8 mice as a neuropathological model of accelerated brain aging and dementia: Toshio Takeda's legacy and future directions. *Neuropathology* 37, 293–305 (2017).

41. Higuchi, K. Hosokawa, M. Takeda, T. Senescence-accelerated mouse. *Meth. Enzymol.* 309, 674-686 (1999).

42. Carter, T. A. et at. Mechanisms of aging in senescence-accelerated mice. *Genome Biol* 6(6), R48 (2005).

43. Pallàs, M. Senescence-Accelerated Mice P8: A tool to study brain aging and alzheimer's disease in a mouse model. *ISRN Cell Biol*., 917167, 1-12 (2012).

44. Wissler Gerdes, E.O., Zhu, Y., Tchkonia, T. & Kirkland, J.L. Discovery, development, and future application of senolytics: theories and predictions. *FEBS J.* 287(12), 2418-2427.

45. Zhang, P. et al. Senolytic therapy alleviates Aβ-associated oligodendrocyte progenitor cell senescence and cognitive deficits in an Alzheimer's disease model. *Nat Neurosci.* 22(5), 719-728 (2019).

46. Ota, H., & Kodama, A. Dasatinib plus quercetin attenuates some frailty characteristics in SAMP10 mice. *Sci Rep*. 12(1), 2425 (2002).

47. Shoji, H., Takao, K., Hattori, S. & Miyakawa, T. Age-related changes in behavior in C57BL/6J mice from young adulthood to middle age. *Mol Brain*. 9, 11 (2016).

48. Pérez-Villalba, A. & Fariñas, I. Behavioral evaluation of aging in experimental animals. In: "Assessments, Treatments and Modeling in Aging and Neurological Disease. The Neuroscience of Aging". (Academic Press, 2021).

49. Ogrodnik, M., et al. Obesity-induced cellular senescence drives anxiety and impairs neurogenesis. *Cell Metab*. 29 (5), 1061-1077.e8.

50. Malerba, H.N. et al. Combined neuroprotective strategies blocked neurodegeneration and improved brain function in senescence-accelerated Mice. *Front Aging Neurosci.* 13:681498 (2021).

51. Ginsburg, G. S. & Phillips, K. A. Precision medicine: From science to value. *Health Aff (Millwood)* 37(5), 694–701 (2018).

52. Khanna, P. & Walt, D. R. Salivary diagnostics using a portable point-of-service platform: A Review. *Clin Ther*. 37(3), 498–504 (2015).

53. Sanjay, S. T. et al. Biomarker detection for disease diagnosis using cost-effective microfluidic platforms. *Analyst.* 140(21), 7062–7081 (2015).

54. Zhang, J. et al. Fluorogenic probes for disease-relevant enzymes. *Chem. Soc. Rev.* 48, 683-722 (2019).

55. Debacq-Chainiaux, F., et al. Protocols to detect senescence-associated beta-galactosidase (SA-βgal) activity, a biomarker of senescent cells in culture and *in vivo*. *Nat Protoc* 4, 1798–1806 (2009).

56. Walf, A.A. & Frye, C.A. The use of the elevated plus maze as an assay of anxiety-related behavior in rodents. *Nat Protoc*. 2(2), 322-328 (2007).

Figure Legends

Figure 1. ***Design, synthesis and validation of WOS-Cy7Gal for SA-β-Gal activity detection.*** **a,** Synthetic route used for the preparation of the WOS-Cy7Gal probe. **b,** X-Gal histochemical staining (left) and confocal images of WOS-Cy7Gal (right) in hUVECs, treated with the senescence-inducing drug palbociclib (senescent) or not (control), for the determination of SA-β-Gal activity. **c,** Phenotypic characterization of senescence in hUVECs by immunocytochemical detection of senescence-associated markers. Note that senescent hUVECs showed a marked decrease in proliferation with lower Ki67 levels, a significant increase in the levels of p21 and DNA damage foci γH2AX, as well as a loss of lamin B1. **d,** Quantification of WOS-Cy7Gal-associated median fluorescence intensity (MFI) in control and senescent hUVECs by flow cytometry. **e**, Confocal images of control and senescent hUVECs labeled with lamin B1 and WOS-Cy7Gal. Notice that senescent cells displayed lower fluorescence levels of lamin B1 and higher of the Cy7 fluorophore, compared to control ones. **f**, Confocal images of control and senescent hUVECs labeled with p16 and WOS-Cy7Gal. Observe that senescent cells showed a brighter signal for both markers compared to control ones. **g**, Flow cytometry histogram of the MFI of probe-released Cy7 and of p16, comparing control and senescent hUVECs. **h**, Percentage of $p16^{-/+}$ senescent cells and flow cytometry histogram of WOS-Cy7Gal-associated MFI within these two cell populations. It is worth noting that the highest levels of fluorescence related to WOS-Cy7Gal corresponds to $p16^{+}$ cells. The graphs show the mean ± SEM. Unpaired Student's t-test was used for statistical analysis. The number of independent biological samples (represented as dots) used and the exact p-values are indicated in the graphs. Images scale bar: 100 μm.

Figure 2. ***In vivo SA-β-Gal selectivity and renal clearance of the Cy7Gal probe.*** **a,** Synthetic route used for the preparation of the Cy7Gal probe, carrying sulfonic groups. **b,** At the top, *in vivo* IVIS® imaging of Cy7Gal-associated fluorescence in bladders of BALB/cByJ female mice bearing 4T1 mammary tumors and orally treated with palbociclib (0, 10, 50, 100 mg/kg), compared to mice treated with the highest dose of palbociclib but non-injected with the probe. At the bottom, the same animal model injected with the WOS-Cy7Gal probe, comparing those receiving 100 mg/kg of palbociclib to untreated mice. **c,** IVIS® readout of Cy7 radiant efficiency ROIs in urine from mice under the conditions described in **b**. Note that the level of fluorescence increases in bladders as a function of palbociclib dose. The fold-change refers to untreated Cy7Gal-injected mice. **d,** Quantification of the amount (μmol) of Cy7 fluorophore excreted in urine after i.p. injection of Cy7Gal, using a calibration curve. **e,** Quantification of the fluorophore recovered after i.p. injection of Cy7Gal or WOS-Cy7Gal in urine and plasma from mice bearing 4T1 tumors and treated or not with palbociclib (100 mg/kg). See that only the probe carrying sulfonic groups is rapidly recovered in urine. **f,** *Ex vivo* IVIS® spectrum imaging of bladders, tumors and kidneys from breast tumor-bearing mice, treated or not with 100 mg/kg of palbociclib, after WOS-/Cy7Gal i.p. injection. **g,** Readout of WOS-/Cy7Gal-associated fluorescence with IVIS® of the organs and experimental conditions exposed in image **f.** Fluorescence or radiant efficiency associated with each ROI is measured in arbitrary units (a.u.). Values are expressed as mean ± SEM. The number of independent biological samples (represented as dots) used are

indicated in the graphs with the exception of **f** (n=3). *p-value<0.05, ***p-value<0.001, ****p-value<0.0001, in one-way ANOVA and Tukey's multiple comparison post-hoc test for statistical analysis.

Figure 3. ***Cy7Gal-based monitoring of age-related senescence in vivo during natural and accelerated aging*****. a,** *In vivo* IVIS® spectrum imaging of bladders from 2- and 14-m BALB/cByJ mice injected or not with the Cy7Gal probe. **b,** IVIS® readout of Cy7 fluorescence in urine from 2- *vs*. 14-m BALB/cByJ mice. **c,** Fluorometer readout of Cy7Gal-associated fluorescence in the urine of 3- and 15-m C57BL/6 mice. Note that this value is multiplied by the total volume of urine recovered (a.u. x ml) to avoid variability in micturition between young and old mice that may alter the concentration of the fluorophore in the bladder and the measurement of fluorescence. **d,** Measurement of the percentage of Cy7Gal probe or free Cy7 fluorophore excreted in the urine of 3- *vs*. 15-m C57BL/6 mice by HPLC. **e,** Fluorescence readout of urine and plasma samples from 15-m SAMP8 mice after i.p. injection of WOS-/Cy7Gal compared to vehicle-injected SAMP8 mice using a fluorometer. **f,** Fluorometer measurement of Cy7 fluorescence in the urine of 7-m SAMP8 and SAMR1 mice. Fold-change is calculated relative to SAMR1 mice values. The graphs show the mean ± SEM. Unpaired Student's t-test was used for statistical analysis. The number of independent biological samples (represented as dots) used and the exact p-values are indicated in the graphs.

Figure 4. Cy7 fluorescence in urine of SAM mice correlates with other senescence markers. a, *Ex vivo* flow cytometry analysis of SA-β-Gal activity based on WOS-Cy7Gal-associated MFI in liver and kidney tissues of 7-m SAMP8 and SAMR1 mice and its histogram representation. **b,** *Ex vivo* flow cytometry analysis of p16 MFI in liver and kidney tissues of SAMP8 and SAMR1 mice and representative flow cytometry histogram. **c,** *Ex vivo* flow cytometry analysis of the percentage of lamin $B1^+$ cells in liver and kidney tissues of SAMP8 and SAMR1 mice and representative histogram of lamin B1 MFI. Fold-change is calculated relative to SAMR1 mice organs for each senescence marker. The graphs show the mean ± SEM. Unpaired Student's t-test was used for statistical analysis. The exact p-values and the number of independent biological samples (represented as dots) used are indicated in the graphs.

Figure 5. ***Monitoring of senolytic intervention with the Cy7Gal probe during natural aging*****. a,** Schedule of the senolytic treatment and its monitoring in C57BL/6 mice. 15-m mice received the senolytic drugs D+Q or the vehicle for 5 weeks and, 13 days after senolysis (DAS), the overall β-Gal activity was assessed with Cy7Gal as a measure of senescence burden. Two days later, anxious behavior was examined. **b,** Cy7 fluorescence measurement in the urine of 17-m C57BL/6 treated with D+Q or vehicle. **c,** Representative map of movement in the open field test comparing young (3-m) with old mice (17-m) that were treated or not with senolytic drugs. **d,** Quantification of the percentage of the time that mice spent in the central area (green zone) of the open field, comparing mice aged 3- to 17-m treated with D+Q or vehicle. **e,** Representative map of movement in the EPM test comparing young (3-m) to old (17-m) mice that were treated with vehicle or senolytic drugs. **f,** Quantification of the percentage of time that mice spent in the open arm of the EPM, comparing of 3- and 17-m mice that were treated or not with D+Q. **g,** Significant linear correlation between Cy7 fluorescence in urine and the percentage of time spent in the center of the open field in mice treated with D+Q or vehicle. **h,** Significant linear correlation between Cy7 fluorescence in urine and the percentage of time spent in the open arm of the EPM test in mice treated with D+Q or vehicle. Fold-change refers to Cy7 fluorescence levels in the urine of untreated mice in both correlation graphs. Graphs represent mean ± SEM. Unpaired Student's t-test was used for statistical analysis of the Cy7Gal fluorescence readout, one-way ANOVA for the assessment of anxious behavior and multiple linear regression to determine the relationship equation between both. Exact p-values and the number of independent biological samples (represented as dots) are showed in the graphs.

Figure 6. ***Monitoring of senolytic treatment with the Cy7Gal probe during accelerated aging*****. a,** Schedule of the senolytic treatment and its monitoring in SAMP8 mice. 7-m mice received a first cycle of oral

treatment with the senolytic drugs D+Q or vehicle, and anxious behavior (open field test) and senescence burden (Cy7Gal) were assessed shortly (15-21 DAS; first cycle, short-term treatment) and long after this treatment (55-58 DAS; first cycle, long-term treatment). In addition, a second cycle was carried out at the age of 10-m and Cy7Gal and behavior were analyzed 15-16 DAS (second cycle, short-term treatment). **b,** Cy7Gal-associated fluorescence measurement of urine samples from SAMP8 mice, administered with D+Q or vehicle, 21 days after the first treatment cycle. **c,** Cy7Gal-associated fluorescence measurement of urine samples from SAMP8 mice, treated or not with D+Q, 58 days after the first treatment cycle. **d,** Readout of Cy7Gal-associated fluorescence in urine samples from SAMP8 mice, treated with D+Q or vehicle, 16 days after the second treatment cycle. **e,** Significant linear correlation found shortly after treatment between the levels of Cy7 fluorescence in urine and the performance in the open field test of mice treated with D+Q or vehicle. **f,** No significant correlation was found between Cy7Gal and anxious behavior when assessed in the long term after the senolytic intervention. Fold-change is calculated relative to Cy7 fluorescence in the urine of untreated mice in all graphs. The graphs represent mean ± SEM. Unpaired Student's t-test was used for statistical analysis and multiple linear regression to determine the equation of relationship between Cy7 fluorescence in urine and the time mice spent in the center of the open field. Exact p-values and the number of independent biological samples (represented as dots) are showed in the graphs.

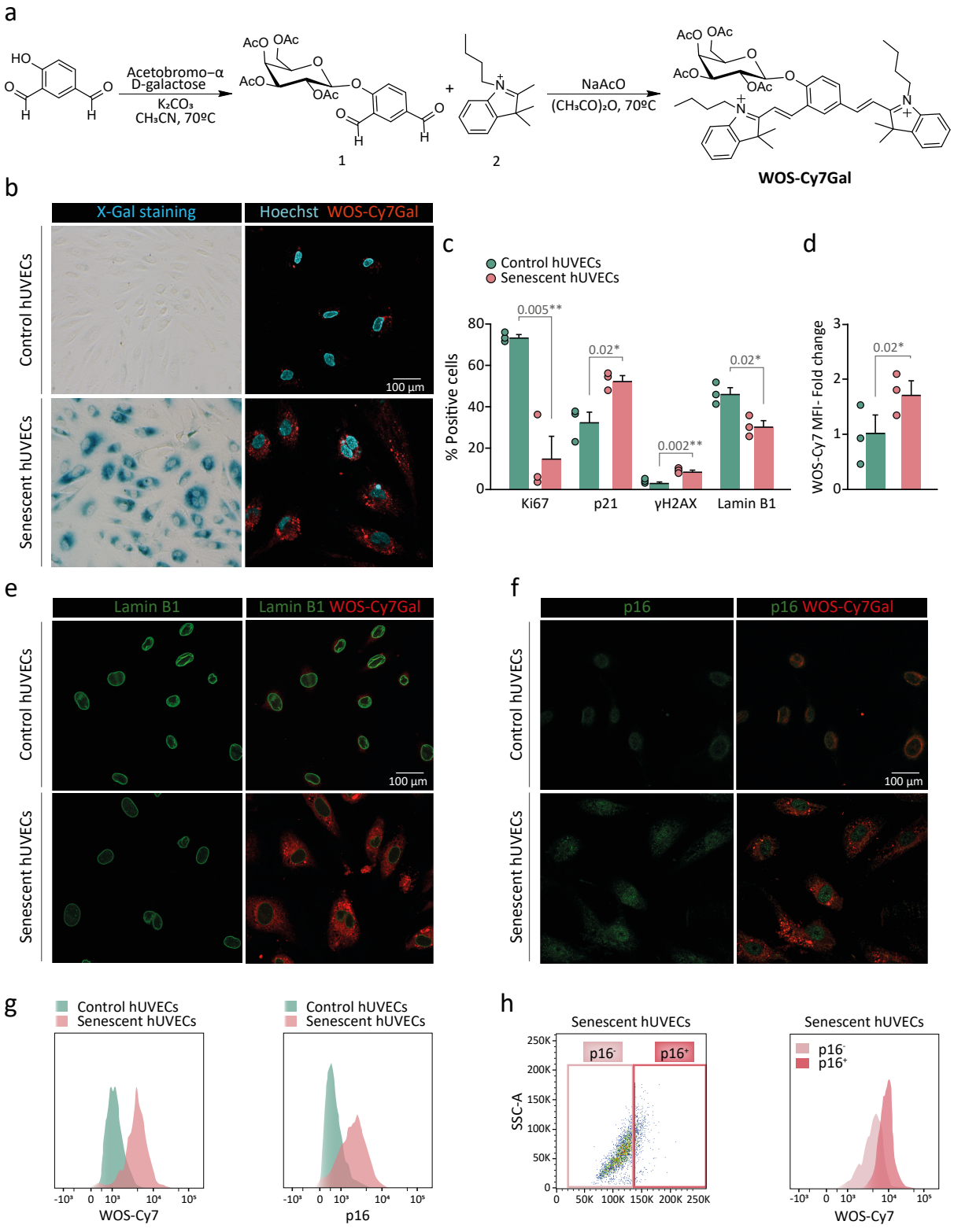
a
Acetobromo−α D-galactose
K2CO3
CH3CN, 70ºC
1
2
NaAcO
(CH3CO)2O, 70ºC
WOS-Cy7Gal
b
X-Gal staining
Hoechst WOS-Cy7Gal
Control hUVECs
Senescent hUVECs
100 µm
c
Control hUVECs
Senescent hUVECs
% Positive cells
0.005**
0.02*
0.02*
0.002**
Ki67
p21
γH2AX
Lamin B1
d
WOS-Cy7 MFI- Fold change
0.02*
e
Lamin B1
Lamin B1 WOS-Cy7Gal
f
p16
p16 WOS-Cy7Gal
g
WOS-Cy7
p16
h
Senescent hUVECs
SSC-A
p16-
p16+

Figure 1.

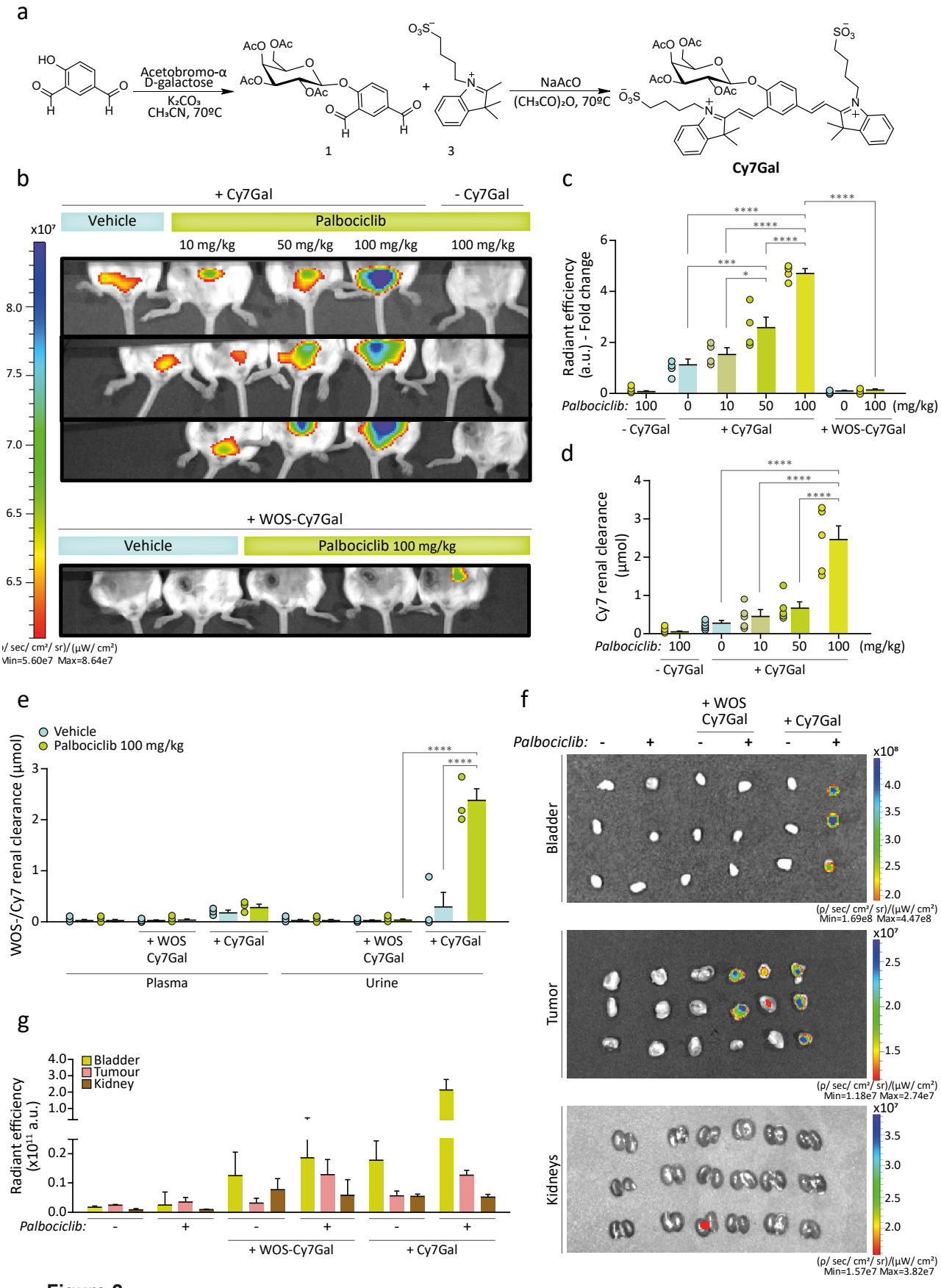
a
Acetobromo-α D-galactose
K2CO3
CH3CN, 70ºC
NaAcO
(CH3CO)2O, 70ºC
1
3
Cy7Gal
b
+ Cy7Gal
- Cy7Gal
Vehicle
Palbociclib
10 mg/kg
50 mg/kg
100 mg/kg
100 mg/kg
+ WOS-Cy7Gal
Vehicle
Palbociclib 100 mg/kg
Vlin=5.60e7 Max=8.64e7
c
Radiant efficiency (a.u.) - Fold change
Palbociclib: 100 0 10 50 100 0 100 (mg/kg)
- Cy7Gal
+ Cy7Gal
+ WOS-Cy7Gal
d
Cy7 renal clearance (µmol)
Palbociclib: 100 0 10 50 100 (mg/kg)
- Cy7Gal
+ Cy7Gal
e
Vehicle
Palbociclib 100 mg/kg
WOS-/Cy7 renal clearance (µmol)
+ WOS Cy7Gal
+ Cy7Gal
Plasma
Urine
f
Palbociclib:
+ WOS Cy7Gal
+ Cy7Gal
Bladder
Tumor
Kidneys
Min=1.69e8 Max=4.47e8
Min=1.18e7 Max=2.74e7
Min=1.57e7 Max=3.82e7
g
Radiant efficiency (x10^11 a.u.)
Bladder
Tumour
Kidney
Palbociclib:
+ WOS-Cy7Gal
+ Cy7Gal

Figure 2.

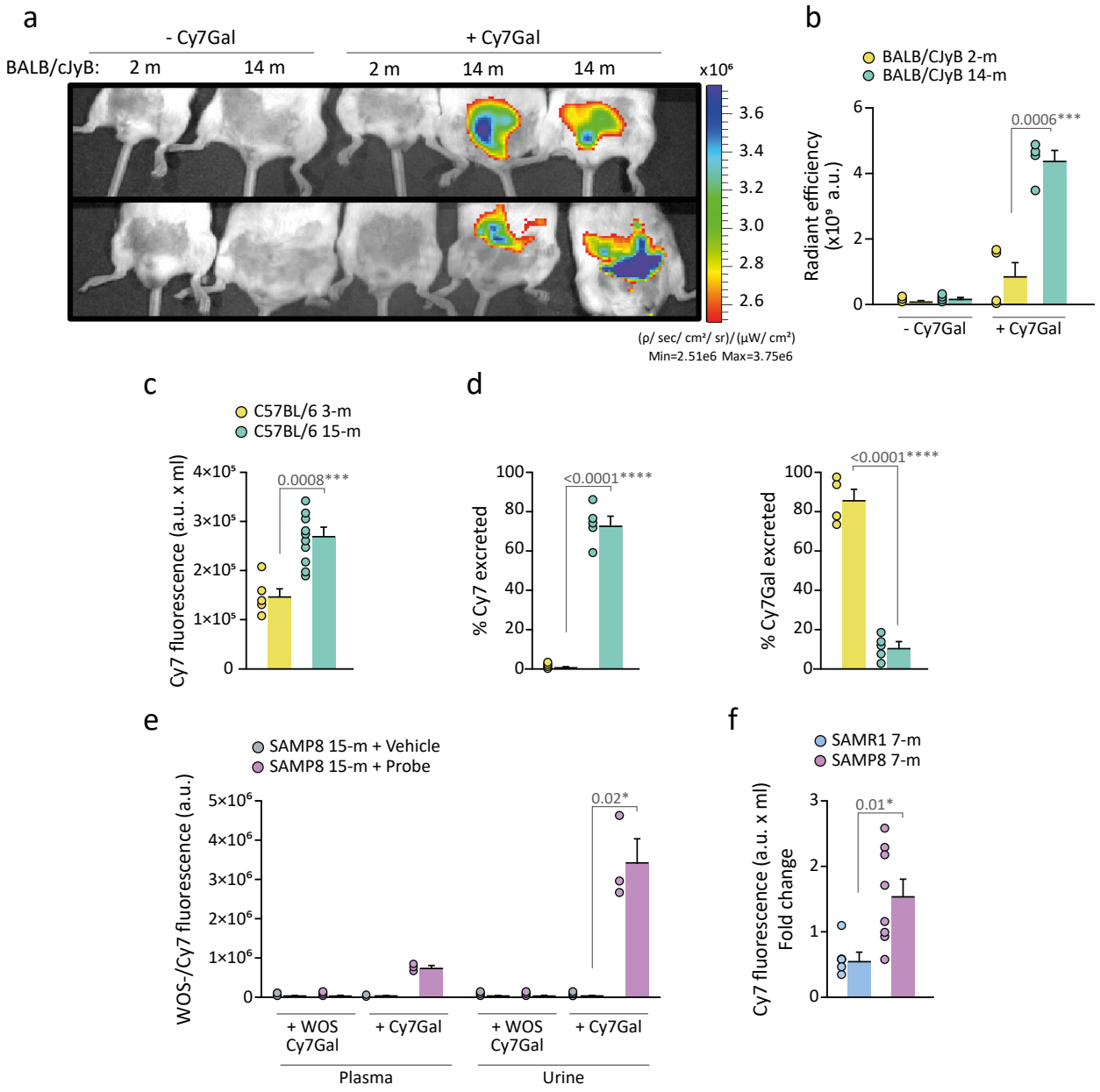
a
- Cy7Gal
+ Cy7Gal
BALB/cJyB:
2 m
14 m
2 m
14 m
14 m
x10⁶
3.6
3.4
3.2
3.0
2.8
2.6
(p/ sec/ cm²/ sr)/(µW/ cm²)
Min=2.51e6 Max=3.75e6
b
BALB/CJyB 2-m
BALB/CJyB 14-m
Radiant efficiency (x10⁹ a.u.)
0.0006***
- Cy7Gal
+ Cy7Gal
c
C57BL/6 3-m
C57BL/6 15-m
Cy7 fluorescence (a.u. x ml)
0.0008***
d
% Cy7 excreted
<0.0001****
% Cy7Gal excreted
<0.0001****
e
SAMP8 15-m + Vehicle
SAMP8 15-m + Probe
WOS-/Cy7 fluorescence (a.u.)
0.02*
+ WOS Cy7Gal
+ Cy7Gal
+ WOS Cy7Gal
+ Cy7Gal
Plasma
Urine
f
SAMR1 7-m
SAMP8 7-m
Cy7 fluorescence (a.u. x ml) Fold change
0.01*

Figure 3.

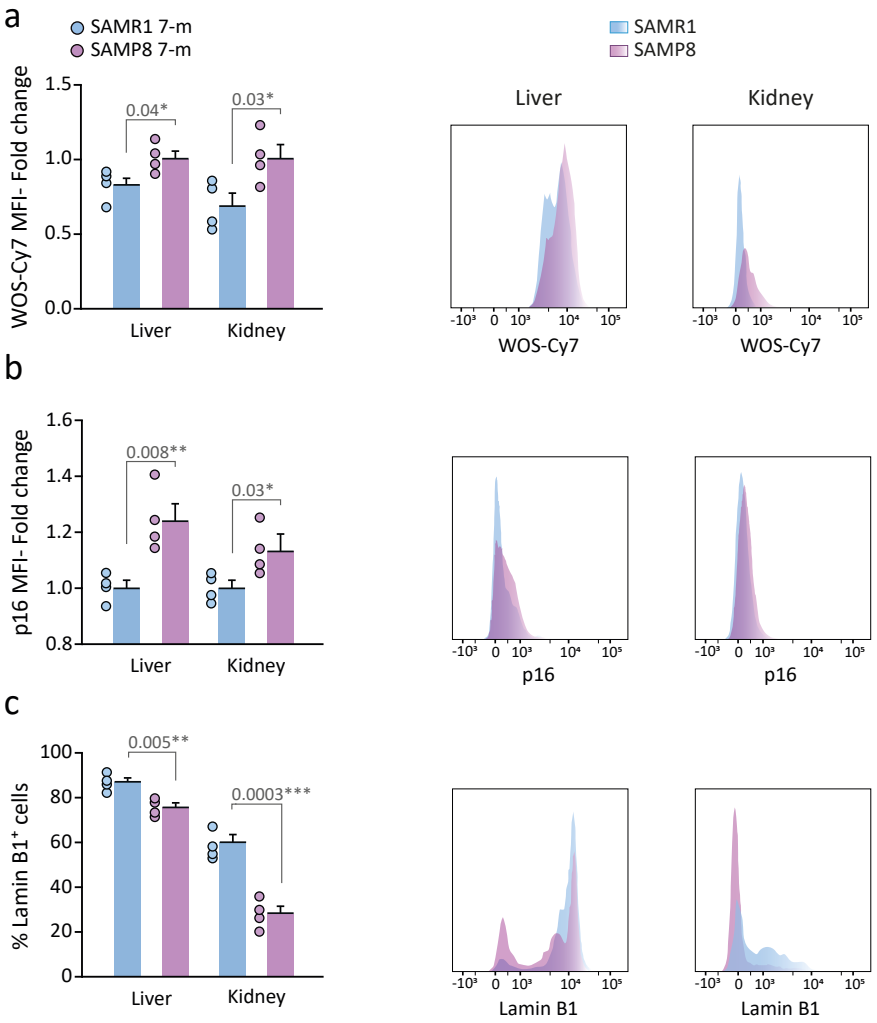
a
SAMR1 7-m
SAMP8 7-m
WOS-Cy7 MFI- Fold change
1.5
1.0
0.5
0.0
0.04*
0.03*
Liver
Kidney
SAMR1
SAMP8
Liver
Kidney
-10³ 0 10³ 10⁴ 10⁵
WOS-Cy7
b
p16 MFI- Fold change
1.6
1.4
1.2
1.0
0.8
0.008**
0.03*
p16
c
% Lamin B1⁺ cells
100
80
60
40
20
0
0.005**
0.0003***
Lamin B1

Figure 4.

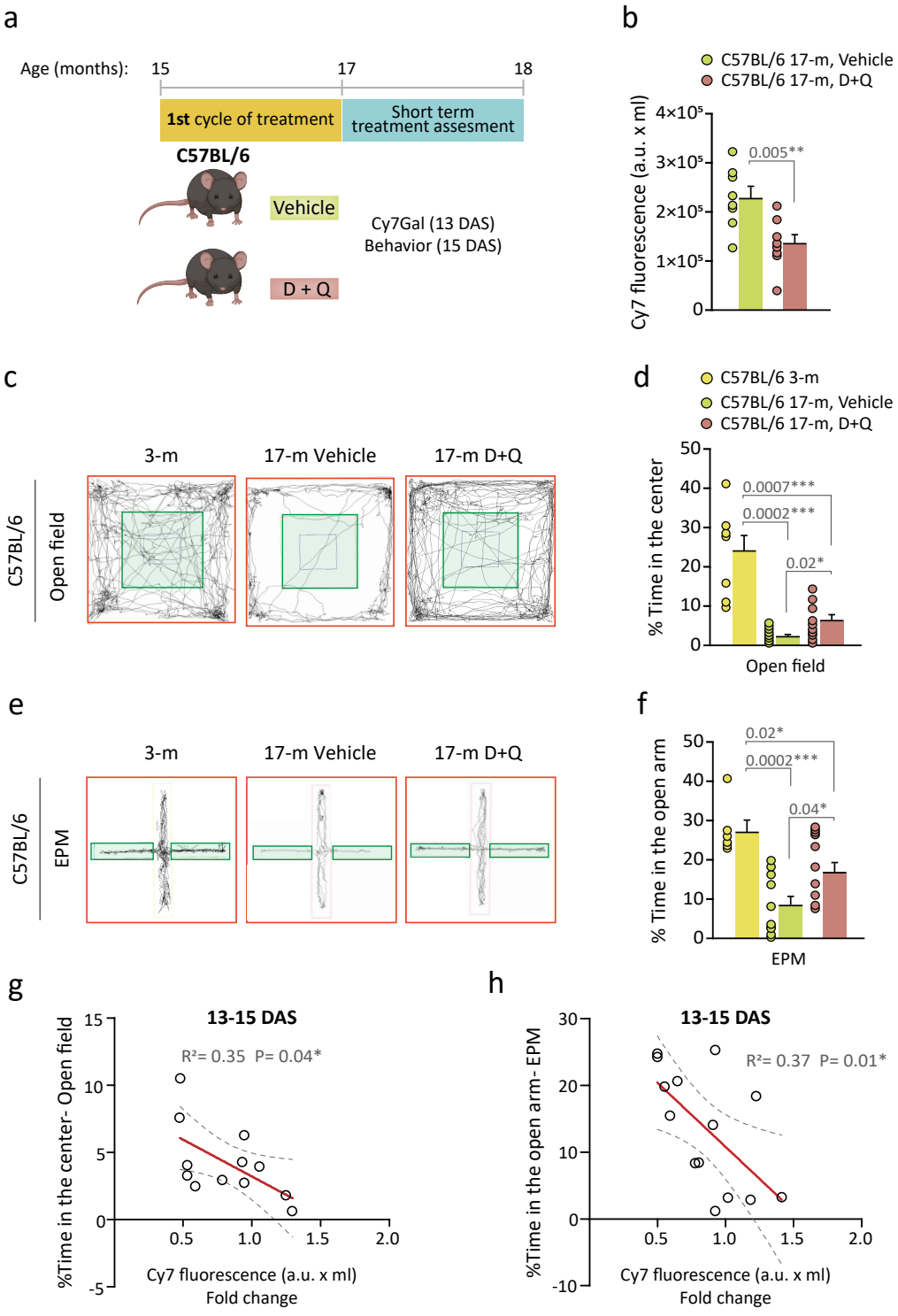
a
Age (months):
15
17
18
1st cycle of treatment
Short term treatment assesment
C57BL/6
Vehicle
D + Q
Cy7Gal (13 DAS)
Behavior (15 DAS)
b
C57BL/6 17-m, Vehicle
C57BL/6 17-m, D+Q
Cy7 fluorescence (a.u. x ml)
4×10⁵
3×10⁵
2×10⁵
1×10⁵
0
0.005**
c
3-m
17-m Vehicle
17-m D+Q
C57BL/6
Open field
d
C57BL/6 3-m
C57BL/6 17-m, Vehicle
C57BL/6 17-m, D+Q
% Time in the center
50
40
30
20
10
0
0.0007***
0.0002***
0.02*
Open field
e
3-m
17-m Vehicle
17-m D+Q
C57BL/6
EPM
f
% Time in the open arm
0.02*
0.0002***
0.04*
EPM
g
13-15 DAS
R²= 0.35 P= 0.04*
%Time in the center- Open field
15
10
5
0
-5
0.5
1.0
1.5
2.0
Cy7 fluorescence (a.u. x ml)
Fold change
h
13-15 DAS
R²= 0.37 P= 0.01*
%Time in the open arm- EPM
30
20
10
0
-10
0.5
1.0
1.5
2.0
Cy7 fluorescence (a.u. x ml)
Fold change

Figure 5.

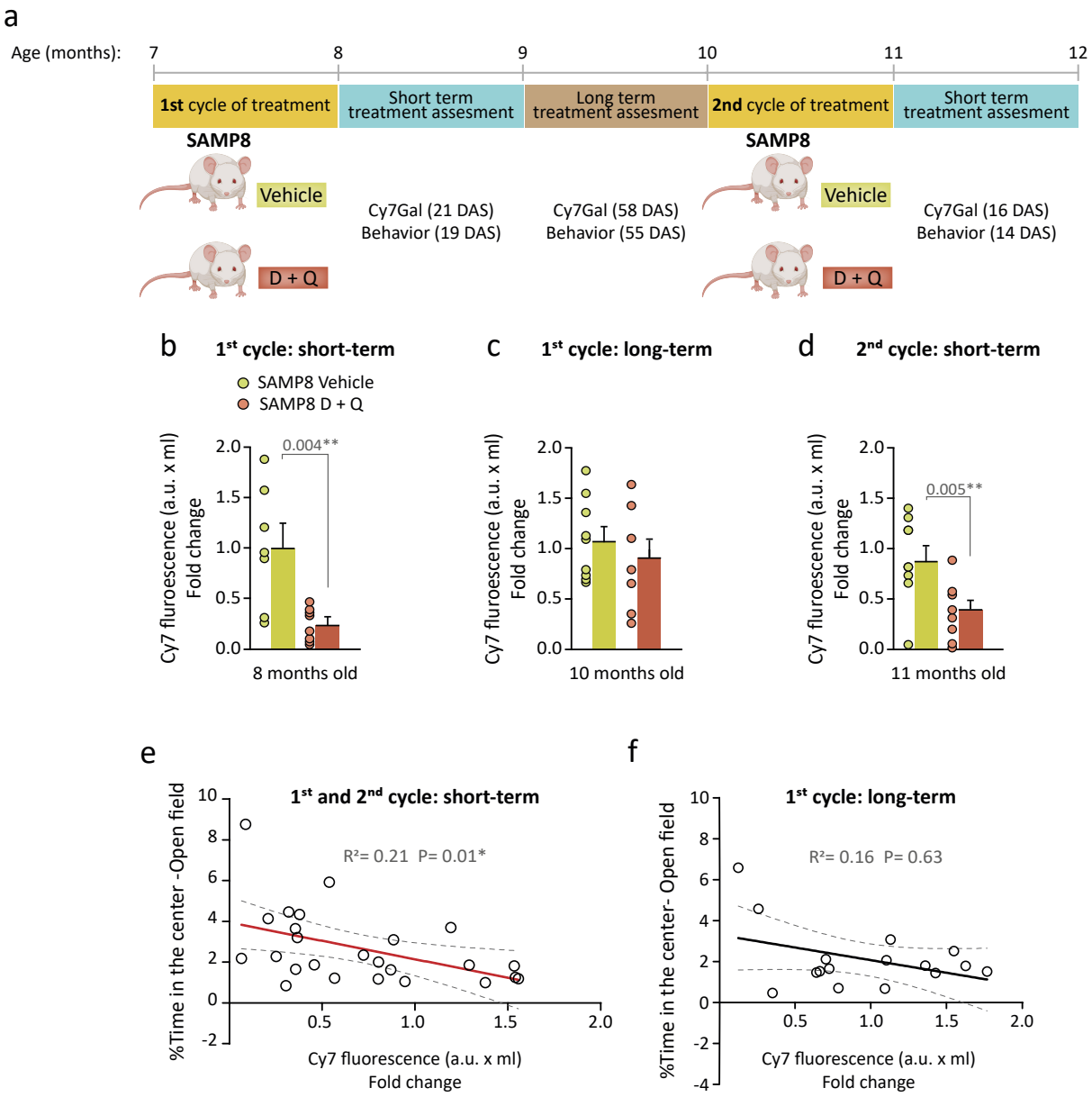
a
Age (months):
7
8
9
10
11
12
1st cycle of treatment
Short term treatment assesment
Long term treatment assesment
2nd cycle of treatment
Short term treatment assesment
SAMP8
Vehicle
D + Q
Cy7Gal (21 DAS)
Behavior (19 DAS)
Cy7Gal (58 DAS)
Behavior (55 DAS)
SAMP8
Vehicle
D + Q
Cy7Gal (16 DAS)
Behavior (14 DAS)
b
1st cycle: short-term
c
1st cycle: long-term
d
2nd cycle: short-term
SAMP8 Vehicle
SAMP8 D + Q
Cy7 fluroescence (a.u. x ml)
Fold change
0.004**
8 months old
10 months old
0.005**
11 months old
e
1st and 2nd cycle: short-term
R²= 0.21 P= 0.01*
%Time in the center -Open field
Cy7 fluorescence (a.u. x ml)
Fold change
f
1st cycle: long-term
R²= 0.16 P= 0.63
%Time in the center- Open field
Cy7 fluorescence (a.u. x ml)
Fold change

Figure 6.

Extended data

A renal clearable fluorogenic probe for the *in vivo* detection of β-galactosidase activity during aging and senolysis

Sara Rojas-Vázquez[1,3,5*], Beatriz Lozano-Torres[1-4*], Alba García-Fernández[1-4], Irene Galiana[1-4], Ana Perez-Villalba[6,7], Pablo Martí-Rodrigo[5,7], M. José Palop[5,7], Marcia Domínguez[1,3], Mar Orzáez[2,8], Félix Sancenón[1-4], Juan F. Blandez[1-4], Isabel Fariñas[5,7] and Ramón Martínez-Máñez[1-4]

[1]Instituto Interuniversitario de Investigación de Reconocimiento Molecular y Desarrollo Tecnológico (IDM), Universitat Politècnica de València-Universitat de València, Spain.

[2]Unidad Mixta UPV-CIPF de Investigación en Mecanismos de Enfermedades y Nanomedicina, Universitat Politècnica de València, Centro de Investigación Príncipe Felipe, Valencia, Spain.

[3]CIBER de Bioingeniería, Biomateriales y Nanomedicina (CIBER-BBN), Spain.

[4]Unidad Mixta de Investigación en Nanomedicina y Sensores. Universitat Politècnica de València, IIS La Fe, Valencia, Spain.

[5]Instituto de Biotecnología y Biomedicina (BIOTECMED), Universitat de València, Spain.

[6]Laboratory of Animal Behavior Phenotype (L.A.B.P.). Facultad de Psicología. Universidad Católica de Valencia, Spain.

[7]Centro de Investigación Biomédica en Red de Enfermedades Neurodegenerativas (CIBERNED), Spain.

[8]Centro de Investigación Príncipe Felipe, Valencia, Spain.

* Equal contribution

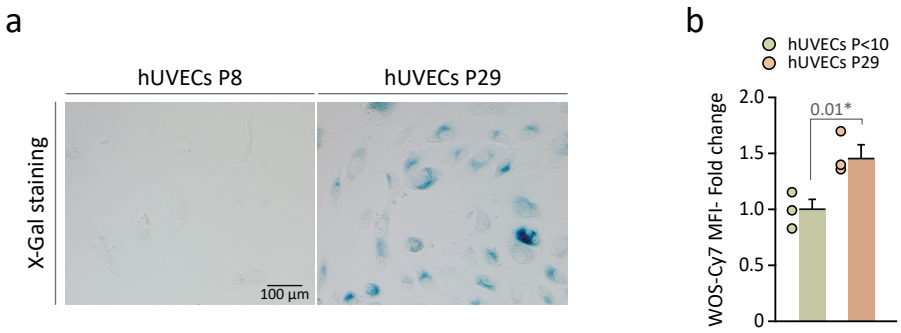

Extended Data Figure 1. WOS-Cy7Gal detects SA-β-Gal activity during replicative senescence. a, X-Gal histochemical staining in hUVECs after being passaged 29 vs. 8 times. **b**, Detection of β-Gal activity in hUVECs passaged either less than 10 times or 29 times by quantifying WOS-Cy7Gal-associated fluorescence using flow cytometry. Unpaired Student's t-test statistical analysis was used to evaluate the detection of SA-β-Gal activity with WOS-Cy7Gal in the replicative senescence model of hUVECs. Images scale bar: 100 µm.

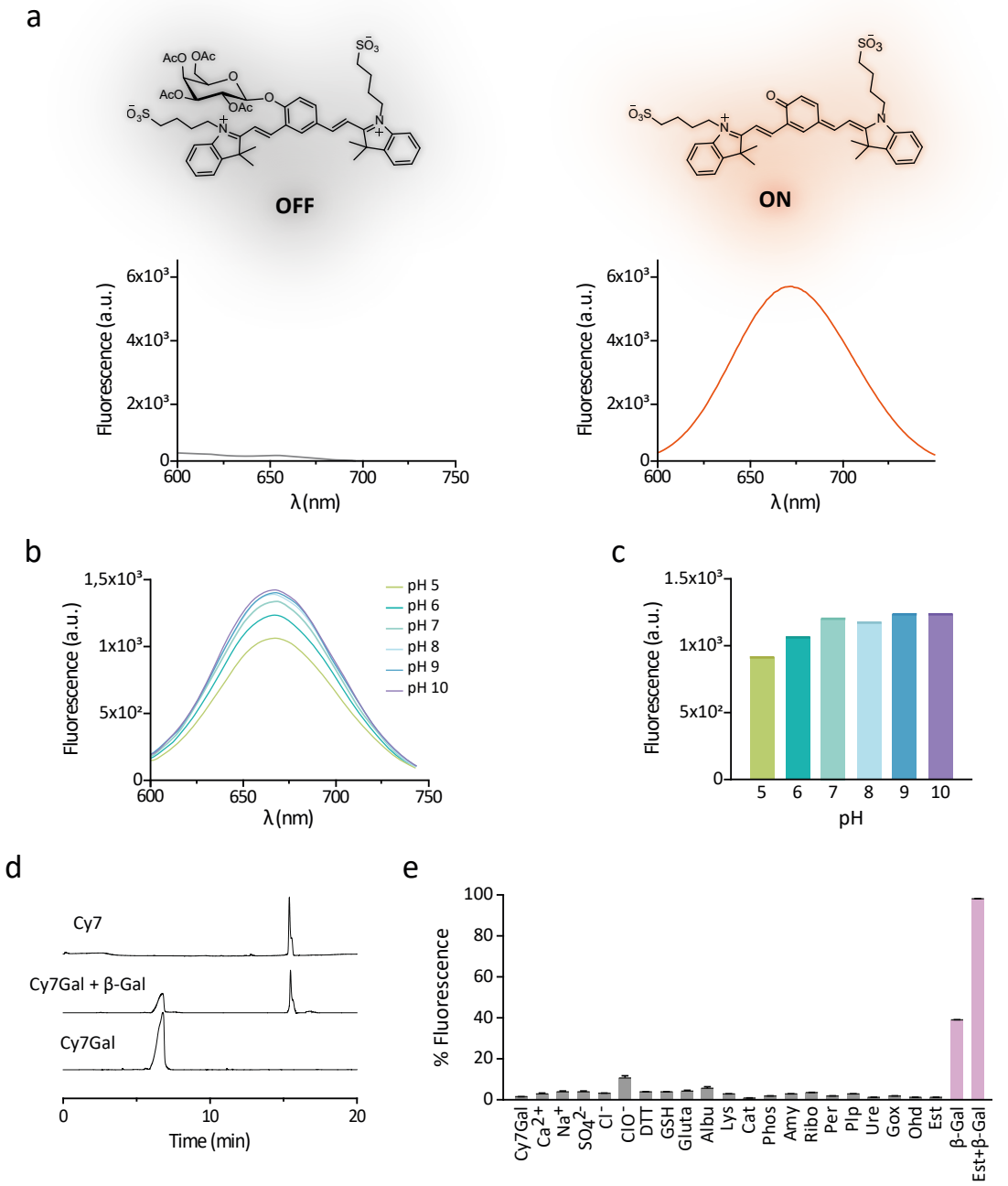

Extended Data Figure 2. Cy7Gal fluorescence emission relies on β-Gal activity. a, Fluorescence emission spectra (λexc = 580 nm) of Cy7Gal (left) and Cy7 fluorophore (right) in aqueous solutions at pH 7. **b**, Fluorescence spectra (λex = 580 nm) of Cy7 (10^{-5} M) H_2O at pH 5, 6, 7, 8, 9 and 10. **c**, Emission intensity at 665 nm (λex = 580 nm) of Cy7 (10^{-5} M) H_2O solutions at pH 5, 6, 7 8, 9 and 10. **d**, Chromatograms of Cy7, Cy7 + β-Gal and Cy7Gal. For hydrolysis studies, aqueous solutions of Cy7 and Cy7Gal at a concentration of 10^{-5} M (pH 7) were prepared. Human β-Gal was then added (5 µl) to Cy7Gal solutions and chromatograms were acquired after 30 min (λabs = 358 nm for Cy7Gal and λabs = 254 nm for Cy7) with a Waters 1525 binary HPLC pump equipped with a Waters 2990 diode array detector. Chromatograms were obtained using Empower 3 software. Conditions: Kromasil-C18 column, 0.8 ml/min, H_2O:MeOH gradient elution: 90:10 to 10:90. Data analysis was performed using OriginPro8 software. **e**, Fluorescence intensity changes of Cy7Gal solutions (20 µM) treated with β-Gal and with

interfering species. From left to right: Blank (only Cy7Gal, 20 μM), Ca^{2+}, Na^{+}, SO_4^{-}, Cl^{-}, ClO^{-}, DTT (DL-dithiothreitol), GSH (γ-L-glutamyl-L-cysteinyl-glycine), Glu (glutamate), Albu (albumin from human serum), Lys (lysozyme from chicken egg white), Cat (catalase from bovine liver), Phos (phosphatase Alkaline from porcine kidney), Amy (alfa-amylase from porcine pancreas), Ribo (ribonuclease A from bovine pancreas), Per (peroxidase from horseradish), Plp (Phosphorylase a from rabbit muscle), Ure (urease from Canavalia ensiformis (Jack bean) Type III), Gox (glucose oxidase from Aspergillus niger), OHd (alcohol dehydrogenase from Saccharomyces cerevisiae), Est (esterase from porcine liver), β-Gal (human β-Gal). Cations (150 μM), anions (150 μM), amino acids (150 μM), proteins (150 μg/mL) and enzymes (150 μg/mL). All measurements were acquired at 37 °C for 0.5 h. The graphs show mean ± SEM in n=3 independent experiments.

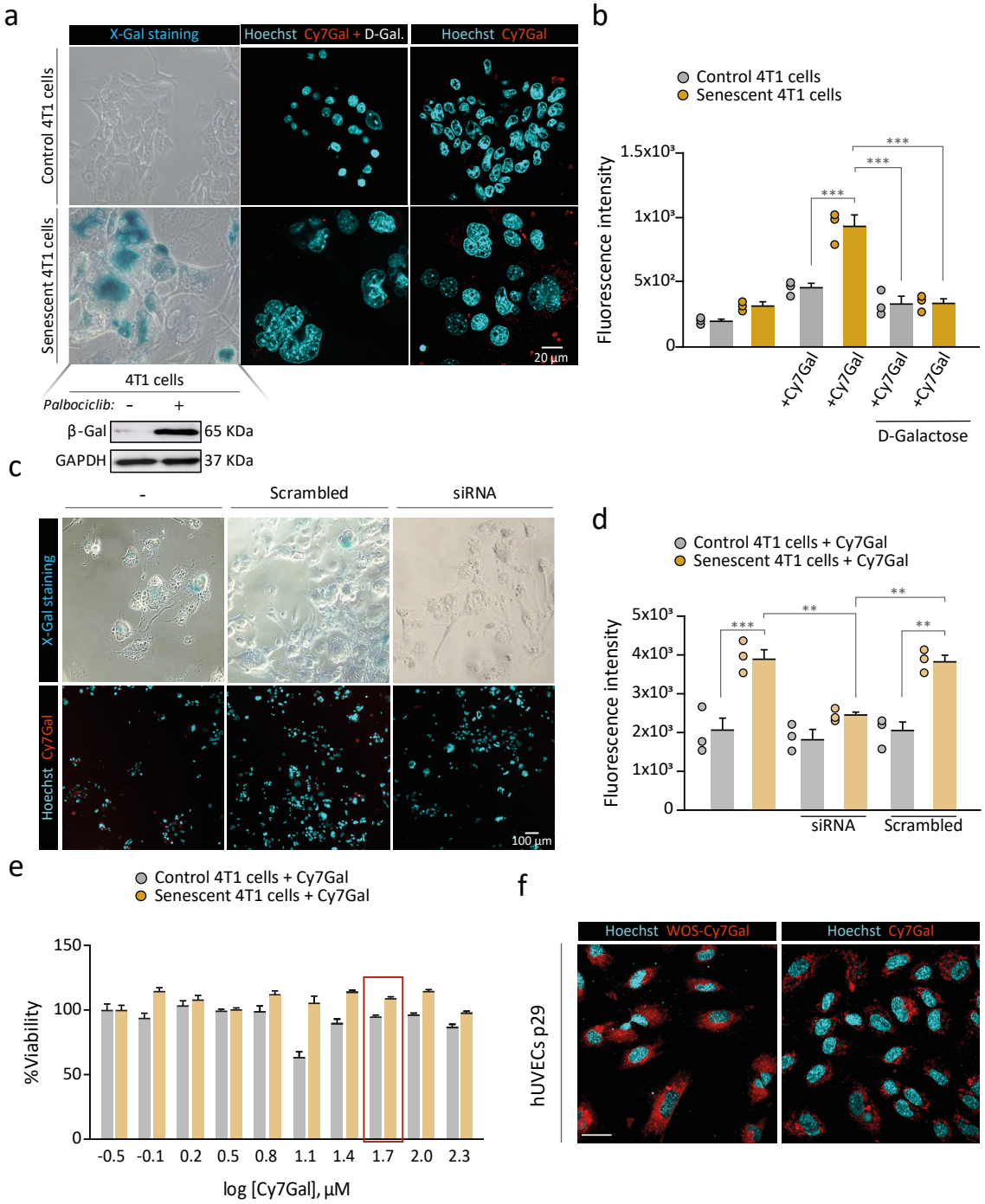

Extended Data Figure 3. Cy7Gal selectively detects SA-β-Gal activity without cytotoxic effects. a, X-Gal histochemistry for SA-β-Gal activity evaluation in control 4T1 cells (top) and palbociclib-treated 4T1 cells (bottom) and determination of β-Gal protein expression by western-blot. Confocal images comparing control 4T1 cells to those treated with palbociclib in the presence of 20 µM Cy7Gal, with and without pre-treatment using a β-Gal enzyme inhibitor (D-galactose). **b**, Quantification of Cy7 dye fluorescence emission intensity from confocal microscopy images of control and palbociclib-treated 4T1 cells. Fluorescence assessment was performed in the absence and presence of 20 µM Cy7Gal, without pre-treating the cells or after pre-treating them with D-galactose. **c**, X-Gal histochemical reaction and confocal imaging with the Cy7Gal probe for the evaluation of SA-β-Gal activity in 4T1 cells treated with palbociclib and exposed to siRNA or scrambled for the *Glb1* gene, encoding the β-Gal enzyme, compared to unexposed (-) cells. **d**, Quantification of fluorescence emission intensity associated with Cy7Gal from confocal images as shown in **c**. **e**, Viability assay of control and senescent 4T1 cells in the presence of Cy7Gal. **f**, Confocal images comparing WOS-Cy7Gal and Cy7Gal signal patterns in

hUVECs passaged 29 times. Note that while WOS-Cy7gal displayed a dotted pattern, Cy7Gal showed a more diffuse one. The graph shows the mean ± SEM. The number of independent biological samples (represented as dots) used are indicated in the graphs with the exception of **e** (n=3). **p-value<0.01, ***p-value<0.001, in one-way ANOVA statistical analysis. Images scale bar: **a** 20 µm, **c** 100 µm.

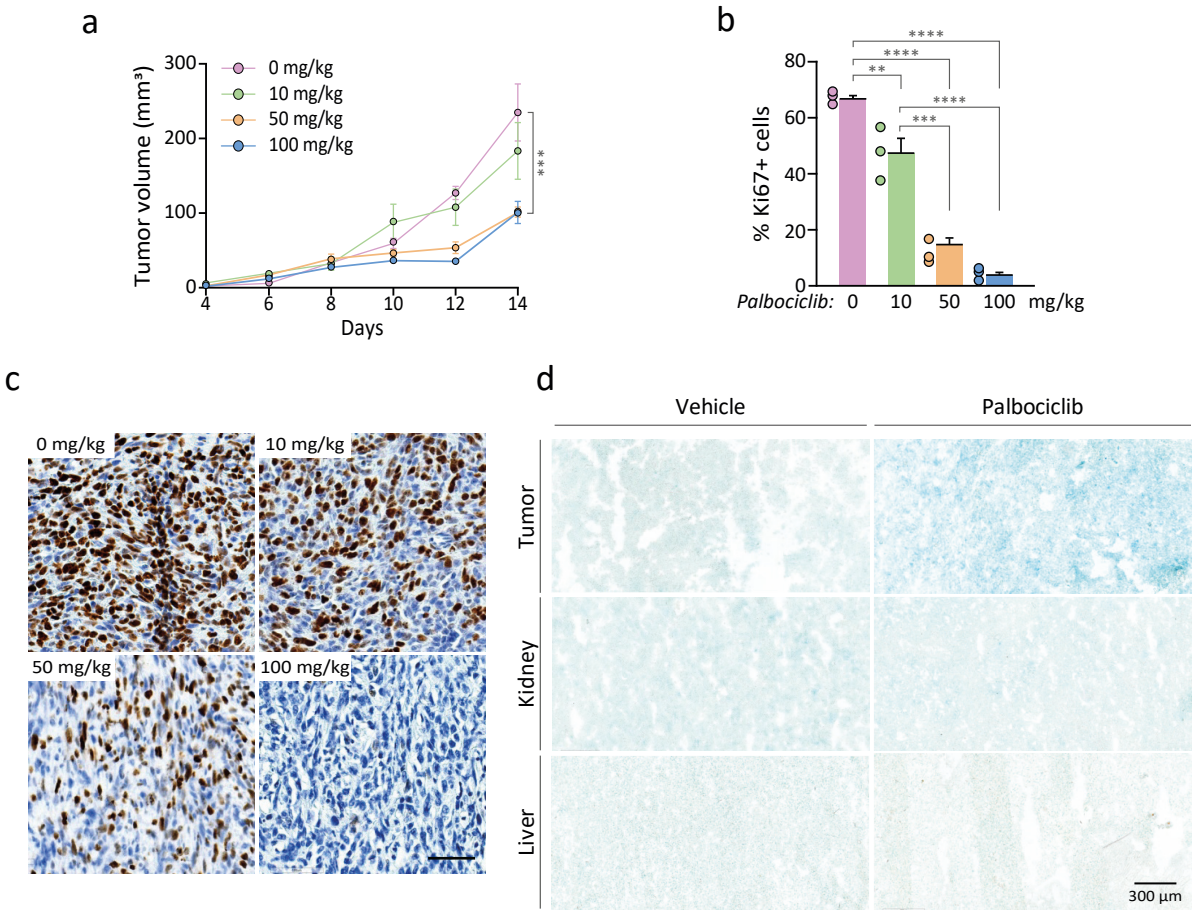

Extended Data Figure 4. Chemotherapy-induction of senescence *in vivo* in a breast cancer animal model. **a**, BALB/cByJ female mice carrying orthotopic 4T1 mammary tumors were treated daily with different doses of palbociclib (oral gavage: 0, 10, 50 or 100 mg/kg). For each tumor, the relative volume change was calculated as V = (a x b²)/2 where a is the longest and b is the shortest of two perpendicular diameters. The graph represents the tumor volume over time (14 days) in palbociclib-treated *vs.* non-treated mice bearing 4T1 tumors. **b**, Quantification of immunohistochemical detection of Ki67 in paraffin sections of tumors. Note that the number of Ki67 positive cells (proliferative cells) decreases as the dose of palbociclib increases. **c**, Images of immunohistochemical detection of Ki67 in paraffin sections of tumors from mice treated with different doses of palbociclib (labeled in the images). **d**, X-Gal staining for SA-β-Gal activity assessment comparing tumors with other organs such as kidneys and liver in vehicle (untreated) or palbociclib-treated mice (100 mg/kg). Images scale bar: **c** 100 µm, **d** 300 µm.

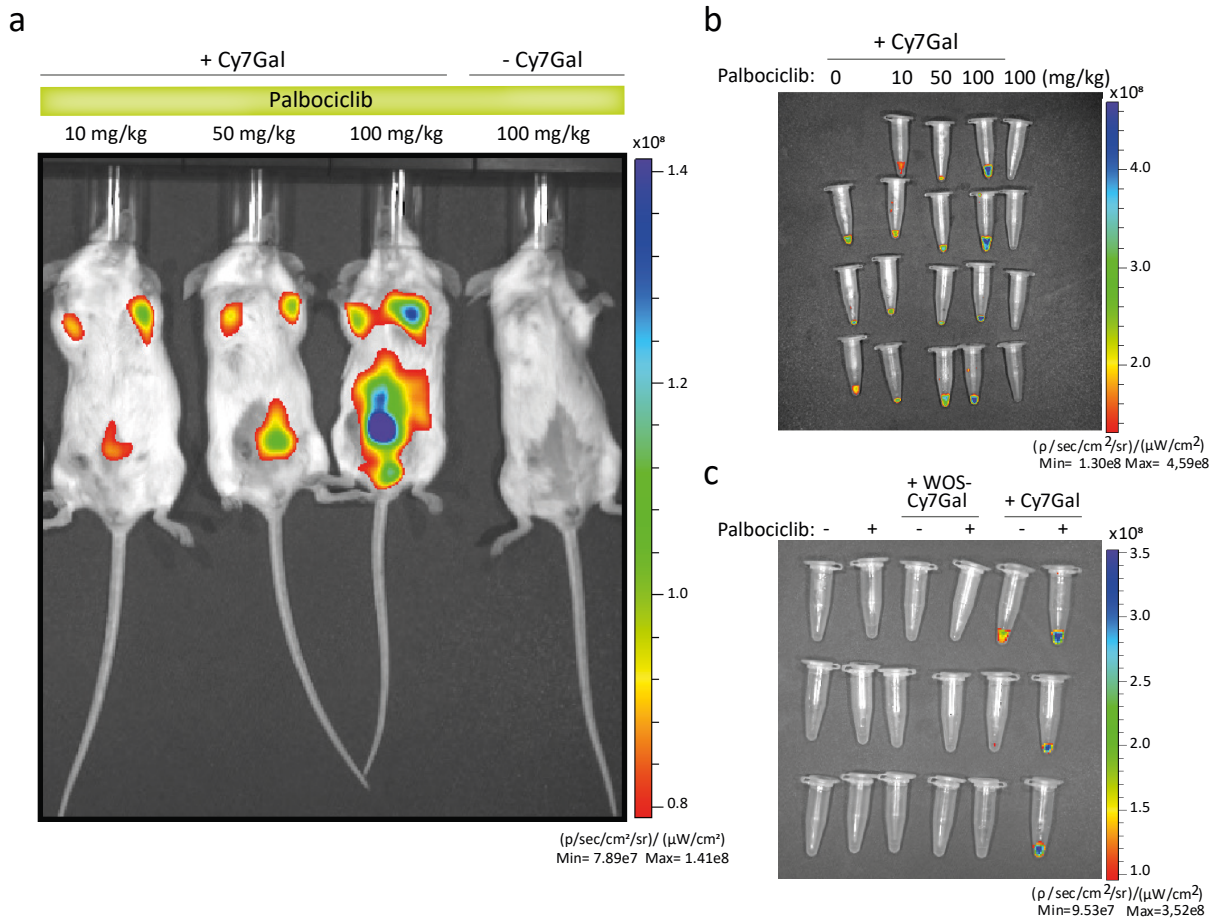

Extended Data Figure 5. Cy7Gal monitors palbociclib treatment in mice bearing mammary tumors. **a**, BALB/cByJ female mice carrying orthotopic 4T1 mammary tumors, treated with varying doses of the senescence-inducing drug palbociclib, and subjected to IVIS® live imaging following injection with Cy7Gal. Note that the fluorescent signal associated with Cy7Gal increases with the dose of palbociclib in the urinary tract, indicating that Cy7Gal recognizes the increased senescence burden in tumors and quickly accumulates in the bladder. **b**, IVIS® imaging of urine samples from mice bearing mammary tumors, treated with increasing doses of palbociclib and injected with Cy7Gal. Observe that the highest fluorescent levels of Cy7 in urine correspond to the maximum dose of palbociclib, while non-injected mice treated with the same dose do not emit any fluorescent signal. **c**, IVIS® imaging of urine samples from palbociclib-treated or untreated mice bearing mammary tumors, and injected with WOS-/Cy7Gal or vehicle (DMEM).

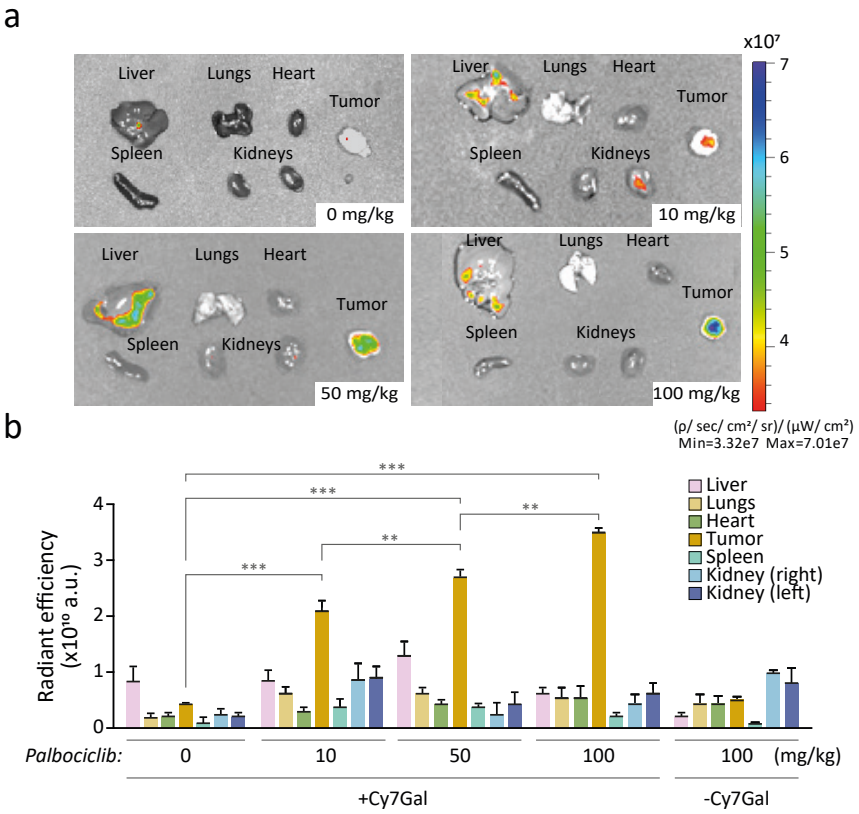

Extended Data Figure 6. *Ex vivo* analysis of Cy7Gal in different organs from mice bearing mammary tumors and treated with palbociclib. **a**, *Ex vivo* IVIS® imaging of a variety of organs (liver, lungs, heart, spleen, kidneys, tumors) from mice bearing orthotopic 4T1 tumors and treated with different doses of palbociclib (0, 10, 50, 100 mg/kg). **b**, Cy7 fluorescence (radiant efficiency) readout of ROIs delimiting each organ in the conditions exposed in image **e**, compared to palbociclib-treated mice (100 mg/kg) that were not injected with the probe. The graphs values show mean ± SEM. The number of independent biological samples in graph **b** is n=3. One-way ANOVA and Tukey's post-hoc multiple comparison test were used for statistical analysis, **p-value<0.01, ***p-value<0.001, ****p-value<0.0001.

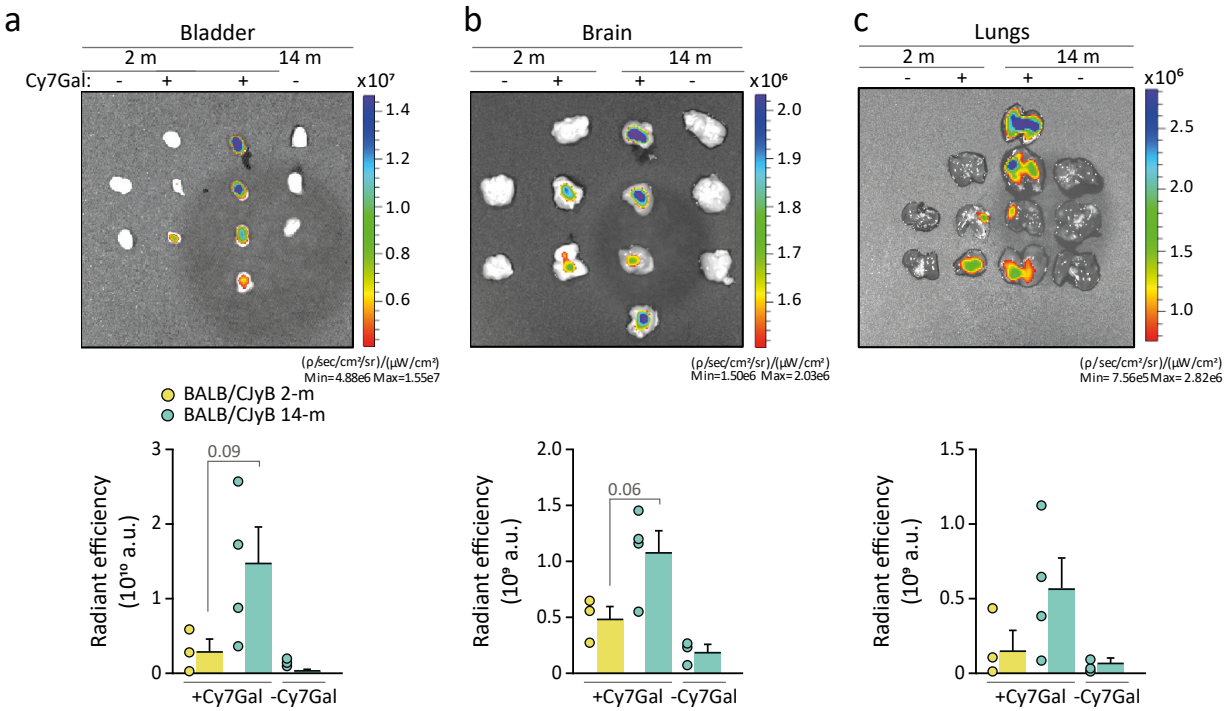

Extended Data Figure 7. An insight into Cy7Gal biodistribution in young *vs.* old BALB/cByJ mice. **a**, *Ex vivo* IVIS® images of the bladder of 2- and 14-m BALB/cByJ mice that were injected i.p. or not with Cy7Gal and measurement of the probe-associated fluorescence in this organ. **b**, *Ex vivo* IVIS® images of the brain of 2- and 14-m BALB/cByJ mice that were injected i.p. or not with Cy7Gal, and readout of the probe-related fluorescence in this organ. **c**, *Ex vivo* IVIS® images of the lungs of 2- and 14-m BALB/cByJ mice that were injected i.p. or not with Cy7Gal and probe-related fluorescence readout in this organ. The graphs show the mean ± SEM. The number of independent biological samples (represented as dots) used and the exact p-values are indicated in the graphs. Unpaired Student's t-test was used for statistical analysis.

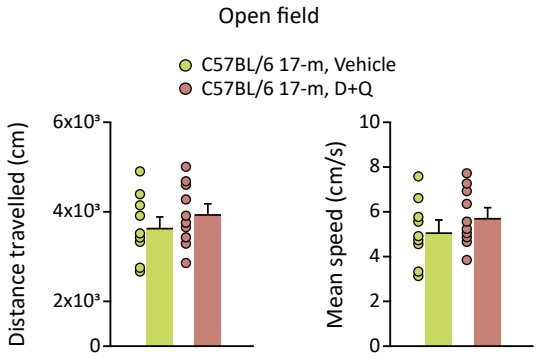

Extended Data Figure 8. Locomotion assessment after senolysis. Locomotion assessment of C57BL/6 mice after senolytic treatment with D+Q. Observe that there are no differences at this level between treated and untreated C57BL/6 mice. The graph shows the mean ± SEM. The number of independent biological samples (represented as dots) used are indicated in the graphs. Statitistical analysis with unpaired Student's t-test showed no significative differences between both groups (p-value>0,05).

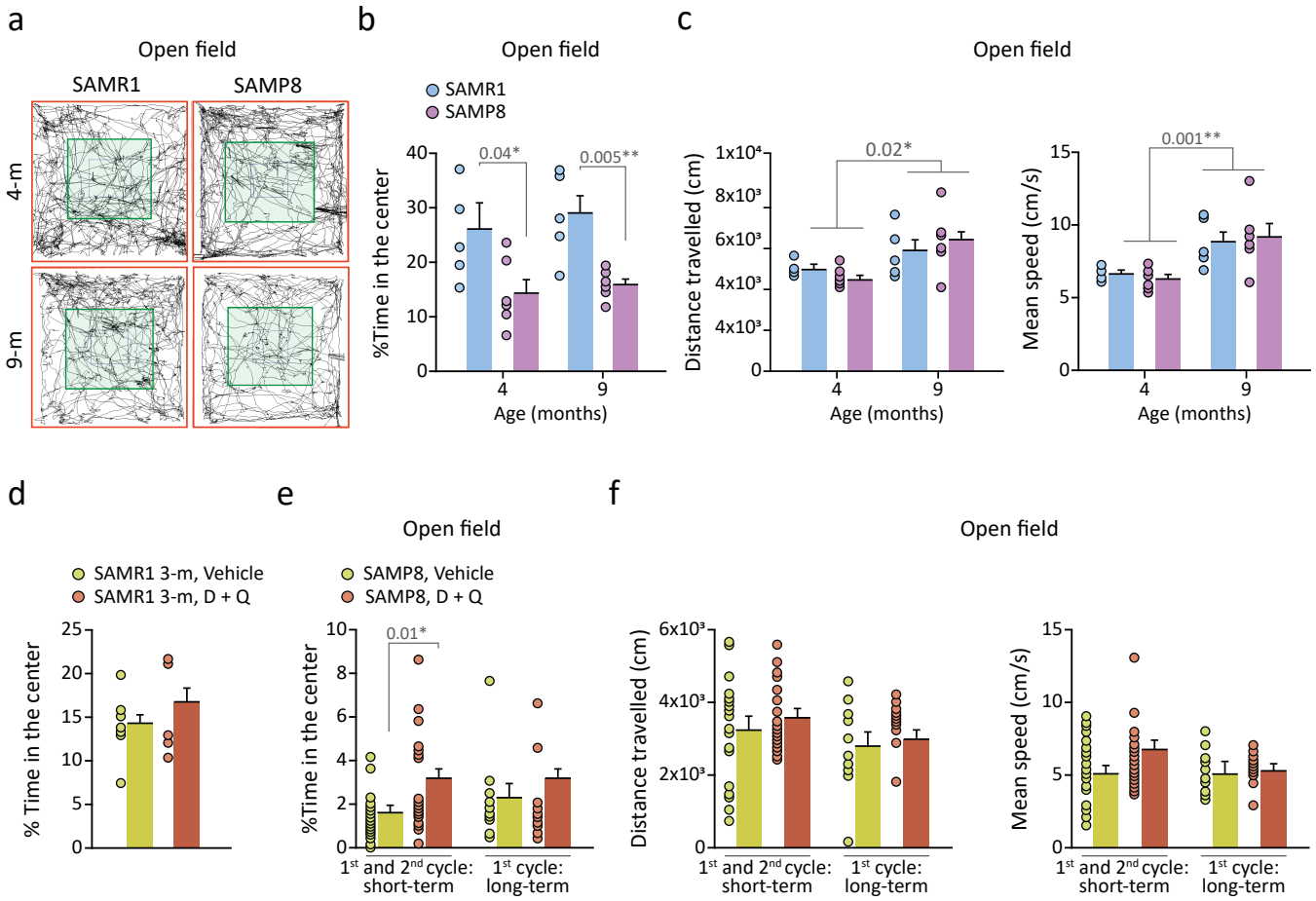

Extended Data Figure 9. Anxious behavior and locomotion assessment during accelerated aging and after senolysis. **a**, Representative map of movement in the open field test comparing 4- and 9-m SAMR1 to SAMP8 mice. **b**, Percentage of time that 4- and 9-m SAMR1 and SAMP8 mice spent in the center of the open field (green area). **c**, Locomotion assessment of 4- and 9-m SAMR1 and SAMP8 in the open field. Notice that differences in avoidance of the center area in the two genetic backgrounds are not due to differences in locomotion. **d**, Percentage of time 3-m SAMR1 mice spent in the center of the open field after 3 days receiving D+Q or vehicle orally. Note that D+Q senolytic drugs per se do not exhibit an anxiolytic effect. **e**, Percentage of time SAMP8 mice, treated with D+Q or vehicle, spend in the central area of the open field. Notice that, only when we assessed short-term anxious behavior after senolytic treatment, a significant improvement in open field test performance (decreased anxiety) was observed in mice treated with D+Q. **f**, Evaluation of locomotion- associated parameters (mouse total distance travelled and mean speed, in the open field test) in SAMP8 mice after senolytic treatment. Note that locomotion is not affected by the treatment, either when assessed in the short- or long-term after the senolytic intervention. The graphs show the mean ± SEM. The number of independent biological samples (represented as dots) used and the exact p-values are indicated in the graphs.Unpaired t-test was used to analyze mice anxious behavior (**b**, **d**, **e**) in the open field test, while locomotor behavior was analyzed with a two-way ANOVA comparing simultaneously SAM background x age (**c**), as well as, SAMP8 D+Q/vehicle x treatment evaluation term (**f**).

This PhD thesis has been supported by a pre-doctoral scholarship from the Spanish Ministry of Universities, “Programa de Formación del Profesorado Universitario (FPU)”, and a technical expert contract funded by the European Commission.

The research has been funded by the following research projects led by Ramón Mártinez Máñez:

- Gobierno de España (RTI2018-100910-B-C41 and PID2021-126304OB-C41).
- Generalitat Valenciana (PROMETEO 2018/024 and CIPROM/2021/007).
- CIBER-BBN- Instituto de Salud Carlos III, Ministerio de Ciencia e Innovación (CB06/01/2012).

And by the following research projects led by Isabel Fariñas:

- 2014-2018. Estudio de células madre en el ámbito de las investigaciones básicas en terapia celular. Fundación Botín-Banco de Santander.
- 2018-2021. Regulación del comportamiento de las células madre neurales por el medio sistémico: el nicho extendido. MINECO (SAF2017-86690-R).
- 2016-ongoing. CIBER en Enfermedades Neurodegenerativas (CIBERNED). ISCIII (Programa de Investigación Cooperativa, CB06/05/0086).
- 2017-2021. Efectos directos y remotos de la respuesta inflamatoria sobre las células madre neurales. Generalitat Valenciana (Proyectos de Excelencia, PROMETEO/2017/030).
- 2017-2021. RETIC de terapia celular ISCIII (RD16/0011/0017).
- 2021-2024 Regulación molecular de la heterogeneidad celular en los nichos neurogénicos adultos MICINN (PID2020- 117937GB-I00).
- 2021-2025. Una aproximación multidisciplinar al estudio de la respuesta al daño genómico en células madre neurales: de levadura a mamíferos y vuelta. Generalitat Valenciana. Programa Prometeo de Proyectos de Excelencia (PROMETEO/2021/028).